UNIVERSITÀ DEGLI STUDI DI MILANO

FACOLTÀ DI SCIENZE E TECNOLOGIE

Dipartimento di Chimica

Corso di Dottorato di Ricerca in Chimica Industriale
XXX Ciclo

Luminescent and nonlinear optical properties of organometallic complexes

ELEONORA GARONI

R10821

Tutor: Chiar.ma Prof.ssa DOMINIQUE MARIE ROBERTO

Co-Tutor: Dr. ALESSIA COLOMBO

A. A. 2016/2017

List of acronyms and abbreviations in alphabetical order

acac	acetylacetonate
BLA	bond-length alternation
CH_2Cl_2	dichloromethane
CH_3CN	acetonitrile
$CHCl_3$	chloroform
DC	direct current
DCM	dichloromethane
DMSO	dimethyl sulfoxyde
dpyb	dipyridylbenzene
DTE	dithienylethene
EFISH	electric field induced second harmonic generation
EL	electroluminescence
Et_2O	diethylether
Et_3N	triethylamine
EtOH	ethanol
HLS	harmonic light scattering
HOMO	highest occupied molecular orbital
HRS	hyper Rayleigh scattering
i-Pr_2NH	bis(isopropyl)amine
ILCT	intraligand charge transfer
LC	ligand centred
LEEC	light-emitting electro-chemical cells
LLCT	ligand-to-ligand charge transfer
LUMO	lowest unoccupied molecular orbital
MeOH	methanol
MLCT	metal-to-ligand charge transfer
MMLCT	metal-metal-to-ligand charge transfer
NIR	near infra-red
NLO	nonlinear optics
NMR	nuclear magnetic resonance
NOESY	nuclear overhauser effect spectroscopy
OLED	organic light-emitting diodes
OPA (1PA)	one-photon absorption
OPE	oligo(*para*-phenyleneethynylene)

OR	optical rectification
phbpy	6-phenyl-2,2'-bipyridyl
PMMA	polimethylmetacrilate
ppy	phenylpyridine
PS	polystyrene
PSS	photostationary state
PTCDI	perylene tetra carboxy diimide
SEM	scanning electron microscopy
SFG	sum frequency generation
SH	second harmonic
SHG	second harmonic generation
TD-DFT	time-dependent density functional theory
TEM	transmission electron microscopy
THF	tetrahydrofuran
TMSA	trimethylsilylacetylene
TPA (2PA)	two-photon absorption
trpy	terpyridine
UV-Vis	ultraviolet-visible
WOLED	white organic light-emitting diodes

AIM OF THE THESIS

Organometallic chromophores with both luminescent[1] and second-order nonlinear optical properties[2] are of growing interest as new molecular multifunctional materials, since they offer additional flexibility compared to organic chromophores by introducing active electronic charge-transfer transitions between the metal and the ligand, which are tunable by virtue of the nature, oxidation state and coordination sphere of the metal centre.

This is the main reason why our interest was brought in this specific research area.

My PhD thesis is divided in two main parts:

1)   Luminescent properties of cyclometallated metal complexes.

2)   Second-order NLO properties of organometallic complexes and third-order NLO activity of organic π-conjugated and coordination compounds.

The first section is dedicated to the preparation and study of the luminescence properties of some novel platinum(dipyridylbenzene) complexes. These organometallic compounds, known for being extremely bright emissive and having long lifetimes, are of particular interest for applications in electroluminescent devices. My aim was to achieve mono- and dinuclear complexes possessing emission properties that can be tuned with external factors. The two dinuclear platinum(II) complexes that I synthesized alternate monomer-like and eximeric emission, depending on the temperature, the solvent and the presence of metal cations in solution. The mononuclear platinum(II) complexes that I studied, instead, bear a photochromic unit linked with different tethers to the metal moiety: this allows the modulation of their switching ability and the study of the effect of the linker. These complexes were prepared in Rennes, France, during my stay in the group of Dr. V. Guerchais.

The second section is dedicated to the second-order nonlinear optical properties of mononuclear platinum(dipyridylbenzene) complexes. In the first place, we will discuss how the second-order NLO properties of such compounds can be modified by virtue of the presence of different π-conjugated pendants linked to the central metal unit with different bridges: this will allow a fine tuning of the NLO properties. Secondly, we will study related photochromic platinum(II) complexes and see that their second-order NLO properties are switchable, too.

The two-photon absorption (TPA) ability of different organic π-conjugated and organometallic complexes will be discussed. At first, the outstanding TPA properties of some 3,4,9,10-perylenetetracarboxylic diimide derivatives will be presented. These purely organic compounds will be used as springboard to achieve new multinuclear ruthenium(II) complexes with a highly π-conjugated ligand. Afterwards, the TPA activity of some ruthenium(II) σ-acetylide and iridium(III) tris-(phenylpyridine) complexes will be discussed. The two-photon absorption measurements were performed in the laboratory of Dr. K. Kamada, in Ikeda, Japan, during my stay there.

Throughout this dissertation, the luminescent, second- and third-order nonlinear optical properties of a new multifunctional cationic iridium(III) complex will also be presented.

I. LUMINESCENT PROPERTIES OF PLATINUM (II) AND IRIDIUM (III) COMPLEXES

1. Introduction to luminescence

1.1. General principles of luminescence

Luminescence is a photophysical phenomenon resulting from emission of light by a substance, originated by the decay of an electronically excited specie. According to the nature of the excitation, many different kinds of luminescence can be defined: here we will discuss photoluminescence, which takes places after the absorption of photons from an incident radiation by a molecule or material.

The interaction of electromagnetic radiation with matter leads to absorption only if a dipole moment is created as a result of such interaction. The strength or intensity of a transition is related to the square of the transition moment integral, and is expressed in terms of oscillator strength.[3] According to the Born-Oppenheimer approximation, being the nuclei much larger and heavier, in the wave function of a molecule the electronic and nuclear components can be separated, and the latter ignored. Also, electronic, vibrational and rotational wave functions can be treated independently and all of them must be taken into account for the calculation of the transition moment integral:

$$|M_{nm}| = \int \Psi_m (e\tau) \Psi_n \, d\tau$$

$$\Psi = \Psi_{electronic} + \Psi_{vibrational} + \Psi_{rotational}$$

The selection rules for electronic transitions can be deduced from this equation:

a - Changes in spin multiplicity are forbidden; there must be a change in the symmetry of a complex and electric dipole transitions can occur only between states of opposite parity (Laporte rule: only $g \rightarrow u$ and $u \rightarrow g$ transitions are allowed).

b - Selection rules can break down if some specific conditions occur:

1. Spin-orbit interaction. Intra and intermolecular perturbations can contribute to the mixing of singlet and triplet states. These perturbations are function of the magnetic field of the nucleus and therefore of the atomic mass (heavy atom effect): second and third row transition metals are heavy enough to allow transitions between singlet and triplet states.

2. Vibronic coupling. Molecular vibrations can allow mixing of states separated by a low energy gap (usually excited states), and consequently symmetry forbidden transitions can occur with low intensities.

Another important rule deriving from the Born-Oppenheimer approximation is the Franck-Condon principle: it states that the most probable transitions between electronic states occur when the wave function of the initial vibrational state most closely resembles to the wave function of the final vibrational state, namely the most intense transition is the so-called vertical transition (Figure 1).
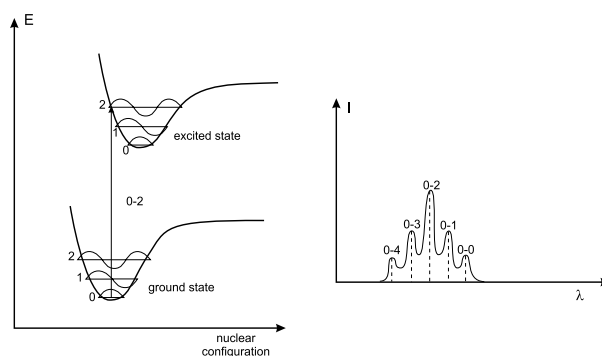
Figure 1. Left: Potential energy diagrams with the vertical transition. Right: shape of the absorption bands.

The transition intensity is proportional to the square of the overlap integral of the two states involved: this gives important information on the shape of the absorption and emission spectra of a molecule.

The ground and excited electronic states of a molecule can be represented with the Jablonski diagram (Figure 2): once a molecule is excited, energy can be released through either radiative or nonradiative pathways.
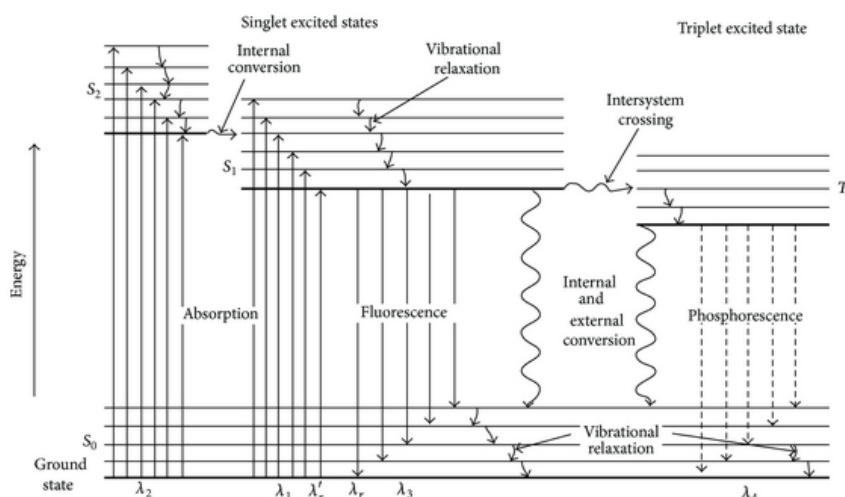
Figure 2. Jablonski diagram describing the electronic levels of common organic molecules and possible transitions between singlet and excited states.

Vibrational relaxation and internal conversion occur extremely rapidly (10^{-12} - 10^{-10} s), while intersystem crossing is slightly slower and more likely in molecules containing heavy nuclei. These processes are faster and compete with radiative transitions as fluorescence (10^{-10} - 10^{-6} s, between electronic states of the same multiplicity) and phosphorescence (10^{-4} - 10^{4} s, between electronic states of different multiplicity). In any case, the rate of radiationless transitions is inversely proportional to the energy gap between the 0-0 electronic levels of the two excited states (energy gap law). This means that emission will always take place from the lowest excited state (Kasha's rule) and, since the gap between

the lowest excited singlet or triplet states and the ground state is bigger, fluorescence and phosphorescence can take place even if their rate is lower than that of the radiationles transitions.

1.2. Organometallic complexes for luminescence

Current active research in metal-organic complexes with optoelectronic applications is due to their long emission lifetime, large Stokes shifts, ability of harvesting triplet states and tuneable excited states.[4] Complexes of 2nd and 3rd row transition metals are of particular interest: the high spin-orbit coupling constant possessed by these metals allow significant mixing of d_{metal} and π_{ligand} orbitals and easier access to triplet states through intersystem crossing.

Possible applications of such complexes include OLEDs and LEECs, solar energy conversion, sensing, cell imaging and photo-catalysis.[5] This first chapter is dedicated to luminescent cyclometalated Pt^{II} and Ir^{III} complexes, in order to evidence how it is possible to modulate their emission properties in solution by a careful choice of the substituents on the ligands and the ligands themselves.

2. Luminescent platinum complexes: introduction and state of the art

2.1. Platinum (II) complexes for luminescence

Platinum complexes have been widely studied in the last decades for their superior luminescent properties[5c,6] and their diverse applications in OLEDs,[7] bioimaging[8] and chemosensing.[9] In contrast to d^6 Ru^{II} and Ir^{III} complexes, the square planar coordination geometry of d^8 Pt^{II} complexes offers the possibility of reactivity by way of axial interactions that are not exploitable in octahedral and tetrahedral complexes. In fact, the d^{z2} orbital is perpendicular to the plane of the molecule and orbitals of adjacent molecules can interact through Pt–Pt interactions (Figure 3, left), with a typical intermolecular separation of the order 3.5 Å.[10]
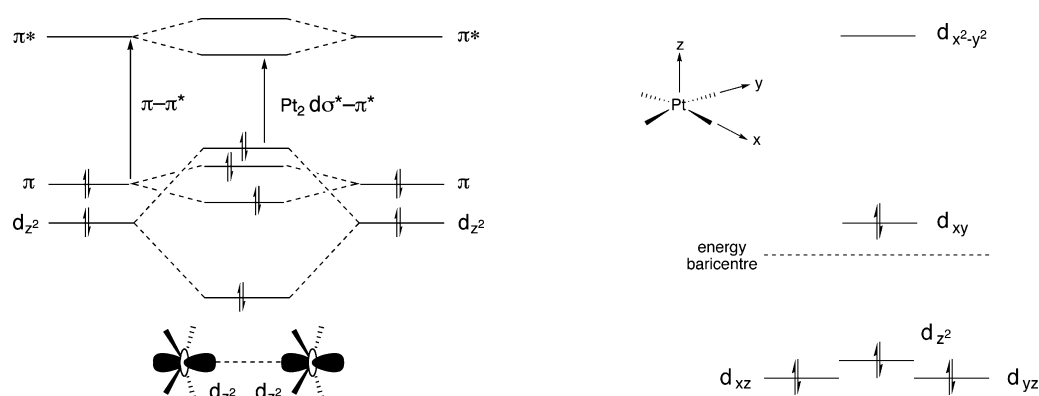
Figure 3. Left: Simplified frontier molecular orbitals showing the effect of intermolecular d_{z2} orbital overlap. Right: Ligand field-splitting diagram for metal d orbitals in a square planar Pt^{II} complex.

One of the consequences of such interaction is that the highest occupied metal-based molecular orbital

is raised in energy compared to that of the isolated molecules, the lowest-energy optical transitions are shifted to lower energies and also switches in the nature of the nature of the lowest-energy state can be induced.[11] Planar, conjugated aromatic ligands can give rise to π–π interactions between adjacent molecules: these are less sensitive to the intermolecular separation but can give the same effects as Pt–Pt interactions. Unfortunately, another effect of the square-planar coordination environment of Pt^{II} complexes is that the unoccupied metal-centred $d_{x^2-y^2}$ orbital becomes strongly antibonding (Figure 3, right). If this orbital is populated after light absorption, the molecule can easily undergo non-radiative decay due to a severe distortion of the excited state that involves the increasing of the Pt-L bond length. Even though other excited states (as d-π^* or π-π^*) may lie at lower energies than the d-d state, the latter can provide a deleterious thermally activated non-radiative decay pathway (Figure 4). This is the reason why platinum complexes with simple inorganic ligands, like [Pt(bpy)Cl$_2$],[12] are rarely emissive in fluid solution.
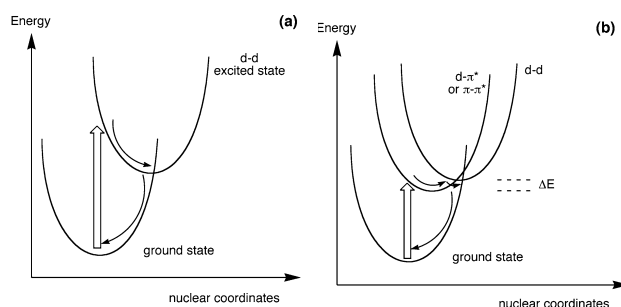
Figure 4. The potential energy surface for d-d excited states in a square planar Pt^{II} complex. They can be thermally accessible even if d-π^* or π-π^* states lie at lower energies.

Different strategies can be adopted in order to favour the radiative decay and promote luminescence in Pt^{II} complexes:

I) *Use multidentate ligands in order to avoid distortions.*

Pt^{II} phosphors with bidentate 2-phenylpyridine C^N[13] and biphenyl C^C based ligands have been largely studied.[14] Nevertheless, terdentate ligands are much less flexible than bidentates, thus being less subject to distortions and subsequently non-radiative decay. By imparting additional rigidity to the complex with terdentate ligands, the D$_{2d}$ distortion that bis-bidentate ligands can undergo by twisting on the two planes can be avoided resulting in enhanced quantum yields.[15]

II) *Switch the emissive state from the usual ^{3}MLCT state to a ^{1,3}ILCT state lying at lower energy.*

This state is not deactivated via the d-d state and emission is thus observable. Examples of this approach are reported by Che and McMillin, who noticed that aromatic and electron-rich substituents on the position 4' of the central ring of the 2,2':6',2''-terpyridyl ligand of [Pt(trpy)Cl]$^+$, chosen for its rigidity but normally weakly emissive, enhance the emission properties in solution at room temperature.[16]

III) *Reduce the influence of the d-d states by raising their energy.*

This can be achieved by using strong-field ligands, as acetylides[17] or cyanides,[18] to replace the chloride

co-ligand in [Pt(trpy)Cl]$^+$ complexes (with cyanide co-ligands, anyway, the lowest-energy excited state is a $^3\pi$-π state with low metal contribution: this reduces radiative rate constants).

IV) *Use of cyclometalated ligands.*

Due to chelation and their coordination with a σ-donor carbon, cyclometalated ligands are very strong field ligands known for conferring rigidity to the molecule, inducing large orbital splitting, strengthening M-L bonds and lifting d-d states to higher energy compared to MLCT and LC states. This strategy led to the synthesis and study of a huge variety of cyclometalated Pt^{II} complexes with terdentate cyclometalated ligands.[19]

2.2. Pt(II) 2,6-dipyridylbenzene complexes and their applications

The terdentate ligands made of interconnected phenyl and pyridyl rings are structurally analogous of terpyridine and isoelectronic with it, except that the σ-donor binding carbon atom acts as an anionic ligand. The most extensively studied ligands of this class are 2,6-diphenylpyridine (C^N^C-dphpy), 6-phenyl-2,2'-bipyridine (N^N^C-phbpy) and 2,6-dipyridylbenzene (N^C^N-dpyb), while 2-([1,1'-biphenyl]-3-yl)pyridine (N^C^C) ligands are quite unusual.[19] Few examples of phosphorescent [Pt(dphpy)X] complexes are reported: emission from a ^{3}LC state can be detected only in a glassy matrix at 77 K[20] and in order to achieve their emission at room temperature thiophene, carbazole or fluorene groups need to be introduced as the anionic carbon donors to extend the π-conjugated system and minimize the distortion of the triplet excited state.[21] This is due to the fact that these complexes are subject to important structural distortions on going from the S0 to the T1 state.[22] As seen for Pt(dphpy)X complexes, simple Pt(phbpy)X complexes are also weakly emissive in solution at room temperature.[23] Again, if the π-conjugated system is extended with quinoline, isoquinoline and benzothiophene groups the luminescent properties in solution at room temperature can be considerably enhanced, emission from ^{3}MLCT state can be observed and quantum yields up to 0.99 can be reached.[24]

Among all cyclometalated platinum complexes, the ones bearing N^C^N ligands are among the brightest emitters in solution. The different position of the cyclometalating phenyl ring respect to N^N^C ligands leads to important differences in the properties of these complexes, which can explain their outstanding luminescent performances. In this case too, ligands have been reported with more extended π-conjugation by the use of fused polycyclic aromatic rings bearing N-acceptor or C σ-donor atoms. However, their luminescent properties are usually worse than those of dipyridylbenzene platinum complexes, because of different electron-withdrawing/donating properties of the cyclometalated ligand or different torsional angles that induce more efficient non-radiative decay.[25]

The first dipyridylbenzene cyclometalated complex to be synthesized by Sauvage and co-workers in the nineties, was a dinuclear mixed valence Ru(II) complex with interesting redox properties.[26] In the following years, several related compounds with other metal ions have been prepared, including Rh^{III}, Ir^{III}, Pd^{II}, Au^{III}, and of course Pt^{II}.[27] The first Pt(dpyb)Cl complex was synthesized by De

Arellano et al. in 1999, with the aim of studying the different coordinating behaviour of 2,6-dipyridylbenzene ligands with Pd and Pt.[28] In the case of Pd[II], coordination to the position C^3 of the phenyl ligand with the formation of multinuclear complexes is preferred. In contrast to Pd[II], the reaction of K_2PtCl_4 with dpybH gave the C^1-metallated product with high yield (78%, Figure 5).
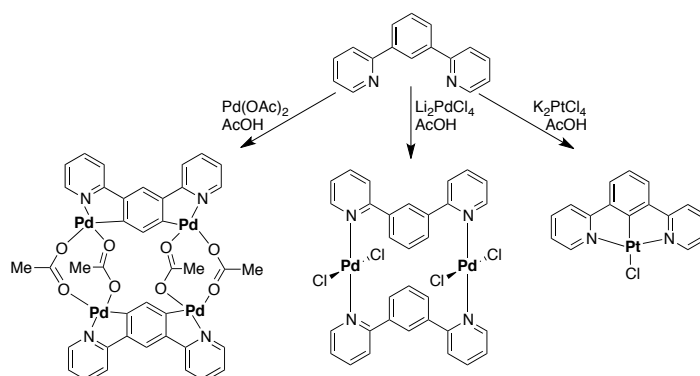
Figure 5. The Pd[II] and Pt[II] complexes reported by De Arellano et al.

2.2.1. Pt dipyridylbenzene complexes with applications in OLEDs

Since then, the studies on Pt(N^C^N) complexes did not advance until Williams and co-workers, in 2003, published the first article about the photophysical properties of Pt(dpyb)Cl.[29] The dipyridylbenzene ligands were synthesized through Stille coupling between the appropriate 3,5-dibromobenzyl derivative and 2-(tri-*n*-butylstannyl)pyridine, while the PtLCl (L = L^1, L^2, L^3) complexes (Figure 6) were synthesized starting from the appropriate dpybH ligand and K_2PtCl_4 at reflux in an acetic acid/water mixture (**PtL^{1,3}Cl**) or an acetonitrile/water mixture (**PtL^{2}Cl**) for three days. The choice of acetonitrile as a solvent is due to the fact that acetic acid could favour the degradation of the ester-substituted ligand.

L^1 R = H
L^2 R = CO$_2$Me
L^3 R = Me
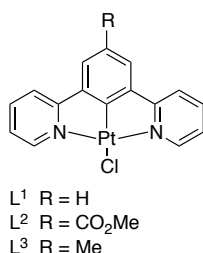
Figure 6. The first Pt(dpyb)Cl complexes studied by Williams et al.

All complexes are highly emissive in dilute CH_2Cl_2 solution at 298 K with emission quantum yields (Φ_{lum}) one order of magnitude greater than those of analogous Pt(phbpy)Cl complexes (0.60 for **PtL^{1}Cl**, 0.58 for **PtL^{2}Cl** and 0.68 for **PtL^{3}Cl**) and lifetimes (τ) in the microsecond range. Crystallographic studies demonstrate that, thanks to the strong cyclometalating ligand, the Pt-C bond length are shorter

than in the analogous N^N^C ligands (1.907 Å for **PtL^{1}Cl** and 1.903 Å for **PtL^{2}Cl** *vs* 2.04 Å for Pt(N^N^C)Cl complexes), and Pt-N bond lengths (2.03 Å) are also shorter than usual.[23] This higher ligand-field strength can account for the enhanced quantum yields of Pt(dpyb)Cl complexes respect to the parent terpyridine (non luminescent at 298 K) and phenylbipyridine complexes: the d-d states are in such manner shifted at very high energy eliminating non-radiative deactivating pathways. The absorption spectra (Figure 7, left) of PtL$^{1-3}$Cl display very intense bands (ε up to 10^3) at wavelengths below 350 nm, assigned to ligand centred ^{1}π-π* transitions of the dipyridylbenzene ligand.

The set of intense bands at 350-450 nm includes at least three contributions:

(I)   The band at higher energy can be assigned to transitions that are independent from the substituent, since its position remains unchanged;

(II)   The bands at lower energies are red-shifted as the 4-substituent becomes more electron-donating and exhibit solvatochromic behaviour: these statements allow their assignment to charge transfer transitions from the Pt and chlorine orbitals to the π* of the N^C^N ligand;

(III) The very weak bands at lower energy (478-495 nm) can be assigned transitions of primarily ^{3}LC character involving direct population of ^{3}π-π* states: these transitions are facilitated by the high spin-orbit coupling associated to the Pt^{II} ion.[30]

The emission spectra (Figure 7, right) display very small Stokes shift and are highly structured, which is typical of emission from primarily ^{3}LC states, the small Stokes shifts being incompatible with emission from charge-transfer states.
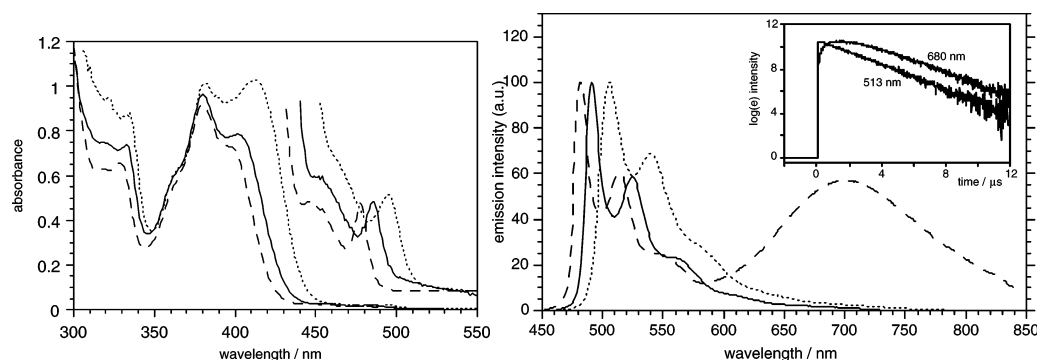
Figure 7. Absorption (left) and emission (right) spectra of **PtL^{1}Cl** (plain line), **PtL^{2}Cl** (dashed line) and **PtL^{3}Cl** (dotted line) in CH$_2$Cl$_2$ at room temperature. The weak, low energy absorption bands are shown on an expanded scale. The emission spectra were registered in dilute solution (2.5x10^{-6} M for **PtL^{1,3}Cl** and 1.0x10^{-4} M **PtL^{2}Cl**). The frame on the right shows the emission kinetic traces of the solution of **PtL^{2}Cl** registered at 513 nm (monomer) and 680 nm (excimer) using 355 nm excitation.

Theoretical calculations showed a significant admixture of MLCT character in the emitting state of the complexes:[31] the long emission lifetimes and efficient quenching of triplet oxygen confirm emission from a triplet state. The increase in concentration leads, for the three complexes, to a decrease in the lifetime and the growing of a broad, structureless emission band at lower energies (ca. 700 nm), which indicates excimer formation. However, the emission decay in the 480-540 nm region remains

monoexponential over the whole range of concentrations, since no significant contribution from the excimer emission is expected.

Such excimer emission is revealed to be a peculiar property of Pt[II] N^C^N complexes, since it was not previously observed in Pt[II] N^N^C and C^N^C complexes, that usually display self-quenching not accompanied by detectable excimer emission.[23]

Further studies demonstrated that the emission wavelength of Pt(dpyb)Cl complexes can be finely tuned by facile ligand modification:[32] different aromatic substituents were introduced in the position 4 (*para*) of the phenyl ring through Stille or Suzuki coupling (Figure 8). The coordination geometries are similar to the previously reported Pt(dpyb)Cl complexes commented before and in the absorption and emission spectra similar sets of bands can be recognized. Interestingly, the band at lowest energy in the absorption spectrum is clearly increasingly red-shifted, from 401 to 431 nm in the order mesityl < 2-pyridyl < 4-tolyl,4-biphenyl < 2-thienly < 4-dimentylamino, effect already observed beforehand (Figure 8a). Furthermore, for each complex, this band undergoes negative solvatochromism: this behaviour is typical of transition with charge-transfer character and means that the excited state has a lower dipole moment than the ground state.[33]
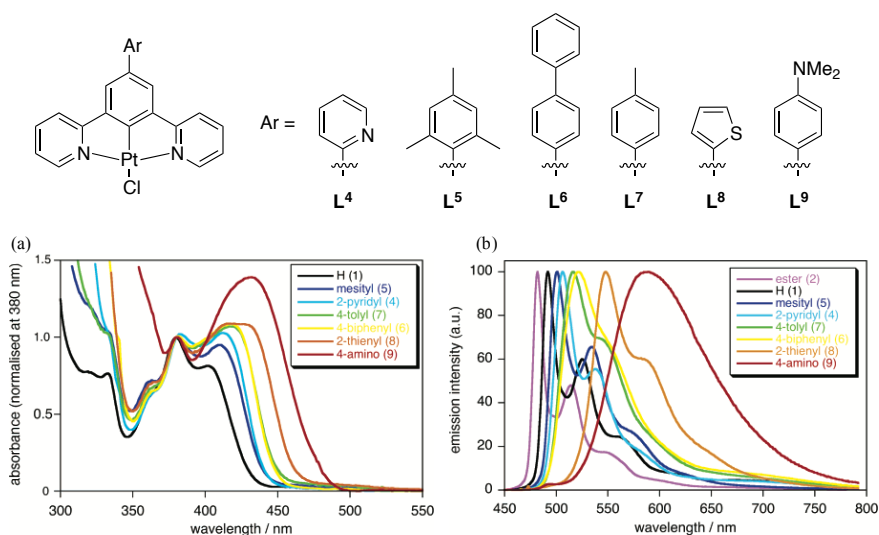
Figure 8. The 4-phenyl substituted Pt(dpyb)Cl complexes with their (a) absorption spectra in CH_2Cl_2 at 295 K, normalised at 380 nm, and (b) emission spectra in 10^{-5} M CH_2Cl_2 solution at 295 K (λ_{exc} = 400 nm).

These complexes, as expected, are brightly luminescent in solution with quantum yields in the range of 0.5-0.6. The emission spectra are highly structured (Figure 8b),[I] the Stokes shifts are small, the band at highest intensity is the one of highest energy and the spectra show very weak negative solvatochromism, confirming the ligand-centred nature of the emission. The emission maxima are increasingly red-shifted following the same trend as the absorption band at lower energy. These considerations on the absorption

---

[I] The amino-substituted complexes displays a broad structureless emission band: its behaviour will be discussed later.

and emission spectra, as well as electrochemistry measurements[32] and TD-DFT calculations,[31,34] reveal that the highest occupied molecular orbital is prevalently based on the cyclometalated aryl ring, the metal and the chloride co-ligand, with a minor contribution from the pyridyl rings, which make nonetheless a more substantial contribution to the lowest unoccupied molecular orbital. Interestingly, the pyridyl 4-position is a node in the HOMO, whereas the 5-position contributes to it. On the other hand, the LUMO receives only little contribution from the 3 and 5 positions of the phenyl rings. The pendent in the 4-position of the phenyl ring gives a major contribution to the HOMO, whereas the LUMO level is substantially unaffected. The red-shift can be rationalised with a destabilisation of the HOMO level, resulting from the increasingly electron-donating ability of the substituent, while the LUMO level remains unchanged. As a result, further modifications of the HOMO-LUMO gap can be achieved by introducing electron-donating or electron-withdrawing substituent on the pyridyl rings.

Some information about the geometry of the excited state can be obtained by studying the emission spectra at low temperature. In the X-ray structures, also informative about the conformation assumed by the ligand at the ground state, a mean dihedral angle of 30° can be observed. In fact, since the lowest energy absorption band, attributed to direct excitation of the ^{3}LC state, appears at almost the same wavelength for all the complexes, there is a remarkable progressive increase in the Stokes shift between the ^{3}LC absorption and emission bands. This can be ascribed to the need for torsional rearrangement, after light absorption, of the aryl substituent with the dipyridylbenzene core for a maximal conjugation in order to achieve an approximately coplanar conformation of the pendent and cyclometalating rings. Emission spectra in frozen glass at 77 K, where torsional rearrangements are inhibited, confirm this hypothesis: the emission maxima are blue-shifted of 5-10 nm compared to the room temperature spectra, except the one of the mesityl-substitued complex. By increasing the concentration, as reported above for **PtL$^{1-3}$Cl**, a new broad and structureless emission band centred at 700 nm becomes progressively more intense at the expense of the shorter wavelength bands. This behaviour demonstrates once more the tendency for these complexes to form excimers at high concentration, even though the introduction of the aryl pendent reduces the propensity to form excimers compared to the methyl substituted parent complex (the self-quenching rate constant k$_Q$ diminishes with the increasing steric demand of the substituent). The evidence of excimers formation even in the presence of the bulky aryl substituents, may suggest a head-to-tail interaction with the aryl groups disposed on opposite sides of the excimers.

The amino substituted complex **PtL^{9}Cl** exhibits a peculiar behaviour in solution: the emission band in polar solvent such as dichloromethane or acetonitrile is red-shifted, broad and structureless, it displays strong positive solvatochromism and is subject to very little self-quenching and excimer formation. This can be ascribed to the introduction of the strongly electron-donating dimethylamino substituent that raises the energy of the aryl pendent to such extent that a high-energy molecular orbital becomes localised predominantly on this group. The lower energy excited state is thus switched from a

LC (π_{NCN}-π^*_{NCN}) state to a ILCT ($\pi_{Me2N-Ar}$-π^*_{NCN}) transition, from which the emission arises: this demonstrates that the substituents on the phenyl ring of the ligand are very important in determining the nature of the emissive state. Williams and co-workers explain that "the initially formed excited state undergoes a radiationless reorganisation in polar solvents to a state in which the amino group is perpendicular to the phenyl ring, and hence electronically decoupled, followed by a charge transfer to the acceptor terminus".[35] Further evidence to the ILCT assignment is provided by the positive solvatochromism in the emission spectrum. By decreasing the polarity of the solvent the emission spectrum resembles to those of the other complexes, it becomes more structured and the emission maximum lies near the one of the pyridyl-substituted complex (Figure 9a): the emissive state is now ^{3}LC.

These observations lead to the conclusion that the energies of the ^{3}LC and ILCT states are very similar and the emission can originate from the first in less polar solvents and from the latter in more polar solvents, where the energy of the ILCT state is reduced due to the high degree of charge separation. The predominant ILCT character in the emission in CH_2Cl_2 can also explain the reduced self-quenching and the absence of excimer formation: the excited state is less susceptible to adduct formation with the ground state molecule.[36] Actually, growing of an excimeric band is observed in saturated solution of toluene (10^{-4} M), which is non-polar enough to force the ^{3}LC to remain lower in energy.
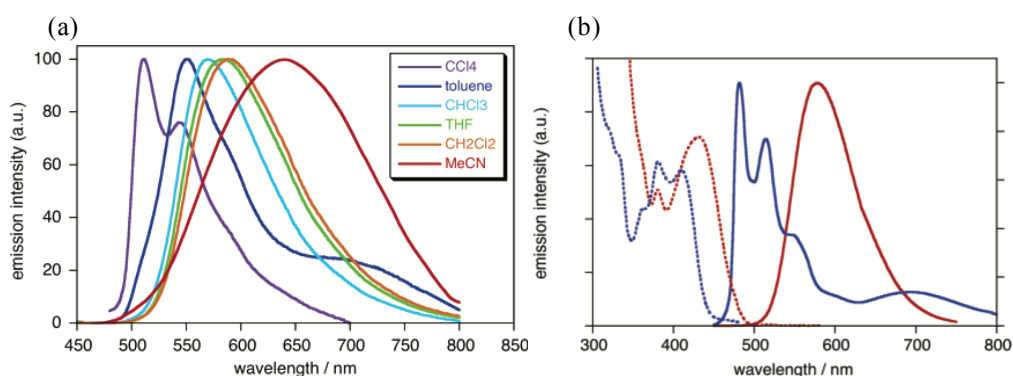
Figure 9. (a) Emission spectra of **PtL^{9}Cl** at 295 K in different solvents; (b) Emission and excitation spectra of **PtL^{9}Cl** in CH_2Cl_2 (6.0 x 10^{-5} M, red lines) and upon addition of trifluoroacetic acid (10^{-2} M, blue lines).

Protonation of the amino pendent by addition of trifluoroacetic acid can perturb the emission properties of **PtL^{9}Cl** as well (Figure 9b): by diminishing the electron-donating ability of the amino group upon protonation, the lowest-energy excited state is switched back to the ^{3}LC state again.[32] The effect of protonation is easily reversible by addition of a base. Unusually, both the neutral and the protonated forms are highly emissive in solution with quantum yields in the order of 0.40.[37] In this work Williams et al. demonstrated that the emission wavelength of a series of Pt(dpyb)Cl complexes can be accurately tuned according to the nature of the substituent on the position 4 of the phenyl ring. This was an

extremely important pioneer study that introduced a very useful and relatively simple way for future modulation of the emission properties of this class of complexes.

The thermal stability and sublimability of complexes **PtL$^{1-3,4,5,9}$Cl** renders them suitable to be tested in OLEDs.[38] In these devices light emission is generated by radiative deactivation of electronic excited states formed by the recombination of charge carriers injected from the electrodes. Phosphorescent emitters, doped into fluorescent materials, are advantageous because they can potentially harvest both singlet and excited states and thus OLEDs can reach a theoretical maximum internal quantum efficiency of 100%.[39] The electroluminescence (EL) spectral emission profiles of the considered complexes are identical to the emission spectra in dilute solution: by using different substituents, the EL emission in the OLED can be tuned in the same way as in solution, from the green-blue region to the red. The maximum external quantum efficiencies (φ_{EL}) are considerably high and range from 4% to 16% in the best case, values comparable to the best reported devices.[40] Complexes **PtL$^{1-3}$Cl** were also used to fabricate near-infrared (NIR) OLEDs:[41] solid state neat films of the complexes display emission from the excimeric form centred at 705-720 nm with a φ_{EL} = 10.5% at a current density of 10 mA/cm^2, largely exceeding the values reported for other Pt-based red emitters.[42] Furthermore, **PtL^{2}Cl** was integrated in a white OLED[43] (WOLED) as electron acceptor in association with (4,4',4''-tris(*N*-(3-methylpnehyl)-*N*-phenylamino)triphenylamine) as electron donor to achieve a combination of monomer, excimer and exciplex emission from the same layer to obtain pure white light. The performances of the device were outstanding: the CIE (*Commission Internationale de l'Éclairage*) coordinates were (0.46,0.45) (those for warm incandescent lamps are (0.41,0.41)) and more importantly the reported CRI (Color Rendering Index) was 90 on a scale of 100.
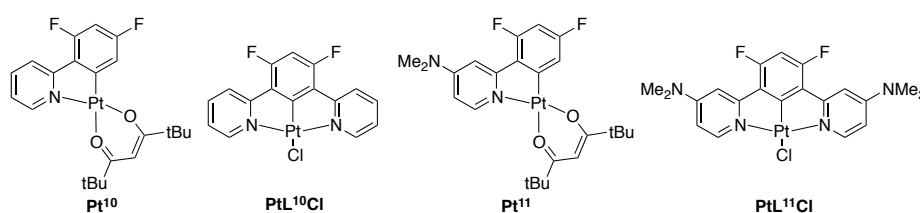
Figure 10. The Pt(dpyb)Cl and Pt(ppy)(acac) complexes studied for their luminescent properties and applications in OLEDs.

The groups of Williams and Jabbour studied the emissive properties in OLEDs of some fluoro and dimethylamino-substituted Pt(dpyb)Cl complexes in relation to their phenylpyridine analogues. The emission properties of **Pt^{10}** and **PtL^{10}Cl** were studied in solution (Figure 10):[44] **PtL^{10}Cl** (sky-blue) demonstrates a higher colour purity if compared to Pt^{10} (turquoise), because the emission bands at higher energy, responsible for contributions in the green, are less intense. Furthermore, for the dipyridylbenzene complex a Φ_{lum} = 0.80 in solution has been reported. This value is, as expected, more than ten times higher than for the phenylpyridine complex, in which the ligand field strength is clearly

lower. The quantum yield of the latter, as well as for **Pt**[10], increases in PMMA films, due to the more rigid environment that minimizes the distortions of the excited state ($\Phi_{lum,PtL10Cl} = 0.85$, $\Phi_{lum,Pt10} = 0.50$). The effect is less important for **PtL**[10]**Cl**, because of the intrinsic rigidity of the terdentate ligand, in solution. When the complexes are tested in an OLED, the performances of PtL[10]Cl are clearly superior to those of the phenylpyridine analogue: the peak φ_{EL} of 16% is almost four times higher than the one of Pt[10].[45] By modulating the dopant concentration, emission of white light can be obtained with CIE coordinates of (0.33,0.36) approaching closely the pure white CIE coordinates (0.33,0.33), which is a very good result for a single-doped white emitting device. The related complexes **Pt**[11] and **PtL**[11]**Cl** were also studied by the group of Williams in order to achieve emission of white light.[46] The fluorine substituents contribute to stabilising the HOMO of **PtL**[11]**Cl**, while the dimethylamino substituents destabilise the LUMO. The HOMO-LUMO gap is increased and the emission is shifted to lower wavelengths: the complex is indeed emissive at 453 nm in solution, still maintaining a high quantum yield of 0.60. Furthermore, the amino substituents destabilise the interaction between pairs of molecules that bring to excimer formation (a similar effect to what observed before for **PtL**[9]**Cl**), blue-shifting the excimeric band and thus preventing energy wasting in the NIR region of the spectrum. The emission throughout the visible range of the spectrum, by combination of the monomer and excimer emission bands, renders this complex of particular interest for WOLEDs. By modulating the concentration of **PtL**[11]**Cl** in the emissive layer (Figure 11) between 20% and 25%, white emission with high CRI values can be obtained. This complex is over 600 times more emissive than the analogue phenylpyridine complex[13a] and shows superior performances when integrated in an OLED device.
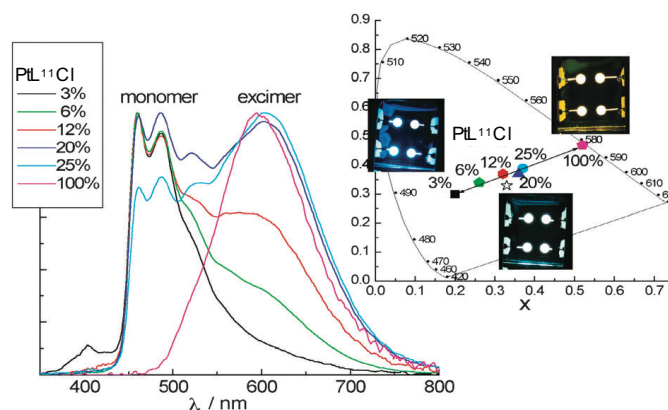
Figure 11. Electroluminescence spectra and CIE diagram with different concentrations of **PtL**[11]**Cl** in the emitting layer.

Williams et al. attained similar results with PtL[12]Cl (Figure 12), whose emission wavelength in an OLED is tunable according to the dopant concentration. It can emit white light and reaches a maximum φ_{EL} of 17% at 35% dopant content.[47,48]
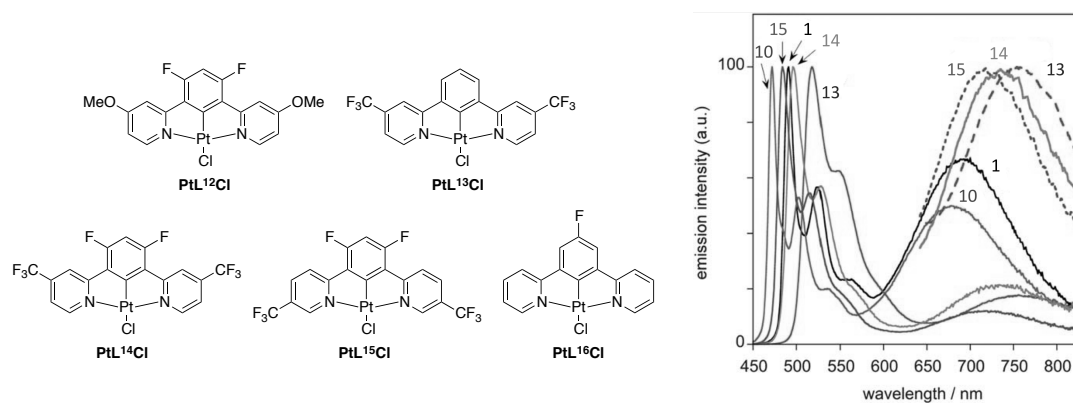
Figure 12. Left: The Pt(dpyb)Cl complexes and the Pt(dpyb)NCS complex studied by Williams and Roberto et al. in solution, OLEDs and WOLEDs. Right: Photoluminescence spectra of the Pt(dpyb)Cl complexes in CH_2Cl_2, 1.5×10^{-4} M. The weak excimer bands of **PtL$^{13-15}$Cl** have been expanded for clarity.

Our group studied the effect of substituting Pt(dpyb)Cl complexes with just electron-withdrawing substituents both on the phenyl and on the pyridyl rings (Figure 12): the fluorine on the central ring are meant to stabilise the HOMO while the CF_3 groups stabilise only the LUMO if they are on the position 4 of the pyridyl ring (**PtL^{13,15}Cl**), while they should stabilise both the HOMO and LUMO levels if they are on the position 5 (**PtL^{14}Cl**).[49,50] By inserting the fluorine on the position 4 of the phenyl ring (**PtL^{16}Cl**), its mesomeric electron-donating effect through the π orbitals attenuates slightly the inductive effect and leads to a red-shift of the emission spectrum of **PtL^{16}Cl**, compared to **PtL^{10}Cl**. Interestingly, the CF_3-containing complexes are relatively insensitive to the quenching by molecular oxygen, probably because of the more electron-poor CF_3-substituted pyridyl rings. As it can be noticed from Figure 12 (right), the excimer emission band of **PtL$^{13-15}$Cl** is clearly red shifted compared to the other Pt complexes: this is in contrast with the monomer emission data and can be explained by considering a donor-acceptor-like interaction in the excimer formation. Excimers are thus stabilised thanks to the presence of the CF_3 groups leading to a red shift, while electron-donating groups have the opposite effect (see above **PtL^{9,11}Cl**). Thin films prepared by sublimation and neat films display uniquely excimer-like emission (quantum efficiencies remain low, $\varphi_{EL} = 2\%-0.35\%$, according to the energy-gap law), while solid-state samples prepared by evaporation from dichloromethane solution exhibit different proportions of monomer and excimer bands. In this study, an analogue of **PtL^{3}Cl** with a NCS co-ligand was also considered: this change did not lead to significant effects, because the co-ligand does not give, in this specific case, a relevant contribution to the HOMO and the LUMO of this class of complexes.

More recently, Pt(dpyb)Cl complexes with alkenyl and alkynyl ligands were synthesised and studied by our group:[51] the presence of such large aromatic substituents, in contrast to the ones reported until here, is expected to extend the π-conjugation of the molecules and to shift the emission to the red. The absorption spectra recall those of the previously studied Pt(dpyb)Cl complexes, but the absorption coefficients' values are much higher. **PtL^{17}Cl** displays a structured emission band in dichloromethane

solution, assigned to emission from a ^{3}LC state, centred at 496 nm and a fairly high $\Phi_{lum} = 0.25$ and a lifetime in the order of microseconds (Figure 13a).
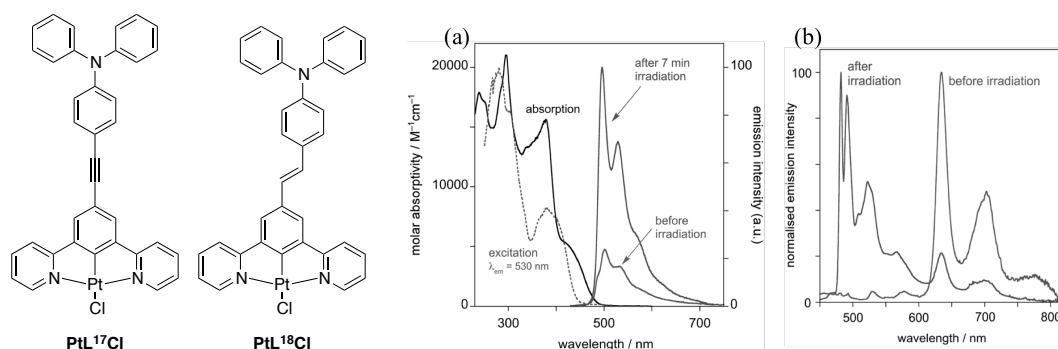
Figure 13. The alkynyl and alkenyl derivatives studied by our group, (a) the absorption and emission spectra of **PtL^{18}Cl** in CH$_2$Cl$_2$ at 298 K before and after irradiation with a UV lamp for 7 minutes and (b) emission spectra of **PtL^{18}Cl** in EPA (ether/isopentane/ethanol, 2:2:1) before and after UV irradiation.

An excimeric band, as for the other complexes of the same family, becomes progressively more intense at elevated concentrations. An analogue of **PtL^{17}Cl** with an NCS co-ligand was also prepared: its luminescent properties do not differ from those of the parent complex, apart that its excimeric emission is blue-shifted. **PtL^{18}Cl** behaves in a more complex way: it absorbs at lower energies than **PtL^{17}Cl**, confirming the better π-conjugating properties of the double bond respect to the triple bond, but the feature at longer wavelength disappears upon exposition to daylight or near-UV light, indicating isomerisation from the *trans* to the *cis* form: TD-DFT calculations predict that the *cis* form emission should be blue-shifted compared to the *trans*. The complex is emissive in the green only when irradiated at wavelength lower than 430 nm, *i.e.* not into the absorption tail, where the *cis* form does not absorb. The emission in the 480-600 nm region at room temperature thus is assigned to the *cis* form: isomerisation occurs as soon as the sample is exposed to the excitation source (which means that the *trans* isomer's emission is not detectable) and the intensity of the green emission band increases upon irradiation with a UV lamp, demonstrating the significant presence of the *cis* form. *Cis-trans* isomerisation is typical of styryl-substituted complexes,[52] and can account for the low emission quantum yield ($\Phi_{lum} = 0.003$). Emission from the *trans* isomer can be observed at 77 K as a set of bands between 600 and 800 nm (Figure 13b). The blue-shifted emission of the *cis* isomer is justified by the fact that the triplet excited state of this form is localised essentially on the Pt(dpyb)Cl moiety with a very small contribution from the pendant (this explains the similarity to the parent **PtL^{1}Cl**), while the triplet state of the *trans* form spans all over the pendent of the highly conjugated unit. Both complexes are good candidates for OLEDs applications but **PtL^{18}Cl** shows better quantum efficiencies (**PtL^{17}Cl** and **PtL^{17}NCS** probably degradate in solution). The emission can be tuned with the dopant concentration from the green to the NIR reaching a maximum emission wavelength of about 800 nm ($\varphi_{EL,max} = 1.2\%$ at a current density of 10 mA cm^{-2}), clearly red-shifted if compared to previously prepared Pt(dpyb)Cl-

based NIR-OLEDs. It is important to underline that the isomerisation process, observed in solution, does not occur under electrically driven conditions.

These complexes also show outstanding nonlinear optical properties, which will be discussed in the following chapter.

We have seen until now that Pt(dpyb)Cl complexes can emit as monomers or form excimers in solution. Nevertheless recently Shinozaki and co-workers demonstrated the possibility for Pt(dpyb)Cl complexes to aggregate forming trimers that allow white emission even in solution (Figure 14).[53] By substituting the pyridyl rings with methyl groups and the phenyl ring with a fluorine, a synergic effect to the blue-shift of the emission wavelength by increasing the energy of the LUMO and at the same time by stabilising the HOMO can be achieved.
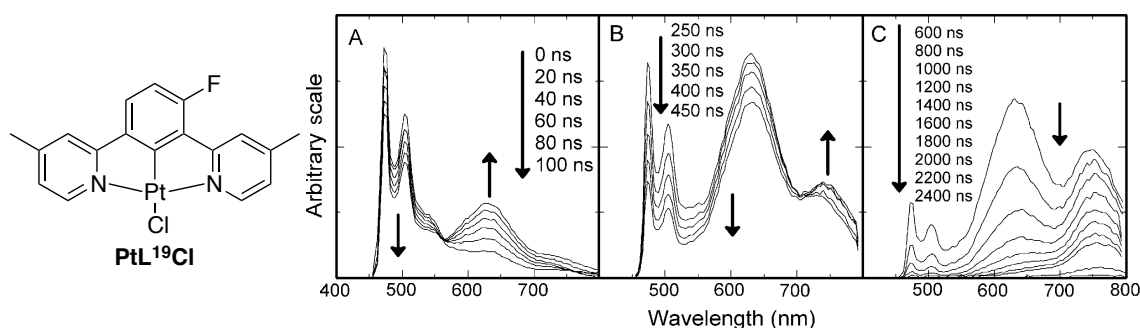
Figure 14. Left: The complex investigated by Shinozaki et al. together with the **PtL^{19}CN** analogue. Right: Time-resolved emission spectra of 1.06 x 10^{-3} M **PtL^{19}CN** in CHCl$_3$ from (A) the early to (B) the middle to (C) the last stage of spectral change.

An analogue of complex **PtL^{19}Cl** with a nitrile co-ligand instead of the chlorine was also synthesized and studied: the co-ligand substitution contributes to shifting the maximum emission energy to the blue, still maintaining a good emission quantum yield (in the order of 0.6-0.7). The emission wavelength is tuned from the blue to the orange by increasing the concentration: **PtL^{19}X** display exceptionally white emission in a 1.04x10^{-4} M CHCl$_3$ solution. At concentrations higher than 10^{-4} M, in addition to the typical excimeric band, a new band centred around 750 nm progressively appears. Time-resolved emission spectra allowed assignation of this new band to an excited trimer formed by reaction of a ground-state molecule with an excimer (Figure 14, right), never observed in parent Pt(dpyb)Cl complexes before and responsible for the emission in the orange.

Platinum dipyridylbenzene thus demonstrated to be an interesting class of complexes, with remarkable emission properties in solution. Their emission wavelength can be easily tuned by facile ligand substitution and emission from monomer, excimers and trimers can be observed. Pt(dbyp)Cl complexes can be tested in electroluminescent devices emitting from the blue to the near-infrared with very good performances.

2.2.2. A dinuclear Pt dipyridylbenzene complex

We have seen above that complexes able to emit in the red are of particular interest for their possible use in OLEDs. Furthermore, complexes that emit at such long wavelengths can be good phosphors for biosensing and bioimaging, since they can emit at wavelengths at which tissues are transparent (see section 2.2.3). Only one dinuclear Pt(dpyb)Cl complex is reported in the literature: Williams and co-workers synthesized a dinuclear Pt(dpyb)Cl complex in which the two units are brought in proximity in a face-to-face manner with a rigid 4,5-substituted xanthene bridge (Figure 15, left) in order to provide deep-red triplet emission in solution.[54]
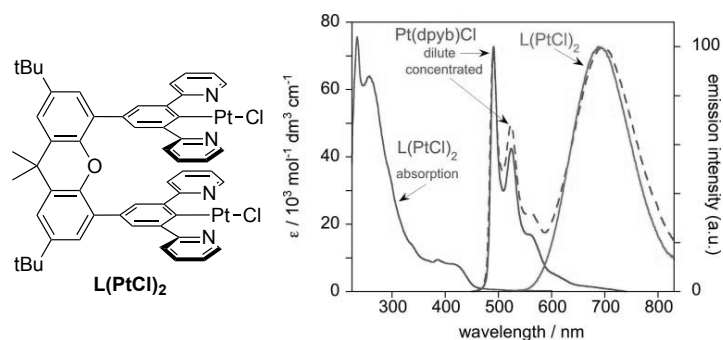
Figure 15. The dinuclear platinum complex (left) and its absorption and emission spectra compared with Pt(dpyb)Cl (*i.e.* PtL[1]Cl) (right).

While the absorption spectrum is typical of this class of complexes, upon excitation the complex emits with a broad unstructured band centred at 690 nm, with a remarkable quantum yield of 0.20, particularly high given the low emission energy.

The band profile is independent from concentration and no emission from the monomeric form can be observed (Figure 15, right). It can be noticed that the low-energy band is superimposed to the excimeric band displayed by the simple **PtL[1]Cl** at high concentrations. The emission spectrum of **L(PtCl)₂** can be thus explained with the extremely rapid formation of intramolecular excimers, at a rate that excludes emission from the monomeric excited state, since the two Pt(dpyb)Cl units lie in very close proximity. The fact that no low-energy band in the absorption or excitation spectra can be recorded and that at low temperature (77 K) only emission from the monomer can be observed, suggest that there are no ground-state interactions. In fact, ground-state aggregates are usually stabilised by lowering the temperature, with red shift in the absorption and emission bands: in the case of **L(PtCl)₂**, the formation of the excimer is a thermally activated process that requires some motion of the two Pt(dpyb) units relative one to another and for this reason it cannot clearly occur at 77 K. The interactions responsible for the stabilisation of the excited stated are probably π-π^* or d-π^* in nature. The distance between the two platinum centres is longer than 4.5 Å because of the conformation of the ligand and is sufficient to account for the stabilisation of the excimer. The complex is also emissive at the solid state, in the red,

although with some variation in the range 670-710 nm according to the different packing of the molecules depending on the solvent from which the sample is evaporated and the evaporation rate.

2.2.3. Pt dipyridylbenzene complexes for bioimaging

Pt(dpyb)Cl complexes also demonstrated good performances as luminescent labels for bioimaging: their emission wavelength can be tuned, as already stressed, by carefully choosing the ligands in order to enter the therapeutic window between 600 and 1300 nm,[55] they are stable to photo- and chemical degradation, they have long lifetimes that allow to distinguish their emission from the background fluorescence of the living substrate and large Stokes shifts.

The group of Williams studied the luminescent properties of complexes **PtL**[1-3,9]**Cl** (already presented in the previous sections) in different cell lines.[56] They observed that low concentrations of the order of 10 μM are needed in order not to cause significant reduction in cell viability even over a period of 24 hours. The complexes are good oxygen sensitizers but showed low cytotoxicity in cells, due to the fact that they are probably protected by oxygen quenching in cells media. They enter cells under diffusion control and are localised mainly in nuclei and nucleoli; confocal microscopy images confirm binding to DNA and, possibly, also to RNA. Time-resolved emission imaging microscopy (TREM) was used for mapping of live cells on a microsecond timescale: in order to use this technique, the probes should have luminescence lifetimes longer than 100 ns, which is the case for Pt(dpyb)Cl complexes. With time-resolved imaging, it was possible to visualise cells thanks to the long-lived emission of the platinum complexes without interferences from the autofluorescence on the background. Similar experiments were performed with a new complex, **PtL**[20]**Cl** (Figure 16), which was the first water-soluble biocompatible Pt(dpyb)Cl complex.[57]
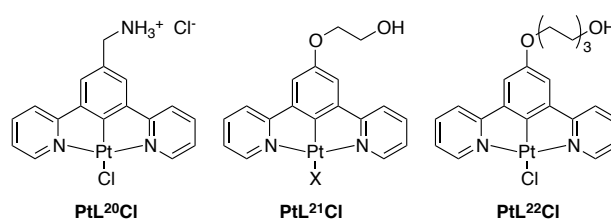
Figure 16. The Pt(dpyb)complexes for bioimaging.

By testing its luminescent properties in cells, it was demonstrated that the emission spectra under two-photon excitation are the same as those observed in solution under one- or two-photon excitation (reminiscent of those of the previously illustrated Pt(dpyb)Cl complexes). Lifetime increases as the complex deeply enters cells and varies depending on the location in the cell, because internal areas of the cells give higher protection by oxygen quenching. In the nucleus lifetimes reach 5.8 μs: this feature can be used to have information about the concentration of oxygen in a particular area of the living

media, opening new possibility for sensing applications. As for the complexes discussed above, two-photon time-resolved emission imaging microscopy was used to register high spatial resolution images free of background emission and allowed discrimination of undesired emission of other fluorophores present in the cells on the basis of lifetime.

Our group, in collaboration with De Cola and co-workers, reported other examples of partially aqueous soluble and biocompatible Pt(dpyb)Cl complexes for bioimaging with a hydrophobic platinum core and a hydrophilic ethylene or triethylenglycol chain as a substituent on the dipyridylbenzene ligand (**PtL**[21,22]**Cl** and the analogue **PtL**[21]**NCS**, Figure 16).[58] The absorption and emission spectra are typical of this class of complexes, with structured emission centred in the green-yellow region of the spectrum and good quantum yields up to 0.66. Interestingly, the emission spectrum of **PtL**[21]**NCS** at 77 K reveals the presence of a low-energy band centred at 625 nm suggesting strong ground-state interaction. The amphiphilic nature of the complexes, with a hydrophilic tail and a hydrophobic head, allows performing aggregation studies in air-equilibrated dioxane (a good solvent) - water (a non-solvent) mixture, from pure dioxane to dioxane-water 1:4. Upon addition of water, a blue shift and decreasing of the absorption band is remarked, but no supramolecular aggregation is detected. The complexes have been integrated in HeLa cells where they localised in cytoplasm and nuclei, and from which emission by confocal microscopy can be detected: the emission resembles to the one in solution and there are again no traces of aggregates. Cellular uptake is fast (within 10 minutes) even at low concentrations (5 µM) and probably occurs with a diffusion-controlled mechanism, even if an energy-driven mechanism cannot be excluded. Nevertheless, **PtL**[22]**Cl** enters cells more slowly due to the presence of the bulkier triethylenglycol chain, even though the slowest cellular uptake rate is that of **PtL**[21]**NCS**, probably because of the different co-ligand.

2.2.4. Emissive Pt(dpyb)Cl complexes in mesophases and in the solid state

After having taken a look to the emission properties of Pt(dpyb)Cl complexes in solution, it is worth to take into account their behaviour as liquid crystals and as aggregates in the solid state (as crystals or powders).
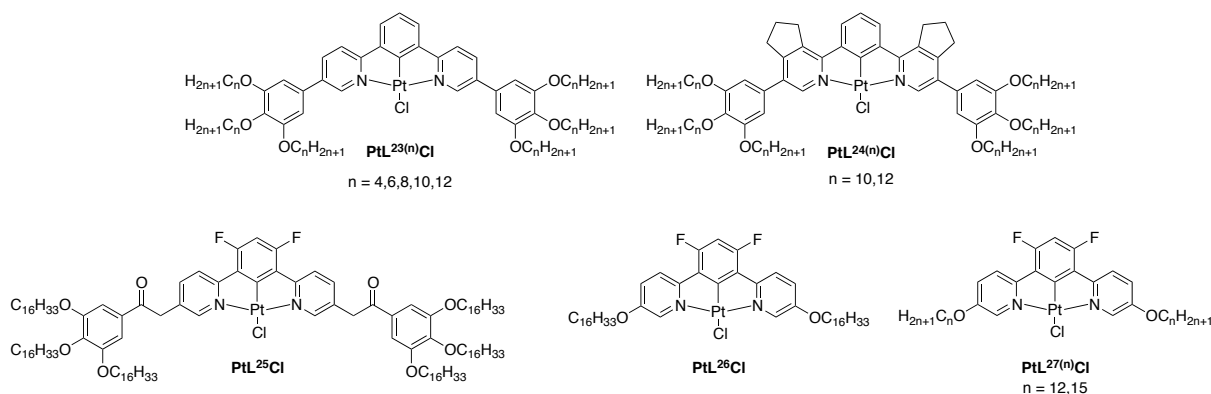
Figure 17. The Pt(dpyb)Cl complexes showing mesophase organisation.

The group of Bruce studied the properties of organisation in mesophases (intermediate state of matter between isotropic liquid and crystalline solid) of several Pt(dpyb)Cl complexes. Generally speaking, when an isotropic melt composed by an opportunely substituted Pt(dpyb)Cl complexes is cooled, depending on the temperature and the cooling rate, differently organised phases can be obtained: these can include, for example, mesophases (liquid crystals), glasses or crystalline phases. According to the organisation, the emission properties of these phases differ one from the other and, in the specific case, emission from the Pt(dpyb)Cl monomeric form or aggregates can be observed. The very first Pt(dpyb)Cl complexes showing mesophase organisation were **PtL[23,24]Cl** (Figure 17): both their emission spectra in solution show typical features with correct quantum yields (Φ_{lum} = 0.07 for **PtL[23]Cl** and 0.12 for **PL[24]Cl**).[59] The blue shifted emission of the cyclopentene-substitued complex as well as its higher quantum yield can be ascribed to a better rigidification of the molecule. If the isotropic melt of **PtL[23,24]Cl** is cooled slowly to 170°C and then fast to room temperature, a columnar mesophase, in which the complexes are organised in an antiparallel manner emitting in the yellow region of the spectrum can be obtained. Otherwise, if the complex is cooled rapidly to room temperature from the isotropic melt, small domains composed by isotropic grain boundaries are obtained: here, the complexes are likely to be organised in excimer-like structures that emit in the red. At last, it is possible to observe excimer emission from thin films obtained by spin coating. With a process of heating and cooling even the emission of the film can be turned to yellow, even though red emission can be re-established by mechanically disturbing the film.

The same group published some years later other Pt(dpyb)Cl complexes showing similar behaviour.[60] Complexes **PtL[25,26]Cl** are luminescent in solution as well as in solid state films: the emission in solution is centred in the blue-green region of the spectrum and at higher concentration, as expected, an excimeric band appears centred at 680 nm. Both complexes exhibit orange luminescence in neat films and from the mesophase, probably due to ground-state aggregates rather than excimers (X-ray diffraction indicates Pt–Pt distances < 3.5 Å). Mesophase organisation can also be observed: complexes **PtL[25-27]Cl** aggregate in different forms according to the temperature and the cooling or heating speed. Some phases can also be emissive.

Some Pt(dpyb) complexes emissive at the solid state were reported by Yang e al. and are showed in Figure 18.[61]
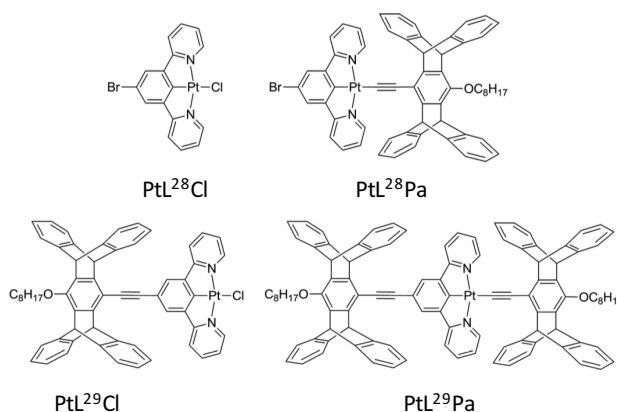
Figure 18. The pentypticene-substituted platinum dipyridylbenzene complexes.

They emit in tetrahydrofuran solution in the green region of the spectrum and they form aggregates by water addition in open atmosphere: aggregation causes an increase in the luminescence quantum yield for **PtL^{28}Pa** and, more incisively, of **PtL^{29}Pa** (oxygen shielding effect), while the emission of **PtL^{28}Cl** is quenched (aggregation-caused quenching) and **PtL^{29}Cl** undergoes a shift in the emission wavelength to the red with the growing of a new band, ascribed to excimer emission, with an enhancement of the emission quantum yield. These phenomena depend essentially on the size of the aggregates, *i.e.* on the size of the substituents (the ideal size of the aggregate to have oxygen shielding effect is 500-1000 nm). The samples for solid-state luminescence were prepared either from a powder from which a film was made (unground sample) or from crystalline powders (crystalline sample): the emission arises primarily from the excimer for the complexes with the less bulky substituents. Nevertheless, by grinding the unground samples the emission changes again in a different way for every complex, showing that the great variety of interactions taking place in the molecules' packing in the solid state importantly influences the emission wavelength. In addition to mechanochromic behaviour, the samples are vapochromic: exposition to dichloromethane vapour restores the initial spectra of the unground samples and exposition of **PtL^{29}Cl** to benzene has the effect of enhancing the monomer emission (also, benzene enlarges the interplanar distance between molecules by intercalation).

The group of Kanbara also prepared some complexes with mechanochromic and vapochromic properties, the best performing of which is showed in Figure 19.[62] This complex is luminescent in solution with a maximum at 480 nm (Φ_{lum} = 0.40) and is interestingly strongly luminescent also at the solid state: the crystals obtained by recrystalisation in dimethylformamide exhibit green luminescence, the luminescence changes to the orange when the crystals are ground and the exposure of the grounded powder to methanol gives yellow luminescence. The orange luminescence can be recovered by grinding or heating at 200°C. This behaviour can be explained with the influence of the solvent in the complex packing. Dimethylformamide and methanol form hydrogen bonds with the platinum molecules even though networks are different: with methanol, the Pt−Pt distances are shorter and the emission is more

likely to arise from the excimer, which explains the red-shifted emission, while when the crystals are ground metal-metal interactions become more important.
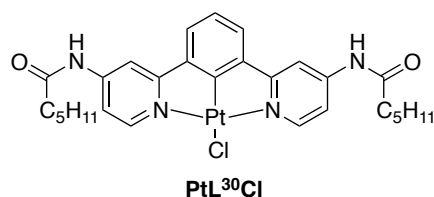
Figure 19. The Pt(dpyb)Cl complex prepared by Kanbara et al.

These results demonstrated that platinum dipyridylbenzene complexes posses interesting luminescent properties not only in solution, but also at the solid state and in organised mesophases, with possible applications in liquid crystals or solid-state emitters. They are able to organise after exposure to solvents, grinding and can aggregate in polar solvents. A very important role is played by the substituent on the dipyridylbenzene ligand and, sometimes, by the co-ligand.

2.2.5. Pt dipyridylbenzene complexes with co-ligands other than chlorine

As already stated in the previous sections, chlorine is not the only co-ligand that can participate to the coordination sphere of Pt(dpyb) complexes: examples of Pt(dpyb)NCS complexes found applications in OLEDs and bioimaging. The absence of the halide is particularly important to improve the operational stability of complexes integrated in OLEDs.

The ligand substitution reaction is quite straightforward: it is sufficient to suspend the Pt(dpyb)Cl complexes and the new ligands in methanol, acetone or a mixture of the two solvents, eventually add a base, and the desired Pt(dpyb)X complex will be obtained in good yields.[63]
The group of Li synthesized a series of Pt(dpyb)Cl complexes and their phenoxide Pt(dpyb)OPh analogues:[64] the emission spectra of the phenoxy-substituted complexes are similar to those of the chlorine-substituted complexes, but the emission quantum yields are the half. This demonstrates that the co-ligand has an influence on the properties of the platinum complex, although not always remarkable in the emission spectral shape and wavelength.

The group of Williams, instead, reported some platinum complexes with a thiolate co-ligand (Figure 20, left).[65] The absorption spectra of the two set of complexes present similar bands to the related parent Pt(dpyb)Cl complexes under 375 nm, but they also feature a new broad band centred at 465 nm, slightly blue shifted for **PtL^{1}SR** and in the meantime red-shifted in the order SPh < STol > SAni. The band is particularly intense in **Pt(dpyb)SNit** complexes.
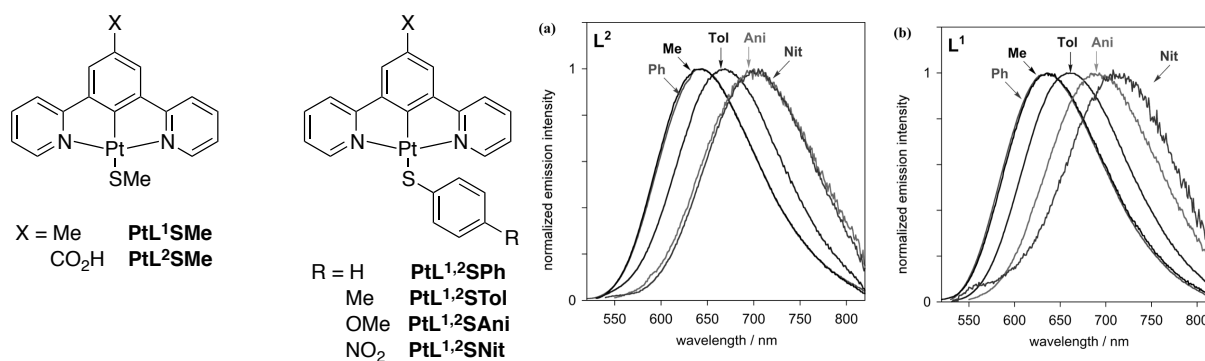
Figure 20. The Pt(dpyb)SR complexes and the emission spectra in degassed CH_2Cl_2 at 298 K of (a) PtL^2SR and (b) PtL^1SR.

The addition of the thiolate co-ligand changes the electronic density distribution in the molecules: the HOMO is now centred on the thiolate and the metal atom, while the LUMO is localised on the pyridyl rings of the N^C^N ligand. The observed band in the red can be attributed to $d_{Pt}/\pi_{RS} \rightarrow \pi^*_{NCN}$ transitions, the red shift of the absorption bands is due to the increasing of the electron-donating ability of the thiolate substituent that destabilises the HOMO, while the blue shift can be explained by the electron-withdrawing ester group stabilising the LUMO. The nitro-thiolate substituted complex behaves differently: the HOMO is localised on the thiolate co-ligand, as for the other complexes, but the LUMO is localised primarily on the NO_2 substituent, giving rise to ILCT $\pi(S\text{-}C_6H_4) \rightarrow \pi^*(NO_2)$ transitions. The emission is centred in the red, and lifetimes and quantum yields are lower than for the Cl-substituted parent complexes. The emission maxima follow the same trends as in the absorption spectra and are all blue-shifted at 77 K, consistently with a charge-transfer excited state. The emission is thus assigned to LLCT (more important as the thiolate ligand becomes more electron-donating, at the expenses of MLCT character) for **PtLSPh**, **PtLSTol**, **PtLSAni** and to ILCT for **PtLSNit**: the assignments are supported by TD-DFT calculations. For this class of complexes there is no evident self-quenching followed by excimer formation, probably due to the bulky thiolate substituent. Anyway, they provide a good example of Pt(dpyb) complexes emitting in the red with good quantum yields considering their long-wavelength emission ($\Phi_{lum, max} = 0.17$).

A very promising class or co-ligands includes acetylides: they are strong-field ligands known to promote luminescence by further raising the energy of d-d states if used instead of the weak-filed halides. In 2009, Che et al. synthesized and studied the solid-state emission properties of a series of Pt(dpyb) acetylide complexes (Figure 21).[66] Curiously, when R^1 is $-CF_3$, the colour of the complex at the solid-state can be easily tuned according to the different substituents on the acetylide co-ligands, while this is not observed if R^1 is -H or $-CH_3$. Different complexes crystallize with different geometries: the strength of Pt−Pt and C-H−π(C≡C) interactions may vary and thus the different colour and emission wavelengths of the complexes can be tuned. The complexes emit intensely in the green (Φ_{lum} up to 52%) in dilute CH_2Cl_2 solution showing a classical structured band; the emission is assigned to a ^{3}LC state.

However, as powders, they show structureless red shifted emission (up to 819 nm), assigned to a ^{3}MMLCT state.
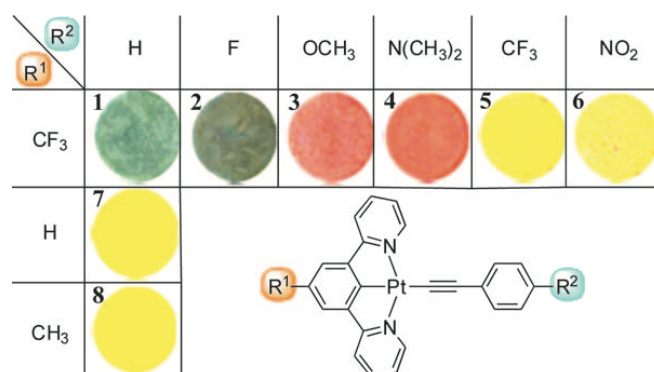
Figure 21. The structure of the complexes studied by Che et al. and their solid-state colours.

Two complexes of the same family were tested by our group in OLEDs (Figure 22).[67] Complex **PtL^3(C≡C)** has a remarkable Φ_{lum} of 0.77 in solution, and at high concentration in both complexes can form excimers that emit around 700 nm. OLEDs were fabricated both using the complex as a dopant and as pure film in order to tune the colour of the device. Interestingly, the OLED with 5% **PtL^6(C≡C)** has a maximum φ_{EL} = 12%, about three times higher than that of the parent chloride complex: this can be attributed to the inhibition of "aggregate-induced quenching" due to the presence of the mesityl substituent.
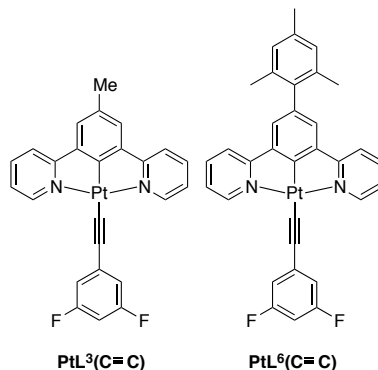
Figure 22. The Pt(dpyb) acetylide complexes tested in OLEDs.

The neutral dipyridylbenzene platinum complexes can be easily converted into cationic complexes by substitution of the chloride with an isocyanide ligand. The groups of Che[68] and Koshevoy[69] studied the properties of Pt(dpyb) complexes carrying a 2,6-dimethylphenyl isocyanide or acetonitrile ligand. They discovered that those cationic complexes easily undergo aggregation at the ground state through π−π stacking or metallophilic interactions. The aggregate properties, as well as the emission wavelength in solution and in the solid state can be easily tuned according to the counterion, the temperature and, in solution, the concentration.

3. Platinum complexes showing changes in luminescence as a response to external stimuli

3.1. State of the art

Platinum complexes, as seen in section 2.2.4, can aggregate at the solid state or in solution thanks to Pt–Pt, π–π and other non-covalent interactions.[70] Most interestingly, orbital overlapping due to aggregation often induces a red-shift of the emission and absorption bands. In addition, the packing of the monomers in the fixed assemblies can lead to the decrease of non-radiative processes.[71]

In this section we will discuss the importance of stimuli-responsiveness imparted to platinum mono- and multinuclear complexes and the resulting switching of their emission properties.

3.1.1. Platinum terpyridine complexes: a significant case study

Differently from the bright luminescent Pt(dpyb)Cl complexes, $[Pt(trpy)Cl]^+$ complexes are not naturally emissive in solution at room temperature: there are no cyclometalating ligands in such complexes and deactivating d-d states are easily accessible.[72] They emit in solution at low temperature and strongly at the solid state: the emission wavelength is determined by the counterion (PF_6, CF_3SO_3..) and by the co-ligand that can be used instead of chlorine (Br, NH_3, SCN...).[16] This led chemists to look for a way to "turn on" the emission of these complexes at room temperature, typically by using strong-field ligands as acetylide[73] or accurately substituting the terpyridyl ligand, as stated in section 2.1.[16] $[Pt(trpy)X]^+$ complexes are known to easily aggregate at high concentrations in solution at the ground state.[74] They reveal once more their different properties respect to Pt(dpyb)X complexes that form aggregate mostly at the solid state, while in solution they usually form excimers. They can also be used as sensors for solvent vapours,[75] cations or small molecules.[76]

In the following sections, we will mostly refer to $[Pt(trpy)X]^+$ complexes, which are among the most widely studied classes of platinum complexes with a terdentate ligand, owing to their interesting spectroscopic behaviour that inspired our work. Platinum complexes with different ligands will be considered when they will provide significant examples.

3.1.2. Mononuclear platinum complexes aggregating in solution

In 1999, the group of Che studied the photophysical properties in solution and in the solid state of some platinum complexes with of 6-phenyl-2,2'-bipyridyl ligands. This class of complexes undergoes d^8–d^8 and ligand–ligand interactions in specific conditions, shifting the absorption and emission wavelength to the red or the NIR (Figure 23).[23,77]
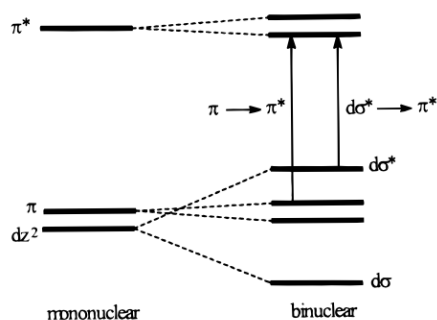
Figure 23. Schematic molecular orbital illustrating d^8–d^8 and π–π interactions in dinuclear platinum polipyridine complexes.

The group of Yam was the first one to study the solvent-induced aggregation properties of platinum terpyridyl complexes.[78] [Pt(trpy)(alkynyl)]$^+$ complexes are emissive in solution (differently from [Pt(trpy)Cl]$^+$ complexes), because alkynyl ligands are strong σ-donors, destabilise the HOMO of metal ions and consequently suppress the non-radiative d-d state deactivation, resulting in long lifetimes and high emission quantum yields. They found that, by increasing the concentration of the [Pt(trpy)(alkynyl)]$^+$ complexes in acetonitrile solution, the growth of an absorption tail at wavelength beyond 550 nm was observed. This indicates the formation of aggregates at concentration higher than 10^{-3} M. The same behaviour was observed in emission at 298 K where, by increasing the concentration, a new band centred between 700 nm and 800 nm grew. The yellow solutions in acetonitrile became blue upon addition of diethyl ether (a non-solvent) to the solution: new absorption and emission bands at longer wavelengths appeared showing the formation of aggregates. The fine behaviour in solution depends strongly on the degree of electron-richness of the substituent on the alynyl ligands and more strongly on the counterions, *i.e.* on the different degree of interaction through Pt–Pt and π–π interactions. For example, with the bulky BPh$_4^-$ counterion aggregation is not observed.

Similarly, some amphiphilic 2,6-bis(benzimidazol-20-yl)pyridine platinum complexes showed aggregation in water/acetone mixture, characterized by the presence of MMLCT absorption and emission bands.[79] The structures of the aggregates can be observed with TEM and SEM techniques: vescicles were found in water and nanofibers in acetone. More recently, amphiphilic [Pt(trpy)(C≡C)]$^+$ complexes with triethylene glycol substituents on the alcetylide ligand and alkyl chains of different lengths on the terpyridine ligand were reported.[80] The nature of the aggregates in solution, and thus the ^{3}MMLCT emission, is controlled by both the alkoxy hydrophilic chains and the hydrophobic alkyl chains, allowing the formation of twisted fibres in water or in a water/DMSO mixture according to the complex.

Aggregation can also be controlled by external factor such as pH, temperature, presence of polyelectrolytes or polymers.

3.1.2.1.   pH induced aggregation

The presence of substituents that can be protonated or deprotonated can allow to observe the effect of the pH on aggregation. Yam and co-workers observed that according to the substituents on the terpyridine ligand or on the acetylide co-ligand of a series of differently substituted $[Pt(trpy)(C≡C)]^+$ complexes, aggregation and deaggregation could be finely tuned at different pH.[81] In fact, by playing with the electrostatic charges on the molecule it is possible to increase the hydrophobicity or hydrophilicity of a specie. As a consequence, according to the polarity of the solvent, aggregates will be more or less stable and emission can be switched from MLCT\LLCT to MMLCT states.

Another way to tune the emission with pH uses the same principle of the work of Williams with complex **PtL⁹Cl** in section 2.2.1.[32] Yam et al. considered a series of $[Pt(trpy)(C≡C)]^+$ complexes with amino substituents on the alkynyl ligand. These complexes are not emissive in solution at room temperature or in the solid state.[82] Upon addition of *p*-toluensulphonic acid to an acetonitrile solution of the complexes and protonation of the amino group, the ^{3}LLCT state is shifted to higher energies, the reductive electron-transfer quenching pathway is supressed, and emission from ^{3}MLCT $[d\pi(Pt)\rightarrow\pi^*(trpy)]$ is allowed.

Such complexes are important because their response to pH can be triggered also in cells, allowing imaging and their use as anticancer agents. In particular, lysosomes of cancer cell have an acidic pH. The group of Che demonstrated that some $[Pt(phbpy)(C≡C)]^+$ complexes can enter cells, aggregate in the acid lysosomes and display anticancer activity.[83]

3.1.2.2.   Polyelectrolite-induced aggregation

Since $[Pt(trpy)X]^+$ complexes carry a positive charge, a counterion is needed for charge balance. If these counterions are assembled in an ordered manner, the organisation of the platinum centres by an aggregation process could be induced. An example of ordered counterions are polyelectrolites, in which negatively charged functional groups are connected to a polymer chain, as presented in Figure 24.

Yam et al. reported a series of $[Pt(trpy)(C≡C)]^+$ whose self-assembly can be induced by a deprotonated polycarboxilate giving UV-Vis and luminescence changes.[84] By adding the complexes to a solution of poly(acrylic acid) and tetrabutylammonium hydroxide as a base, the growing of MMLCT absorption and emission bands is observed. This is due to the electrostatic binding of the platinum complexes to the polyelectrolyte (Figure 24) forming self-assembled structures.
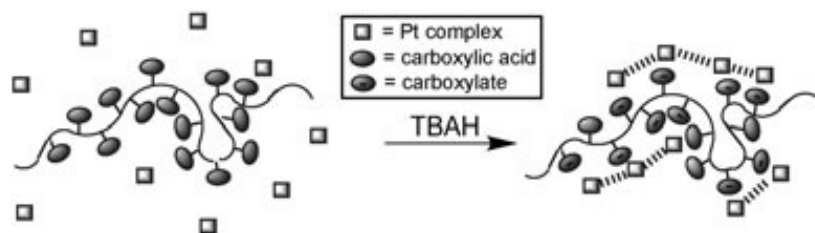
Figure 24. Schematic representation of the aggregation of the platinum complex ions in the presence of a polycarboxylate.

The aggregation process is fully reversible by addition of HCl. As the concentration of the polyelectrolyte is diminished (*i.e.* more sites are deprotonated by a base, whose concentration is constant), or the concentration of the platinum complex is increased (*i e.* more complexes are available to bind the negatively charged sites), the MMLCT bands become more intense reaching a maximum plateau. The same process can be observed in water medium, by opportunely substituting the $[Pt(trpy)(C \equiv C)]^+$ complexes in order to make them hydrophilic and by choosing water-soluble electrolytes.[85]

DNA can be also considered as a polyelectrolyte: at neutral pH nucleic acids carry multiple negative charges. $[Pt(trpy)(C \equiv C)]^+$ can intercalate in the nucleic acid structure and give rise to self-assembled chiral helical aggregates.[86] These aggregates show absorption and emission from MMLCT states. Obviously, the substituents on the pyridyl ligand must be accurately chosen, because the ability to self-assembly depends also on the size of the complex. With bulky *tert*-butyl group on the pyridines, aggregation with nucleic acids does not occur.[87]

3.1.4. Multinuclear platinum complexes aggregating in solution

Multinuclear platinum complexes, of which dinuclear are the most studied, have the possibility of undergoing both inter- and intramolecular interactions. The distances between the different units can be adjusted by the bridging ligand, that can be rigid (as for the xanthene linker discussed in section 2.2.2 and as reported by Yam[88] and Che[89]), semi-rigid or flexible.

3.1.3.1. Complexes bearing a semi-rigid linker

Platinum-platinum interactions can assist the formation of chiral supramolecular aggregates, mimicking the folding of proteins and DNA.

Yam et al. reported examples where two platinum terpyridine complex units are incorporated into the single-turn backbone of a binaphthol derivative (Figure 25).[90] According to the length of the tether, different behaviours can be observed. If n = 1 (Figure 25) the linker is not long enough to allow a folding. If n = 2 the two platinum centres can stack to form a chiral P-helix that cannot be observed in the organic counterpart.[91] The presence of metal-metal interactions is confirmed by the growth of a band in the red

in the absorption spectrum, assigned to MMLCT transitions. If n = 3, the stacking effect is less pronounced probably due to a misalignment of the two platinum terpyridyl units.
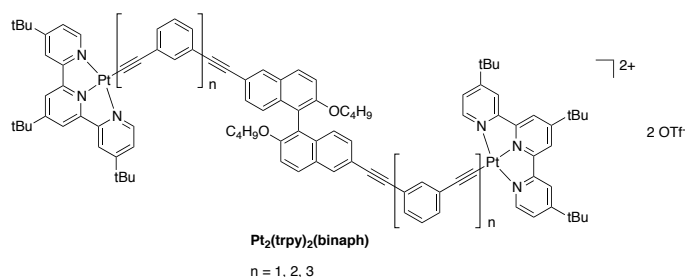
Figure 25. Structure of the complex with a binaphthol derivative tether studied by Yam et al.

It is important to mention that not only the presence of the linker is important for the aggregation, but also that it has to be of the right size and length in order to allow correct interactions between the metal centres upon folding. If the tether is too long or too short, stacking will not occur, or occur in a not efficient way.

The group of Patrick reported a dinuclear platinum terpyridine complex in which the two units are linked by a terthiophene backbone (Figure 26).[92]
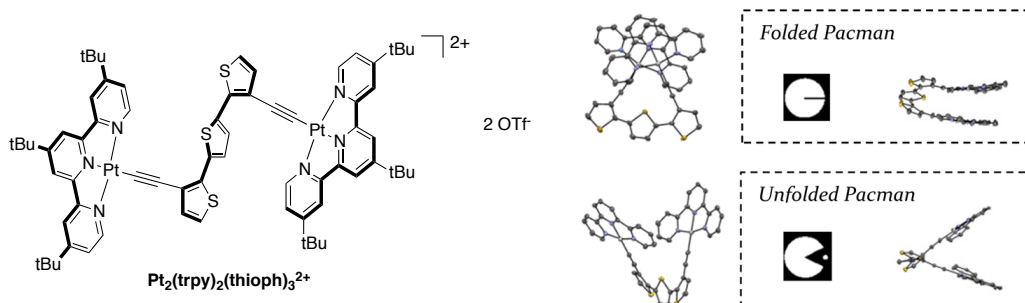
Figure 26. Structure of the dinuclear **[Pt$_2$(trpy)$_2$(thioph)$_3$]$^{2+}$** complex (left) and "folded" and "unfolded" Pacman-like structures (right).

This molecule has a "Pacman-like" behaviour: it can fold and unfold in relation to the polarity of the solvent. In the more polar acetonitrile it forms chiral helical columns, while it is present as a racemic mixture in dichloromethane. Crystals of the two forms can be isolated. The presence of the aggregates can be confirmed by UV-Vis absorption (presence of the MMLCT band) and by NOESY ^{1}H-NMR. Aggregation can also be triggered by lowering the temperature, as reported by the group of Kato for a [Pt(trpy)]$^+$ trimer with (2-mercapto-5-methyl-1,3,4-thiadiazole) linkers.[93] At low temperature, typical sharp signals are observed in the ^{1}H-NMR and a MMLCT band grows in the absorption spectrum.

An interesting family of ligands is the one of poly(phenyleneethynylene)s (PEs): a carbon-rich

material with extended π conjugation. *Meta-* and *orto-*PEs can undergo folding, affected by solvent, temperature and hydrogen-bonding.[94] Also, Pt–Pt interactions, π-stacking and solvophobic interactions can stabilise the foldamers (see below). The group of Che studied some dinuclear Pt(trpy) complexes in which the two platinum units are bound by *orto-*PEs.[95] They found that by increasing the content of water in an acetonitrile solution of complexes with appropriate length of the linker (from 3 to 8 units, Figure 27) the emission wavelength is red-shifted, and the emission lifetime and quantum yields increased. This behaviour can be ascribed to Pt–Pt and π–π interactions that favour the formation of aggregates, whose presence can be observed by TEM microscopy. Aggregates formation is favoured also in pure acetonitrile by lowering the temperature: ^{1}H-NMR at 213 K shows broad upfield-shifted signals typical of aggregates. On the other hand, Yam et al. studied the properties of dinuclear [Pt(trpy)(C≡C)]${}_2^{2+}$ with *meta-*[96] and *para-*PEs linkers[97] (Figure 27). In the first case, they found that by increasing the amount of acetonitrile in a dichloromethane solution or by lowering the temperature, ^{1}H-NMR signals become broad and upfield-shifted. In the same conditions, a new band that can be assigned to MMLCT transitions can be observed in the absorption and emission spectra of complexes with an appropriate linker length (n = 5, 6). Dinuclear platinum complexes with *para-*PEs linkers behave in a different way: the folding of the chain is not possible, but the linear complexes manage to self-assembly in an intermolecular fashion by forming lamellar packing in DMSO.
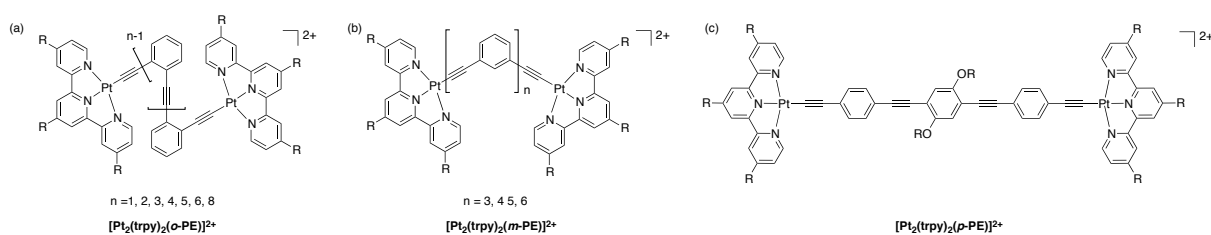
Figure 27. Schematic representation of the complexes studied by (a) Che et al. and (b), (c) by Yam et al.

3.1.3.2.   *Complexes bearing a flexible linker*

A frequently chosen group of flexible linkers is oligo(oxyethylene). As for the semi-rigid linkers, they can be of different lengths and thus influence the aggregation properties of the considered complexes. Yam et al. studied the behaviour in solution of some dinuclear [Pt(trpy)(C≡C)]${}^+$ complexes bearing the flexible oligo(oxyethylene) chain on the terpyridyl ligand or on the acetylide co-ligand (Figure 28).[98]
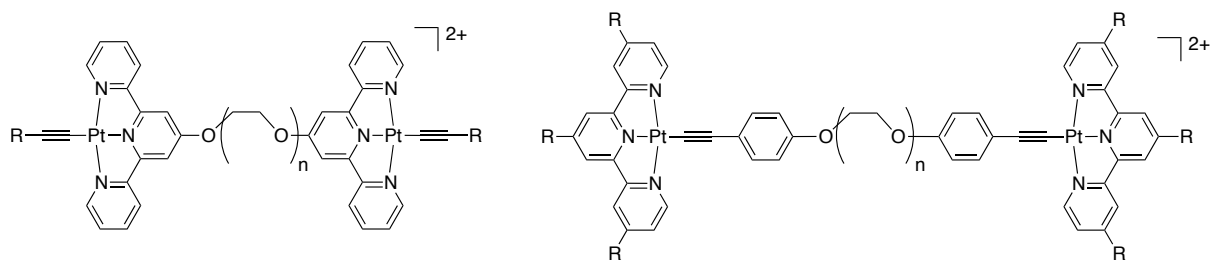
Figure 28. Schematic representation of the [Pt(trpy)(C≡C)]$_2^{2+}$ complexes bearing an oligo(oxiethylene) chain studied by Yam et al.

First of all, they studied the effect of the length of the oligo(oxyethylene) bridge. If it is too short (*i.e.* less than three units) self-association at room temperature at the ground state does not occur: the length of the bridge is shown to play once more an essential role in governing the occurrence and extent of the intramolecular aggregation (Figure 29, left). Complexes bearing from three to ten −O−CH$_2$−O− units undergo intramolecular aggregation at low and room temperature, while de-association occurs at higher temperature (complete de-association at T > 333 K). The aggregation can be followed by ^{1}H-NMR and by UV-vis absorption and emission spectroscopies. At low temperature ^{1}H-NMR signals are broad and poorly resolved, while they become well defined at higher temperature, revealing the occurrence of de-aggregation. Bands ascribed to MMLCT transitions can be observed both in absorption and emission at low and at room temperature, while they disappear by heating the sample. In some cases, interestingly, if the concentration of the sample is increased (10^{-3} M) both the MMLCT bands assigned to the inter- and intramolecular assemblies can be distinguished in the UV-Vis absorption spectrum. It should be pointed out that the intermolecular aggregate disassembles more rapidly by increasing the temperature. Mononuclear analogues of these complexes can also aggregate but they do it at much lower temperatures (T > 223 K).

If the oligo(oxyethylene) chains are substituted by polymer co-blocks, the dinuclear complexes can form micelles in solution. Yam and co-workers used a poly(ethyleneoxide)-*block*-poly(propyleneoxide)-*block*-poly(ethyleneoxide) triblock copolymer (PEO-PPO-PEO), consisting of hydrophilic PEO segments and hydrophobic PPO segments.[99] In water, when the critical micelle temperature is reached, polymeric micelles form and platinum terpyridyl moieties aggregate, giving rise to MMLCT bands in absorption and emission (Figure 29, right). If the complexes are substituted with charged group, a pH aggregation response can be observed.
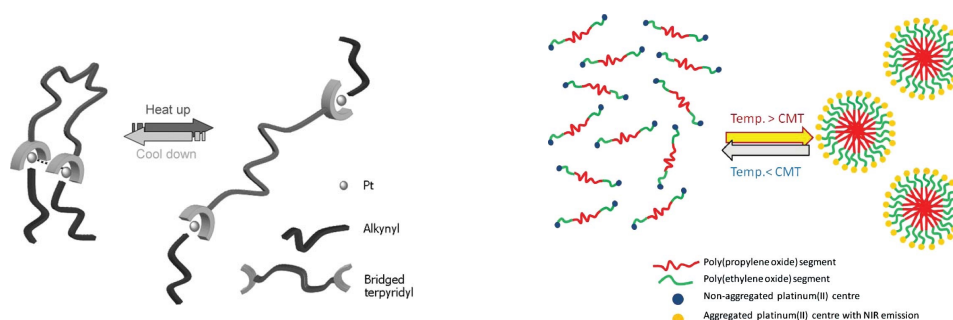
Figure 29. Schematic representation of aggregation and deaggregation by temperature modulation of (left) the [Pt(trpy)(C≡C)]$_2^{2+}$ complexes and (right) the [Pt(trpy)(C≡C)]$_2^{2+}$ complexes bearing a PEO-PPO-PEO linker.

Temperature-depending aggregation can also be observed in a series of dinuclear [Pt(phbpy)(CNR)]$^+$ complexes with a oligo(oxyethylene) linker studied by Che and co-workers: they were found to form aggregates at room temperature and could also be used to obtain nematic hydrogels.[100] Bäuerle et al studied the behaviour of some dinuclear platinum bipyridyl complexes in which the two units are linked by a small alkyl chain or by an oligo(oxyethylene) chain.[101] The formation of aggregates was not evident from spectroscopic studies, but was confirmed by electrochemistry.

3.1.4. Platinum complexes with cation sensory functions

Transition metal based luminescent systems capable of detection of environmental changes have grabbed the attention of chemists because of their rich photophysical properties.[102] Platinum based sensors can be obtained by modification of the ligands with suitable substituents[103] and the signal response of those luminophores can be governed by different mechanisms:[102d,103]

(I) *Blocking of the photoinduced electron transfer (PET).*

The excited state of a molecule can be deactivated by transfer of an electron from a donor, whose orbitals are located at an intermediate energy between the HOMO and the LUMO, to the HOMO when a hole is generated upon excitation. This process is followed by back electron transfer from the LUMO to the singly occupied molecular orbital of the donor, resulting in non-radiative deactivation of the excited state. Upon cation binding to the donor, the energy of its molecular orbitals can be decreased, resulting in the blocking of the PET and consequent switching on of the radiative emission (Figure 30).

(II) *Photoinduced charge transfer (PCT).*

Molecules containing a luminophore conjugated with donors and acceptors are subject to PCT upon excitation, but complexation with the cation can alter the energy of the excited state. Cation binding to the donor moiety of the molecule would reduce its electron-donating ability, stabilising the HOMO and leading to a blue-shift of the emission. On the other hand, cation binding to the acceptor would enhance its electron-withdrawing ability, destabilising the LUMO and leading to a red-shift.

MLCT transitions in particular are susceptible to stabilisation or destabilisation through interactions

with cations that perturb the energetics of either the metal-based or ligand-based orbitals.

(III) *Förster resonance energy transfer (FRET)*.

FRET occurs upon dipole interactions between the donor and the acceptor. If the distance and orientation of the energy donor and acceptor after cation binding are altered, the FRET efficiency can be modulated and signal the binding of the cation.[104]
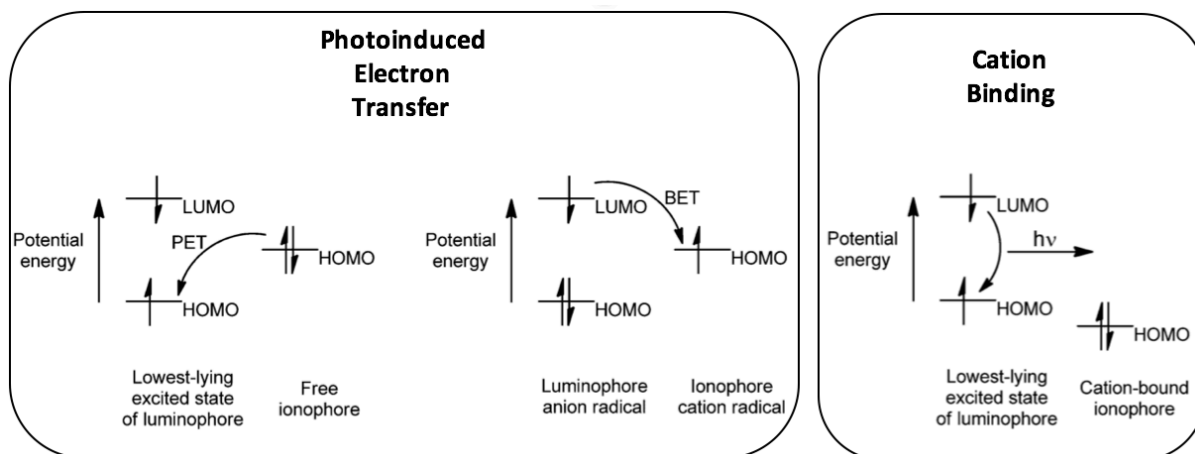
Figure 30. Mechanism of PET-based cation sensors.

Among the many possible host receptor units, crown and azacrown ethers are the most exploited because they can form relatively stable complexes with metal cations.[105] Nakahara et al. reported fluorophores based on the presence of two pyrenes linked by a crown ether whose excimer emission is modulated by the presence of metal cations in solution.[106] Some platinum (II) complexes with crown ether substituent on the terdentate ligand or on the alkynyl co-ligand have been reported.

Yam. et al found that in [Pt(trpy)(S-benzo-15-crown-5)]PF$_6$[107] and [Pt(trpy)(C≡C-benzo-15-crown-5)]PF$_6$[108] the LLCT and MLCT absorption band, respectively, are blue shifted upon cation binding of the crown ether substituents (Figure 31). In particular, a 1:1 binding stoichiometry was found for Na$^+$, 1:1 and 2:1 for K$^+$, and 1:1 for Ba^{2+}. Interestingly, the binding constant is bigger in CH$_3$CN than in DMSO because the more polar solvent solvates better the metal cations in solution so that their binding in the cavity is less favoured. They also found that the emission of [Pt(trpy)(C≡C)]$^+$ complexes can be switched on upon cation binding.[109]
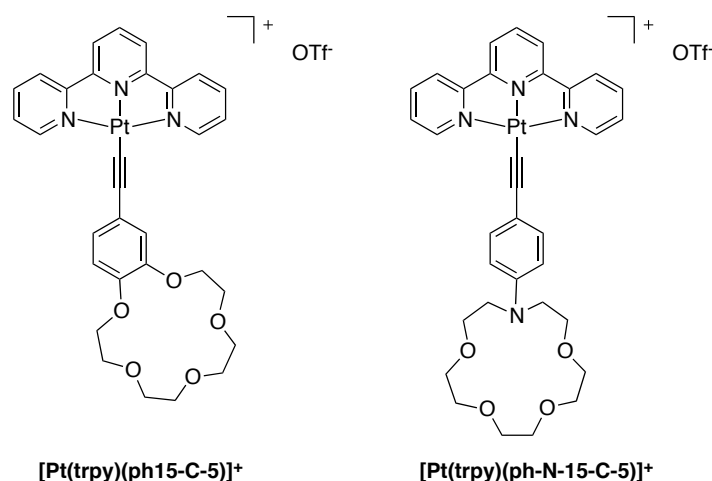
Figure 31. Two platinum terpyridine complexes with a crown or an azacrown moiety studied by Yam et al.

Changes in the UV-Vis absorption bands of both **[Pt(trpy)(ph15-C-5)]**[+] and **[Pt(trpy)(ph-N-15-C-5)]**[+] are remarkable upon cation addition (Li^+, Na^+, Mg^{2+}, Ca^{2+}, Cd^{2+}, Zn^{2+}). The spectral changes are ascribed to the decrease in the electron-donating ability of the alkynyl ligand upon metal ion complexation. Complex **[Pt(trpy)(ph-N-15-C-5)]**[+], containing an azacrown moiety, binds more tightly divalent metal ions giving rise to dramatic changes in the UV-Vis absorption spectrum, according to the soft-hard principle. On the other hand, **[Pt(trpy)(ph15-C-5)]**[+] has higher affinity for alkali and alkaline earth metal ions. Only **[Pt(trpy)(ph15-C-5)]**[+] demonstrates an enhancement of the emission intensity upon binding of Mg^{2+} and Ca^{2+} ions while the luminescence of **[Pt(trpy)(ph-N-15-C-5)]**[+] can not be switched on. The behaviour of the first complex is ascribed to the blocking of the PET upon ion binding. In another work, Yam et al. reported that similar tuning of the UV-Vis absorption bands can be obtained in a series of Pt(dphpy)(C≡C-crown ether) complexes, that are also emissive in solution, differently from the [Pt(trpy)][+] analogues.

The group of Tung studied the emission properties of a 6-phenyl-2,2'-bipyridyl analogue of complex **[Pt(trpy)(ph-N-15-C-5)]**[+]:[110] they observed a similar behaviour in the UV-Vis absorption spectrum. The complexes emit from a structureless band upon addition of Mg^{2+} ions, but not with the addition of Li^+, Na^+, K^+, Ca^{2+}, Ba^{2+}, Zn^{2+}. The emission change is explained with a shift of the ^{3}LLCT state to higher energy, resulting in emission from the lowest-lying ^{3}MLCT state. They explain the lack of emission of complex **[Pt(trpy)(ph-N-15-C-5)]**[+] and its 6-phenyl-2,2'-bipyridyl analogue by the kinetic scheme showed in Figure 32.
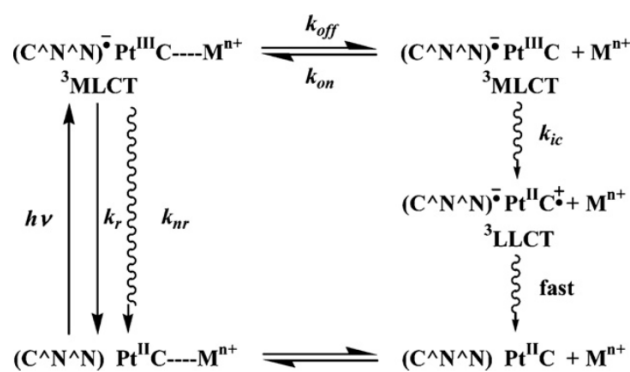
Figure 32. The deactivation pathway as explained by Tung et al.

In this scheme (C^N^N) and C represent, respectively, the terpyridyl ligand and the acetylide bearing the azacrown. Excitation of the platinum complex bound to the cation produces the ^{1}MLCT state, which undergoes an intersystem crossing to the ^{3}MLCT state. The metal centre in MLCT excited states (Pt^{III}) is much more electrophilic than that in the ground state (Pt^{II}) and the charge density on the amino group of the azacrown ether is diminished. The binding ability of the azacrown is thus reduced and the complexed cation is released by the azacrown during the lifetime of the MLCT state, resulting in the non-radiative quenching of the excited state.

The group of Williams studied the effect of cation binding on a crown ether pendant localised on the position 4 of the phenyl ring of some Pt(dpyb)Cl complexes (Figure 33).[35]
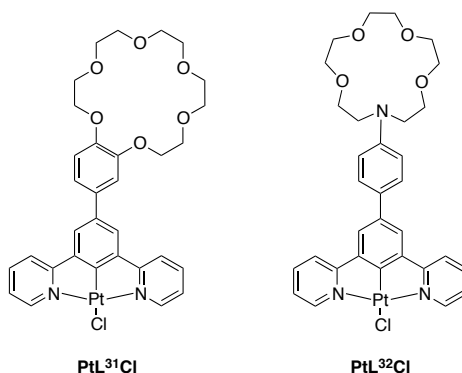
Figure 33. The two Pt(dpyb)Cl complexes bearing a crown and an azacrown ether studied by Williams et al.

Emission spectra of both complexes show an unstructured broad emission band, similarly to **PtL^{9}Cl**. Complex **PtL^{31}Cl** shows high affinity for double charged metal cations as Mg^{2+}, Ca^{2+} and Zn^{2+}: the absorption band at lowest energy is red shifted (especially for Zn^{2+}). This can be explained by the fact that the binding of the metal cation renders the phenolic oxygens less electron-donating and lowers the HOMO. On the other hand, the shape of the emission band is not changed upon addition of a metal cation (only slightly diminished in intensity). This can be explained by the fact that the metal ion has a poorer affinity for the excited state than for the ground state.

36

cation (Li⁺, Na⁺, K⁺). On the other hand, the presence of a divalent metal (Mg²⁺, Ca²⁺, Ba²⁺, Zn²⁺) cation leads to a remarkable change. The strongest response is induced by Ca^{2+}: the emission intensity is increased and the emission band is blue-shifted, with an analogous effect as **PtL⁹Cl** upon protonation. The spectral change can thus be interpreted with the presence of a twisted intermolecular charge transfer for the free-metal ligand, with the ³LC becoming the low-lying emissive state upon cation binding.

Recently, De Cola et al. reported a dinuclear Pt(2,6-bis(triazolyl)pyridine) complex in which the two units are linked by an 18-crown-6 ether localized on the pyridyl co-ligand.[111] The complex shows prevalently emission from an ³MMLCT state in THF solution, due to the facial proximity of the two platinum units. They found that, in the presence of K^+ cations, the aggregate emission band is decreased, while the monomeric emission band is increased. This demonstrated that the binding of the K^+ to the 18-crown-6 moiety distances the two platinum fragments, diminishes the aggregation and allows the increasing of the emission from the monomeric form (Figure 34). Upon addition of 18-crown-6, which competitively bind K^+ ions, this process is reversed and can be cycled about three times before the effect of the salt load affects the cation binding ability of the switch.
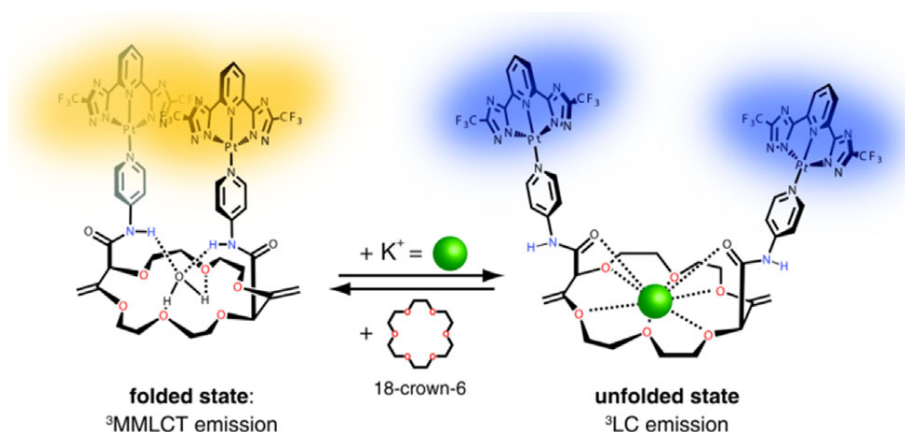
Figure 34. Reversible emission switch of the platinum complex studied by De Cola et al.

Crown ethers revealed to be efficient substituents to allow switching of the absorption and, sometimes, emission properties of a complex bearing them as substituents on the appropriate ligand. Nevertheless, the study of the effect of the presence of cations in solution on an flexible chain is rare, and we will focus on this aspect from now on.

3.2. Controlling the emission of a dinuclear platinum dipyridylbenzene complex

In section 2.2.2 we discussed the properties of the only dinuclear platinum dipyridylbenzene complex present in the literature in which a 4,5-disubstitued rigid xanthene unit locks the two Pt(dpyb)Cl units into a face-to-face configuration. This efficiently promotes the formation of intramolecular excimers upon excitation in solution.

Inspired by the work of the groups of Che and Yam about aggregating dinuclear platinum complexes linked by an oligo(oxyethylene) bridge (section 3.1.3.2), we decided to synthesize and study two dinuclear dipyridylbenzene platinum complexes in which the two metal units are linked by a flexible tetra(oxyethylene) tether via either the central phenyl ligand (**Pt₂(4-eg)**), or the phenylacetylide ligand (**Pt₂(alk-4-eg)**) (Figure 35).[112] The length of the chain was chosen considering that the complexes undergoing more easily aggregation are those with three to five ethyleneglycol blocks linking the two platinum units.[98] We compared the behaviour of **Pt₂(4-eg)** to that of the corresponding mononuclear complex **Pt(3-eg)**. Unfortunately, **Pt₂(alk-OMe)** was not stable even under inert atmosphere and decomposed right after purification: it was thus not possible to compare the properties of **Pt₂(alk-4-eg)** to the corresponding mononuclear complex.
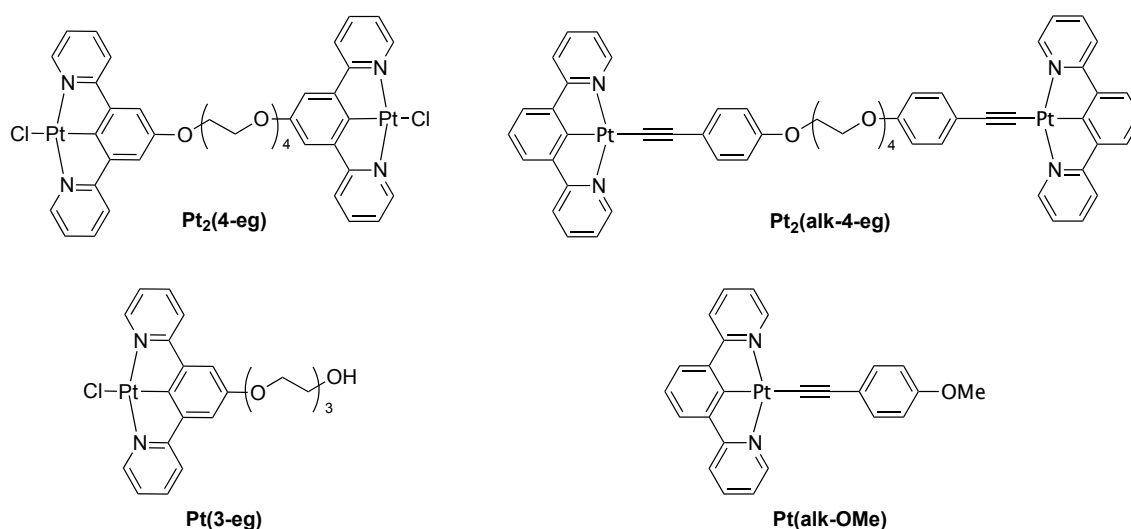
Figure 35. Chemical structures of the mono- and dinuclear Pt[II] complexes.

We will show that *(i)* the presence of a flexible bridge can allow the coexistence of an extended *vs* a face-to-face conformation, *i.e.* a folded state which is likely to favour Pt–Pt and π–π interactions and consequently have an impact on the luminescence properties, and *(ii)* how the different location of the tetra(alkoxyethylene) chain, on the dipyridyl ligand or on the alkynyl co-ligand, can influence the behaviour of the binuclear platinum complexes in solution.

We will also demonstrate that, thanks to the amphiphilic nature of the complex, the ratio between the two forms can be modulated by different external factors, such as solvent and presence of metal cations.

3.2.1. Preparation and characterization of the Pt(dpyb) complexes

Different methods can be used for the synthesis of 2,6-dipyridylbenzene ligands:[27]

a - The first dpybH ligands were prepared in 90% yield by reaction of 1,3-dicyanobenzene with acetylene, catalysed by Co(Cp)(COD), under 10 atm pressure at 130°C.[26] This method was later abandoned due to the fact that acetylene is potentially explosive under pressure.

b - The classical procedures developed by Kröhnke, variants of the Tschitschibabin pyridine synthesis, can also be used.[59] Nevertheless, the limited availability of diacetylbenzene derivatives as starting materials limits the use of this method.

c - Palladium-catalysed cross coupling reactions are the most widely used methods for the synthesis of dpybH and ideal for the formation of a carbon-carbon bonds in aryl derivatives. Typically, Stille reactions (using aryl-stanannes), Suzuki reactions (using less toxic aryl-boronic acid or esters, even though pyridyl-2-boronic acid is not stable) and Negishi reactions (using aryl-zinc derivatives) can be used, even sequentially, to obtain aryl substituted dpybH.[113] This is the method we used.

The platinum complexes can be synthesized upon reaction with K_2PtCl_4 at reflux in an acetic acid/water mixture or an acetonitrile/water mixture in inert atmosphere for 2 days[32] and then purified by filtration and crystallisation. The detailed synthetic procedure for the preparation of complexes **Pt(3-eg)Cl**, **Pt$_2$(4-eg)** and **Pt$_2$(alk-4-eg)** will be described in Chapter III.

Complex **Pt$_2$(4-eg)** was synthesized starting by linking two 3,5-dibromophenols with the tetra(oxyethylene)chain. Then the dipyridylbenzene ligand was obtained through a Stille coupling with 2-(tri-*n*-butylstannyl)pyridine. Reaction of K_2PtCl_4 with the bis-(dpyb)H ligand to afford **Pt$_2$(4-eg)** in a $CH_3CN:H_2O$ mixture (3:1 *v/v*) at 80°C for 18 hours afforded both the desired dinuclear complex together with **Pt(3-eg)** as a side product arising from the cleavage of a $C(sp^3)$-O bond. The two complexes were isolated as pure compounds after fractional crystallisation in a CH_2Cl_2/Et_2O mixture and were fully characterized by standard spectroscopies. The complexation of the ligand to the platinum centres was confirmed by ^{1}H-NMR spectroscopy. The signal corresponding to the H in the position 6 of the pyridyl ring is shifted downfields (at about 9.2 ppm) respect to the signal of H in the same position of the pyridyl ring before complexation and displays the typical coupling with [195]Pt. Furthermore, the signal corresponding to the proton 4' on the phenyl ring disappears (Figure 36).
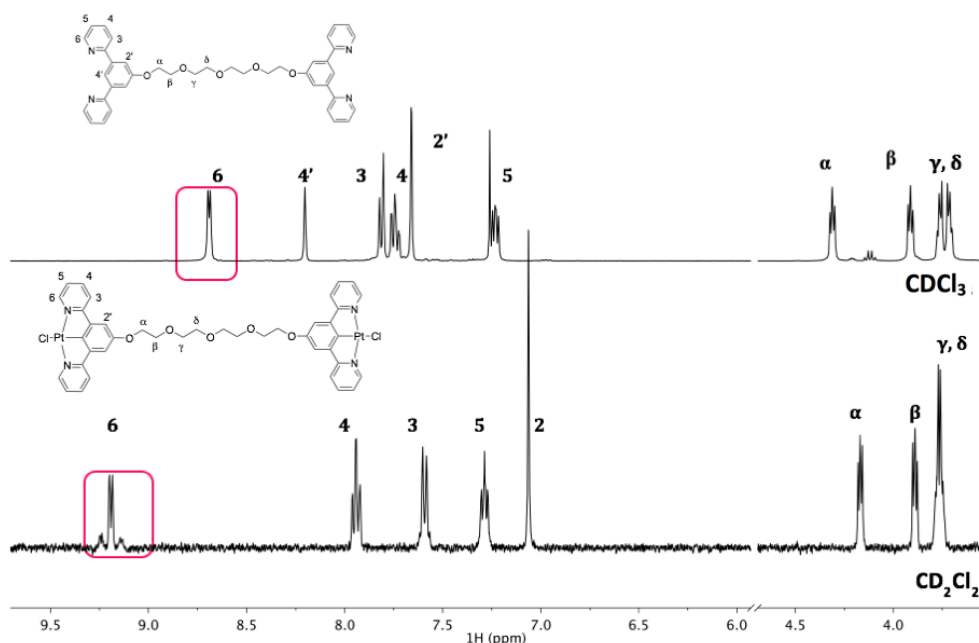
Figure 36. ^{1}H-NMR spectra of the ligand and the corresponding binuclear platinum complex **Pt$_2$(4-eg)**.

Complex **Pt(3-eg)** displays a set of signals similar to **Pt$_2$(4-eg)** but, of course, the integration accounts for a minor number of protons, and the signal assigned to the chain are less symmetrical than those of the binuclear complex.

Crystals of **Pt(3-eg)**, suitable for X-ray analysis, were grown by slow diffusion of Et$_2$O into a concentrated CH$_2$Cl$_2$ solution and its crystallographic structure is described in Figure 37.
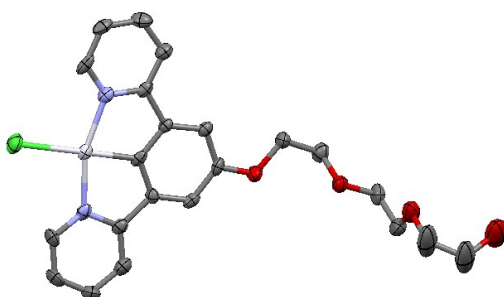
Figure 37. ORTEP diagram of **Pt(3-eg)**. Thermal ellipsoids correspond to a 60% probability level.

The bond lengths and angles (reported in Chapter III) are consistent with the structures previously reported for other Pt(dpyb)Cl complexes.[32] The platinum ion, the dipyridylbenzene ligand and the chloride ligand are on the same plane, but the N-Pt-N axis is distorted from linearity with a typical angle of 161.0(6)°. This non linearity reflects the chelate ring strain that the terdentate ligand experiences upon complexation. The Pt–C bond length [1.899(8) Å] is as expected considerably short when compared to

the one found for Pt(phbpy)Cl complexes,[23] accounting for the stronger ligand field of the dipyridylbenzene ligand that shifts the deactivating d-d states at very high energy.

The precursors for the synthesis of **Pt₂(alk-4-eg)**, Pt(dpyb)Cl and the bis-alkynyl tetra(oxyethylene) tether, were prepared following reported methods and synthetic details are provided in Chapter III. Complex **Pt₂(alk-4-eg)** was prepared from Pt(dpyb)Cl and the appropriate bis-alkyne in basic conditions at room temperature. It was isolated as a yellow powder in 47% yield. This complex decomposes rapidly in solution and slowly in the solid state at room temperature: the lack of stability can be attributed to the detrimental *trans* effect of the electron-rich alkynyl co-ligand.

3.2.2. Photophysical properties in solution: experimental and theoretical

The photophysical properties of the complexes were studied in a dichloromethane solution. The UV-visible absorption spectra of **Pt(3-eg)**, **Pt₂(4-eg)** and **Pt₂(alk-4-eg)** measured in CH_2Cl_2 at 298 K are shown in Figure 38, whereas the photophysical data are listed in Table 1. The electronic absorption spectrum of **Pt(3-eg)** displays an intense absorption band in the UV region, ranging from 250 to 350 nm, which can be ascribed to $^1(\pi\text{-}\pi^*)$ transitions of the dipyridylbenzene ligand. A moderately intense band appears at lower energy, from 380 to 450 nm, and is attributed to charge-transfer transitions $(d(Pt)/n p(Cl) \rightarrow \pi^*(dpyb))$ typical of this family of complexes.[29] The UV-vis absorption spectrum of **Pt₂(4-eg)** is almost identical to the mononuclear analogue, but the epsilon values are doubled, as expected from the presence of two platinum centres.
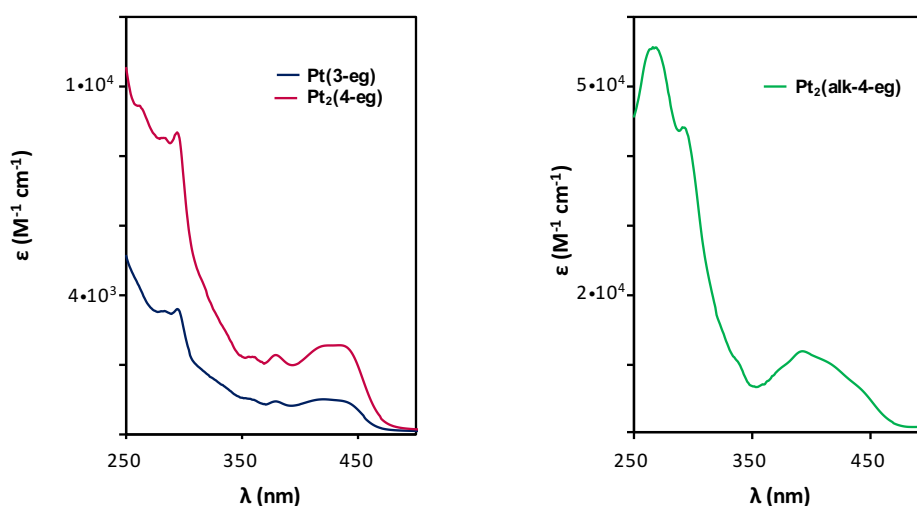
Figure 38. UV-vis absorption spectra of (left) **Pt(3-eg)**, **Pt₂(4-eg)** and (right) **Pt₂(alk-4-eg)** in CH_2Cl_2 solution at 298 K.

The absorption bands of **Pt₂(alk-4-eg)** are located at about the same wavelengths as the other two complexes, but they are less well resolved and significantly more intense, with evidence of a tail at

longer wavelengths. This tail might tentatively be attributed to a $\pi(C\equiv C) \rightarrow \pi^*(dpyb)$ LLCT transition, by analogy with other platinum acetylide complexes.[63]

The three complexes are emissive in degassed dichloromethane solution at room temperature (Figure 39) and their photophysical data are compiled in Table 1.

Pt(3-eg) emits in the green-yellow displaying a structured spectrum with a typical vibrational spacing of 1040 cm^{-1}, with the 0-0 band at 547 nm (10^{-5} M, λ_{ex} = 400 nm). The spectral shape is typical of predominant emission from a $^3(\pi$-$\pi^*)$ state, which is attributed to a dominant triplet LC excited state with a small contribution of the metal. The long lifetime (τ = 11 µs) and the fair quantum yield (Φ_{lum} = 0.24) confirm the triplet origin of the emission. The small Stokes shifts are not compatible with emission from a charge-transfer excited state. The emission's features are in good accordance with that of the related complexes studied by our group.[58]
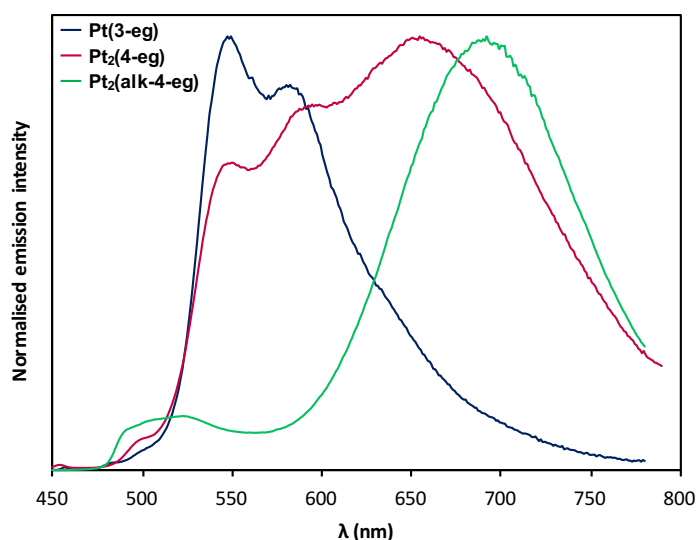
Figure 39. Emission spectra of the three platinum complexes in degassed CH$_2$Cl$_2$ solution (10^{-5} M, 298 K, λ_{ex} = 400 nm).

The room temperature emission spectrum of complex **Pt$_2$(4-eg)** (10^{-5} M in CH$_2$Cl$_2$) appears as a very broad band featuring several peaks. It can be interpreted as the sum of different electronic transitions: a monomer-like emission profile, for which the maxima are located at 547 and 588 nm (with a vibrational spacing of 1275 cm^{-1}), and a red-shifted emission band at 670 nm. The assignment of the first is justified by the comparison with the spectrum of the parent complex **Pt(3-eg)** which displays a similar structured emission profile at the same wavelength. The low-energy band is likely to arise from the emission from an excimeric excited state: it remembers that of the xanthene-based dinuclear complex studied by Williams[54a] (section 2.2.2) for which the intramolecular excimeric band in CH$_2$Cl$_2$ is centred at 690 nm. The shorter lifetime (τ = 2.2 µs at 590 nm) and the lower quantum yield (Φ_{lum} = 0.087) can be ascribed to the presence of the flexible chain that allows vibrational rearrangements of the two units relatively

one to each other. The typical shorter lifetime registered at 690 nm (τ = 1.5 µs), is assigned to the excimeric specie.[29]

The emission spectrum of **Pt$_2$(alk-4-eg)** 10^{-5} M at room temperature in CH_2Cl_2 is clearly dominated by the excimer emission. The complex displays a strong luminescence band centered at 692 nm, accompanied by a very weak band at 523 nm. The low-energy band is attributed to the excimer whereas the high-energy band is attributed to a π-π* ^{3}LC state mixed with a π(C≡C) $\rightarrow \pi$*(dpyb) LL'CT excited state. The lifetime at 520 is monoexponential (τ = 2.7 µs) and similar to the one registered for **Pt$_2$(4-eg)**; the quantum yield remains low (Φ_{lum} = 0.074) for the same reasons discussed above. The decline at 690 nm is biexponential (τ = 4.1 µs (25%) and 1.2 µs (75%)), and is tentatively assigned to the presence of both the excimeric specie and a tail of the monomeric emission.

Complex	λ_{abs} / nm ($\varepsilon \times 10^3$ / $M^{-1}cm^{-1}$)^a	λ_{em}/nm^b	τ/µs^b	Φ_{lum} %^{b,c}
Pt(3-eg)	294 (3.5), 379 (0.9), 419 (1.0)	547, 580	11 (550 nm)	24
Pt$_2$(4-eg)	293 (8.5), 379 (2.3), 438 (2.5)	547, 588, 670	2.2 (590 nm), 1.5 (670 nm)	8.7
Pt$_2$(alk-4-eg)	291 (32.4), 393 (10.9), 450 (4.45)	523, 692	2.7 (520 nm), 4.1 - 1.2 (690 nm)	7.4

Table 1. Photophysical data for complexes **Pt(3-eg)**, **Pt$_2$(4-eg)** and **Pt$_2$(alk-4-eg)**. [a] In CH_2Cl_2 solution (10^{-5} M) at 298 K. [b] In degassed CH_2Cl_2 solution (10^{-5} M) at 298 K, λ_{ex} = 400 nm. [c] Ref: Ru(bpy)$_3$Cl

In order to further explore the nature of the excimers in solution, the emission of the three complexes was studied at variable concentrations ranging from 10^{-6} M to 10^{-4} M. The emission of solutions at lower concentration could not be clearly distinguished by the noise by the spectrometer, while the complexes were not soluble enough to allow emission measurement of solutions at concentrations higher than 10^{-4} M: they started to precipitate right after the preparation of the sample.

Different kinds of interactions are expected in solution. The binuclear complexes can aggregate intramolecularly in a face-to-face manner or intermolecularly in a face-to-face or head-to-tail manner. The intermolecular face-to-face aggregates are believed to form by following the tendency of dimers to aggregate in a face-to-face manner, while the intermolecular head-to-tail aggregates can form by random interactions. Chart 1 shows some possible intra- and intermolecular arrangements for **Pt$_2$(4-eg)**. Similar arrangements of the two platinum units are expected for **Pt$_2$(alk-4-eg)**.
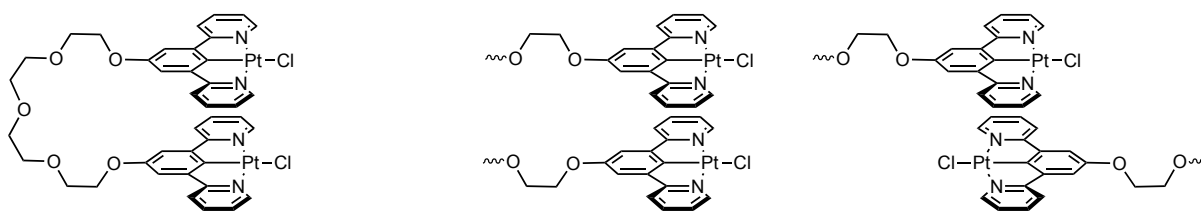
Chart 1. Proposed intra- and intermolecular arrangements of **Pt$_2$(4-eg)**.

By increasing the concentration of **Pt$_2$(4-eg)** in CH$_2$Cl$_2$ solution, the low-energy band becomes progressively more intense at the expense of the shorter wavelength bands (Figure 40a). Irrespective of the considered concentration, the excitation spectrum closely resembles the corresponding absorption spectral bands of **Pt$_2$(4-eg)**. This leads to the exclusion of the possibility of formation of aggregates at the ground state, since they should be visible as a band or a tail at long wavelength.

The chain linking the two complexes is flexible enough to allow interactions between the two Pt(dpyb)Cl units within the same molecule, but at higher concentrations interactions between different molecules can become more significant. The fact that the excimer emission band grows by increasing the concentration is indicative of the presence of intermolecular excimers. Indeed, intramolecular excimers are not supposed to vary in number depending on the concentration. However, the formation of intra- and intermolecular excimers cannot be readily distinguished, since no significant shift of the emission maximum was observed by increasing the concentration.

Pt$_2$(alk-4-eg) displays a similar behaviour but, in this case, the excimer is the prevalent specie in solution even at the lower concentration of 10^{-5} M (Figure 40b). This confirms our previous statement: excimers form more readily for **Pt$_2$(alk-4-eg)** respect to **Pt$_2$(4-eg)**.

In addition, for the parent monomer **Pt(3-eg)** no clear evidence of near-IR emission can be found in a 10^{-4} M solution in CH$_2$Cl$_2$ (Figure 40c), which suggests that the flexible bridge may significantly help to form excimers in solution.
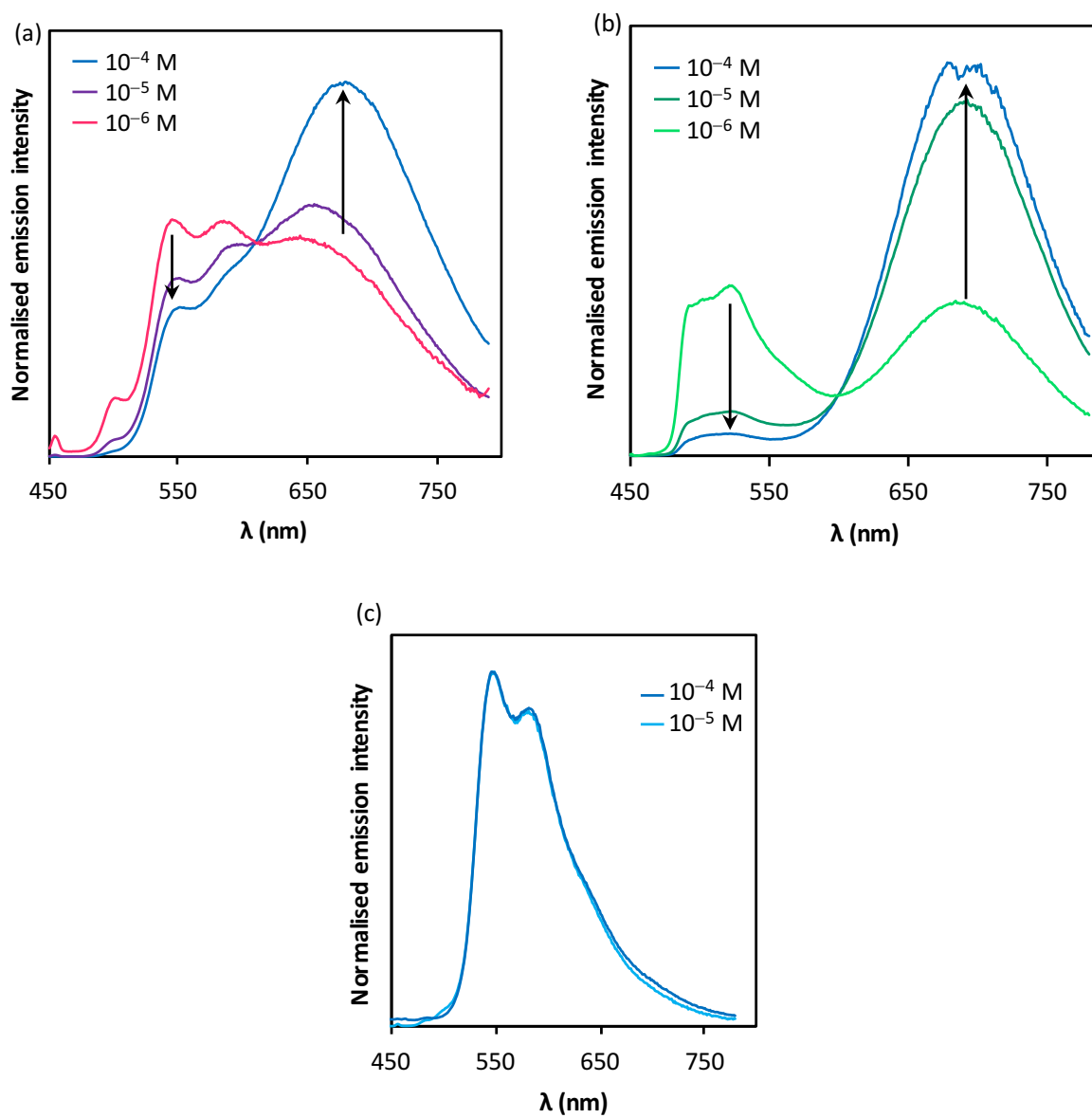
Figure 40. Emission spectra of (a) **Pt₂(4-eg)**, (b) **Pt₂(alk-4-eg)**, (c) **Pt(3-eg)** at various concentrations in CH_2Cl_2 (298 K, $\lambda_{ex} = 400$ nm).

The differences in the emission spectra of the three complexes can be explained by considering the presence of the alkoxy substituent in the *para* position of the phenyl ring of the dipyridylbenzene ligand and the linker between two units in the dinuclear complexes.

Alkoxy substituents are electron donors. When the poly-ethylenglycol chain is in the position 4 of the phenyl ring of the dipyridylbenzene ligand, it has the effect of lowering the energy of the ILCT transition, resulting in a destabilisation of the Pt–Pt and $\pi-\pi$ interactions bringing to excimer formation. The same, even though more pronounced, phenomenon was as reported by Williams et al.[32] when they studied the effect of an amino substituent in the same position. This explains the lack of excimer emission even in more concentrate solution (10^{-4} M) for **Pt(3-eg)**. The fact that the alkoxy substituent has actually the function of a linker reverses the effect. In **Pt₂(4-eg)** its presence is crucial to help to bring together the two Pt(dpyb)Cl moieties via a face-to-face configuration for the intramolecular association although the electron-donating ability of the chain slightly destabilizes these interactions in the meantime.

The prevailing eximeric emission for **Pt₂(alk-4-eg)** can be explained by the presence of the chain, as for **Pt₂(4-eg)**, and also by the fact that the tetra(oxyethylene) linker is now placed on the alkynyl co-ligand and not in the position 4 of the phenyl ring of the dipyridylbenzene ligand anymore. The detrimental effect of the electron-donating alkoxy substituent that lowers the energy of the ILCT transition is in such way abolished.

In order to definitely confirm that the band in the NIR is due to the presence of an excimer an not of a ground-state aggregate, we measured the absorption spectra of the three complexes at 77 K in EPA glass (EPA = ethanol/isopentane/diethylether : 2/2/1) (Figure 41).
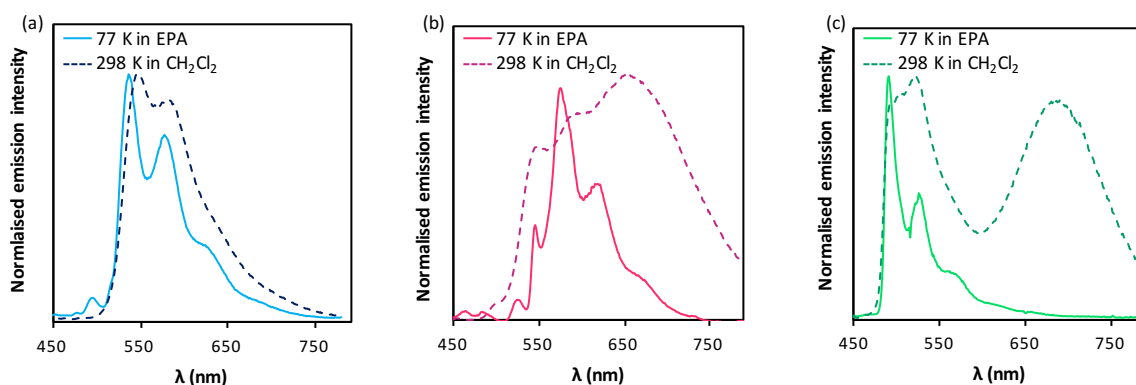
Figure 41. Emission spectra of (a) **Pt(3-eg)**, (b) **Pt₂(4-eg)**, (c) **Pt₂(alk-4-eg)** in CH₂Cl₂ at room temperature (10^{-5} M, λ_{ex} = 400 nm) and in EPA at 77 K.

The three complexes present a highly structured emission band: the maxima values are reported in Table 2. Emission is centred between 550 and 650 and there is no evidence of a band at long wavelength, differently from the room-temperature spectra. This is in accordance with the attribution of the emission band in the NIR to an excimer.

At low temperature we observe the emission only from the monomer-like extended form because the formation of an excimer is a thermally activated process for which the motion of the two platinum units relatively one to each other is required. At such low temperature the two units do not have enough energy to move and approach: this is why the excimer can form only at higher temperature when enough energy is furnished to the system.[54]

Complex	λ_{em}/nm
Pt(3-eg)	538, 576, 628
Pt$_2$(4-eg)	546, 577, 620
Pt$_2$(alk-4-eg)	491, 527, 570

Table 2. Emission maxima in EPA (ethanol/isopentane/diethylether : 2/2/1) glass at 77 K for the three platinum complexes (λ_{ex} = 400 nm).

For the binuclear platinum complexes self-assembling at the ground state studied by Yam et al. the emission in the NIR was observable even at low temperature, and more intensely, because the formation of ground state aggregates is favoured at low temperature in a more rigid environment (see section 3.1.3.2).

The experimental results were corroborated by TD-DFT calculations, done in collaboration with Prof. D. Jacquemin. For what concerns the absorption spectra, calculation showed that for **Pt(3-eg)** the first singlet excited state is located at 421 nm: it presents a significant oscillator strength (f = 0.156) and it is responsible for the low-energy band observed experimentally together with the second state at 418 nm (f = 0.013). It can be mainly ascribed to a HOMO-LUMO transition, which corresponds to a charge transfer from the metal and the phenyl to the pyridyl moieties, *i.e.* it presents a mixed MLCT/ILCT character. The measured optical absorption spectrum in CH$_2$Cl$_2$ of **Pt$_2$(4-eg)** displays a similar profile with higher molar extinction coefficients, as expected for a "*dimeric*" structure (Table 1). For **Pt$_2$(4-eg)**, both the extended (a) and the intramolecular face-to face (b) forms (Figure 42, top) were optimized at the DFT level. For **Pt$_2$(4-eg)-a**, the computed spectrum is almost perfectly the double of that of **Pt(3-eg)**. Four nearly degenerated states can be found at 421 nm (f = 0.041), 420 nm (f = 0.253), 418 nm (f = 0.015) and 418 nm (f = 0.025), that correspond to a peak centred at 420 nm for a total oscillator strength of 0.334, almost perfectly twice the total f of **Pt(3-eg)** (0.338). In **Pt$_2$(4-eg)-b**, the Pt–Pt separation is 3.49 Å according to DFT. Compared to **Pt$_2$(4-eg)-a**, the computed absorption spectrum encompasses many more transitions but the convolution of the TD-DFT states still indicates a band centred at ca. 420 nm with a total f of 0.308, again similar to the one of a "double" **Pt(3-eg)**. Therefore, the absorption spectrum in itself is probably not the best indicator of the form of **Pt$_2$(4-eg)** in solution: aggregation has a relatively moderate impact on the band shape of the lowest peak.

If the total DFT free energies of **Pt$_2$(4-eg)-a** and **Pt$_2$(4-eg)-b** are compared, it can be found that the latter is favoured by 18 kcal·mol^{-1}. To ascertain this value, the interaction energy in both gas and solvent phases were computed using a single-point calculation made with a very larger atomic basis set, namely *def2*-QZVP, and very similar interaction energies were obtained: 21 and 19 kcal·mol^{-1}, respectively. This indicates that the stacked form **Pt$_2$(4-eg)-b** should predominate in solution at the thermal equilibrium at room temperature.
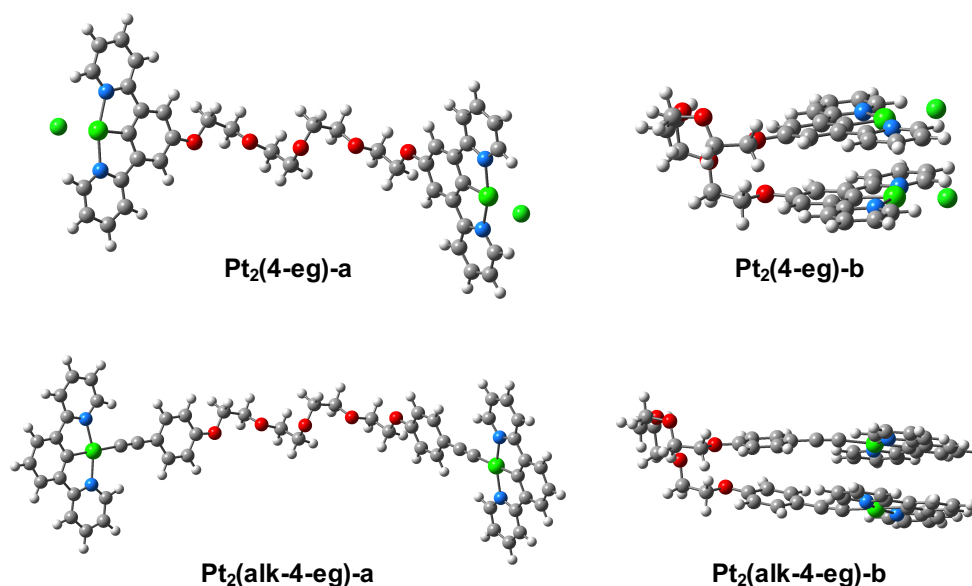
Figure 42. Representation of the DFT-optimized extended and the intramolecular face-to face forms of (top) **Pt$_2$(4-eg)** and (bottom) **Pt$_2$(alk-4-eg)**.

For **Pt$_2$(alk-4-eg)**, we also considered the extended (a) and the intramolecular face-to face (b) conformers for the theoretical calculations (Figure 42, bottom) and found that the latter is more stable than the former by 17 kcal·mol^{-1} on the free energy scale. In **Pt$_2$(alk-4-eg)-b**, the Pt–Pt separation attains 3.57 Å, quite similar to the value in **Pt$_2$(4-eg)-b**. For the extended conformer, **Pt$_2$(alk-4-eg)-a**, TD-DFT yields absorption that are in the same spectral range as both **Pt(3-eg)** and **Pt$_2$(4-eg)**, but that are significantly more intense, as observed experimentally (Table 1). Indeed, the four lowest singlet transitions are at 455 nm (f = 0.200), 454 nm (f = 0.151), 436 nm (f = 0.058) and 436 nm (f = 0.077). The nature of the frontier molecular orbitals of **Pt$_2$(alk-4-eg)-a** is essentially unmodified compared to **Pt(3-eg)** but the spectral properties of the stacked form **Pt$_2$(alk-4-eg)-b**, reveal broader absorption with excited-states located by TD-DFT at 484 nm (f = 0.003), 462 nm (f = 0.043), 456 nm (f = 0.203), 421 nm (f = 0.008). Nevertheless, the strongest band remains located at the same position as in **Pt$_2$(alk-4-eg)-a**, and again, the absorption spectra in themselves are probably not the best indicator of aggregation at the ground-state in the present case.

Using DFT, the "excimer" in both **Pt$_2$(4-eg)-a** and **Pt$_2$(4-eg)-b** were modeled. We considered one of the two structures is in its singlet state and the other in its triplet state. The stabilization of the latter compared to the former is 21 kcal·mol^{-1}, that is slightly higher than for the corresponding ground-state structure (18 kcal·mol^{-1}, see above). Concomitantly, the separation between the two Pt atoms is slightly smaller in the excimeric form of **Pt$_2$(4-eg)-b** (3.31 Å) than its ground-state counterpart (3.49 Å). For **Pt$_2$(4-eg)-a**, the computed 0-0 phosphorescence wavelength is 565 nm whereas the vertical value is 602 nm. In contrast, for **Pt$_2$(4-eg)-b**, theory predicts 607 nm and 666 nm for the 0-0 and vertical emission, respectively, illustrating the redshift obtained due to the stacking. Nevertheless, it is noticeable that this effect is significantly smaller with DFT (+64 nm within the vertical approach) than the one experimentally measured (+123 nm). The density plots (Figure 43, top) indicates that as expected the triplet state is purely localized on one moiety in **Pt$_2$(4-eg)-a**, but that in **Pt$_2$(4-eg)-b**, there is a partial delocalization on the two platinum units.

DFT calculations were performed for both the extended **Pt$_2$(alk-4-eg)-a** in which the two complexed do not interact and **Pt$_2$(alk-4-eg)-b**, in which a strong stacking is present (Figure 43, bottom). For **Pt$_2$(alk-4-eg)-a**, the emissive state is still localized only on one side of the compound, but is significantly more delocalized than in both **Pt(3-eg)** and **Pt$_2$(4-eg)-a**. For this structure, DFT returns a 0-0 phosphorescence at 593 nm, too red-shifted if compared to experiment as in **Pt$_2$(4-eg)-a**. More interestingly, the density difference of **Pt$_2$(alk-4-eg)-b** shows a full delocalization on the two complexes, contrasting clearly with the case of **Pt$_2$(4-eg)-b**. This result, obtained though we started the geometry optimization with one complex in its ground-state geometry and one in its excited-state (T$_1$) geometry, clearly indicates that excimeric interaction is stronger in **Pt$_2$(alk-4-eg)-b** than in **Pt$_2$(4-eg)-b**.
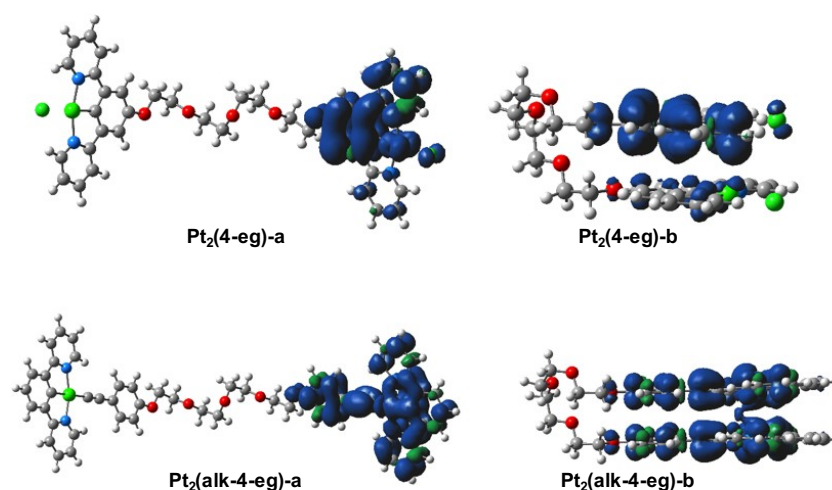
Figure 43. Representation of the spin density difference for the emissive structures of (top) **Pt$_2$(4-eg)** and (bottom) **Pt$_2$(alk-4-eg)**.

Also, the computed 0-0 phosphorescence energy is of 663 nm for **Pt$_2$(alk-4-eg)-b**, strongly red-shifted compared to **Pt$_2$(4-eg)-b** (607 nm) and the Pt–Pt separation is much smaller in the excimeric form of

Pt₂(alk-4-eg)-b (2.94 Å) than in both the **Pt₂(4-eg)-b** excimer (3.31 Å) and the **Pt₂(alk-4-eg)-b** ground-state (3.57 Å). This confirms again the higher propensity of **Pt₂(alk-4-eg)** to form excimers in solution.

3.2.3. Modulation of the emission with external factors

Owing to the amphiphilic nature of the complexes, possessing hydrophobic Pt(dpyb) units and a hydrophilic tetra(oxyethylene) chain, we reasoned that it should have been interesting to test their response to solvents of various polarity.

We started by studying the changes in the emission of **Pt₂(4-eg)** in different solvents (Figure 44 emission maxima listed in Table 3). We firstly measured the emission of a 10^{-5} M solution of the complex in a very polar solvent such as DMSO. We observed a broad and unstructured band centred at 567 nm that can be attributed to the monomer emission. The band is well superimposable with the emission of complex **Pt(3-eg)** in dichloromethane. The photophysical behaviour is very different in a 10^{-5} M solution of the complex in the less polar THF. Here the excimer band prevails, leading to a significant red-shift of 125 nm of the emission, now centred at 692 nm.
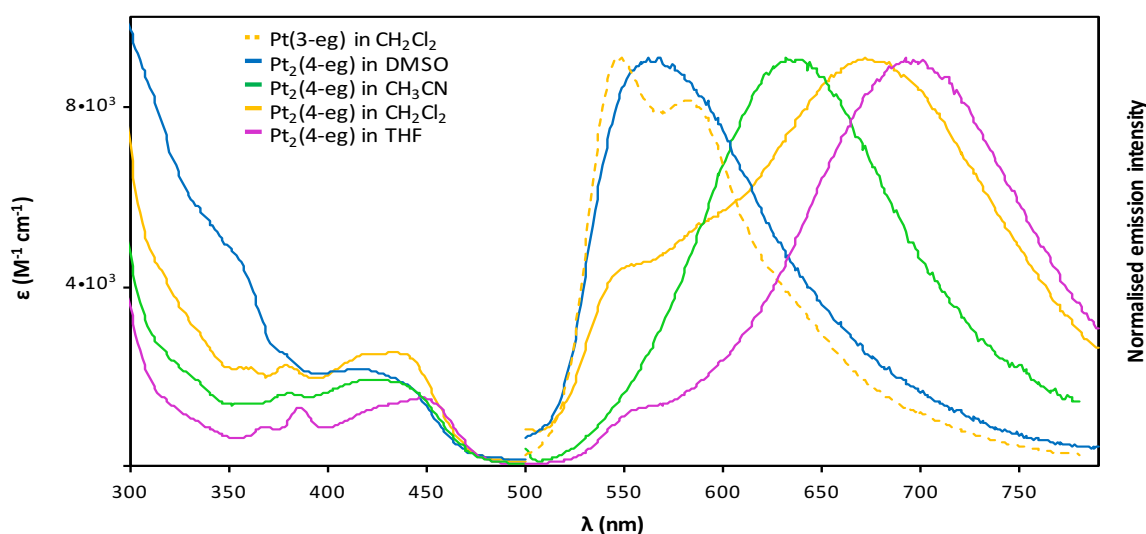
Figure 44. Absorption (left) and emission (right) spectra of **Pt₂(4-eg)** in various solvents, superimposed with the emission spectrum of **Pt(3-eg)** in CH₂Cl₂ (10^{-5} M, 298 K, λ_{ex} = 400 nm).

	Pt₂(4-eg)		**Pt₂(alk-4-eg)**	
Solvent	λ_{em}/nm[a]	Φ_{lum} %[b,c]	λ_{em}/nm[a]	Φ_{lum} %[b,c]
CH₃CN	632	8.1	489, 520, 684	17
DMSO	567	0.8	531, 678	0.2
THF	692	1.5	493, 526, 700	22

Table 3. Emission data for **Pt₂(4-eg)** and **Pt₂(alk-4-eg)** in various solvents. [a] Recorded in degassed solution (10^{-5} M, λ_{ex} = 400 nm). [b] 10^{-5} M; [c] Ref: Ru(bpy)₃Cl₂.

It can be assumed that the association process is controlled by the nature of the solvent as the result of the amphiphilic nature of **Pt$_2$(4-eg)**, featuring a hydrophobic head, *i.e.* the platinum core, and a hydrophilic chain. The oligo(oxyethilene) chain is well stabilised in its extended form by the strongly polar DMSO: this leads to emission prevalently from the monomer-like conformer. On the other hand, a less polar solvent like THF tends to worse solvate the chain, leading to its folding and consequent emission from the excimer.

A different and peculiar effect is observed in acetonitrile (Figure 45, left). Significant spectral emission changes are observed by adding CH$_3$CN in a CH$_2$Cl$_2$ solution: the spectrum gradually displays a structureless and very broad band centred at 632 nm, to which both the monomer and the excimer contribute.
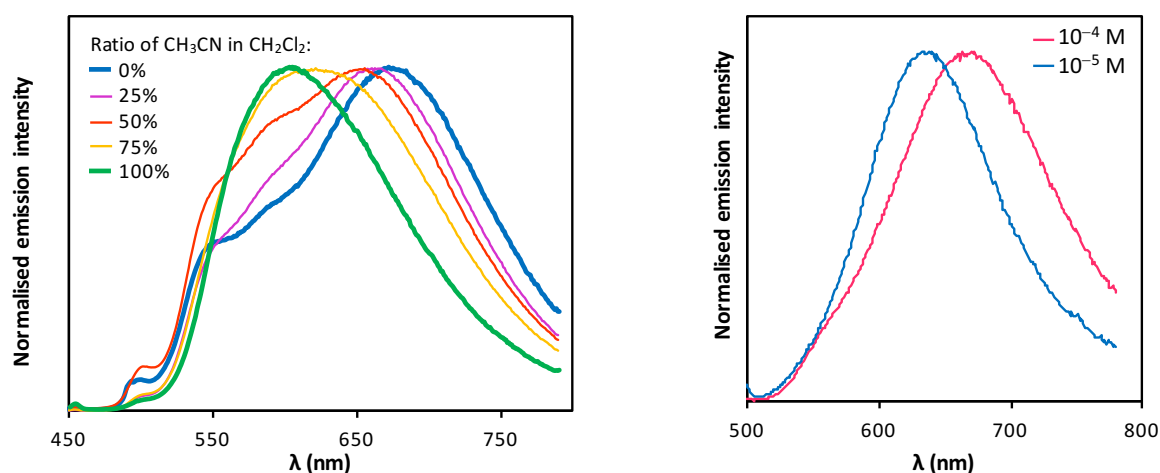
Figure 45. (Left) Emission spectra of **Pt$_2$(4-eg)** in a mixture of CH$_2$Cl$_2$ and CH$_3$CN (10^{-5} M, 298 K, λ_{ex} = 400 nm); (right) Emission spectra of **Pt$_2$(4-eg)** in CH$_3$CN at different concentrations (298 K, λ_{ex} = 400 nm).

Since the structureless band is clearly shifted towards the blue, it can be stated that CH$_3$CN favours the extended form. Furthermore, the "monomeric" **Pt$_2$(4-eg)** displays a positive solvatochromism, *i.e.* a bathochromic shift due to the ILCT character of this 4-alkoxy substituted derivative,[32] while the excimer band displays a negative solvatochromism, *i.e.* a blue shift, leading to the overlap of the two bands. Moreover, at higher concentration (10^{-4} M), the emission band is red-shifted to 672 nm. The intensity of the red-end tail of the spectrum is increased in concomitance with a decrease of the emission proportion of the monomer relative to the excimer. This arises from a greater extent of intramolecular excimeric interactions as observed previously by varying the concentration of the complex in a CH$_2$Cl$_2$ solution.

Varying the concentration of solutions of the complexes in DMSO or THF does not lead to any significant change in the proportion of the monomer and excimer in solution, nor in the emission wavelength. These features allow the modulation of the luminescence of **Pt$_2$(4-eg)** from the green to the red the solvent or the concentration in solution.

It is relevant that the absorption spectra do not undergo any significant change upon changing the solvent (Figure 44), except in DMSO, where the band centred at 350 nm is slightly more intense. This confirms that the phenomena we are discussing are related to the excited state properties of the molecule. The values of the molar absorption coefficient remain of the same order of magnitude, too.

Conversely, the emission quantum yields vary over one order of magnitude in different solvents. While in CH_3CN the value of Φ_{lum} is almost the same as in CH_2Cl_2, quantum yields drop both in THF ($\Phi_{lum} =$ 0.015) and DMSO ($\Phi_{lum} = 0.008$). Statistically, the chain can have different degrees of bending at the ground state. Upon excitation, the extended conformer is stabilised in DMSO, while the folded conformer, *i.e.* the excimer, is stabilised in THF. The need of rearrangement for the unstable conformer in order to allow the emission from the favoured species can be translated in energy losses under the form of vibrational motion. This motion leads directly to a dispersion of energy via non-radiative decay and subsequent dropping of the quantum yields. On the other hand, both forms are stabilised in CH_2Cl_2 and in CH_3CN: there is less need for immediate rearrangements, resulting in higher quantum yields.

Again, the emission of **Pt(3-eg)** in different solvents does not present any variation. The only noticeable effect is that the emission band in CH_3CN becomes less structured, but still remains at the same wavelength as the ones in other solvents (Figure 46).
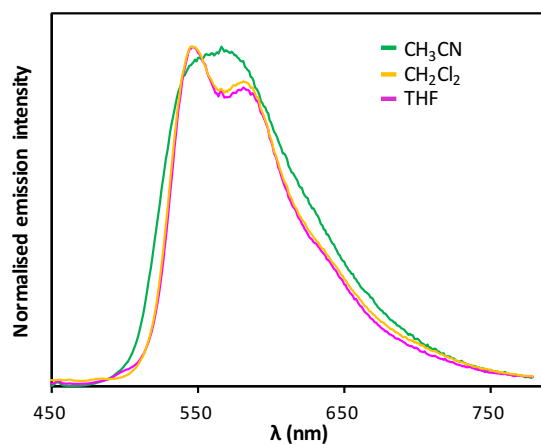
Figure 46. Emission spectra of **Pt(3-eg)** in various solvents, (10^{-5} M, 298 K, $\lambda_{ex} = 400$ nm).

At last, we studied the changes in the emission of **Pt₂(alk-4-eg)** in different solvents Figure 47 (photophysical data listed in Table 3).
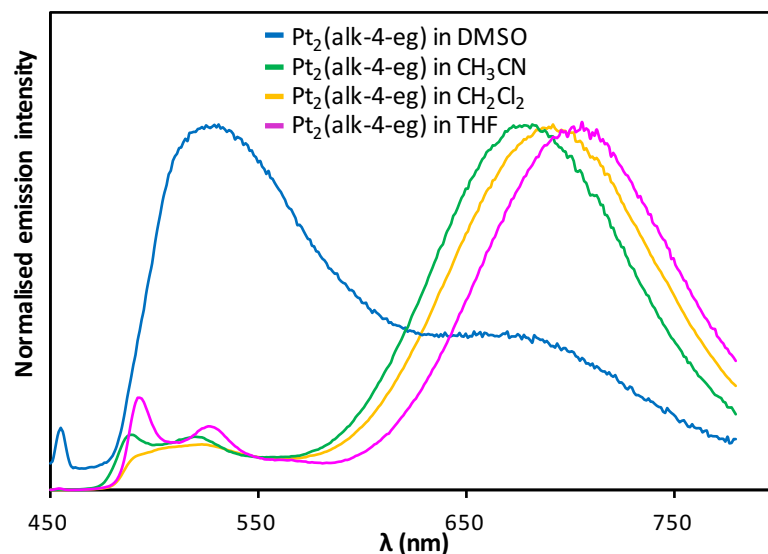
Figure 47. Emission spectra of **Pt₂(alk-4-eg)** in various solvents, (10^{-5} M, 298 K, λ_{ex} = 400 nm).

By going from CH_2Cl_2 to CH_3CN or THF, no significant spectral changes were observed. These results confirm that **Pt₂(alk-4-eg)** has a high propensity to self-assembly in the excited state. The emission is thus prevalently centred in the red, with bands of very low intensity attributable to the emission of the extended form, and a small bathochromic shift by going from CH_3CN to THF. Emission from a solution of a very polar solvent such as DMSO displays an unstructured broad band centred at 531 nm with a shoulder at 698 nm ascribed to the emission of the excimer. The stability of the folded form of the complex is so high that it can not be broken event in a very polar solvent.

Differently from complex **Pt₂(4-eg)**, emission quantum yields are highly enhanced both in CH_3CN and in THF (Φ_{lum} = 0.17 and 0.22 respectively). This can be ascribed to the fact that the folded conformer is naturally stabilised in this solvents and, upon excitation, it does not undergo any rearrangement prior to emission. On the other hand, once again the quantum yield drops in DMSO (Φ_{lum} = 0.002) and is even lower than that of **Pt₂(4-eg)** (Φ_{lum} = 0.008). This is possibly due to the fact that, upon excitation, the complex need to rearrange in order to allow emission from the favoured species, causing energy losses.

Emission can also be perturbed by binding of cations. Upon addition of aliquots of different monovalent (Na^+, K^+) and divalent (Zn^{2+}, Pb^{2+}) metal cations in CH_3CN to a CH_2Cl_2 solution of **Pt$_2$(4-eg)**, the emission spectrum is clearly modified (Figure 48a), leading to a decrease of the low-energy emission band, while no modification of the absorption spectrum was observed.[II]
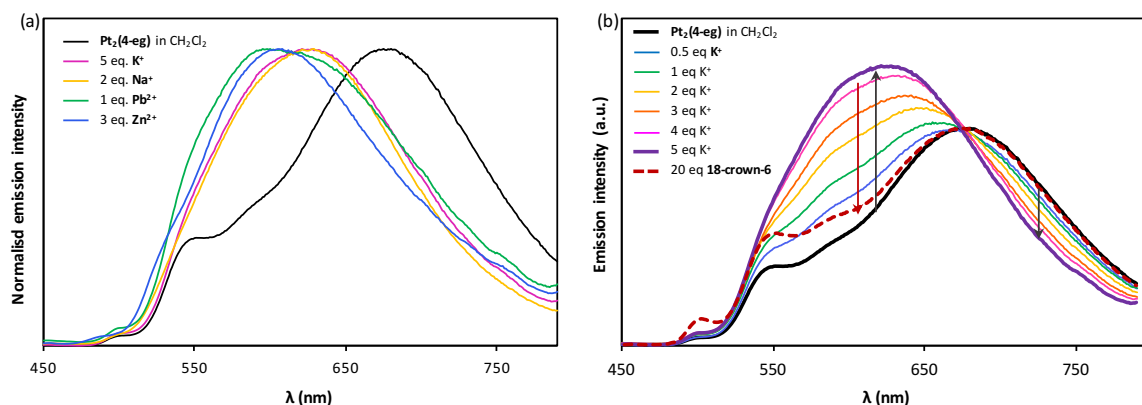
Figure 48. Emission spectra of **Pt$_2$(4-eg)** in CH_2Cl_2 (8.9 10^{-5} M, 298 K, λ_{ex} = 400 nm) (a) with addition of different metal salts ($NaPF_6$, KPF_6, $Zn(OTf)_2$ and $Pb(ClO_4)_2$ in CH_3CN) and (b) with addition of aliquots of KPF_6 and after addition of 18-crown-6.

The complex does not bind selectively to a specific metal cation, and apparently the charge and the softness of the cation do not have an influence on the binding ability to **Pt$_2$(4-eg)**. The binding stoichiometry also is almost aleatory: 5 equivalents of K^+ are needed in order to obtain the maximum modification of the spectrum, while only 3 equivalents of Zn^{2+}, 2 of Na^+ and 1 of Pb^{2+} are required to obtain the same effect. The lack of selectivity can be attributed to the extremely flexible nature of the chain that can interact with different cations in a similar way irrespectively of their size and charge.

It is likely that the binding of M^{n+} to the oxygen atoms of the linker significantly reduces or inhibits the excimer formation by "opening" the chain and increasing the distance between the two platinum moieties.[111] The excimeric emission band disappears and only a broad unstructured band centred between 595 and 620 nm grows, the maximum emission wavelength depending on the added cation.

The evolution of the emission curve can be followed upon addition of KPF_6 (Figure 48b) : an isosbestic point is observed at 673 nm by increasing the quantity of K^+ in solution and, interestingly, the spectral changes are reversible with addition of 18-crown-6.[111] The crown ether is expected to complex K^+ more

---

[II] We discussed above the effect that CH_3CN has on the emission of **Pt$_2$(4-eg)**, *i.e.* shifting the emission wavelength to 632 nm. In the present experiments, some μL of CH_3CN solution containing the metal cation were added to 3 mL of a CH_2Cl_2 solution of the platinum complex. The amount of CH_3CN in solution is so small that it is not supposed to have an influence on the emission of the complex. This assumption was confirmed by adding the corresponding total volume of CH_3CN to a CH_2Cl_2 solution of **Pt$_2$(4-eg)**: no changes were observed in the emission spectra.

strongly than **Pt₂(4-eg)**, allowing the initial emission spectrum to be recovered (dashed line in Figure 48b).

Even though addition of K$^+$ did not lead to any observable change in the absorption spectrum, the ¹H NMR spectrum (in CD₂Cl₂) of **Pt₂(4-eg)** is also modified when an excess of KPF₆ is added. Splitting of all signals with a 1:1 integration ratio occurs: the molecule is de-symmetrised, two Pt moieties become magnetically non-equivalent indicating also a change at the ground state (Figure 49). This phenomenon is also reversible upon addition of 18-crown-6: the ¹H-NMR signals merge to give the initial pattern. Strangely, a new signal can be observed at 8.05 ppm: it is tentatively assigned to an interaction between the crown ether and the binuclear platinum complex.
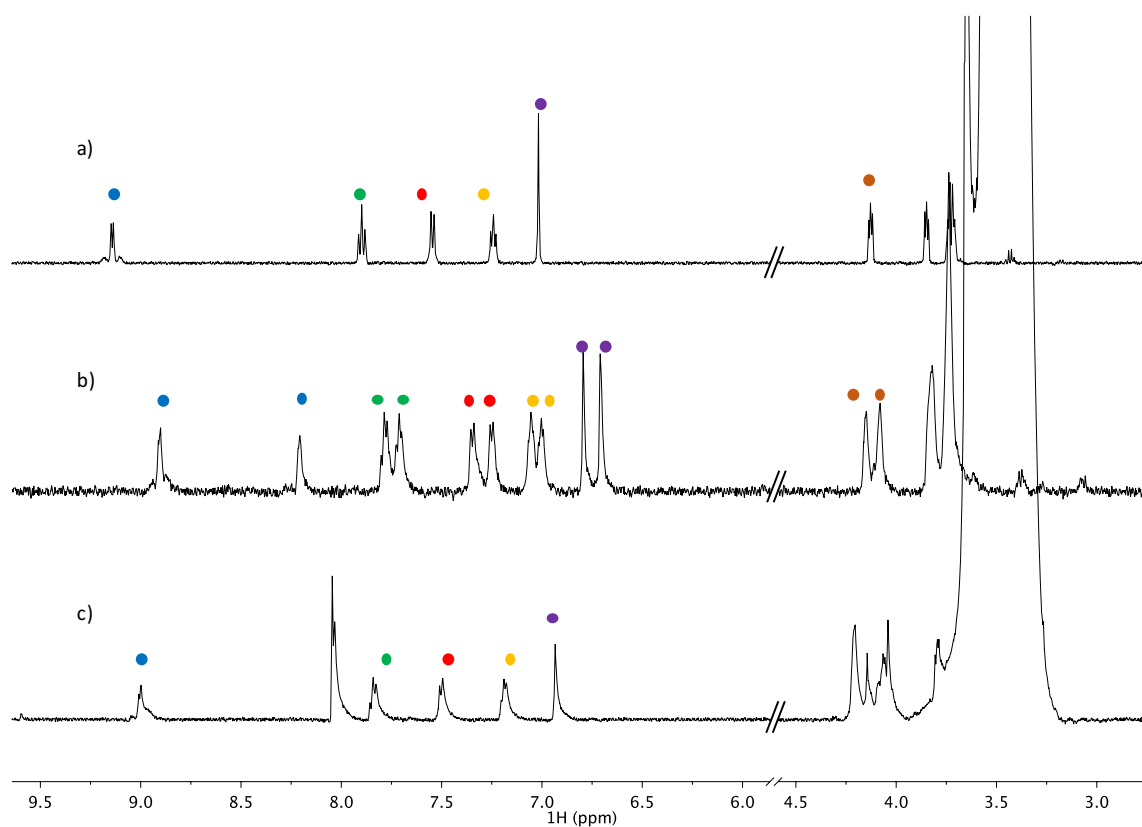
Figure 49. ¹H NMR spectra of (a) **Pt₂(4-eg)** in CD₂Cl₂, (b) after addition of 10 equivalents of KPF₆ in CD₃CN, (c) after further addition of 20 equivalents of 18-crown-6 in CD₂Cl₂.

Addition of K$^+$ to **Pt(3-eg)** and **Pt₂(alk4-eg)** did not lead to significant modification of the emission spectra (Figure 50).
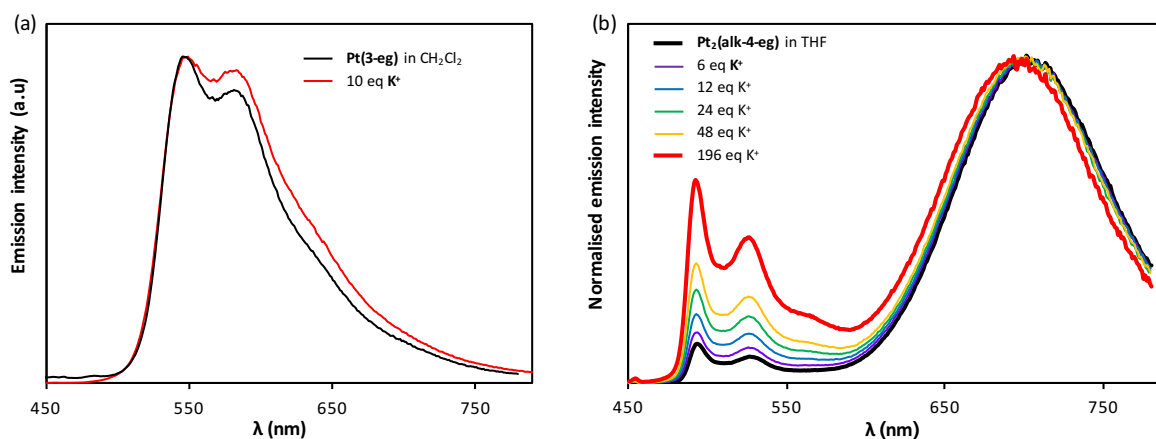
Figure 50. Emission spectra of (a) **Pt(3-eg)** in CH_2Cl_2 (10^{-5} M, 298 K, λ_{exc} = 400 nm) with addition KPF_6 and (b) **Pt$_2$(alk4-eg)** in THF (10^{-5} M, 298 K, λ_{ex} = 400 nm) with addition of aliquots of KPF_6.

In the case of **Pt(3-eg)** this can be explained by the fact that the complex is mononuclear and naturally does not form excimers, because there are not two platinum units capable of interacting upon addition of the metal cation. The fact that the emission spectrum remains almost unchanged confirms that the alteration of the emission for **Pt$_2$(4-eg)** are not due to a change in the emissive state (ILCT or LC) but specifically to the interactions of the two moieties linked by the tetra(oxyethylene) chain. In the first case, *i.e.* if modification of the emissive state occurred, the emission spectrum of **Pt(3-eg)** would also have been modified, since the emissive state (^{3}LC) is the same for the mononuclear and the extended dinuclear complex.

In the case of **Pt$_2$(alk4-eg)** the emission spectra undergoes some changes and after addition of K$^+$ the monomeric emission band grows in intensity. Nevertheless, in order to obtain a significant increase of the monomeric emission, almost 200 equivalent of salt are needed. The folded form is thus confirmed to be the most stable for **Pt$_2$(alk4-eg)** even in the massive presence of a cation, which should manage to "open" the excimer.

3.2.4. Conclusion

In summary, two new flexibly-linked dinuclear platinum(dipyridylbenzene) complexes and a mononuclear reference have been designed, synthesized, fully characterized and studied.
We demonstrated the crucial role of the flexible linker in the formation of excimers:

1. The mononuclear **Pt(3-eg)** with a tri(oxyethylene) chain in the position 4 of the dpyb ligand does not emit as excimer in solution. This is due to the presence of the electron-donating alkoxy substituent.

2. The dinuclear **Pt$_2$(4-eg)** complex gives rise to an additional emission band in the near-IR attributed to excimer emission in solution. Strategies to finely tune the emission colour by controlling the noncovalent interactions of luminophores (Pt−Pt and π−π interactions) have been tested: by controlling

the solvent and reversibly binding metal cations the emission wavelength has been modulated from the green to the red. We explained how the ratio between the excimeric and the extended form can be controlled by the solvent polarity, through stabilisation of one of the two forms and solvatochromic shift.

3. The dinuclear **Pt$_2$(alk-4-eg)** shows higher propensity to form excimers in solution, due both to the presence of the flexible linker and the absence of the electron-donating substituents on the dipyridylbenzene ligand.

These are the first examples of binuclear platinum complexes in which the two metal centres are linked by a flexible chain and that exhibit spectral changes purely due to excimeric formation. The obtained results should be useful for the future design of switchable and deep-red triplet emitters.

4. Platinum complexes bearing photochromic substituents

4.1. Organic photochromes: molecular design principles

Photochromism is a reversible photoinduced transformation of a molecule between two forms whose absorption spectra are perceptibly distinguishable. Photoresponsive materials, whose intrinsic properties can be modulated with the use of light as an external trigger, are of central importance for the development of molecular devices. Such compounds have already found applications in a wide variety of consumer products such as toys and cosmetic products,[114] photochromic inks for security markings,[115] ophthalmic and sunglass lenses,[116] biomolecular labels,[117] optical filters[118] and optoelectronic devices such as optical memories.[119]

Some of the most important classes of photoresponsive compounds with mechanisms operating through reversible chemical transformations, such as *cis-trans* isomerization and pericyclic ring-opening and ring-closing reactions, are shown in Figure 51.[120]
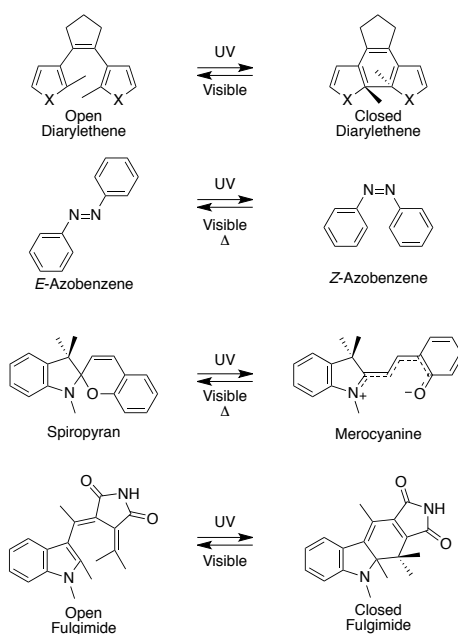
Figure 51. Main families of organic photochromic compounds and their isomerisation reactions.

In order to be integrated in optoelectronic devices, photochromic molecules need to fulfil some technical requirements:

1. Thermal stability of both isomers;
2. Low fatigue (possibility to be cycled many times without significant loss of performance);
3. High sensitivity and rapid response;
4. Non-destructive readout capability;
5. Sensitivity at diode laser wavelengths;
6. Reactivity in the solid state (polymer matrix or crystalline phase).

Among these requirements, the most important are thermal stability and fatigue resistance: dithienylethene derivatives stand out as a highly efficient class of reversible photochromes satisfying these requirements.

The molecule that inspired the development of photochromes of the dithienylethene family is stilbene. It is known to undergo a photocyclization reaction to produce dihydrophenantene,[121] which returns to stilbene in the dark in a deaerated solution. Unfortunately, in the presence of air dihydrophenantene converts irreversibly to phenantrene by hydrogen elimination. When methyl groups are introduced at the 2- and 6- position of the phenyl rings, the last reaction is suppressed but still the photogenerated cyclic form is unstable and quickly reverts to the open form.[122] In order to extend the lifetime of the closed form and render it thermally stable, phenyl rings can be replaced with heteroaromatic rings.[123] In fact, thermal stability of diarylethene photochromes depends on the aromatic stabilization energy: the destabilization resulting from the loss of aromaticity upon photocyclization is reflected in an increase in the ground-state energy of the closed form, which, in turn, results in thermal instability and tendency to re-open.[122] Heterocyclic aryl groups have low aromatic stabilization energies and can grant the stability of both isomers of diarylethene photochromic compounds. However, the thermal stability strictly depends on the type of heteoaryl groups: the closed form of compounds bearing furan, thiophene, selenophene or thiazole rings are stable and do not return to the open ring isomers even at 80°C.[124] On the other hand, compounds bearing pyrrole and indole rings are thermally unstable.[125] This is why thiophenes are very often chosen as heteroaromatic rings for photochromic molecules.

Diarylethenes with thiophenes as heteroaromatic aryl groups belong to the class of thermally stable (P-type) photochromic compounds. Anyways, it should be noticed that the presence of electron-withdrawing or bulky substituents on the thiophene rings can still decrease the thermal stability of the closed isomer by weakening the central carbon-carbon bond.[126]

To avoid cis-trans isomerisation of the double bond, different rigid groups, as maleic anhydride, maleimide or the most largely used perfluoroyclopentene can be inserted on the vinyl group of stilbene.[127] Perfuorocyclopentenes are used instead of simply cyclopentenes because the latter have inferior performances, such as minor fatigue resistance and spectral splitting of the two isomers.[128] Actually, the size of the perfluorinated cycloalkene can range from a four to a six-membered ring: the absorption maxima of the closed-ring isomers are shifted to longer wavelength upon decreasing the size of the ring, while the cyclization quantum yield increases if the size of the ring is extended.[129] Therefore, taking into account the two factors, the five-membered ring results the most appropriate cycloalkene structure.

Taken into account all the features needed to achieve a variety of well performing chromophores, we should also consider that all photochromic reactions, accompanied by definition by the rearrangement of chemical bonds, are vulnerable to undesirable side reactions: this limits the number of on-off cycles.

$$B' \xleftarrow{\Phi_S} A \underset{\lambda_2, \Phi_{B \to A}}{\overset{\lambda_1, \Phi_{A \to B}}{\rightleftarrows}} B$$
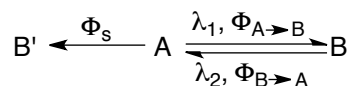
Even though the side reaction quantum yield Φ_S is 1% and B perfectly converts back to A, after 1000 cycles 63% of the initial product A will decompose.

Irie and co-workers managed to isolate the byproduct of the photochromic reaction of a dithienylethene compound (Figure 52).[130] They showed that it formed efficiently from the closed-ring form by UV irradiation.
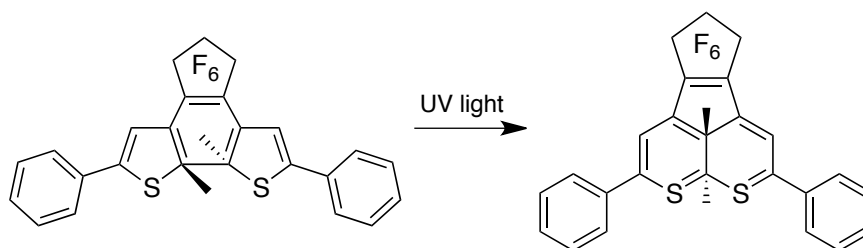
Figure 52. The formation reaction of the byproduct and its chemical structure.

In order to have photochromes with high sensitivity, high molar absorption coefficient and high cyclization quantum yields are required. Diarylethenes with five membered heterocyclic rings have two conformations: parallel, with the two rings in mirror symmetry, and antiparallel, with the two rings in C_2 symmetry (Figure 53).[122] Photocyclization reaction, according to Woodward-Hoffman rules,[131] can only proceed from the antiparallel conformation and, since the population of the two conformations is generally 1:1, cyclization quantum yield (Φ_{cy}) could not exceed 0.5.

Antiparallel   Parallel
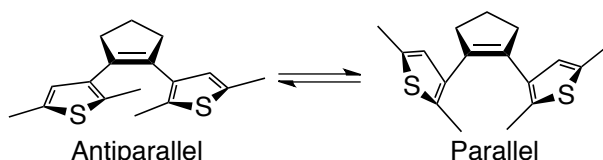
Figure 53. Parallel and antiparallel conformations of DTE.

The ratio of the antiparallel conformation should be augmented to increase Φ_{cy} and there are several methods to do so as introducing bulky substituents on the thiophene rings[126b] or incorporate dithienylethene into a polymer backbone.[132]

Of course, since one of the main interests of photochromic compounds is in their colour change, the absorption spectra of the open and closed form hold great importance. Despite the wide variety of existing DTE derivatives, their fundamental spectroscopic behaviour in solution can be described in general terms. The open-ring isomers absorb at shorter wavelengths, while upon irradiation with UV light, new absorption bands attributed to the closed-ring isomer appear at longer wavelengths. Most diarylethenes show very large spectral shifts upon photoisomerization from the open- to the closed-ring

isomers, because in the latter π-electrons delocalize throughout the two condensed thiophene rings.[133] Common features of the absorption spectrum of the ring open form are the thiophene n-π* and π-π* bands at around 300 nm. Irradiation into these bands using UV light results in photocyclization and consequent coloration of the solution due to the growth of the characteristic highly red-shifted [1]IL absorption band of the closed DTE moiety in the red visible region of the spectrum. The absorption wavelengths of the open and closed forms can be tuned by using different substituents on the thiophene rings and from the point of view of applications, especially to optical media, it is desired to develop photochromes with absorption in the range of 650-800 nm.[134]

With these principles in mind, several efficient organic photochromes with various applications have been synthesized.[134] We highlighted that diarylethene derivatives, to which we are most interested, fulfil all of the desired requirements and their properties can be summarized as follows:[135]

1. Both isomers are thermally stable: a well-designed derivative has a half-life time at room temperature as long as 470 000 years;

2. Coloration/decoloration cycles can be repeated more than 10^5 times;

3. The quantum yield of coloration is close to 100%;

4. Response times of both coloration and decoloration are less than 10 ps;

5. Many diarylethene derivatives undergo photochromic reactions even in single-crystalline phase.

In the following sections, we will provide a rapid overview on how DTE derivatives can be coordinated to metals giving complexes with remarkable photochromic properties.

4.2. Organometallic dithienylethene derivatives

Metal complexes whose active component is a DTE-derived molecular switch are quite common and have attracted the interest of chemists during the last decades.[136] The binding to a metal of a DTE fragment can modulate the electron transfer, fluorescence and NLO responses of the resulting switch.[137] A wide number of different metal centres (Fe, Ru, Os, Ir, Pd, Pt, Cu, Au, Re, W...) have been combined to DTE-based ligands, mostly by using the DTE fragment as a substituent on a classic pyridyl or polipyridyl ligand, and the effect of such combination have been studied.[138] Interestingly, in some cases photochemical reactions can be triggered by irradiation in the [1]MLCT band of the metal moiety.[139] The [3]MLCT state is thus populated by intersystem crossing and it undergoes internal conversion to the excited [3]IL based on the DTE fragment that subsequently closes. This process can take place because the [3]MLCT state lies at approximately the same or slightly higher energy than the [3]IL state, otherwise internal conversion would not be possible. It is relevant to notice than the closure of the DTE involves the quenching of the emission of the complexes.

This led to the idea of using DTE-substituted metal complexes as on-off luminescent switches, in which only one of the two forms, open or closed, is emissive.[140]

In the following sections, we will focus on the photophysical properties of platinum complexes bearing a DTE fragment and their ability to switch from the open to the close form.

4.2.1. Platinum complexes bearing a DTE-derived ligand

As we discussed in sections 2 and 3, platinum complexes possess superior photophysical properties and find a wide range of applications.[3-7] By combining an emissive platinum centre with a DTE-based ligand and by associating their photoluminescence properties, chemists envisaged to obtain sensitive and efficient photoswitches resulting in multifunctional materials. Also, perturbations caused by a simple change in the metal centre would help to directly influence the photochromic behaviour of dithienylethenes and help to tune it in the desired way.

4.2.1.1.   DTE-functionnalized pyridyl ligands

By using the same method exploited in the synthesis of a previously cited rhenium complex,[139b] Yam et al. synthesized the first platinum complex bearing a DTE fragment:[141] the photochrome is directly linked to the bipydiryl ligand. They observed that photocyclization, characterized by the growing of an absorption band centred around 550 nm, can be triggered by excitation both in the IL band (based on the photochrome) and MLCT absorption bands and is fully reversible. They explained this phenomenon by a rapid internal conversion from the ^{3}MLCT/LLCT state to the ^{3}IL state and, since the photocyclization quantum yield is the same by irradiating in any of the two bands, they assumed that this energy transfer is very efficient (Figure 54). They also noticed that the open complex is luminescent in dichloromethane solution and at 77 K by irradiation in the MLCT band, but the emission quantum yield is quite low. This can be ascribed to the presence of the intramolecular energy transfer to the ^{3}IL band followed by quenching by photocyclization. The closed form is emissive too, but at slightly longer wavelengths: due to the similarity with the emission of the bipyridyl ligand alone, the ^{3}IL excited state is considered responsible for the emission.
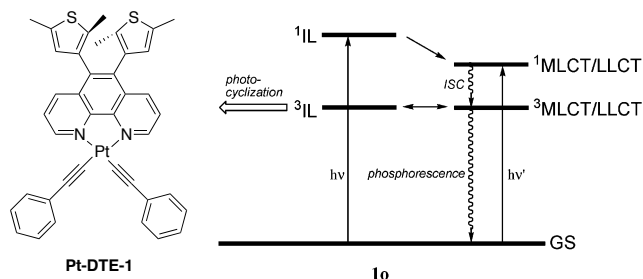
Figure 54. The complex studied by Yam and a qualitative energy diagram of its excited states.

Similar properties were reported for a series of alkynyl platinum complexes bearing DTE-functionalized 2-(2'-pyridyl)imidazole or 2-(2'-thienyl)pyridyl) ligands, with minor variations of absorption and

emission energies according to the substituents on the ligands.[142] Interestingly, if the DTE fragment is on a 2-(2'-thienothienyl)pyridyl ligand, any or little photochromism is observed.[142a]

Recently, Gamez et al. reported a *trans*-[Pt$_2$(pyridyl)Cl$_4$(DMSO)$_2$] complex with a DTE fragment on the pyridyl ligand possessing photochromic properties and emissive in the open form.[143] The two photoisomers interact differently with DNA duplex and exhibit a different cytotoxic behaviour against various cancer cell lines: this properties render them suitable for applications in photoactivated chemotherapy.

4.2.1.2. *DTE-functionnalized alkynyl ligands*

Alkynyls are classical ligands for platinum complexes and can be easily functionnalized with different substituents through coupling reactions.

The first platinum complex with DTE-functionnalized alkynyl ligands was a cyclic macromolecule incorporating four DTE units and two platinum moieties.[144] Upon irradiation with UV light, two of the four DTE units could close with a total cyclization quantum yield of 0.64.

Some complexes bearing a central DTE units substituted with two alkynes linked to a corresponding platinum centres have also been studied. Raithby et al. reported a symmetrical DTE[(C≡C)Pt(PEt$_3$)$_2$] that can undergo reversible photocyclization by irradiation with UV or visible light both in the crystal form or in solution.[145] The group of Guerchais synthesized two binuclear platinum complexes linked either on the reactive carbon atoms or on the lateral non-reactive carbon atoms of the photochrome (Figure 55).[146]
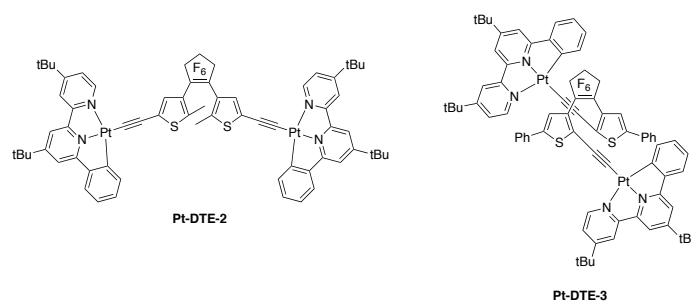
Figure 55. The complexes studied by the group of Guerchais.

Complex **Pt-DTE-2** can easily undergo photocyclization, even if it was proved that only a small amount of antiparallel form is present in solution. Anyway, the closed form is more stable and the triplet sensitization pathway allows a barrierless ring closing. On the other hand, even though the most stable form of **Pt-DTE-3** in solution is the antiparallel, photocyclization does not occur. This is due to the fact that the closed form is less stable and a high energy barrier should be overcome both in the singlet and triplet sensitization pathway to obtain it. The emission behaviour is also the opposite for the two

complexes: while **Pt-DTE-2** is not emissive because of the competitive ring-closing, **Pt-DTE-3** is emissive as an intramolecular excimer.

Several examples of platinum complexes linked to two DTE fragments through alkynyl bridges have also been reported. The group of Wolf synthesized a platinum bis-DTE complex (Figure 56, left) in which both photochromes can photocyclize by exploiting the fact that ligand-localized triplet states can be populated by excitation with visible light and trigger the cyclization of both DTE photoswitches without the transfer of the excited-state energy of the ring-open DTE to the adjacent ring-closed DTE.[147] This is possible thanks to the presence of the metal. Without it, the triplet states are not accessible and electron transfer from the open to the closed DTE prevents the closing of the first one.
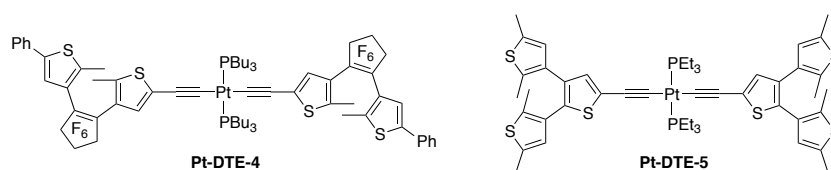
Figure 56. The complexes studied by the group of Wolf (left) and Yam (right).

The group of Yam compared the properties of analogue complexes substituted with one or two DTE units (Figure 56, right).[148] The complexes are all emissive in solution at 298 K and 77 K, in the solid state at 77 K and show photochromism. Nevertheless, **Pt-DTE-5** does not undergo dual photochromism, because of electron transfer from the open to the closed DTE: it has thus a different behaviour from the complex studied by Wolf.

The group of Chen studied a series of symmetric and asymmetric Pt complexes bearing DTE substituents linked through alkynyl ligands.[149] They noticed that the ability to undergo single of double photocyclization, and also the photocyclization quantum yield, depend strongly on the design of the molecule and on the substituents on the DTE fragments. In some cases, by following the ring-closing reaction by UV, a red-shift of the absorption band attributed to the photochrome can be remarked when the second unit starts to close. This is ascribed to the more extended π-conjugation of the molecule upon ring-closure. In particular, they found that in an asymmetrically substituted complex the closing and opening of only one of the two DTE units could be triggered by selectively choosing the wavelength at which irradiate a solution of the complex.

Wolf et al. also studied the effect of using a different linker between the platinum centre and the DTE unit (Figure 57).[150]
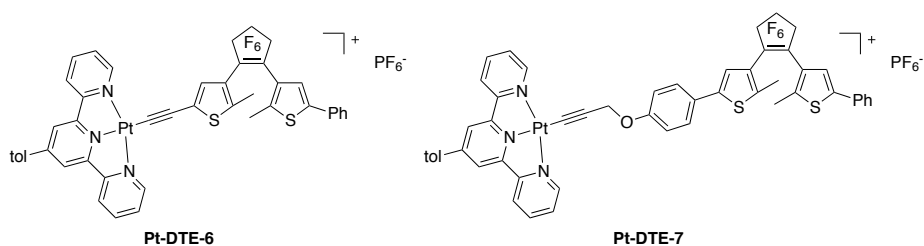
Figure 57. The complexes with different linkers between the platinum moiety and the DTE studied by Wolf et al.

Complex **Pt-DTE-6** shows photochromism even if irradiated in the MLCT/LLCT absorption bands in the visible, while the process is less efficient for **Pt-DTE-7**. The longer, non-conjugated tether inhibits sensitized ring closing, and the DTE is converted into its cyclized isomer only when directly irradiated with UV light: the thienyl-based molecular orbitals do not participate in the MLCT/LLCT transitions anymore. On the other hand, this allows emission of **Pt-DTE-7** from the ^{3}MLCT/LLCT excited states, while emission is quenched by DTE ring-closing in **Pt-DTE-6**.

All of these studies highlight the necessity for the metal and the DTE units to be linked with π-conjugated linkers and in a correct fashion for energy transfer to occur. Minor differences in the geometry of the complexes or in the ligands' structures allow relatively facile tuning of the photochromic properties of these complexes.

Recently, Yam and co-workers synthesized some mononuclear N^C^N 1,3-bis(*N*-alkylbenzimidazol-2′-yl)benzene platinum complex bearing an DTE group on the alkynyl co-ligand.[151] The complexes are emissive form the ^{3}IL excited state centred on the N^C^N ligand, probably mixed with ^{3}MLCT upon irradiation in the MCLT/LLCT absorption band. They show photochromic behaviour upon excitation in the visible with the appearance of an isosbestic point in the absorption spectrum and a new absorption band at longer wavelength assigned to the closed DTE. Upon photoexcitation at the isosbestic wavelength, the emission intensity decreases. This can be attributed to the quenching of the emissive excited state via energy transfer processes to the closed DTE fragment.

4.3. Tuning the emission of DTE-dipyridilbenzene Pt(dpyb) complexes

So far, there are no reports of platinum(II) dipyridylbenzene complexes bearing DTE substituents. Since, as previously discussed, they represent a class of bright luminophores with tunable emission wavelength, we decided to combine their optical properties with the photochtomic performances of diarylethenes.

We thus synthesized and studied two Pt(dpyb)Cl complexes bearing on the position 4 of the central phenyl ring a DTE fragment linked by different spacers to the N^C^N Pt centre (Figure 58): **Pt-DTE** and **Pt-O-DTE**. It would have been interesting to compare their properties to those of **Pt-alk-DTE**, but we could not manage to achieve it. Instead, we only obtained the corresponding DTE-alk-dpybH ligand, which will be briefly presented.

In the following paragraphs, we will present the luminescent and photochromic properties of the complexes and the influence of the different connectors on them.
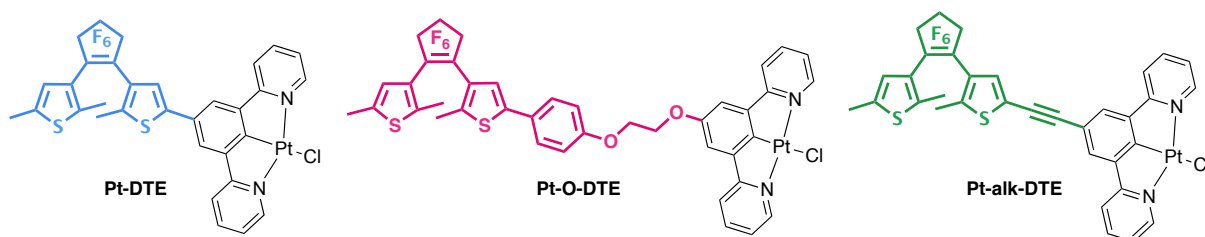
Figure 58. The three new Pt(dpyb)Cl complexes with a DTE fragment.

4.3.1. Preparation and characterization of the Pt-DTE complexes

Detailed synthetic procedures will be described in Chapter III. Complex **Pt-DTE** was synthesized by H. Zhao, a master student in Rennes, and it synthesis will not be reported in details here.

To prepare the **DTE-dpybH** ligand, we started by synthesizing dpybH by classical methods,[32] by selective Stille cross-coupling between 2-(tri-*n*-butylstannyl)pyridine and two brominated positions of 1,3,5-tribromobenzene. The remaining bromine atom on the phenyl ring was converted in a boronic group to be linked through a Suzuki cross-coupling with the appropriate bromo-DTE precursor, to obtain thus DTE-dpybH (Figure 59a).

The **DTE-O-dpybH** ligand was prepared starting by the dpybH fragment: the 4-OH substituted dpybH was synthesized by Stille coupling between 2-(tri-*n*-butylstannyl)pyridine and 3,5-dibromophenol.[58] The ethylene glycol chain was added by nucleophilic substitution of the phenolic OH group with a 2-hydroxyethyltosilate. The DTE fragment was linked by a nucleophilic substitution of the phenolic function on its phenyl group with the oxyethyltosylate-functionalized dpybH (Figure 59b).

The **DTE-alk-dpybH** ligand was prepared by Sonogashira coupling between 4-bromo-2,6-dipyridylbenzene obtained as described above and the appropriate alkynyl-DTE precursor (Figure 59c).
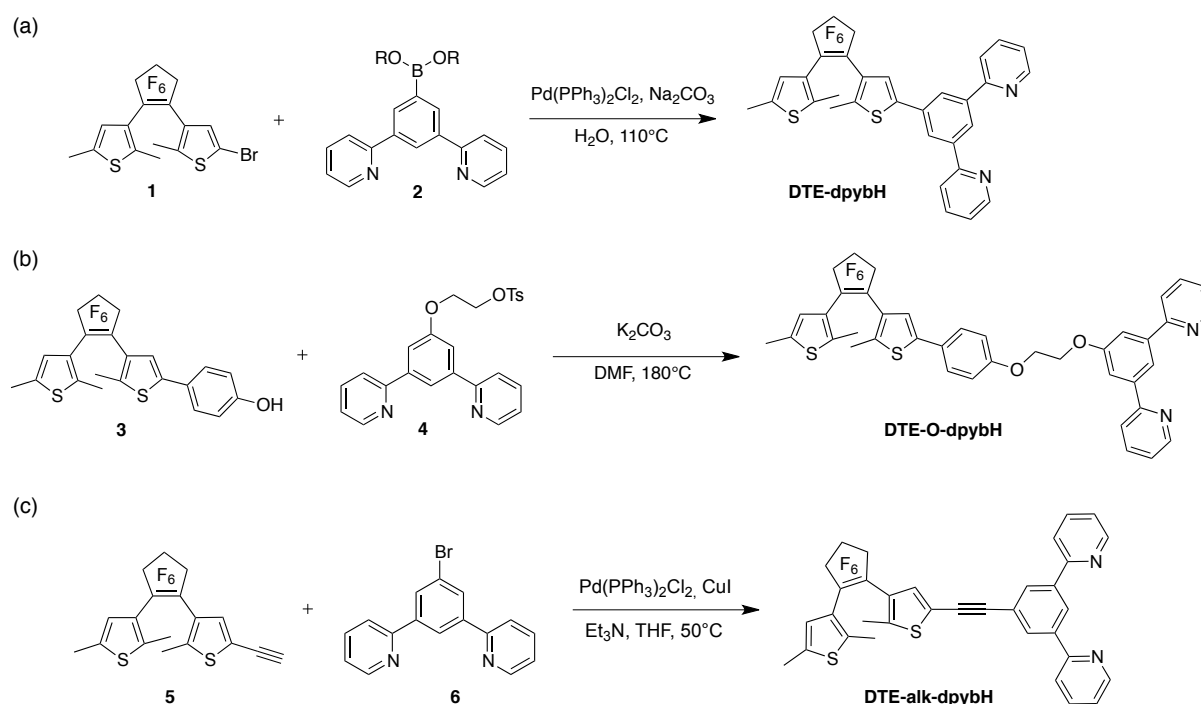
Figure 59. Synthetic routes for ligands (a) **DTE-dpybH**, (b) **DTE-O-dpybH** and (c) **DTE-alk-dpybH**.

The cyclometalated platinum(II) complexes **Pt-DTE** and **Pt-O-DTE**, were prepared upon reaction of the appropriate ligand with K_2PtCl_4 in an AcOH:H_2O mixture (3:1 *v/v*) at reflux.[32] The complexes were isolated by filtration and dried in vacuo. Ligands and complexes were fully characterized by ^{1}H and ^{13}C NMR, elemental analysis and mass spectroscopies.

The open and closed forms of the ligands and complexes bearing the DTE photochromic unit will be denoted as open **(o)** and closed **(c)**.

Single crystals of **Pt-DTE(o)** were grown at room temperature by slow diffusion of diethyl ether vapour into concentrated dichloromethane solution of the open complex (Figure 60, left), while crystals of **Pt-DTE(c)** were obtained in similar conditions, from a concentrated solution of **Pt-DTE** at the photostationary state (Figure 60, right). Unfortunately, it was not possible to obtain crystals of neither the open or closed forms of **Pt-O-DTE**.

Crystallographic data of closed dithienylethenes are rare: up to now only one example of closed DTE-functionalized platinum complex has been described[145] and no examples of crystals of cyclometalated platinum complex containing a closed DTE fragment are reported to date.
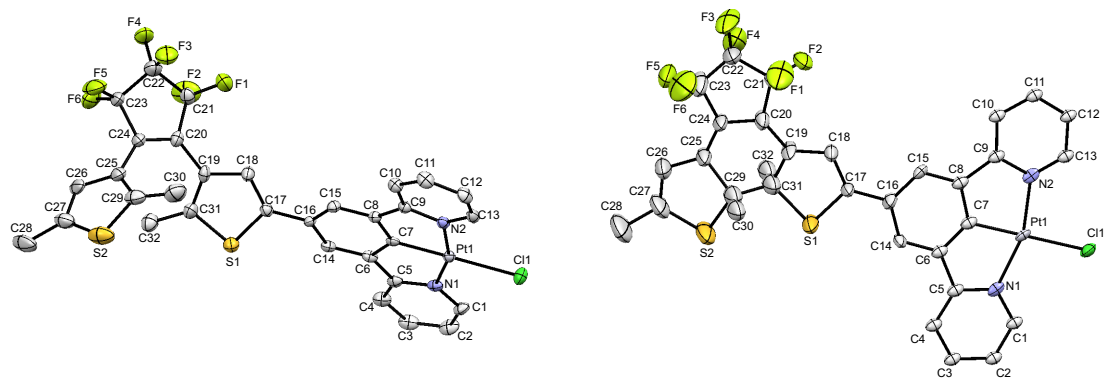
Figure 60. ORTEP view of **Pt-DTE(o)** (left) and **Pt-DTE(c)** (right). Thermal ellipsoids are shown at the 50 % probability level.

In **Pt-DTE(o)**, the cyclometalated dipyridylbenzene displays typical distorted square-planar geometry with an N-Pt-N angle of 161.01(18)°, consistent with the structures previously reported for complexes of the same family.[32] The dithienylethene typical bond metrics for an "open form" are shown with C20 – C24 and C20 – C19 distances of 1.359 and 1.462 Å, characteristic of carbon - carbon double and single bond distances respectively. The open dithienylethene moiety adopts the anti-parallel configuration suitable for photocyclization, with a C31 – C29 through space distance of 3.569 Å. In reason of a twist angle (C18 – C17 – C16 – C15) of 37.03° between the thiophene and the central phenyl ring, only a weak electronic delocalization is expected between the DTE and the dipyridylbenzene moieties, due to a poor orbital overlap. This can be ascribed to repulsive interactions between protons on C18 and C14/C15.

Photo-isomerization of the DTE unit in **Pt-DTE(c)** does not affect the geometry of the Pt(dpyb)Cl fragment: the distorted square-planar geometry similar to that of **PtDTE(o)** is maintained. The major change in the structure is the new bond between C29 and C31 with a distance of 1.402 Å typical of a carbon - carbon single bond. Consequently to the rearrangement of the π-system upon ring-closure, the bonds between C24 – C20 (1.415 Å) and C20 – C19 (1.355 Å) are now single and double bonds, respectively. The relative position of the DTE unit and the cyclometalated pincer was also affected: they twist angle became almost planar (C18 –C17 –C16 –C15) of 6.7° with an evident bending of the molecule, suggesting that now the π-delocalization over the complex is more efficient.

Analysis of the crystal packing for **Pt-DTE(o)** and **Pt-DTE(c)** revealed a comparable offset head-to-tail arrangement. The molecules are organized in columnar arrangements of cyclometalated Pt centers assembled through Pt–Pt and π–π interactions (Figure 61). The DTE moieties do not significantly participate in the columnar stacking: hence, similar packing distances were observed for the open and the closed isomer (between 3.448 and 3.365 Å for **Pt-DTE(o)** and 3.227 and 3.263 for **Pt-DTE(c)**).
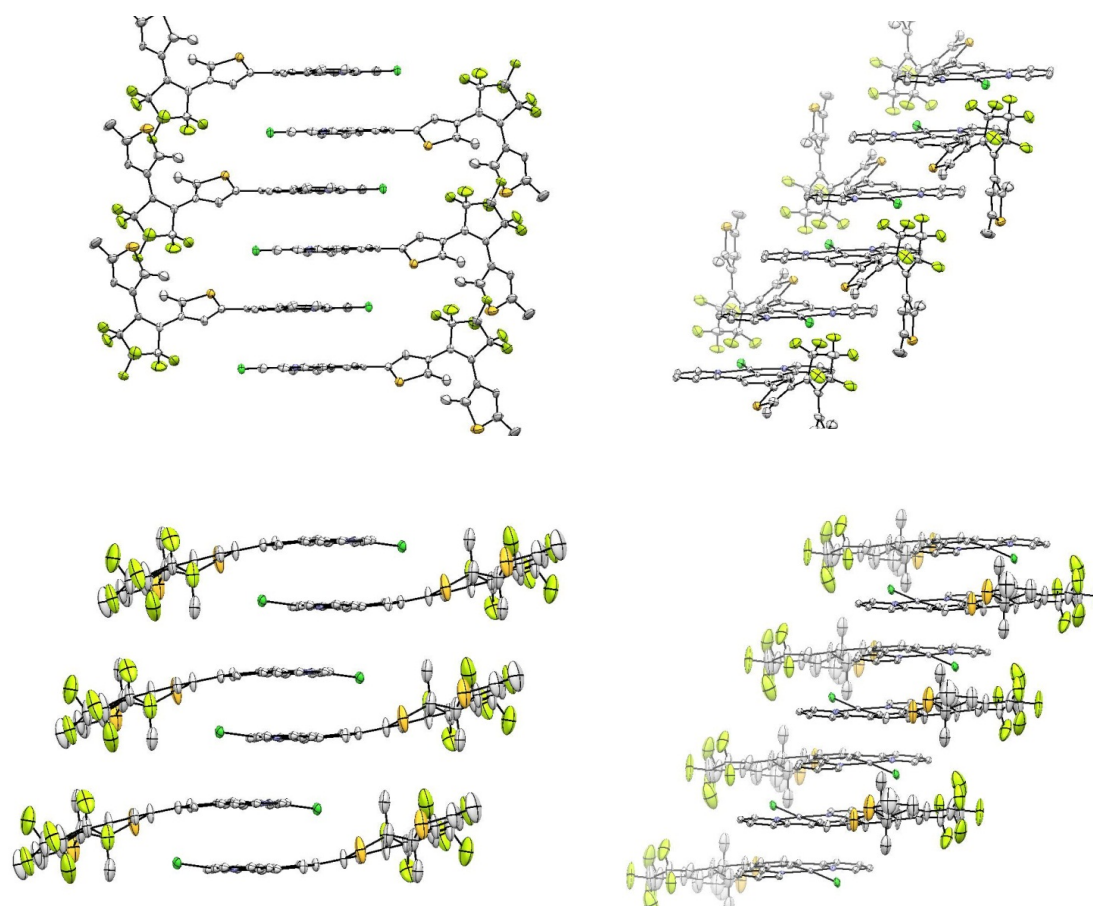
Figure 61. ORTEP view of the crystal packing of **Pt-DTE(o)** (top) and **Pt-DTE(c)** (bottom). Thermal ellipsoids are shown at the 50 % probability level.

4.3.2. Photophysical properties in solution: experimental and theoretical

The photophysical properties of the complexes were studied at room temperature in a dichloromethane solution.

The steady-state absorption spectra of the complexes measured in CH_2Cl_2 at 298 K are presented in Figure 62 whereas the photophysical data are summarized in Table 4.

The electronic absorption spectra of **Pt-DTE(o)** and **Pt-O-DTE(o)** show intense absorption bands in the UV region, between 270 and 350 nm, assigned to ligand centred $^1(\pi\text{-}\pi^*)$ transitions of the dpyb ligand and to additional $^1(\pi\text{-}\pi^*)$ transitions belonging to the photochromes, responsible for the high absorptivity. The weaker absorption bands in the visible part of the spectrum, from 400 to 480 nm, are attributed to mixed MLCT/LLCT transitions from the platinum centre and the chloride to the pyridine of the dpyb ligand (d(Pt)/np(Cl) $\rightarrow \pi^*$(dpyb)), typical of this family of complexes.[32] The lowest-energy absorption bands of **Pt-DTE** are slightly blue-shifted compared to the reported (4-(2-thienyl)-1,3-dibromobenzene)PtCl complex,[32] probably because of the electron-withdrawing effect on of perfluorocyclopentene moiety. Absorption features of **Pt-O-DTE(o)** are in agreement with the reported

4-(methoxy-dpyb)PtCl complex,[58] according to the presence of the ethylene glycol bridge between the DTE and the Pt(dpyb) centre.
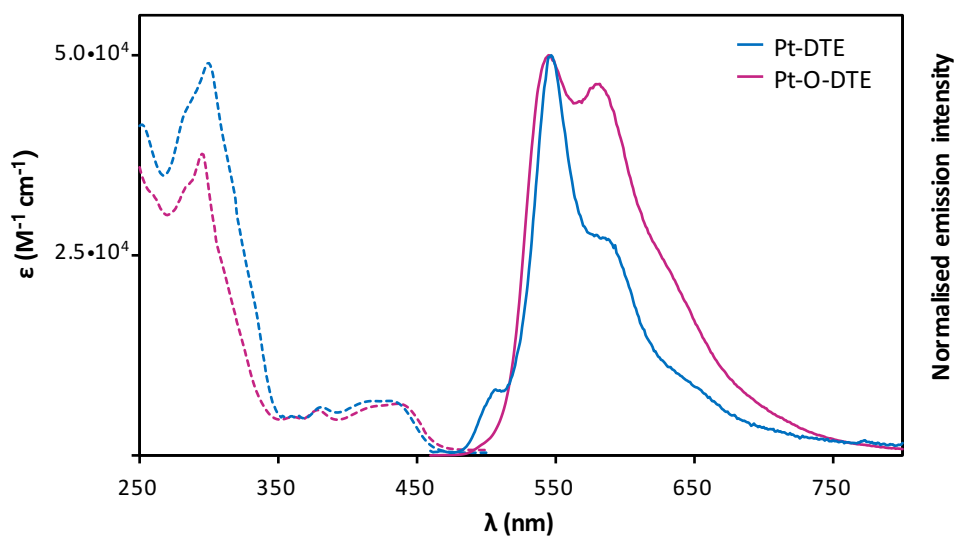
Figure 62. Absorption (dashed line) and emission (plain lines) spectra of the opened forms of **Pt-DTE** and **Pt-O-DTE** ($\sim 10^{-6}$ M, λ_{exc} = 440 nm).

Room temperature emission measurements were performed in degassed dichloromethane solution at a concentration of about 10^{-6} M, in order to exclude excimeric emission.

Pt-DTE(o) and **Pt-O-DTE(o)** (Figure 62), emit in the green region of the spectrum: the emission is centred at 560 nm. The structured band with a vibrational spacing of about 1300 cm^{-1} is typical of a ^{3}LC emission with a small contribution from the metal, as previously reported for the parent Pt(dpyb)Cl complexes (see section 2.2.1). The emission lifetimes in the order of μs confirm that the emission originates from a triplet state.

Complex	λ_{abs} / nm ($\varepsilon \times 10^3$ / M^{-1}cm^{-1})[a]	λ_{em}/nm[b]	τ/μs[b]
Pt-DTE	300 (48.8), 382 (5.9), 418 (6.7), 432 (6.6)	547, 588, 655 sh	6.1 (547 nm)
Pt-O-DTE	296 (40.8), 379 (6.0), 420 (6.4), 437 (6.5)	545, 578	7.0 (545 nm)

Table 4. Photophysical data for complexes **Pt-DTE** and **Pt-O-DTE**. [a] In CH$_2$Cl$_2$ solution (10^{-5} M) at 298 K. [b] In degassed CH$_2$Cl$_2$ solution (10^{-5} M) at 298 K, λ_{ex} = 440 nm.

The open forms of the complexes are weakly luminescent in these conditions: as stated above, DTE-based platinum(II) complexes are subject to metal-sensitized DTE ring-closure reaction which compete with the complex luminescence. For this reason, it has no sense to register a luminescence quantum

yield for these complexes. Luminescence arises from the little amount of open form present in solution that is not subject to DTE ring-closure quenching. Even though a Φ_{lum} value was given, it would be unreliable because referred not to the 100% of the molecules in solution, but only to the small quantity of open molecules left.

The luminescence at 77 K in EPA matrix (diethyl ether/isopentane/ethanol: 2/2/1) was also investigated (Figure 63). Complexes **Pt-DTE** and **Pt-O-DTE** display similar structured profiles with typical vibrational spacing of about 1450 cm^{-1}: the photocyclization reaction does not occur in a rigid matrix at low temperature. The highest energy emission band (0-0 transition) of complex **Pt-DTE** lies at longer wavelengths than **Pt-O-DTE**. This effect is attributed to the diminished electron-donating strength of perfluorothiophene in **Pt-DTE** respect to the ethoxy chain in **Pt-O-DTE**.
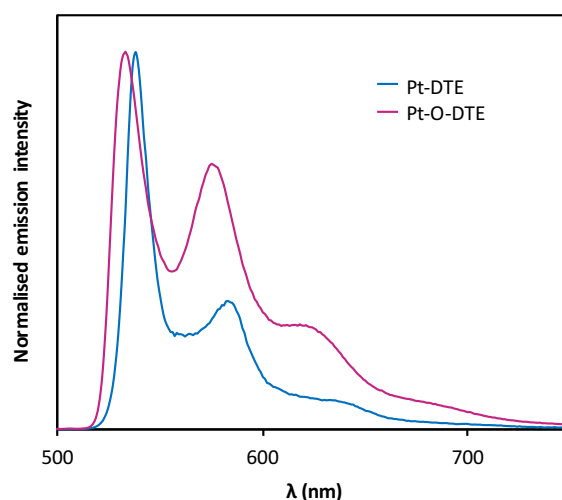
Figure 63. Emission spectra of **Pt-DTE** and **Pt-O-DTE** in EPA (diethyl ether/isopentane/ethanol: 2/2/1) glass at 77 K (λ_{ex} = 440 nm).

4.3.3. Photochromic behaviour in solution

The photocyclization reactions were conducted in airtight cuvettes to avoid solvent evaporation during light irradiations. The cyclization and the cycloreversion reactions were triggered by 350 nm (or 450 nm) and 580 nm excitation wavelengths, respectively.

UV-visible absorption was used as a first technique to monitor the ring closing and opening reactions of the DTE unit.
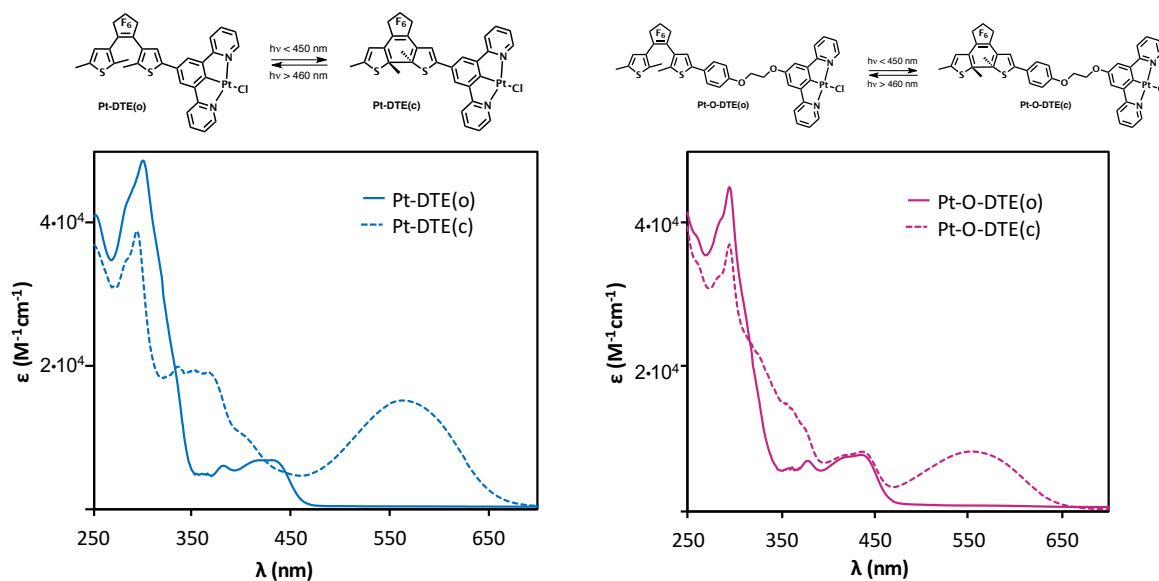
Figure 64. Absorption spectra of a) **Pt-DTE** and b) **Pt-O-DTE**, before (plain lines) and after (dashed lines) irradiation at 350 nm (CH$_2$Cl$_2$, 298 K, C ≈ 10^{-5} M).

A solution of **Pt-DTE(o)** is initially yellow, but it turns dark blue upon irradiation at 350 nm. The colour change is accompanied by the appearance of a broad absorption band in the visible, centred at 567 nm, attributed to ^{1}IL transitions of the closed DTE unit (Figure 64a).[134] Irradiation of **Pt-DTE(c)** in the visible absorption band at 580 nm recovers quantitatively the open form showing the good reversibility of this system. Interestingly, the absorption bands attributed to charge-transfer transitions in **Pt-DTE(o)** are altered upon ring-closure reaction: they are red-shifted and become overlapped with the broad band in the visible. This can mean that the rigid π-conjugated bridge in **Pt-DTE** promotes the electronic coupling required for energy transfer between adjacent ^{3}IL states on the DTE and ^{3}MLCT/LLCT states on the Pt(dpyb)Cl unit, as already foreseen with the crystallographic data.

Pt-O-DTE exhibits similar absorption spectral changes upon UV irradiation, with the appearance of the broad DTE closed absorption centred at 551 nm (Figure 64b) and a solution colour change from yellow to violet. The PSS is reached after 30 miutes of irradiation. As for complex **Pt-DTE**, the open from **Pt-O-DTE** can be fully re-obtained upon 580 nm irradiation. In this case the absorption bands attributed to CT transitions are not shifted upon ring-closure, demonstrating the effectiveness of the ethylene glycol bridge in inhibiting ground-state electronic communication between the DTE moiety and the Pt(dpyb)Cl fragment.

The ligand **DTE-alk-dpybH** also undergoes reversible spectral changes upon irradiation at 320 nm for ring closing and 580 nm for ring opening (Figure 65). In this case, the PSS is reached after 105 minutes of irradiation, the triple of time needed for the complexes discussed above. This can suggest that the presence of the metal favours the photocyclization reaction and makes it faster.
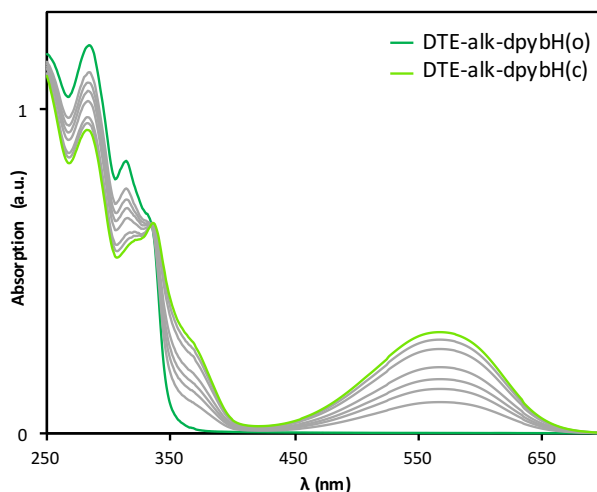
Figure 65. Absorption spectral changes of **DTE-alk-dpybH** upon irradiation at 320 nm (CH$_2$Cl$_2$, 298 K, C ≈ 10^{-5} M).

The percentage of conversion at the PSS state can be calculated by following the photocyclization reaction by ^{1}H-NMR.

After irradiation at 350 nm, both **Pt-DTE** and **Pt-O-DTE** show characteristic spectral evolution due to photocyclization (Figures 66, 67). The singlets corresponding to the thienyl protons are typically upfield shifted (**Pt-DTE**: from 7.36 to 6.80 ppm and from 6.77 to 6.06 ppm; **Pt-O-DTE**: from 7.17 to 6.57 ppm and from 6.74 to 6.04 ppm) and at the same time the singlets corresponding to the methyl protons nearest to the newly formed DTE C-C bond are downfield shifted (**Pt-DTE**: from 1.91 and 1.94 to 2.14 and 2.16 ppm; **Pt-O-DTE**: from 1.87 and 1.91 to 2.10). On the other hand, the singlet corresponding to the methyl protons further to the DTE C-C bond are upfield shifted and, in the case of **Pt-O-DTE** they merge with the singlet corresponding to the other methyl groups (**Pt-DTE**: from 2.44 to 2.23 ppm; **Pt-O-DTE**: from 2.41 to 2.10). The relative integration of the methyl and thienyl signals showed that both **Pt-DTE** and **Pt-O-DTE** reached almost quantitative open → closed photo-conversion at the PSS (higher than 95%).

Interestingly, the coordinated platinum atom seems to impart stability to the photochrome: the ligand **DTE-dpybH** attains only 50% of photo-conversion before degradation under similar irradiation conditions, **DTE-O-dpybH** too shows lower photochromic stability (≈ 30% conversion) than its complex analogue and **Pt-alk-DTE** reaches only ≈ 17% of conversion (Figure 68).
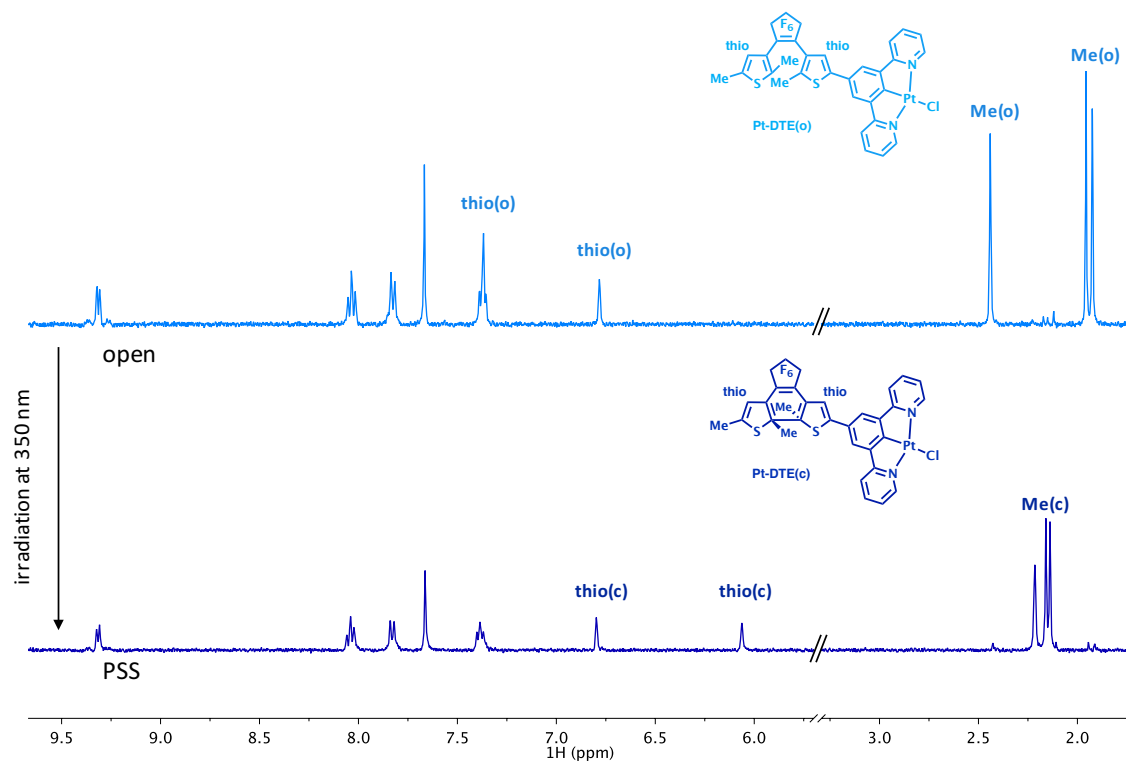
Figure 66. Partial ^{1}HNMR spectra of **Pt-DTE** in CD$_2$Cl$_2$, before (top) and after (bottom) irradiation at 350 nm.
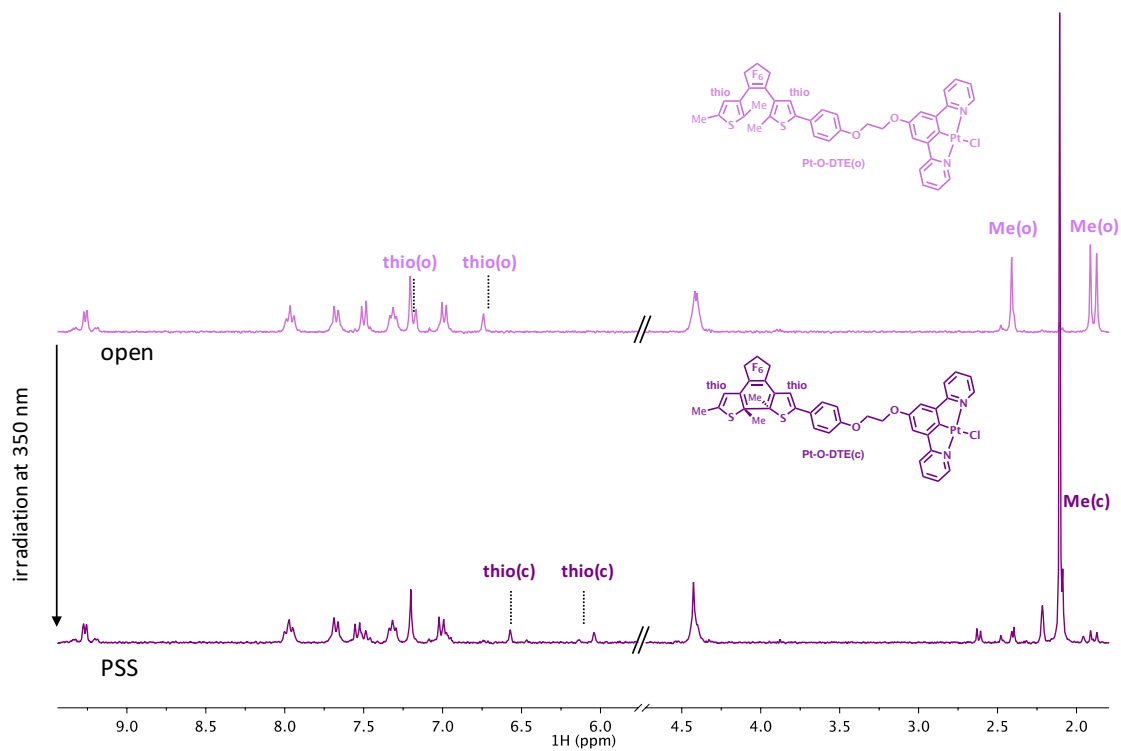
Figure 67. Partial ^{1}HNMR spectra of **Pt-O-DTE** in CD$_2$Cl$_2$, before (top) and after (bottom) irradiation at 350 nm.
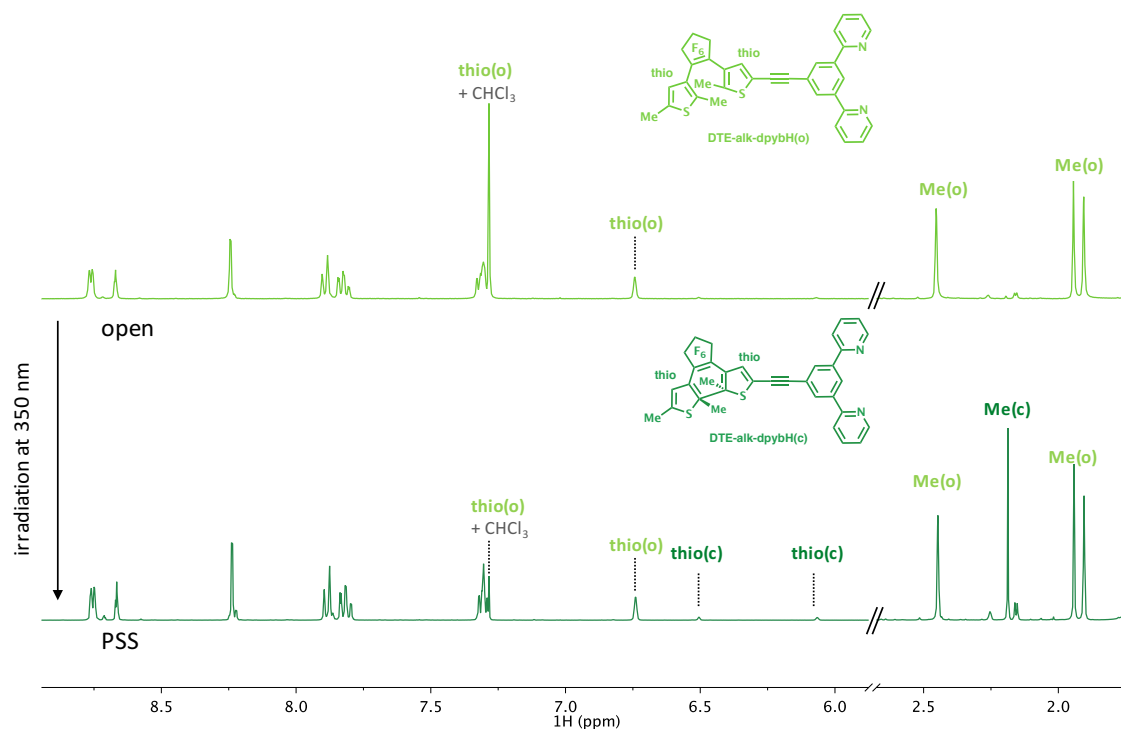
Figure 68. Partial ^{1}HNMR spectra of **Pt-alk-DTE** in CDCl$_3$, before (top) and after (bottom) irradiation at 350 nm.

Upon selective irradiation in the MLCT/LLCT absorption band of the complexes at 450 nm, both **Pt-DTE** and **Pt-O-DTE** show conversions almost as high as with 350 nm excitation (≈ 95%). The DTE ring-closure sensitization upon selective excitation of the charge transfer transitions has been previously observed for DTE-based Pt(trpy) acetylide analogues: ring closing occurs by energy transfer from a triplet charge-transfer state involving the metal to a localized triplet intraligand state on the DTE.[150] However, it was previously demonstrated by Branda et al. that introduction of a long non-conjugated linker between the DTE and the platinum fragments prevents sensitized ring-closing upon irradiation into the CT band.[150b] In our case it looks like that even though the platinum centre and the DTE units are linked by a non π-conjugated bridge, some electronic communication still exists between them.

The photocyclization phenomenon was also studied in relation to changes in the emission by variating the temperature (Figure 69). As discussed above, both complexes are emissive at 77 K because the low temperature prevents ring closing, while they are only weakly emissive at room temperature in solution. By slowly increasing the temperature from 85 K to 250 K, progressive decrease of the luminescence intensity was observed. The structured emission of **Pt-DTE** becomes less intense by warming the sample, until complete quenching occurs at 155 K. A similar behaviour was observed for **Pt-O-DTE**, but its emission was quenched only at 250 K, a higher temperature respect to those at which **Pt-DTE** becomes not emissive. Similar emission changes have been reported for a related photochromic Pt(trpy) acetylide complex.[150b] The different temperature at which emission is quenched can be tentatively related to the different binding mode of the DTE to the platinum moiety in the two complexes.

A rigid π-conjugated bridge as the triple bond allows better communication between the metal and the photochrome: in such way the energy transfer to the DTE upon irradiation in the CT band is more effective and emission is quenched already at lower temperature. On the other hand, a flexible and not π-conjugated linker makes the electronic communication between the two moieties less easy and emission is maintained even at higher temperature.
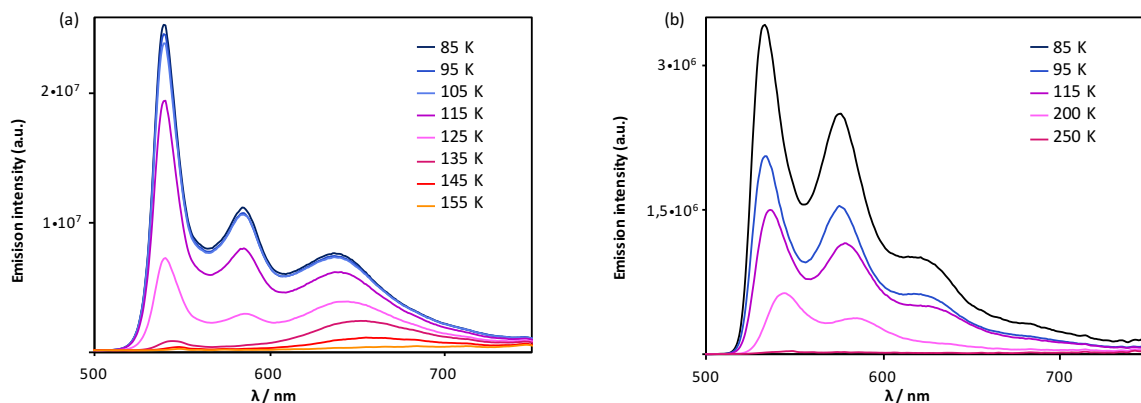
Figure 69. Emission spectra in degassed EtOH/MeOH 4:1 mixture of a) **Pt-DTE**, b) **Pt-O-DTE** by raising the temperature from 85 to 250 K (λ_{ex} = 440 nm).

The complete conversion to the non-emissive close form of both complexes is in contrast with the fact that at room temperature a residual emission due to the presence of a small amount of open DTE at the PSS is detectable. It was already reported that the efficiency of photocyclization and photocycloreversion reactions in some photochromic compounds can vary according to the temperature.[152] Lowering the temperature was found to affect the height of the thermal activation barriers, inhibiting the ring-opening or closing process while the reverse reaction remained almost unaffected. In our case, it is evident that ring-opening reaction is suppressed below 130 K for both complexes while photocyclization can still occur. This process leads to an accumulation of the closed isomer, which brings to full conversion when the temperature is increased. On the contrary, by recording the emission spectrum directly at room temperature, where no high energy barriers prevent photocycloreversion, there is still a possible presence of a small amount of open isomer even at the PSS, which leads to a weak but detectable residual phosphorescence.

These observations demonstrate that the temperature dependent photochromic reactivity of the DTE fragment can be employed to thermally control the luminescent behaviour of the DTE-based platinum complexes under exam.

4.3.4. Conclusion

In summary, two platinum(dipyridylbenzene) complexes bearing a photochromic dithienylethene fragment have been successfully designed, synthesized and studied.
Both complexes show photochromic behaviour in absorption in solution with almost quantitative conversion from the open to the closed form upon irradiation. These properties are superior to those of the corresponding ligands. ^{1}H-NMR spectroscopy revealed to be a useful technique to establish the percentage of conversion at the photostationary state.

The complexes are scarcely emissive in solution because the photocyclization reaction of the DTE fragment effectively quenches the fluorescence. Nevertheless, emission at low temperature (77 K) could be easily detected and emission studies by warming the sample demonstrated that the presence of different linkers between the platinum and the DTE moieties has an influence on the photochromic properties of the complexes.

The tunable second-order nonlinear optical properties of complexes **Pt-DTE** and **Pt-O-DTE** will be discussed in the following chapter.

5. Luminescent iridium cationic complexes

In recent years, attention on photoactive iridium(III) complexes grew exponentially, due to their remarkable luminescent properties that allow, for example, applications in OLEDs,[153] as dyes in solar cells,[154] in bioimaging[155] and photocatalysis.[156] Charged iridium(III) complexes have attractive properties, respect to the neutral. Their ionic nature, good solubility, ease of molecular design, synthesis and purification allow numerous applications, among which their use in LEECs, that require the presence of a charged chromophore.[157]

5.1. $[Ir(ppy)_2(bpy)]^+$ complexes

$[Ir(ppy)_2(bpy)]^+$ complexes, in which the Ir^{III} centre is coordinated by two cyclometalated 2-phenylpyridine ligands and by a 2,2'-bipyridine ligand, have had a great success as luminophores in electroluminescent devices and thanks to this they are among the most studied cationic platinum luminophores. Their design has mostly been optimized for their applications in LEECs, in fact they are usually synthesized as PF_6^- salts, because Cl^- counterions, naturally present after synthesis, impact negatively on the performances of the devices for which these complexes are designed.[158]

The archetipal $[Ir(ppy)_2(bpy)]PF_6$ complex was synthesized and studied by Güdel et al. in 1993 (Figure 70, left).[159] They found that at room temperature the emission spectrum consisted in a broad structureless band centred at 585 nm, assigned to emission from a $(Ir \rightarrow bpy)$ ^{3}MLCT state. Subsequent studies of complexes belonging to the same family were meant to further investigate absorption and emission properties. Serroni et al. investigated similar $[Ir(ppy)_2(bpy)]PF_6$ complexes and assigned the absorption bands under 270 nm to LC transitions of the phenylpyridine, bands between 270 and 300 nm to the bipyridine and bands above 370 nm to mixed MLCT and LLCT transitions.[160] On the other hand, emission was found to be dominated again by ^{3}MLCT transition with a small participation of ^{3}LLCT transitions. In 2004, a $[Ir(ppy)_2(bpy)]PF_6$ complex was tested for the first time in an electroluminescent device (Figure 70, right),[161] opening the way for all futures applications and studied of this class of complexes.
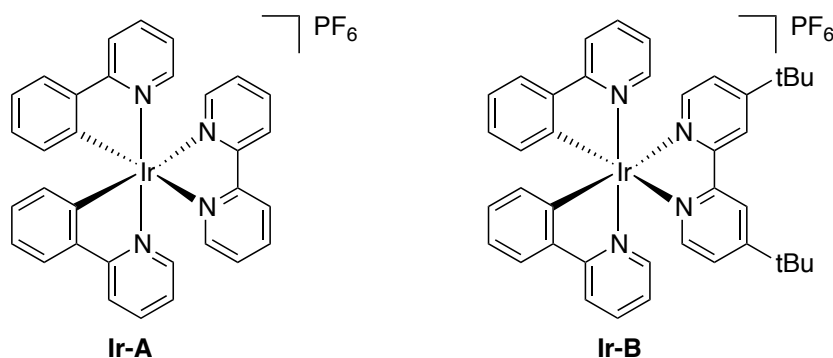
Figure 70. The first $[Ir(ppy)_2(bpy)]PF_6$ complex synthesized by Güdel et al. (left) and the first one used in an electrochemical device (right).

In order to rationalize the way to tune the emission wavelength, DFT calculations have been performed. It was shown that the HOMO of these compexes is essentially localized on the phenyl rings of the 2-phenylpyridine ligands with a contribution from the metal centre, while the LUMO is localised principally on the 2,2'-bipyridine (Figure 71).[162]
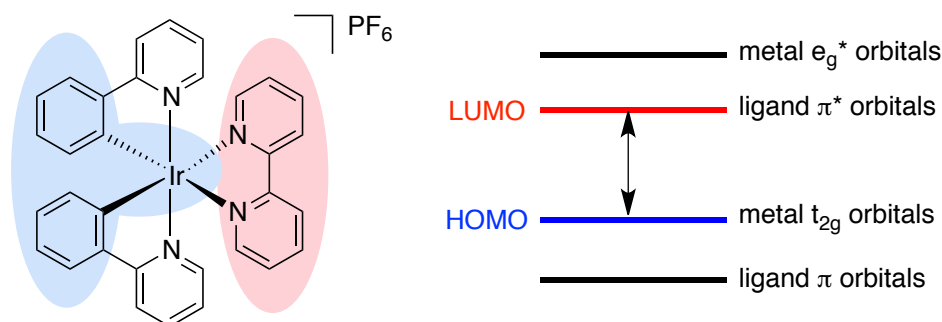
Figure 71. Representation of HOMO and LUMO levels in an $[Ir(ppy)_2(bpy)]PF_6$ complex.

By appropriately substituting the ligands, the emission should be easily tunable from deep red to the blue.[163] Modifications can include appending electron-withdrawing or electron-donating substituents on the ligands,[164] using different heterocyclic rings (*e.g.* instead of the pyridines)[165] or other kinds of C^N and N^N chelating ligands.[166] In particular, red emission can be obtained either acting on the HOMO-LUMO gap with substituent on the ligands[167] or by increasing the conjugation of the 2,2'-bipyridine,[168] as we will explain in the following section.

5.1.1.   Luminescent $[Ir(ppy)_2(bpy)]^+$ complexes with π-conjugated substituents

A well-known method to shift emission wavelength towards the red is to increase the conjugation length of a complex. By adding π-conjugated substituents on the ligands, typically styryls, on the easily functionalizable position 4 of the pyridines,[169] the emission of $[Ir(ppy)_2(bpy)]^+$ complexes can be shifted at longer wavelengths. Examples of iridium(III) cationic complexes with 2-phenylpyridine rings functionalized with a styryl derivative are rare,[170] but substituted 2,2'-bipyridyl ligands are more common.

Spichiger-Keller et al. studied an $[Ir(ppy)_2(4,4'-bis(2-(4-N,N-methylhexylaminophenyl)ethyl)-2-2'-bipyridine)]Cl$ complex emissive in the red (Figure 72).[171]
While in dichloromethane solution the quantum yield is low ($\Phi_{lum} = 0.1$), if incorporated in a polymeric support the complex revealed a high luminescence quantum yield of 0.58, long-term stability and luminescence lifetime in the order of 102 μs. The complex was used as oxygen sensors, since the luminescence was quenched upon exposure to atmosphere.
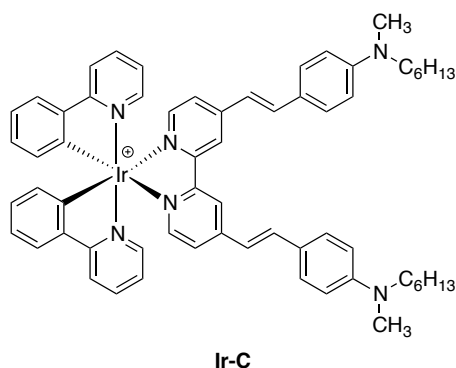
Figure 72. The complex studied by Spichiger-Keller et al. for oxygen sensing.

Guerchais et al. reported a similar complex with di(2-pycolil)amino substituents on the styrylpyridyl fragment, used for cations sensing.[172] They noticed that the complex was not emissive at room temperature, while at 77 K it displayed a ^{3}IL emission band centred at 650 nm. The lack of emission at room temperature can be explained by competitive deactivation of the excited state by the faster *cis-trans* isomerization process of the double bond triggered by excitation light,[52] while in a rigid matrix at 77 K the *cis-trans* isomerization process cannot occur, allowing emission to be observed. More recently, the same group studied some other complexes with this design.[173] The emission was registered at 77 K: the complexes display highly structured luminescence spectra with vibronic progressions of 1500 cm^{-1}, typical of aromatic and double C-C bond vibrations (Figure 73).
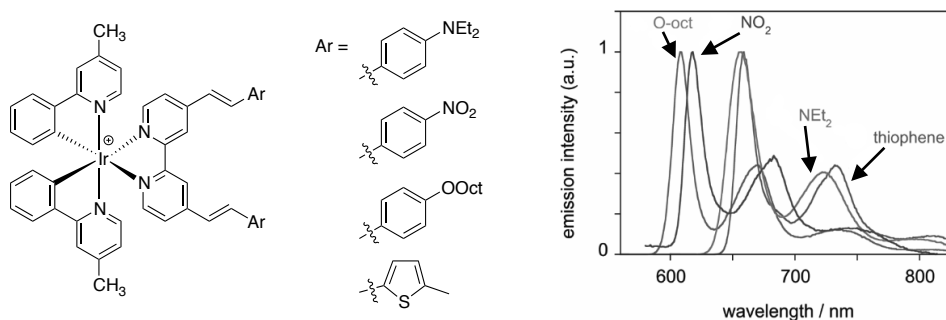
Figure 73. The series of complexes studied by Guerchais et al. (left) and the respective emission spectra at 77 K (right).

The long lifetimes low-energy, and highly structured spectra are indicative of emission from a triplet state predominantly localized on the styryl-appended ligands, rather than from the MLCT state. Anyways, the participation of the metal is required in order to promote the formally forbidden triplet radiative decay.

Gupta and co-workers studied the isomerization phenomenon in detail.[174] They irradiated with UV light ($\lambda = 366$ nm) the 2,2'-bipyridyl ligands and the relative Ir^{III} complexes (Figure 74) and observed *cis-trans* isomerization with the ^{1}H-NMR technique. In fact, the ^3J constant is 16 Hz for protons bound to carbons in a *trans* double bond, while it is halved if the bond is in *cis* conformation. The reported

complexes are emissive in the green from a ^{3}MLCT/^{3}LC state in solution upon irradiation at 410 nm. They noticed that emission intensity diminishes slowly upon irradiation of the complexes with UV light, because the isomerization to the *cis* form occurs (Figure 74, right).
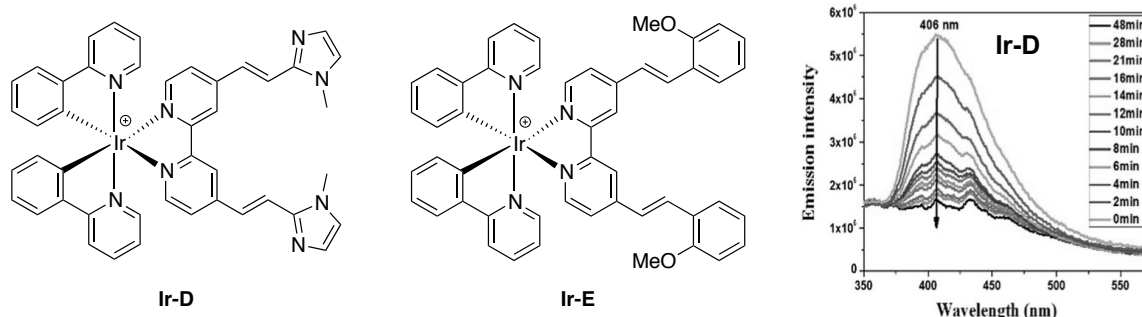
Figure 74. The Ir^{III} cationic complexes studied by Gupta et al.

Examples of complexes in which both the pyridines of the 2-phenylpyridine and 2,2'-bipyridyl ligands are substituted with styryl fragments are rare: only Grätzel et al. reported a complex of this kind in a patent.[170b]

5.2. A highly π-conjugated [Ir(ppy)$_2$(bpy)]$^+$ complex

The group of Guerchais studied the luminescent properties of some neutral Ir(ppy)$_3$ complexes with π-extended vinyl-aryl substituents at the *para* position of the pyridyl rings,[175] emissive at 77 K. This work and the other reports described above prompted us to synthesize and study a new [Ir(ppy)$_2$(bpy)]PF$_6$ complex with extended π-conjugated styryl substituents on the *para* positions of the pyridines of the 2-phenylpyridine and the 2,2'-bipyridine ligands.[176]
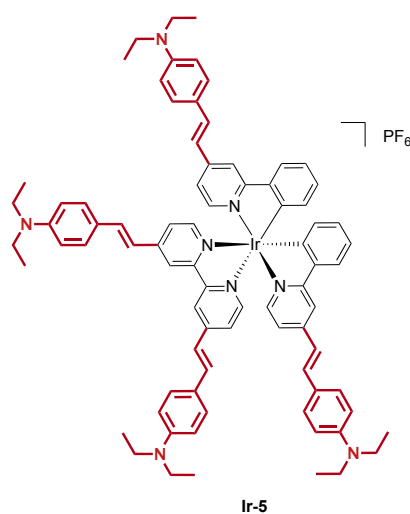
Figure 75. The [Ir(ppy)$_2$(bpy)]PF$_6$ complex under study.

5.2.1.   Synthesis and characterization of the Ir (III) complex

In order to obtain complex **Ir-5**, we started by synthesizing the ligands 4,4'-*p*-[(*N,N*-diethyl)aminostyryl]-2,2'-bipyridine[177] by deprotonation of the methyl in the *para* position of the pyridine and subsequent condensation with *p*-(*N,N*-diethyl)aminobenzaldehyde, following a procedure reported in the literature. To achieve 4-(*N*-diethyl)aminostyryl]-2-phenylpyridine,[178] we started by synthesizing 4-methyl-2-phenylpyridine by reaction of phenyllithium with 4-picoline. Then, the methyl in the *para* position of the pyridine was deprotonated and the desired ligand was obtained upon condensation with *p*-(*N,N*-diethyl)aminobenzaldehyde. The μ-dichloro-bridged cyclometalated iridium dimer intermediate was isolated, heating at reflux $IrCl_3 \cdot 3H_2O$ and 4-*N,N*-diethylminostyryl-2-phenylpyridine in a 2-ethoxyethanol/H_2O 3:1 mixture for 24 hours.[178]

The desired complex was prepared by ligand substitution, in the presence of 4,4'-*p*-[(*N,N*-diethyl)aminostyryl]-2,2'-bipyridine in 1,2-dichloroethane at reflux for 2 hours. The complex was obtained as a dark red powder ad was characterized by ^{1}H-NMR and elemental analysis.

5.2.2.   Photophysical properties

The UV-visible absorption spectrum in CH_2Cl_2 at 298 K and the emission spectrum at 77 K in EPA matrix of Ir-5 are shown in Figure 76, whereas the photophysical data are listed in Table 5.

With reference to previous studies on $[Ir(ppy)_2(bpy)]^+$ complexes, the absorption bands under 350 nm can reasonably be assigned to ${}^1(\pi\text{-}\pi^*)$ transitions of the styrylphehylpyridine and styrylbipyridine ligands, the intense band between 350 and 550 nm can be assigned to mixed (d(Ir) → π*(ppy/bpy)) MLCT and LLCT transitions,[160] while the weaker band centred at 620 nm may be due to direct population of triplet CT states.[175]
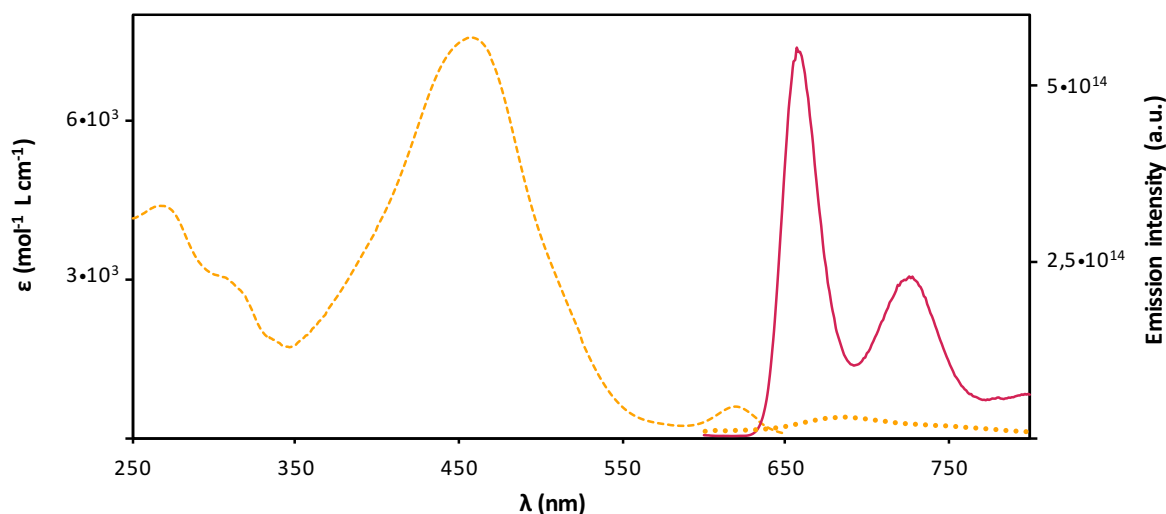
Figure 76. Absorption spectrum in CH_2Cl_2 at 298 K (orange dashed line) and emission spectra in CH_2Cl_2 at 298 K (orange dotted line) and in EPA (diethyl ether/isopentane/ethanol: 2/2/1) glass at 77 K (λ_{ex} = 460 nm, red plain line) of **Ir-5**.

As expected, the complex is only very weakly emissive at room temperature (Figure 76) because the radiative decay is quenched by the competitive non-radiative *cis-trans* isomerization process of the double bond, triggered by excitation with light before emission.

Complex	λ_{abs} / nm $(\varepsilon \times 10^3 / M^{-1}cm^{-1})^a$	λ_{em}/nm^b	$\tau/\mu s^b$
Ir-5	267 (4.38), 309 (2.97), 457 (6.67), 620 (0.56)	657, 726	57

Table 5. Photophysical data for complex **Ir-5**. [a] In CH_2Cl_2 solution (10^{-5} M) at 298 K. [b] In EPA (ethanol/isopentane/diethylether : 2/2/1) glass at 77 K (λ_{exc} = 460 nm).

On the other hand, **Ir-5** is emissive at 77 K in EPA matrix: the luminescence spectrum is highly structured and the emission is centred in the red region of the spectrum, as predicted upon substitution of the ligands with extended π-conjugated substituents. With reference to previously reported $[Ir(ppy)_2(bpy)]^+$ complexes,[173] considering the highly structured spectrum and the long lifetime (> 50 μs) luminescence can be assigned to radiative decay from a triplet state predominantly localized on the styryl-substituted ligands, rather than from the MLCT state. In any case the participation of the metal in the emission is necessary to promote the population of the formally forbidden triplet emissive state.

5.2.3. Conclusion

In summary, a novel $[Ir(ppy)_2(bpy)]PF_6$ complex with *p*-(*N,N*-diethyl)aminostyryl substituents on the pyridines of both the 2-phenylpyridine and 2,2'-bipyridyl ligands has been successfully synthesized and characterized. The complex is luminescent in the red region of the spectrum at low temperature, with a long lifetime and a structured emission typical of this class of compounds.

The interest of synthesizing this complex is in the possibility of studying also its second and third order nonlinear optical properties: they will be discussed in the following chapter.

II. SECOND AND THIRD-ORDER NONLINEAR OPTICAL PROPERTIES OF ORGANIC Π-CONJUGATED DYES AND ORGANOMETALLIC COMPLEXES

1. Second-order nonlinear optics

1.1. Principles of second-order nonlinear optics

The study of linear optics started being developed by the Greeks: Euclid's *Optics* sets the basis for the progress of this branch of physics. On the other hand, nonlinear optics had its origin in more recent times: its first appearance as an experimental science can be dated to 1961, after laser invention in 1960, when Franken and his colleagues observed for the first time the phenomenon of frequency doubling in ruby laser.[179] Since then, scientists carried through a series of experimental discoveries in the nonlinear optics field.[180] NLO studies optical phenomena caused by the interaction of a strong oscillating electromagnetic field (light) with specific molecules or bulk materials, followed by the emission of new electromagnetic fields, which differ in frequency, phase or other optical properties from the incident ones.

The interaction of an electromagnetic field with matter induces a polarization in that matter. If a weak electromagnetic field irradiates the medium, its propagation is linear, with a harmonic polarization of the electrons near the nuclei and the production of a wave of the same intensity and phase delay of the incoming one. When a molecule is subjected to an oscillating external electric field produced by an incident radiation, the induced polarization effect can be described as:

$$\vec{P} = \mu_0 + \alpha\vec{E}$$ Eq. (1)

where μ_0 is the molecular ground state electric dipole moment, α the linear polarizability tensor and $\vec{E}$ the applied electromagnetic field.

If the applied electromagnetic field is strong, namely an intense laser beam, the propagation of the electromagnetic wave in the medium is not linear anymore, electrons near the nucleus become polarized anharmonically and produce new fields altered in phase, frequency, amplitude or other propagation characteristics from the incident fields.[181] So, if the electric field strength of the incident radiation is very high, as is the case with laser pulses, the induced polarization is better expressed by a power series:

$$\vec{P} = \mu_0 + \alpha\vec{E} + \beta\vec{E}^2 + \gamma\vec{E}^3 + \cdots$$ Eq. (2)

where β and γ are the nonlinear quadratic and cubic hyperpolarizability tensors, respectively, responsible for second and third order nonlinear optical effects.

The fact that α >> β, γ is the reason why NLO was not commonly observed before the introduction of lasers and associated large electric fields. The nonlinear optical response, in fact, can be triggered only if the incoming electric field has a minimum strength: $\vec{E} \geq 10^3$ V/cm. Such electric fields are powerful enough to perturb the electronic system of a material or a molecule, naturally subject to of microscopic and atomic electric fields in the order of 10^8-10^9 V/cm.

When the order of the nonlinear optical effect increases, the hyperpolarizability tensors values decrease considerably, since the efficiency η of a nonlinear process is given by:

$$\eta \approx \frac{1}{\lambda_{laser}} \left(\frac{\vec{E}_{laser}}{\vec{E}_{atom}} \right)^{n-1}$$

Eq. (3)

Since $\vec{E}_{atom} > \vec{E}_{laser}$, for the major part of the materials the effects higher than the third order are not observable, because of their low efficiency.

Let us observe now what can happen at a macroscopic level. The polarization effect induced by a strong external electromagnetic field can be expressed by:

$$\vec{P} = \vec{P}_0 + \chi^{(1)}\vec{E} + \chi^{(2)}\vec{E}^2 + \chi^{(3)}\vec{E}^3 + \dots + \chi^{(n)}\vec{E}^n$$

Eq. (4)

where $\vec{P}_0$ is the static dipole of the sample and $\chi^{(1)}$, $\chi^{(2)}$ and $\chi^{(3)}$ are, respectively, the linear, second-order and third order electrical susceptibilities that control the nonlinear optical response of the material ($\chi^{(1)}$ = Σα, $\chi^{(2)}$ = Σβ…). In the case of linear phenomena, the polarization of the medium is proportional to the field strength. However, in the case of second and third order nonlinear phenomena the polarization of the medium is not proportional to the field strength, but to its square or third power.

From a graphical point of view, the linear perturbation induced by the electric field $\vec{E}$ can be expressed only as a function of the susceptibility $\chi^{(1)}$ ignoring the terms depending on $\vec{E}^2$ or $\vec{E}^3$:
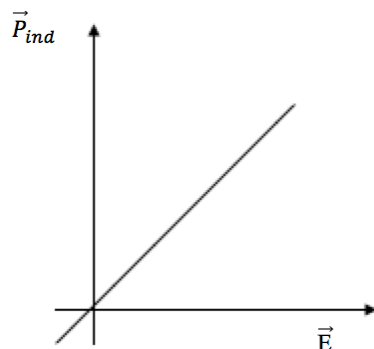
Figure 77. Weak electric field applied.

In this case the response is linear and the material has a linear optical behaviour. When the electric field applied is very strong, the induced polarization in the material does not have a linear response and can be represented by the following diagrams:
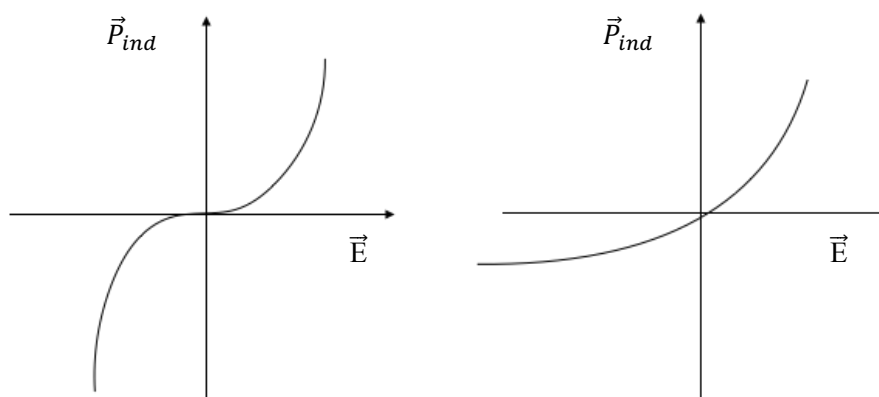
Figure 78. Strong electric field applied in centrosymmetric (left) and non-centrosymmetric (right) media.

It is also important to underline that both β and $\chi^{(2)}$ go to zero in centrosymmetric molecules or materials, respectively. This can be explained by the fact that if a field +E is applied to a molecule the first nonlinear term will induce a polarization of $+\beta E^2$. On the contrary, if a field $-E$ is applied, the predicted polarization becomes $-\beta E^2$ if the molecule is centrosymmetric. Since the absolute value of $\vec{P}_{ind}\left(+\vec{E}\right) = \vec{P}_{ind}\left(-\vec{E}\right)$, β (and $\chi^{(2)}$) = 0 in centrosymmetric media. This is not valid for γ and $\chi^{(3)}$: γ can be shown to be the first nonzero nonlinear term in centrosymmetric media, as +E gives $+\gamma E^3$ while $-E$ produces $-\gamma E^3$.

To obtain molecular materials displaying significant second-order NLO effect it is therefore necessary to have high values of β. In 1977, Oudar and Chemla gave a theoretical interpretation of the electronic origin of the quadratic hyperpolarizability.[182] By studying nitroanilines, they found that β can be separated into two contributions:

$$\beta = \beta_{add} + \beta_{CT}$$
Eq. (5)

where β_{add} is due to the interactions between the substituents and the π-conjugated system and β_{CT} is due to donor-acceptor charge transfers in the molecule. Assuming that in one-dimensional molecules the second-order NLO response is dominated by one major charge-transfer process, the contribution of β_{add} is small and can be neglected, and β_{CT}, the principal contribution in the direction z of the charge transfer, can be expressed as:

$$\beta_{CT} = \beta_{zzz} = \frac{3}{2h^2c^2} \frac{v_{eg}^2 r_{eg}^2 \Delta\mu_{eg}}{(v_{eg}^2 - v_L^2)(v_{eg}^2 - 4v_L^2)} \qquad \text{Eq. (6)}$$

where h is the Planck constant, c is the speed of light in vacuum, v_{eg} is the frequency of the charge-transfer transition, r_{eg} is the transition dipole moment, $\Delta\mu_{eg}$ is the difference between the excited state and ground state molecular dipole moment (μ_e - μ_g) and v_L is the frequency of the incident radiation. The equation above represents the two-level approximation, a simple way to estimate the values of β taking into account only the highest occupied and the lowest vacant molecular orbitals and considering the main charge-transfer transition aligned with the π-conjugation axis.

Extrapolation to zero frequency allows an estimation of the static quadratic hyperpolarizability β_0, a useful figure of merit to evaluate the basic second-order NLO properties of a molecule:

$$\beta_0 = \beta_\lambda \left[1 - \left(\frac{2\lambda_{max}}{\lambda}\right)^2\right]\left[1 - \left(\frac{\lambda_{max}}{\lambda}\right)^2\right] \qquad \text{Eq. (7)}$$

where β_λ is the quadratic hyperpolarizability value at the incident wavelength λ and λ_{max} is the absorption wavelength of the charge-transfer transition considered.

This model allows to evaluate the necessary requirements that a molecule must fulfil to show a significant second-order NLO response:

1. Asymmetric charge distribution;
2. Charge-transfer transitions at low energy (excited state close in energy to the ground state);
3. Large transition dipole moment r_{eg};
4. Large difference between ground and excited state dipole moments $\Delta\mu_{eg}$.

Molecules typically satisfying these requirements are push-pull linear organic dipolar chromophores, in which an electron-donating group and an electron-accepting group are connected by a long and highly polarizable π-conjugated spacer.[181] More recently, multipolar systems, in particular octupoles, started attracting growing attention.[183] These systems offer the advantages of a reduced efficiency-transparency trade off (*i.e.* they have higher transparency), and of easier non centrosymmetric arrangements in crystals and materials. Nevertheless, the vectorial part of the quadratic hyperpolarizability is cancelled and only the octupolar contribution remains.

Materials and molecules possessing second-order NLO properties are of interest for a variety of NLO processes, that can be classified in two main categories:

1.   Frequency conversion: the interaction between the incident electromagnetic radiation and the NLO material causes a variation of the output beam frequency with respect to that of the incoming wave. An example of frequency conversion is second harmonic generation.[184] This process is generated by the mixing of two incident electromagnetic waves of frequency ω that interact with the molecule or the material possessing NLO properties to produce a third wave of frequency 2ω, named second harmonic. Other wave-mixing phenomena are optical rectification, *i.e.* simple polarization of the material with the generation of a static electric field,[185] and sum and difference frequency generation, where two input waves at different frequencies generate an output beam with the sum or difference of the optical frequencies of the pump beams.
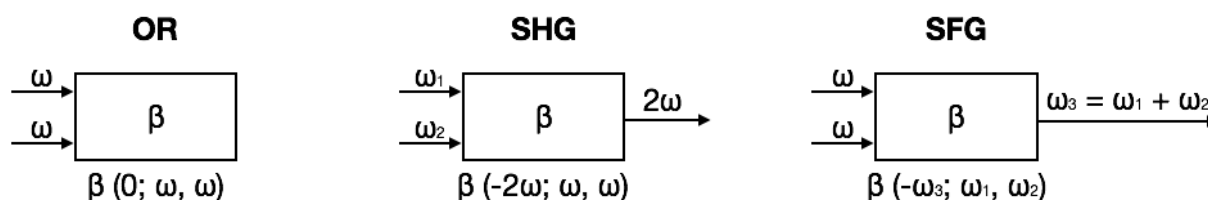
Figure 79. Representation of wave-mixing phenomena.

2.   Modulation of the refraction index: the interaction of a laser radiation with a NLO material, in the presence of electric field which produces a variation of the refraction index of the material, can modulate the speed of the laser propagation, but not its frequency. When the applied field is an electric field, we can talk about electro-optic effects.[186] In some materials, the change in refractive index is linearly proportional to the strength of the applied electric field. This change is known as the linear electro-optic effect or Pockels effect. Since the linear electro-optic effect can be described by a second-order nonlinear susceptibility, a linear electro-optic effect can occur only for materials that are non-centrosymmetric. On the other hand, in centrosymmetric materials (such as liquids and glasses), the lowest-order change in the refractive index depends quadratically on the strength of the applied field. This effect is known as the Kerr electro-optic effect or as the quadratic electrooptic effect. These phenomena can be exploited in devices such as optical switches and modulators.

1.2.   Measurement of quadratic hyperpolarizability in solution

1.2.1.   Electric Field Induced Second Harmonic Generation

The EFISH technique (Electric Field Induced Second Harmonic Generation) is one of the two most important techniques used to measure the value of the quadratic hyperpolarizability and has been widely used for the experimental measurement of β in NLO active polar molecules (Figure 80, top).[187]

This technique is suitable for dipolar neutral molecules and tight ion-pairs and allows to calculate both the sign and the absolute value of the scalar product $\vec{\mu} \cdot \vec{\beta}$, where μ represents the ground state molecular dipole moment and β is the projection of the vectorial component of the tensor of the quadratic hyperpolarizability along the dipole moment axis. The ground state dipole moment can be measured independently, with theoretical or experimental methods (*e.g.* the Guggenheim method) and consequently the value of β can be easily extrapolated with EFISH measurement.

In order to exclude overestimation of β, operating conditions require an incident beam of fundamental wavelength of 1.604 μm produced by a Nd:YAG laser or 1.907 μm obtained from a hydrogen Raman cell converted from the 1.604 μm beam of the Nd:YAG laser. The choice of an input laser whose second harmonic is far from any electronic absorption of the molecule is necessary to avoid reabsorption of the radiation.

Experimentally, once the sample dissolved in a suitable solvent (usually $CHCl_3$, CH_2Cl_2 or DMF), the molecules in the solution are aligned by a strong DC electric field (*ca*. 30 KW/cm), required to break the statistical centrosymmetry of the solution.

A laser beam at fundamental frequency ω is then directed through the cell in the presence of the DC field and during the measurement the cell is translated perpendicularly to the laser beam. It should be noted that the cell has a cuneiform shape: it is constituted by two quartz windows opportunely angled and assembled on a stainless steel support (Figure 80, bottom). By translating it perpendicularly to the laser beam, the optical path that the beam will cover will be different at different times, thus causing the generation of Maker interference fringes: these fringes are generated by the interference between the fundamental and harmonic wave into the medium. Finally, by recording the second harmonic intensity as function of position, the value of β can be evaluated.
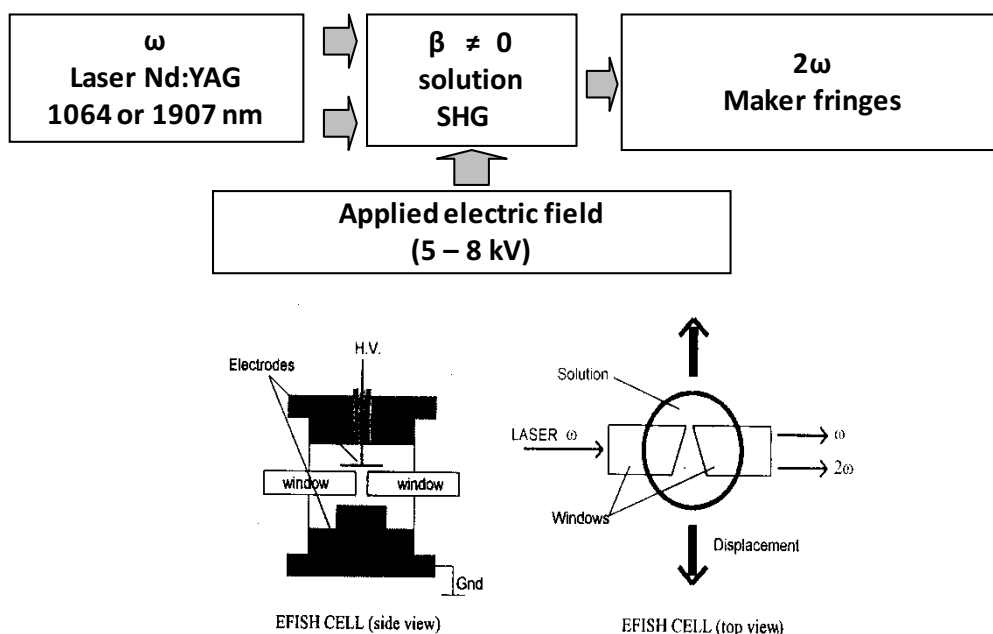
Figure 80. Schematic representation of the EFISH equipment (top) and of the EFISH cell (bottom)

Two radiations are present as output: the incident radiation (with frequency ω) and the second harmonic with frequency 2ω, generated by the interaction between the laser and the sample. The fundamental radiation is removed with a filter, so that only the second harmonic radiation is sent to the photomultiplier. The value of β is measured by referring to a crystal as a reference.

The width and the periodicity of the Maker fringes are correlated to the macroscopic susceptibility Γ(x) of the solution according to the relation:[188]

$$\Gamma(x) = \frac{1}{l_c(x)}\left[A\sqrt{\frac{I^{2\omega}(x)}{I^{2\omega}(0)}} \cdot \frac{E(0)}{E(x)} + B \right] \cdot 10^{-12} \qquad \text{Eq. (8)}$$

where $I^{2\omega}(x)$ is the intensity of the harmonic at x concentration (0 is the solvent), E(x) is the intensity of the electric field and A and B are constants depending on the solvent. Since:

$$\gamma_{EFISH} = \frac{M}{\rho N_a f x}[(1 + x)\Gamma(x) - \Gamma(0)] \qquad \text{Eq. (9)}$$

where N_a is the Avogadro's number, M the molecular weight of the solute, ρ the density of the solvent, x the molar fraction of the solute and f a correction factor of the applied electric field E, it is possible to obtain the value of β (projection of the vectorial component of the tensor of the quadratic hyperpolarizability along the dipole moment axis) by the relation:

$$\gamma_{EFISH} = \frac{\mu\beta\ (-2\omega; \omega, \omega)}{5kT} + \gamma(-2\omega; \omega, \omega, 0) \qquad\qquad \text{Eq. (10)}$$

where $\mu\beta$(-2ω; ω, ω)/5kT represents the dipolar orientation contribution, and γ (−2ω; ω,ω,0), a third-order term at frequency ω of the incident wavelength, is a purely electronic contribution which is negligible for many molecules with a limited electronic polarizability. In this way the $\mu\beta_{VEC}$ value can be calculated directly from γ_{EFISH} value.

In summary, the advantages of the EFISH technique include:

a - Well established calculation methodologies;

b - Good sensibility (10^{-3}-10^{-5} M);

c - Direct evaluation of $\mu\beta$.

Some disadvantages are:

a - Possibility to be used only for dipolar and neutral molecules and tight ion-pairs;

b - Need for a reliable measure of μ;

c - Gives only the value of the projection of the vectorial component of β along the dipole moment direction;

d - For highly polarizable molecules, the third order term is not always negligible.

Nevertheless, the EFISH technique is the most widely used to measure the values of first hyperpolarizability of dipolar neutral organic molecules and metal complexes.

1.2.2.   Hyper-Rayleigh Scattering

The HRS technique can be used to measure the first hyperpolarizability value of dipolar, octupolar, neutral or charged molecules (as salts). HRS can be used to measure the values of β of dipolar and charged molecules because it works without a strong applied external electric field. The incoherent harmonic diffusion of the incident laser radiation, that is the basic process of HRS, has been largely used to investigate the quadratic hyperpolarizability of ionic molecules by Persoons et al.[189] With the HRS technique, values of β can be obtained without having to independently determine the dipole moment μ and the second hyperpolarizability γ, this creating an advantage over the EFISH technique. Furthermore, this kind of measure gives the sum of the dipolar (or vectorial) and octupolar components of the quadratic hyperpolarizability tensor, rendering the measure more complete. However, the high intensity of the used laser can generate some spurious signals, not always easily distinguishable from the weak harmonic emission and also the fluorescence of the sample can potentially interfere with the second harmonic signal.[190]

1.2.3. Solvatochromic method

The solvatochromic method gives access to the value of β along the major charge-transfer direction (β_{CT}).[191] This method exploits the shift of the absorption or the emission band of a compound in solvents of different polarity, in particular by using a series of solvents covering a large dielectric constant and refraction index range. By applying Oudar's two-states model, the value of β_{CT} can be obtained. This value can be compared with the value of β_{EFISH} only when the dipole moment axis and the charge-transfer transition lie in the same direction.

1.3. How to increase the second-order NLO properties of organic molecules

The two-states model of Oudar and Chemla described above anticipated some requirements needed to design molecules with high values of β. It can be used as a guide for the preparation of second-order NLO chromophores.

Traditionally used inorganic crystals such as $LiNbO_3$ and KH_2PO_4 have high efficiency in optoelectronic devices, but their synthesis is difficult and the response time is relatively slow. So, in the last fifteen years many studies have been dedicated to organic compounds for second-order NLO. They offer several advantages, as lower production cost, high NLO properties, faster responses, and great flexibility of design.[192] To increase the second-order NLO properties, an ideal molecule should feature a π-delocalized push-pull system, with heteroatoms in order to increase polarizability and strong electron-donating and electron-withdrawing groups.

i) Increasing the push-pull structure of the molecule

Oudar and Chemla were pioneers in exploring the second-order NLO properties of nitroanilines, taken as a model for many push-pull systems studied from then on.[182a] They observed that the value of β could be modulated according to the relative position of the strong electron-donating (amine) and withdrawing (nitro) substituents on the phenyl ring. β was drastically enhanced in the case of *orto-* and *para*-nitroaniline (Table 6): this is directly related to the intramolecular charge transfer between the donor and the acceptor group through the extended π bonds of the benzene. In fact, charge-transfer interactions between substituents are often represented by resonance structures which connect charge-neutral and charge-separated states with alternating single and double bonds.

Enhancement of the NLO properties for *ortho-* and especially for *para*-nitroaniline is due to a more efficient intramolecular donor-acceptor charge transfer, oppositely to the *meta*-substituted.
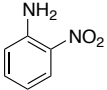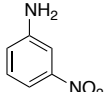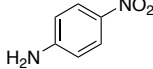
Chromophore	β_{exp} (10^{-30} esu[III])
NH$_2$ / NO$_2$ (ortho)	10.2
NH$_2$ / NO$_2$ (meta)	6
NO$_2$ / H$_2$N (para)	34.5

Table 6. Experimental β values of nitroaniline isomers.

The effectiveness of substitution with such kind of groups with opposite electronic effects has proved to be generally valid.[193] Marder and co-workers showed that, while monosubstituted benzenes have low β values, *para*-disubstituted benzenes take advantage of the cooperative effect of donor and acceptor groups, displaying higher values of first hyperpolarizability.[194] On the other hand, if more substituents are added on the same ring, their effect on the NLO properties can be detrimental: alterations of conjugation, geometry or hybridization of the substituted site can sometimes lead to less effective delocalization and reduced nonlinearity.

ii) Increasing the extension of the π-conjugated system

Among higher conjugated molecules directly derivate from benzene there are styrenes and stilbenes. As expected, their β values are higher than those of the corresponding benzenes:[195] in organic systems the β value increases when the length of the π conjugated system increases and depends on the electronic nature of the spacer. In stilbenes, the presence of substituents at the vinyl or phenyl position makes a difference: acceptor substituents at the vinyl position have been experimentally proved to be more effective in enhancing hyperpolarizability. Interestingly, the addition of a vinyl going from benzene to styrene causes a much greater enhancement of β than the phenyl addition going from the styrene to the stilbene structures.

Oudar et al. compared the second-order NLO properties of variously substituted stilbenes.[182b] Unsubstituted *cis*- and *trans*-stilbene are non-polar molecules so, as expected, they do not exhibit second-order NLO properties. Nevertheless, when substituted stilbenes are considered, it can be noticed that their values of quadratic hyperpolarizabilities are about 10 times larger than those of the corresponding benzenes, an evident consequence of the increase in the length of the conjugated system. Furthermore, the highest values of β were registered for 4-nitro-4'-dimethylaminostilbene, as expected in the presence of strong electron-donating and electron-withdrawing groups.

[III] 1 esu (electrostatic unit) = 1 cm / statvolt; 1 statvolt = 299.79 volt

If we consider the second-order NLO properties of diphenylacetylenes,[195] with a triple bond linking the two phenyls instead of the double bond of *trans*-stilbenes, we can observe a decrease of β of almost a half. This difference can be ascribed to the fact that the p orbitals of the sp-hybridized acetylenic carbons, electron rich because of the low energy of the σ orbitals, lead to less effective π delocalization due to the orbital energy mismatch with the neighbour p orbitals of the sp²-hybridized phenyl carbons. Moreover, phenyls loose aromaticity in resonance forms if triple bonds are used as linkers (allenic resonance forms). In structures as *trans*-stilbene, where all carbons are sp²-hybridized, a more effective delocalization of all the π electrons is allowed due to the better interaction between orbitals.

In general, we can state that the effectiveness of conjugation arises from the delocalisation of π-electrons, directly linked to properties as planarity and bond equivalence. Planarity and small torsional angles allow a better electronic overlap of the orbitals that favours donor-acceptor charge-transfers in the molecule. This can be observed, for example, in the increased values of β for the more rigid fluorenes respect to biphenyls. Anyways, torsional dependence is weak for small torsional angles, but becomes quite important for highly conjugated structures that offer more torsional possibilities. The second important factor to consider when evaluating the π-conjugation of a system is the bond-length alternation (BLA: average length difference between double and single bonds in the ground state). The value of β maximizes at a combination of donor and acceptor groups for a given conjugated bridge.[196] The ground state structures can be seen as a combination of two resonance forms:
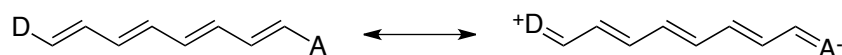
In substituted polyenes with weak donor and acceptor groups, the neutral resonance form dominates the ground-state wavefunction, and the molecule has a high degree of bond-length alternation. With stronger donors and acceptors, BLA decreases because the contribution of the charge-separated resonance form to the ground state increases. When coulombic and resonance factors balance, the two resonance forms contribute equally to the excited and the ground state and the molecule exhibits no BLA: this state is called the cyanine limit in reference to the structure of a cyanine molecule. Going from the neutral polyene limit to the cyanine limit, β first increases, peaks in a positive sense for an intermediate structure, decreases and passes through zero at the cyanine limit (Figure 81). Then, going towards the charge-separate resonance structure, β decreases, peaks in a negative sense, and decreases again arriving to the charge-separate structure.[197]

The use of a combination of donor-acceptor strength and bridge topology to alter the relative energetics of the two resonance forms allows the design of molecules with higher second-order NLO properties. It should be in any case remembered that, if the alternating double bond chain contains more than 9 carbons, a plateau is reached: β will not be enhanced if the length of the chain is increased.
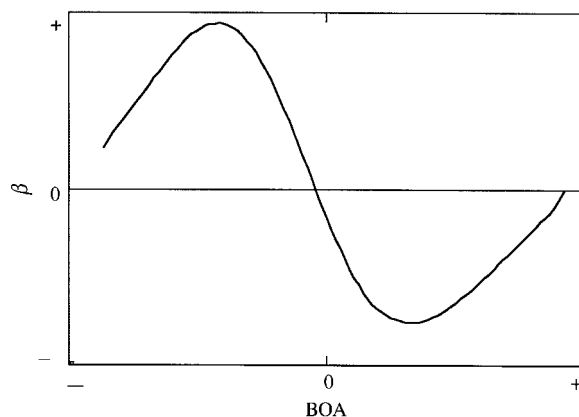
Figure 81. Plot of β versus bond-order alternation (BOA: difference in π-bond order between adjacent C-C bonds) for a simple donor-acceptor polyene polarized to increasing extents by application of an external field along the dipole vector of the molecule.

iii) Presence of highly polarizable heteroatoms

The hyperpolarizabilities of conjugated structures containing phenyl units can be enhanced by replacing phenyls with other aromatic groups with reduced aromatic stabilization and more polyene-like structures.[198] The magnitude of increase or decrease of β, with respect to that of the model stilbene derivative, depends on both the nature and the position of the heteroaromatic ring in the molecular framework (Table 7).

Chromophore	β_{exp} (10^{-30} esu)
Me$_2$N— ⬡ —CH=CH— ⬡ —NO$_2$	73
Me$_2$N— ⬡ —CH=CH— (O) —NO$_2$	83
Me$_2$N— ⬡ —CH=CH— (S) —NO$_2$	98

Table 7. Experimental β values of 4-nitro-4'-dimethylamino-stilbene and analogues with five-membered heteroaromatic rings in dioxane.

Usually, the replacement of the benzene ring on the donor with rings containing one heteroatom such as thiophene, furan or pyrrole results in higher β values. Substitution with pyrrole has a more positive effect than by furan and thiophene. On the other hand, in molecular systems where the same heteroaromatic rings are present on the acceptor end, the opposite trend is reported.[199]

The first hyperpolarizability of several molecules featuring a thiophene instead of a phenyl has been extensively studied.[200] It was found that thiophenes offer a better conjugation than benzenes and in particular there is a significant increase in the value of μβ if both the benzene rings in a stilbene-type molecule are replaced with thiophenes.[201]
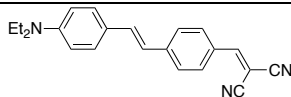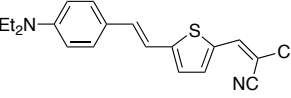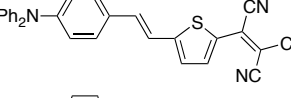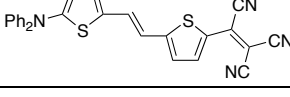
Chromophore	$\mu\beta_{exp}$ (10^{-48} esu)
	1100
	1300
	3250
	10200

Table 8. Experimental $\mu\beta$ values in dioxane of various push-pull systems containing aromatic and heteroaromatic thiophene rings.

In Table 8 the values of $\mu\beta$ of thiophene-substituted stilbene analogues are reported. The effect of the donor and acceptor groups are important even when the backbone of the molecule is made of heteroaromatic rings: compounds bearing tricyanovinyl acceptor have significantly larger hyperpolarizabilities than those with a dicyanovinyl acceptor[202] and even though diphenylamino is a less effective donor than the diethylamino group, it confers better stability to the molecule when used in a device.[203]

Currently, an organic molecule is used in electro-optic polymers: disperse red ($\beta_0 = 50 \cdot 10^{-30}$ esu).[204] It must not be forgotten that, since the molecules we consider are conceived for being integrated in a device, the properties of good solubility, stability, processability and possibly easy synthetic access should be preserved.[205]

1.4. Measurement of quadratic hyperpolarizability in bulk materials

At the bulk level, the most common method to investigate the second-order NLO activity of powder samples is the one developed by Kurtz and Perry in 1968.[206] This simple and fast technique allows an initial screening of the NLO properties of the system by the measure of the intensity of the second harmonic radiation and gives an indirect evaluation of the order of magnitude of $\chi^{(2)}$. The need for the sample to be in a crystalline powder form allows very large applicability.

A typical instrument to determine the second harmonic generation of powders consists of a Nd:YAG Q-switched laser. A very thin section (ca. 0.2 mm) of the powder is irradiated with a pulsed laser and the second harmonic emitted light is collected by a photomultiplier and compared to that of a reference compound such as urea or quartz.

In general, the results obtained with this technique are semiquantitative because they are influenced by the size of the particles. Therefore, for qualitative measure and for initial screening it is possible to use a thin film of the powder with unknown granulometry upon a slide for microscope, while the procedure

is more complex for quantitative measurements. In this case, in fact, grains of a fixed size (usually 75-150 μm) are selected by standard sieves and then put in a quartz cell with a defined thickness. A regular packaging is obtained through a vibrator, while the particle dimensions are controlled by optical microscopy.

1.5. From molecules to devices

From an application point of view, the main issue to consider is that dipolar molecules, which demonstrate second-order NLO properties, tend to crystallize in a centrosymmetic way with antiparallel disposition of the molecular dipoles. A way to overcome this problem is to use pre-organised materials such as poled films, Langmuir-Blodgett films and organic or inorganic scaffolds bound to a support. Molecules in polymeric films can be oriented by increasing the temperature of the film over the glass transition temperature, applying a strong orienting electric field and rapidly cooling the sample while the electric field is switched off. The main problem of this technique is, unfortunately, that the temporal stability is not very long.[207]

The most common technique to measure the nonlinearity of a material was introduced by Maker and co-workers in 1962[208] and thus named the "Maker fringes" method. In this technique, the second harmonic wave produced by a sample is compared to a known reference, such as quartz.[209] In the Maker fringe experiment the second harmonic intensity is determined as a function of the incidence angle of the fundamental beam and normalised with respect to that of a calibrated quartz crystal wafer. The sample is rotated around the Y-axis, which increases the path length that the light must travel through to exit the sample. In SHG the fundamental and the SH waves do not travel at the same speed, so they are not always in phase: constructive interference of the two waves causes an increase in the generated second harmonic, while destructive interference causes a decrease of it. The SHG signal goes thus periodically from a maximum to a minimum, generating peaks that appear as "fringes", from which the name of the technique. The periodicity of this effect is quantified by the coherence length, calculated by the analysis of the positions of the minima of the Maker fringes, which can be experimentally determined with better accuracy than the maxima, for a wide range of θ. This is essentially a measure of the maximum length of the nonlinear material. There is a small discrepancy in the angle between the fundamental and second harmonic. However, this is quite small and can be neglected.
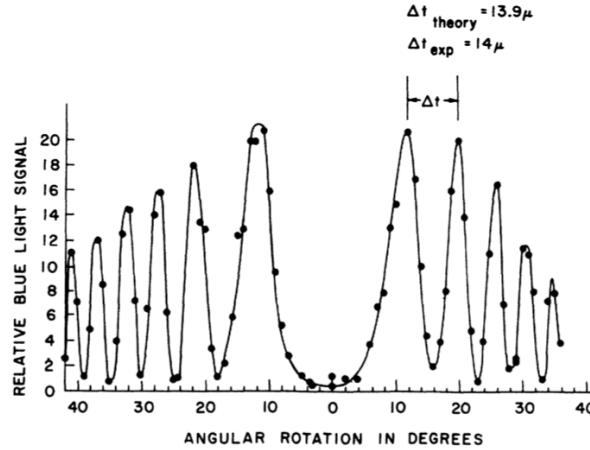
Figure 82. Blue light generation vs inclination in thick quartz platelet as represented by Maker et al.

The standard corrected expression used to fit the SHG intensity in a Maker fringe measurement[209b] takes into account the absorption coefficient of the film at the harmonic frequency. This equation considers the SHG intensity proportional to the square of the effective nonlinear optical coefficient (d_{eff}) which depends on polarizations of the fundamental and SH beam.[210] Considering the $C_{\infty v}$ symmetry expected for poled films and the polarizations of the fundamental and SH beam, the coefficient d_{eff} can be expressed as:

$d_{eff} = d_{31} \sin \theta_2$ for s → p configuration

$d_{eff} = d_{15} \sin \theta_1$ for 45 → s configuration

$d_{eff} = 2d \sin \theta_1 \cos \theta_1 \cos \theta_2 + \sin\theta_2 (d_{31} \cos^2\theta_1 + d_{33} \sin^2\theta_1)$ for p → p configuration

where d_{ij} are the components of the nonlinear optics coefficient tensor, θ_1 and θ_2 are, respectively, the angles of refraction inside the poled film for the fundamental and SH beam with refractive indexes n_ω and $n_{2\omega}$ ($\sin \theta_m = \sin \theta / n_{m\omega}$, m = 1,2) and p and s indicate the polarization of the beam in the plane parallel and orthogonal to the incident one, respectively.

The components of the nonlinear optics coefficient and the susceptibility tensor are related by $2d_{ij} = \chi_{ij}^{(2)}$. By fitting the Maker fringe measurements using the expressions reported above, the three nonzero coefficients of the second-order susceptibility tensor for a poled film $\chi_{33}^{(2)}$, $\chi_{31}^{(2)}$, and $\chi_{15}^{(2)}$ can be evaluated. The error in these data can be estimated to be less than 20%.

2. Second-order NLO properties of coordination compounds

2.1. Organometallic NLO-phores: structure-properties relationships

In the last twenty years, organometallic and coordination complexes have emerged as a new interesting class of molecular NLO-phores. Compared to traditional organic chromophores, their offer additional electronic advantages acting on the NLO response, such as:

I.   Presence of low-energy charge-transfer transitions, as MLCT with significant values of β;

II.   Polarizable d electrons that can improve conjugation and the number of low-energy excited states;

III. Different oxidation states of the metal centre, which can help to further modulate the electronic distribution of the ground and excited states;

IV. Wide choice of coordination sphere, ligands and geometries.

Metal centres are of particular interest for their versatility, in fact they can act as the electron-donor or the electron-acceptor species, or even as the bridge of a donor-acceptor network, depending on the nature of the metal, its oxidation state and the ligand environment.[181] A large variety of organometallic complexes has been taken under examination for their second-order NLO properties[211] and some specific classes of compounds have been mostly studied due to their better response.

Since the earliest reports of Green and co-workers, who studied the NLO properties of *cis*-1-ferrocenyl-2-(4-nitrophenyl)ethylene,[212] the interest in using metallocenes as donor groups brought them to be one of the most widely investigated classes of organometallic complexes for NLO.[213] The ferrocenyl group represents a moderate donor group. Its donor capability, comparable to that of the methoxy-phenyl organic group, can be attributed to the low ionization energy of the metal, which is relatively easy to oxidize.
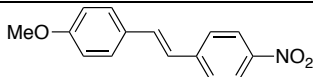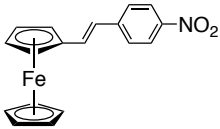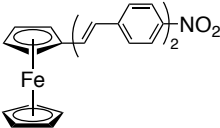
Chromophore	β (10^{-30} esu)
	28^a
	31^a
	403^b

Table 9. Example of second-order NLO ferrocenyl complex. The stilbene derivative is reported for comparison. a: $\beta_{1.91}$, EFISH, dioxane; b: $\beta_{1.06}$, HRS, CH_2Cl_2.

On the basis of binding energies and redox potentials, the molecular hyperpolarizabilities might be expected to be larger than the observed values. The poor coupling between the metal centre and the substituent, because of the π binding mode, most likely lowers the effectiveness of the metal centre as a donor.[214] Similarly to what observed for organic chromophores, extending the π-conjugation of the system results in the red-shift of the charge-transfer absorption bands and subsequent increase of the β values of these complexes.[215] It must also be noticed that, if the conformation of the double bonds is Z instead of E, the hyperpolarizability values diminish. The interest in this class of NLO chromophores is also due to their capability to crystallize in noncentrosymmetric structures characterized by a high SHG, because the acceptor substituents are usually bulky species.[216]

Related ruthenocene species show lower quadratic hyperpolarizabilities compared with those of ferrocenyl complexes: replacing iron by ruthenium results in a blue shift of the absorption bands and in a decrease of β values, according to the higher ionisation energy of ruthenium compared to iron.[217] Interestingly, by changing the function of the metallocene, its nonlinear optical properties can be highly increased. In fact, recently, multidecker sandwich complexes of general formula V_nBz_{n+1} ($n = 1, 2, 3, 4$, Bz = benzyl) were used as the polarizable bridge in push-pull systems of the form donor-(V_nBz_{n+1})-acceptor.[218] It was found that the hyperpolarizability of these complexes increases with the number of layers and can reach an extremely high value of $\beta_0 = 6638 \cdot 10^{-30}$ esu for V_3Bz_4-3CN.

Alkylphosphine$-$M$-\sigma$-acetylide complexes of group 8, 10 and 11 metals also represent a widely investigated class of second-order NLO chromophores, mainly developed by Humphrey et al.[219] They can bear cyclopentadienyl rings and the metal usually behaves, as in metallocenes, as the donor group of a donor-acceptor π-conjugated system. The second-order NLO properties are controlled by MLCT transitions. The largest β values have been obtained with the readily oxidizable Ru^{II} centres, followed by Ni^{II} and Au^{I}. Compared to 18-valence-electron metallocenes, σ-acetylides, which possess an almost linear M$-$C$\equiv$C$-$R structure, allow a better electronic coupling between the d metal orbitals and the π^* system of the σ-acetylide bridge and, consequently, larger second-order nonlinearities.

In-plane MLCT transitions in σ-acetylides result thus more effective than out-of-plane MLCT transitions in metallocenes. Recently, ruthenium dialkynyl complexes have been synthesized and their NLO properties have been studied.[220] In these systems, the ruthenium centre acts as the polarizable bridge between the donor and the acceptor: the NLO response of such complexes can be readily modulated by the nature of the alkynyl substituents to obtain high values of $\mu\beta_{EFISH}$ (up to -1700 $\cdot 10^{-48}$ esu, $\beta_{EFISH,max}$ = -225 $\cdot 10^{-30}$ esu).

A widely explored class of compounds that exploits the ambivalent donor or acceptor ability of the metal are metal(carbonyl)(pyridine) complexes. The most studied molecules are σ-complexes bearing a pyridine or a stilbazole ligand.[221]

M = Rh, Ir, Os, Cr, W
X = Cl, Br
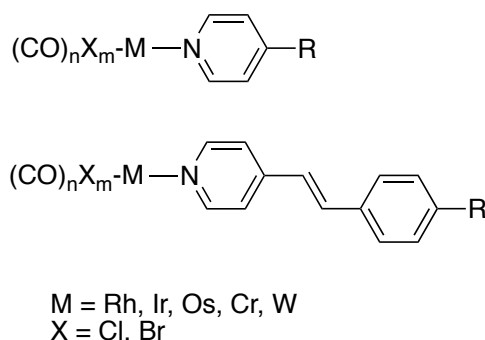
Figure 83. Schematic structure of the metal carbonyl complexes under investigation.

The absorption spectra of metal complexes bearing pyridyl or stilbazolyl ligands with electron-donating substituents in the *para* position of the pyridine or the stilbazole are dominated by intra-ligand charge-transfer bands. Upon coordination, these bands are red-shifted compared to those of the free ligands, the shift being more significant if the ligand is the more π-delocalized stilbazole.[222] The red shift of ILCT bands produced upon coordination is consistent with the lower energy necessary to reach the lowest excited state of the ILCT transition, which should induce an increase of the second-order NLO response respect to that of the pyridyl ligands. As stated in the two-level model, a smaller energy gap for charge-transfer transitions results in larger β value:[182] this entails obviously that the NLO properties of such ligands are enhanced upon coordination to a metal centre. Related complexes in which ligands carry weak donor or strong acceptor substituents in the *para* position are characterized by more complex UV-visible spectra. In fact, both carbonyl and pyridine ligands may contribute with additional MLCT transitions, which, being of comparable energy to the ILCT, produce more than one significant charge-transfer absorption band.[222] The second-order NLO values for these complexes can be measured with the EFISH technique, because the charge-transfer axis lies along the dipole direction and other contributions are negligible. β_{EFISH} values for these complexes are strongly dependent on the nature of the substituent R: β is positive with strong electron-donating groups but negative with strong electron-withdrawing groups, and the magnitude of the nonlinear response increases in the first case.[223] The negative sign of β can be explained by the reduction of the dipole moment upon excitation and by the fact that the dominant MLCT transition is vectorially opposed to the dipole moment.

The effect due to coordination becomes modest by increasing the length of the π-delocalized bridge, *i.e.* by passing from pyridines to stilbazoles. Furthermore, the NLO response seems quite insensitive to the derivatization of the styryl moiety, in contrast to what observed with π-conjugated organic architectures, in particular if it bears electron-withdrawing substituents.[224] This can be explained by considering that, in complexes bearing donor substituents, the hyperpolarizability is dominated by ILCT transitions from the donor to the metal-carbonyl moiety, in the same direction of the ground state dipole moment, which justifies the positive value of β. On the other hand, in complexes bearing acceptor substituents, the aromatic ring adjacent to the metal centre (the pyridine) serves as the primary acceptor of electron density instead of the acceptor group itself, especially in complexes containing less strong electron-

withdrawing groups.
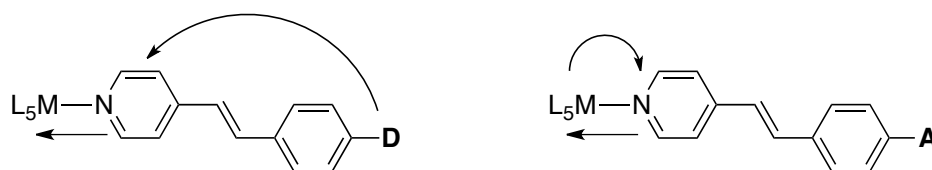
Figure 84. Charge-transfer mechanisms in metal complexes bearing stilbazole ligands.

The effect of the ancillary ligands is also important to modulate the electronic character of the metal. In fact, if electron-withdrawing groups like trifluoromethanesulfonate co-ligands are used, the accepting nature of the metal centre is accentuated and high values of β can be obtained with the appropriate metal.[225] Nevertheless, due to the acidic nature of this ligand, at low concentration the complex dissociates causing an unnatural increase of the NLO values measured with the EFISH technique.

The second-order NLO properties of ruthenium amine metal complexes bearing pyridyl ligands have been proved to be increased by using *N*-methyl-4,4′-bipyridinium[226] or *trans*-[2-(4-pyridyl)vinyl]pyridinium as ligands[227] instead of their neutral counterparts. Furthermore, β_0 can be increased by the presence of ligands that enrich the electron density of the metal centre (up to $458 \cdot 10^{-30}$ esu)[228] and by *N*-arylation of the pyridinium acceptor groups (up to $410 \cdot 10^{-30}$ esu).[229] On the other hand, extension of the π-conjugated system through addition of multiple double bonds between the two pyridines of *trans*-[2-(4-pyridyl)vinyl]pyridinium ligands does not systematically increase the NLO properties of the complexes, because of the concurrent presence of MLCT and ILCT transitions.[230] The same trends can be observed in V-shaped ruthenium amine complexes bearing more than one 4-styryl-pyridyl ligand of this kind.[231]

The NLO properties of several metal complexes bearing one 4-4'-styryl-2,2'-bipyridyl ligand have been reported.[232] Even in this case, it was noticed that the hyperpolarizability was dependent on the characteristics of the metal, the ligand and the co-ligands. In particular, β increases with the strength of the electron-donor substituents on the bipyridyl ligands and with the Lewis acidity of the metal centre: Zn is more acid than Hg and its complexes have higher β. Interestingly, Re complexes were less efficient than the corresponding Zn complexes due to the presence of two vectorially opposed charge-transfer transitions. More electro-withdrawing co-ligands (OTf > Br, Cl > OAc) also contribute to enhance the NLO properties of the complexes.[233]

The effect of chelation can be remarked by going from complexes bearing two 4-styrylpyridines to those bearing one 4-4'-styryl-2,2'-bipyridyl ligand: the better coplanarity and π-conjugation of the second result in an enhancement of μβ of the complex (Table 10).[232b,234]

Chromophore	$\mu\beta_{1.34}$ (10^{-48} esu)
	706
	1420

Table 10. Second-order NLO properties of a bis(styrylpyridine)ZnCl$_2$ vs a (4-4'-styryl-2,2'-bipyridyl)ZnCl$_2$ complex measured in CHCl$_3$ with the EFISH technique.

Tetrahedral D_{2d} metal complexes of Cu^{I}, Ag^{I} and Zn^{II} bearing two 4-4'-styryl-2,2'-bipyridyl ligands have been studied for their NLO properties with the HRS technique.[235] The magnitude of β_0 in these complexes is related to the nature of the metal ion. For a given geometry, stronger Lewis acidity of the central metal diminishes the energy of the ILCT transition that dominates the NLO response and, consequently, induces a significant enhancement of the NLO activity. The β_0 values are thus higher for the Zn^{II} complex than for the Cu^{I} and Ag^{I} ones.

The Zn ion is particularly versatile: its d^{10} electronic configuration and absence of ligand field effects allow the synthesis of octahedral D_3 tris(4-4'-styryl-2,2'-bipyridyl)Zn complexes.[236] The second-order NLO properties of this complex have been compared to those of related Cu^{II}, Ni^{II}, Fe^{II}, Ru^{II} complexes with the same ligands.[237] Concerning the ligands, it was observed that the length of the π-conjugated backbone has a stronger influence on β than the strength of the terminal donor group and an increase in the coordination number also results in an enhancement of the NLO response. Octaedral tris-bipyridine complexes of Cu^{II} and Ni^{II} have lower β values respect to the corresponding Zn^{II} complex ($\beta_{1.91, \text{HRS,}}$ $_{\text{CH2Cl2}} = 340 \cdot 10^{-30}$ esu) because of distortions from the ideal octahedral geometry. On the other hand, Fe^{II} and Ru^{II} complexes also show an MLCT band in the visible region that contributes to their NLO activity. The ILCT and MLCT transitions are roughly parallel but in opposite directions and should lower the value of β. This is valid for the Fe^{II} but not for the Ru^{II} complex: the contribution of the MLCT transition to the molecular hyperpolarizability still remains unclear and a more complex model involving extended delocalisation through the metal centre should be elaborated to explain these results.

The second-order NLO properties of some Ir^{III}, Zn^{II} and Ru^{III} complexes bearing one electron-donating terpyridyl ligand and electron-withdrawing co-ligand have also been examined.[238] As expected, respect to that of the free terpyridyl ligand, the hyperpolarizability is enhanced upon coordination to an

acid metal centre, mainly because of a stabilizing effect of the terpyridine π^* orbitals upon coordination. Furthermore, while the sign of β is positive for the Zn^{II} complex, it is negative for the Ir^{III} and Ru^{III} complexes: it was shown for the first time that the metal centre can influence not only the absolute value but also the sign of the quadratic hyperpolarizability of a nitrogen donor π-delocalized ligand bearing a strong electron-donor group. This can be explained by the dominating ILCT transition for the Zn^{II} derivative, while for the Ir^{III} and Ru^{III} complexes an important role is also played by MLCT and LMCT transitions, respectively. Recently, it was reported that the Ru^{III} centre in a bis(terpyridyl)Ru complex can act as the polarizable bridge between an electron-withdrawing and an electron-donating terpyridines.[239]

The second-order NLO properties of complexes with macrocyclic ligands, as porphyrins and phtalocyanines, have been investigated.[240] Most frequently, the porphyrin ring acts as a spacer within a push-pull system: one of the first examples of this kind of complexes are push-pull (arylethynyl)porphyrins.[241] The β values of metal porphirinates are respectable, but special attention should be paid to the incident wavelength: in fact, early studies overestimated the hyperpolarizability of such complexes because of resonance enhancement.[242] Moreover, it was recently found that the β values of metal porphirinates in non-polar solvents can be overestimated because of aggregation.[243] Interestingly, the second-order NLO properties of this family of complexes can be further enlarged if the (porphinato)Zn core is linked to two metal(polypyridyl) via an ethylene bridge, to have strongly polarizable push-pull systems.[244]

Schiff-bases, arising from condensation of substituted salicylaldehydes with various bridging diamines, represent useful templates to generate non-centrosymmetric molecular architectures: in this regard, divalent Fe, Co, Ni, Cu and Zn complexes have been investigated as second-order NLO-phores. In Schiff base complexes, the metal centre can act both as the donor of a push-pull system involving MLCT transitions and as a polarizable bridge in the presence of strong donating and accepting substituents on the chelating ligand.[245]

The compounds presented until now are only some important examples of organometallic NLO-phores. In the following paragraphs, the NLO properties of platinum and iridium complexes, with particular attention to those with cyclometalated ligands, will be explored in more detail.

2.2. Platinum complexes with second-order NLO properties

Metal σ-acetylides, as discussed in the previous section, represent a widely investigated class of second-order NLO chromophores, where the metal acts as the donor group of a donor-acceptor system connected by a π-conjugated linker. Pt^{II} alkynyl complexes have been studied as excellent candidates for optical power limiting,[246] solar cells,[247] two-photon absorption[248] or reverse saturable absorption.[249] These complexes take advantage of the almost linear M–C≡C–R structure, which allows a good coupling

between the d orbitals of the metal and the π^* system of the σ-acetylide bridge affording a significant NLO response controlled by low-energy MLCT excitations.

The first example of platinum σ-acetylide complexes for second-order NLO was reported in 1997 by Marder et al.[250] The advantage given by the presence of $-C\equiv C-$ fragments consists in the reduction of the molecular charge-transfer character: this allows to achieve materials with improved optical transparency. On the other hand, the disadvantage of the increased transparency is a decrease of β. In order to improve the second-order NLO activity while maintaining good optical transparency, the π-conjugated system of the complexes was expanded by using a bis(phosphine) platinum moiety as the central element bridging the phenylethynyl donor and acceptor moieties. By comparing the Pt σ-acetylide complexes with the organic analogues, it was noticed that a moderate improvement in $\mu\beta$ could be registered for the platinum complexes: the platinum centre can be thus considered a reasonably efficient component to be used to synthesize NLO materials.

Later, our group studied a push-pull binuclear complex in which two donor Pt σ-acetylide units are linked to a 2,1,3-benzothiadiazole moiety that acts as acceptor (Figure 85). [251] In this complex, the HOMO is composed by Pt orbitals combined with the π orbitals of thiophene and benzothiadiazole, while the LUMO is completely localized on the benzothiadiazole moiety without any contribution from the metal.

Pt₂(btdz)
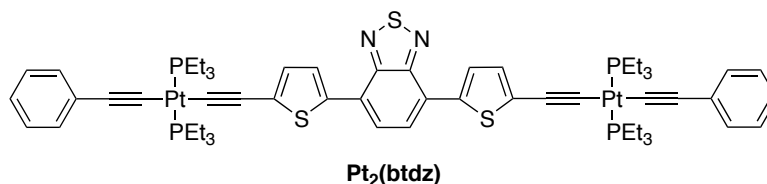
Figure 85. The binuclear Pt σ-acetylide complex studied by our group.

The complex has a $\mu\beta_{EFISH}$ value of $-520 \cdot 10^{-48}$ esu: its second-order NLO response is good, but analogue ruthenium complexes have better $\mu\beta_{EFISH}$ response.[251] Our group also investigated the second-order NLO properties of push-pull systems containing a donor platinum σ-acetylide moiety bound to an electron-deficient fullerene. The NLO properties of these complexes have been compared to analogue organic chromophores bearing a trimethylsyil moiety instead of the platinum fragment. The $\mu\beta_{EFISH}$ values were largely increased upon conjugation to platinum, up to $-3200 \cdot 10^{-48}$ esu . This revealed the effectiveness of the fullerene as electron-acceptor and the metal centre as electron-donor, that allowed to reach the highest absolute value of $\mu\beta_{EFISH}$ ever reported for a platinum alkynyl complex.

More recently, the group of Le Guen studied the second-order NLO properties of some unsymmetrical push-pull diacetylide platinum-based complexes with pyranylidene ligands as donor groups, diazine rings as electron-withdrawing groups and styryl or thienylvinyl bridges as π-linkers that separate the donor and the acceptor group from the platinum diacetylide unit.[252] The complexes exhibit high and

positive $\mu\beta_{EFISH}$ values, especially if the acceptor is a positively-charged methylated pyrimidine ($\mu\beta_{EFISH,max} \approx 2300 \cdot 10^{-48}$ esu). Neutral complexes exhibit slightly lower $\mu\beta$ values than their organic analogues, but the NLO response is significantly enhanced when a platinum fragment is included into the π-conjugated core of a pyrimidinium derivative.

Another performing class of platinum-based second-order NLO-phores consists in cyclometalated platinum complexes. Some examples of cyclometalated neutral Pt^{II}(ppy)(acac) complexes have been studied (Figure 86).[253]
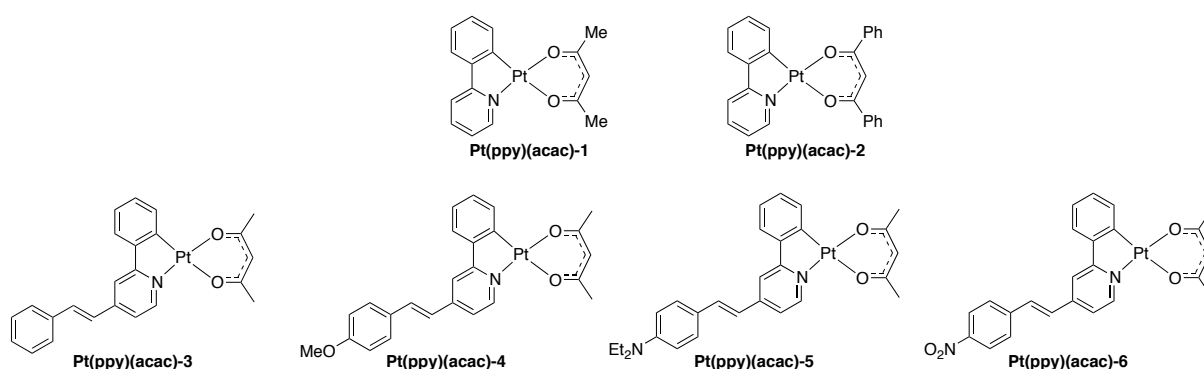
Figure 86. The Pt(ppy)(acac) complexes for second-order NLO.

Pt(ppy)(acac)-1 and **Pt(ppy)(acac)-2** have a good transparency trade off, *i.e.* they do not absorb at long wavelengths, the HOMO is mostly localized on the platinum centre and on the phenyl of the phenylpyridine ligand, while the LUMO is localized on the pyridine of phenylpyridine ligands. The major contribution to the dipole moment is along the direction connecting the pyridine and phenyl rings of the phenylpyridine. The NLO properties are thus dominated by mixed MLCT-ILCT transitions going from the phenyl to the pyridine: the $\mu\beta_{EFISH}$ values for these complexes are negative and moderately high ($\mu\beta_{EFISH,(Pt(ppy)(acac)-2)} = -770 \cdot 10^{-48}$ esu), even though lower than the related Ir(ppy)(acac) complexes with which they were compared. The NLO response was enhanced and became positive for those complexes bearing a styryl substituent on the pyrydyl ring (Figure 86, lower row). The increased π-delocalization of the pyridine moiety of the cyclometalated ligand leads to an inversion of the sign of $\mu\beta_{EFISH}$. This is attributable to the direction of the dipole moment: the major contribution of the dipole moment is along the styryl moiety whose ILCT transitions dominate the β_{EFISH} value. The situation is different for **Pt(ppy)(acac)-6** that bears the electron-withdrawing nitro group: the calculated dipole moment is almost perpendicular to the styryl moiety and the NLO response can reasonably be attributed to MLCT transitions. The $\mu\beta_{EFISH}$ values of the complexes increase by increasing the electron-donating ability of the substituent of the 4-styryl-2-phenylpyridine ligand: this is explainable by an increase of the ground state dipole moment.

It is also interesting to point out that the $\mu\beta_{EFISH}$ value of **Pt(ppy)(acac)-4** is almost 4 times higher than that of the related uncoordinate 4-styryl-2-phenylpyridine ligand bearing a methoxy group ($\mu\beta_{EFISH,complex}$

$= 1330 \cdot 10^{-48}$ esu vs $\mu\beta_{EFISH,ligand} = 370 \cdot 10^{-48}$ esu), showing that cyclometalation to a platinum(II) center allows a large enhancement of the second-order NLO response of such kind of compounds.

Second-order NLO properties of terdentate N^C^N Platinum(II) complexes have lately grabbed attention. Van Koten and co-workers presented, in an early work, the second-order hyperpolarizability values of a series of 2,6-(dimethylamino)methyl-4-styrylbenzene Pt^{II} complexes with different electron-donating and electron-withdrawing groups on the styryl moiety.[254] The PtCl moiety acts as a donor, while the acceptor group is located at the other edge on the stilbenoid ligand (Figure 87). In these complexes, the metal is on the same plane as the aryl ligand and this should contribute to the enhancing of the NLO properties of the system.

R = NPh$_2$, NMe$_2$, OMe, SiMe$_3$, H, I, CN, NO$_2$
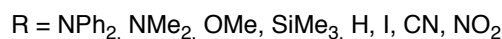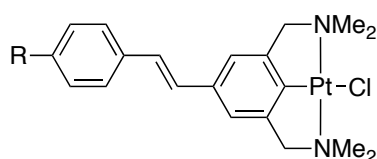
Figure 87. The platinum(II) complexes studied by Van Koten and co-workers.

The complexes show good hyperpolarizability values, measured with the HRS technique, better than their ferrocene analogues.[216] This can be ascribed to the in-plane alignment of the Pt-Cl fragment respect to the stilbazole ligand, which facilitates π-conjugation and charge-transfer transitions. The maximum value of $\beta_{zzz,800}$ of $1324 \cdot 10^{-30}$ esu is obtained for the compound bearing the iodine as a substituent, probably because of the high polarizability of the halide.

Asselberghs et al. compared the second-order NLO properties of a series of terpyridine and dipyridylbenzene platinum(II) complexes with chloride or arylacetylide co-ligands.[255] The terdentate ligand has the function of acceptor, while the platinum centre together with the co-ligands act as the donor moiety. An increase in the acceptor strength of the terdentate ligand leads to an enhancement in hyperpolarizability, as suggested by the red-shift of the MLCT absorption band. Furthermore, the Pt(dpyb)Cl complexes possess higher β values, compared with the Pt(trpy)Cl$^+$ parent complexes: this can be attributed to the presence of the intense, low energy charge transfer bands for the firsts, absent for the latter. The introduction of the arylacetylide ligand induces a reduction of the β value of Pt^{II} dipyridylbenzene complexes, while it induces the opposite effect on Pt^{II} terpyridyl complexes, thus increasing the hyperpolarizability. Some of these effect could not clearly be explained with the two-state model. This study demonstrated for the first time that Pt(dpyb)Cl complexes are good candidates for second-order NLO, since a maximum value of $\beta_{zzz,1064}$ of $460 \cdot 10^{-30}$ esu was obtained for the best performing of such compounds.

Our group systematically studied a series of Pt^{II} 1,3-di(2-pyridyl)benzene complexes with chlorine or phenylacetylide as co-ligands (Figure 88).[256] The absorption spectra of the complexes bearing a chlorine as co-ligand present mixed CT/LC absorption bands between 350 and 450 nm, while those of complexes bearing a phenylacetylide co-ligand show a set of less resolved LLCT bands in the same area.
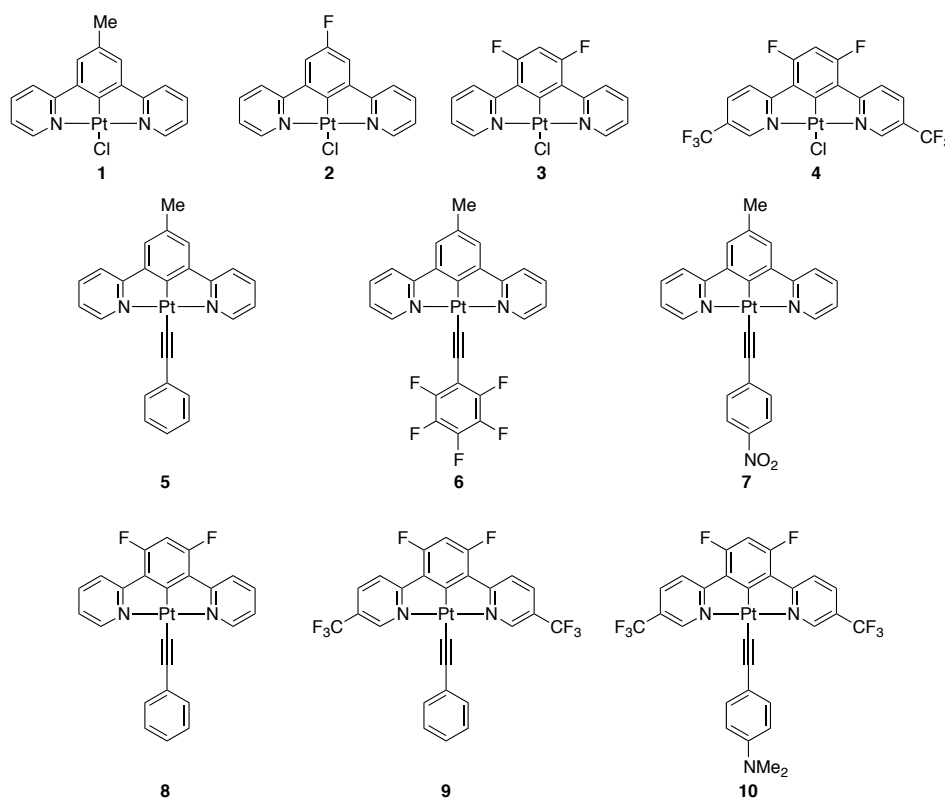
Figure 88. The platinum dipyridylbenzene complexes studied by our group.

This family of complexes is known for having outstanding emission properties, as discussed in Chapter I, but they also demonstrated to be good NLO-phores. The HOMO is primarily located on the central phenyl ring of the dpyb ligand, on the Pt centre and on the chloride or phenylacetylide co-ligands, while the LUMO is delocalized on the pyridyl ligands. For complexes **8**, **9** and **10**, bearing electron-withdrawing substituents on the dipyridylbenzene, the HOMO is principally on the phenylacetylide co-ligand, while the LUMO is on the pyridines and partially on the central phenyl ring.

The $\mu\beta_{EFISH}$ values were calculated in DMF solution with the EFISH technique: the values are negative, because of the decrease of the dipole moment upon excitation, and dominated by the charge transfer from the platinum centre to the cyclometalated ligand. Complex **4** is the one with the highest $\mu\beta_{EFISH}$ value ($-2470 \cdot 10^{-48}$ esu) because of its significant dipole moment, while the largest value of β_{EFISH} was reported for complex **10** ($-470 \cdot 10^{-30}$ esu, $\mu\beta_{EFISH} = -2020 \cdot 10^{-48}$ esu). This study underlined how the addition of electron-withdrawing substituents on the dipyridylbenzene ligand and the

substitution of the chloride with the phenylacetylide co-ligand can enhance the second-order NLO properties of these complexes, by decreasing the HOMO-LUMO gap.

Guerchais et al. studied the second-order NLO properties of N^C^N Pt^{II} complexes with symmetric 1,3-bis(benzoxazolyl)benzene or asymmetric 2-[3-(benzothiazol-2-yl)phenyl]benzo[d]oxazole or 2-[4-fluoro-3-(1-methyl-$1H$-benzoimidazol-2-yl)phenyl]benzothiazole cyclometalated ligands (Figure 89).[257]
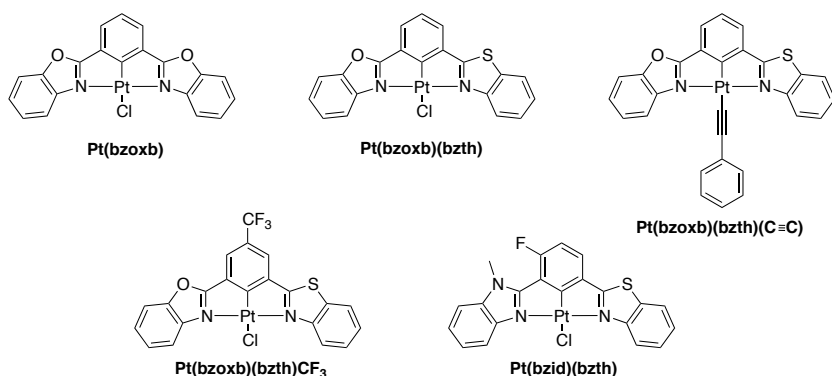
Figure 89. The N^C^N Pt^{II} complexes studied by Guerchais et al.

The absorption spectra of the complexes show typical bands assigned to $\pi \rightarrow \pi^*$ transitions in the UV and MLCT transitions at longer wavelengths. The HOMO is primarily localized on the chloro and on the phenyl unit of the cyclometalated ligand as for the Pt(dpyb)Cl complexes, while the LUMO is delocalized mainly on the electron-withdrawing fragment of the N^C^N ligands (the benzothiadiazole). The $\mu\beta_{EFISH}$ values are fair, and in particular complex **Pt(bzoxb)** has a slightly higher $\mu\beta_{EFISH}$ value than the corresponding Pt(dpyb)Cl complex. Substitution of the benzoxazole group with a benzothiadiazole causes an enhancement of the NLO response, because of the lowering of the LUMO level, while substitution with a benzoimidazole causes an increase of $\mu\beta_{EFISH}$ due to a higher dipole moment. The presence of the phenylacetylide and the electron-withdrawing CF$_3$ group also positively contribute to the enhancement of the NLO response The higher $\mu\beta_{EFISH}$ value was registered for **Pt(bzid)(bzth)** ($-950 \cdot 10^{-48}$ esu), while **Pt(bzoxb)(bzth)(C≡C)** possess the highest β_{EFISH} value ($-178 \cdot 10^{-30}$ esu).

In summary, Pt^{II} N^C^N complexes, and in particular Pt^{II} 1,3-di(2-pyridyl)benzene complexes have a competitive second-order NLO response. In particular, it can be increased by favouring charge-transfer transitions between the dipyridylbenzene ligand and the platinum centre and the ancillary co-ligands.

2.2.1. Platinum-based NLO switches

As introduced in the previous chapter, complexes bearing a photoswitching unit have been largely studied for their luminescent properties.[141−151] Species with commutable NLO properties are promising candidates also for the design of photoswitchable NLO materials, to increase their potential for original applications in emerging optoelectronic and photonic technologies.[258] To achieve efficient switches the molecule must be stable in both "on" and "off" states and the response time must be relatively fast.

Metal centres have been introduced in chromophores for NLO because of the availability of different oxidation states. By acting directly on the oxidation state of the metal, redox NLO switches can be obtained, as first demonstrated by Coe et al with a Ru^{II}-4,4'-bipyridinium complex:[259] when the Ru^{II} is oxidized to Ru^{III}, the second-order NLO response is switched off.

Acido-base switches have also been studied: Humphrey et al. reported ruthenium complexes with acetylide ligands that can easily convert to protonated vinylidene, with a lower NLO response, in presence of an acid and switch back with a base.[260]

The third class of NLO switches includes a photochrome, frequently dithienylethene (DTE), a highly efficient group. Ru^{II}, Re^{I}, Ir^{III} and Zn^{II} metal complexes bearing a 2,2'-bipyridyl ligand bis-substituted with a DTE fragment on the 4 and 4' positions have been reported.[173−261] The Zn^{II} complexes show the best performances: a dramatic (21-fold) increase of the second-order NLO activity is observed after UV irradiation. The second-order NLO response of such complexes is dominated by ILCT and the large enhancement of $\mu\beta$ values after ring-closing reflects the delocalization of the π-electron system in the closed forms. The Re^{I} complex shows slightly inferior performances, due to the presence of vectorially opposed MLCT and ILCT transitions. On the other hand, Ru^{II} exhibits NLO activity even in the open form, attributed to low-energy MLCT $d\pi(Ru) \rightarrow \pi^*(bipy)$ transitions. The Ir^{III} complex does not show any significant modification of its NLO response after photocyclization, because its hyperpolarizability is dominated by mixed LLCT/MLCT transitions, not involving the DTE substituent. Octupolar Cu^{I} and Fe^{II} complexes with two or three 2,2'-bipyridyl ligands, respectively, bearing each two DTE fragments have been studied.[262] The Cu^{I} and Fe^{II} complexes have a fairly high NLO response even in the open form, dominated by MLCT transition. Nevertheless, a high enhancement of the NLO activity is observed upon UV irradiation. Theoretical calculations confirm that the increase of the NLO response is related to additional IL transitions rather than in variations of the MLCT bands.

Knowing that cyclometalated platinum complexes display rich photophysical properties (see Chapter I) and preparation of related photochromic complexes for modulation of their luminescence properties has been developed, their NLO properties recently started to be investigated.

Qiu et al. studied the second-order NLO switching properties of some Pt(acetylacetonate)(2,2'-thiophenylpyridine) derivatives (Figure 90) with theoretical methods.[263]
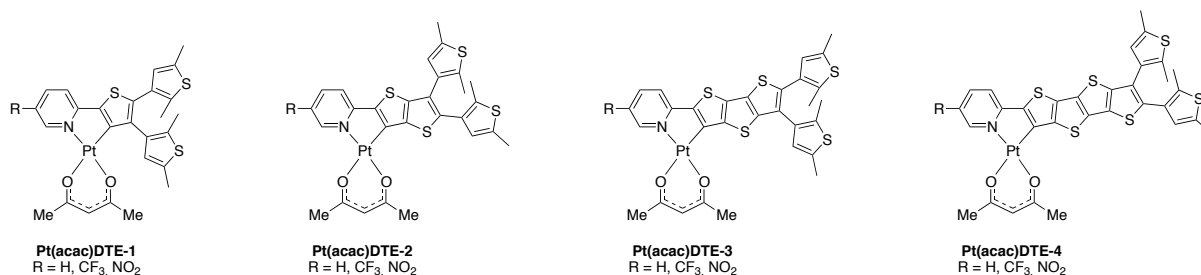
Figure 90. The Pt[II] complexes studied by Qiu et al.

They found that the β value of the complexes increases by substituting the pyridine with electron-withdrawing groups and by increasing the number of condensed thiophene rings. As expected, the NLO response of the closed form is superior to that of the open form. A related theoretical study by Wu et al. demonstrated that by simple substitution of the pyridyl or the thienyl rings the β values can still be enhanced.[264]

The NLO activity of Pt(II) complexes featuring photochromic units was explored by our group.[265] The NLO response of the "regular" complexes (Figure 91) is dominated by ILCT/MLCT transitions for complex **Pt(phbpy)(DTE)-1a**, while in complex **Pt(phbpy)(DTE)-1b**, due to the presence of the donor dimethylamino group, IL transitions also contribute.
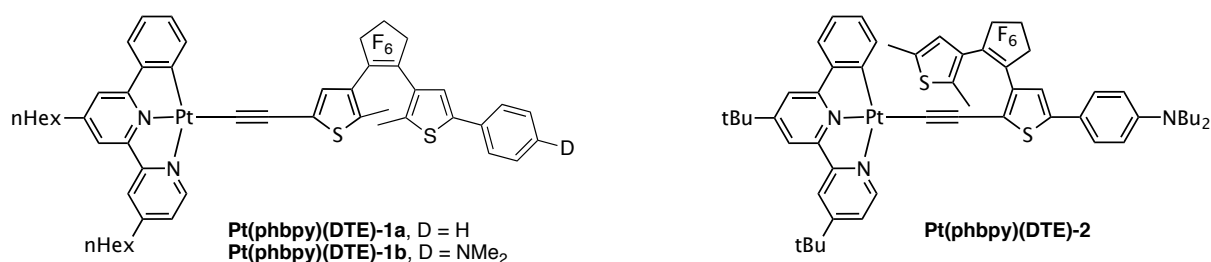
Figure 91. The regular and reverse Pt(phbpy) complexes studied by our group.

The NLO activity of these complexes were studied in solution with the EFISH technique: as expected, the open forms have a weaker NLO response than the closed isomers. Upon ring-closing, the values of $\mu\beta_{EFISH}$ are increased 6-fold for **Pt(phbpy)(DTE)-1a** and even 12-fold for **Pt(phbpy)(DTE)-1b**, reflecting the improved delocalization of the π-system in the closed form followed by a decrease of the HOMO-LUMO gap. The outstanding increase of the NLO response of **Pt(phbpy)(DTE)-1b** upon photocyclization can be ascribed to the longer charge-transfer distance and therefore to a lager difference of dipole moment between the ground and excited states.

For the first time, the properties of such complexes were studied in the solid state in thin films of the chromophore dispersed in PMMA matrix. The complexes were deposited in the closed form, possessing a higher dipole moment, in order to optimize the orientation of the chromophores during the electric poling. By fitting the Maker fringes the values of the nonzero coefficients of the second-order

susceptibility tensors could be extrapolated, revealing to be largely increased upon ring-closing. Furthermore, the NLO response in the solid state was managed to be switched by alternating visible and UV irradiation. The observed NLO contrast was higher than that of purely organic DTE chromophores.[210] Nevertheless, some SHG signal was lost during the switches because of irreversible loss of orientation through the photoisomerization processes.

On the other hand, complex **Pt(phbpy)(DTE)-2** does not show any photoreactivity upon irradiation with UV light, but its photochromic reactivity can be restored upon protonation (Figure 92).
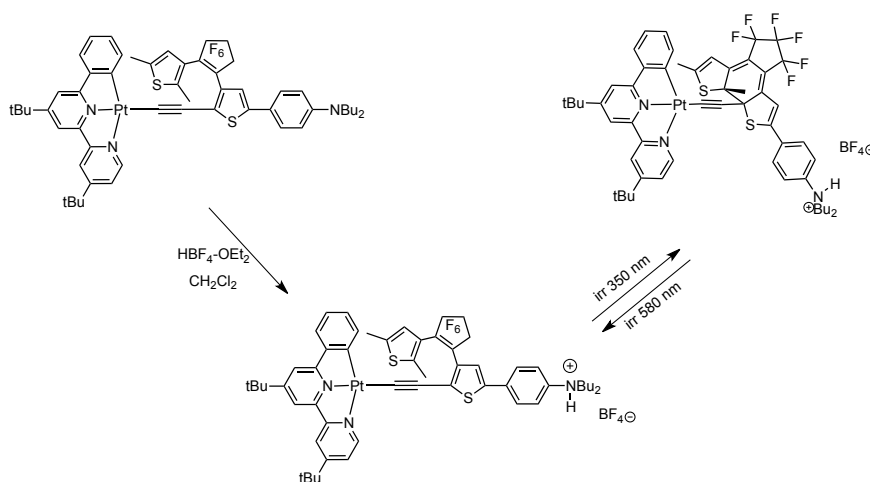
Figure 92. The acido-triggered photochromism of **Pt(phbpy)(DTE)-2**.

The NLO response was investigated with the EFISH technique. It was found the neutral complex is characterized by a large negative value of $\mu\beta_{EFISH}$, dominated by LLCT ($\pi_{amino} \rightarrow \pi^*_{N^\wedge N^\wedge C}$) with a small contribute of MLCT transitions, that doesn't change upon irradiation in agreement with the lack of photochromism of the complex. The protonated open complex also has a large value of $\mu\beta_{EFISH}$, dominated now by $\pi_{DTE} \rightarrow \pi^*_{N^\wedge N^\wedge C}$ transitions, but with opposite sign respect to the neutral complex. Irradiation in the UV leads to ring-closing and to a high negative value of $\mu\beta_{EFISH}$: the formation of a tetrahedral centre at the C_2 carbon of the protonated closed form induces a new conjugated pathway centred on the DTE unit. Theoretical studied confirmed that all three systems have $\mu\beta$ values of the same order of magnitude, in agreement with the experiments. This novel DTE-based Pt[II] complex is the first example of an in situ sequential double NLO switch, modulated both by protonation and by UV light irradiation.

2.3. Novel Platinum(II) NLO-phores

The large NLO response of Pt^{II} 1,3-di(2-pyridyl)benzene complexes presented before, prompted us to prepare a new series of platinum complexes with this kind of ligand for applications in second-order NLO.[266,267]

From an NLO point of view, the effect of a π-delocalized electron-donating substituent on the cyclometallated 1,3-di(2-pyridyl)benzene ligand of such Pt(II) complexes has not been investigated yet. These complexes are expected to demonstrate a good NLO response, because their absorption bands are red shifted by increasing the donor ability of the substituent at the central position of the cyclometallating ring (see Chapter I) stabilising thus charge transfer states. It is also known that the presence of charge-transfer transitions at low energy can lead to a high quadratic hyperpolarizability.

The considered complexes are represented below:
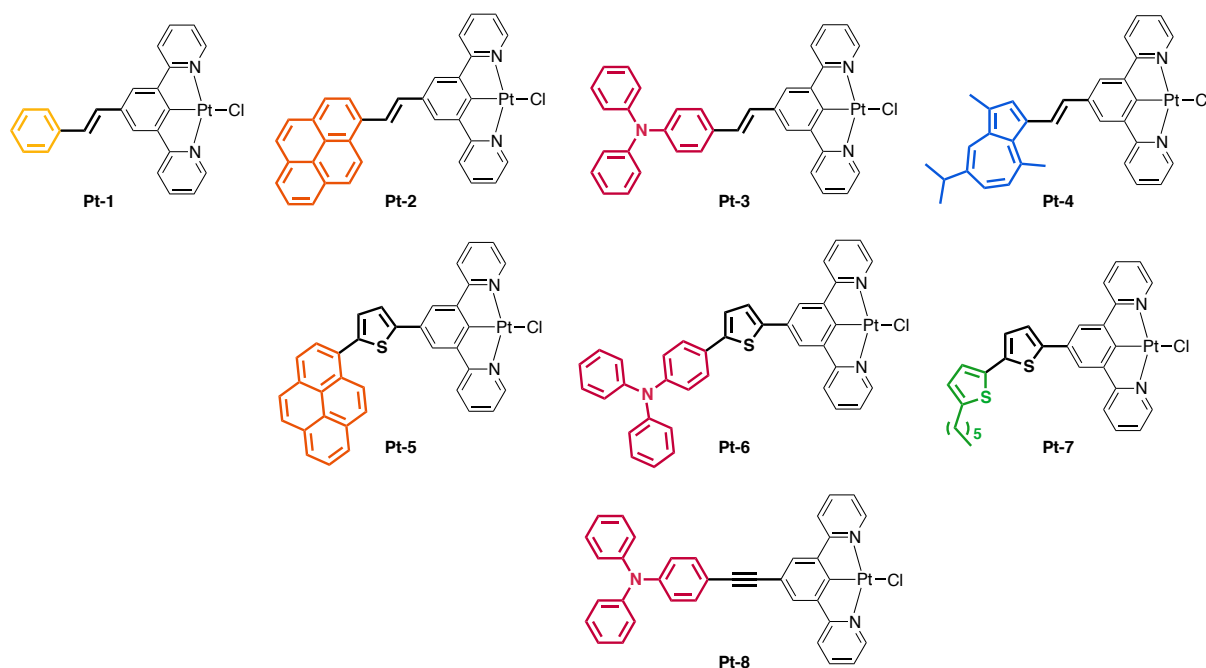
Figure 93. The Pt(dpyb)Cl complexes whose second-order NLO properties were investigated.

The luminescent properties of complexes **Pt-3** and **Pt-8** were already discussed in Chapter I, relatively to their efficiency in OLEDs.

The complexes possess different π-conjugated donating substituents, *i.e.* simple phenyl, pyrene, triphenylamine, guaiazulene and 4-hexylthiophene, linked to the central phenyl unit of the pincer ligand through different linker, *i.e.* a double bond, a triple bond or a thiophene. The double bond is expected to allow a better conjugation respect to the triple bond, because of the sp^2 hybridized carbons, instead of the alkynyl sp carbons. On the other hand, the thiophene linker is expected to enhance the NLO response of such complexes because it increases the rigidity and planarity of the π-conjugated structure and

because of the highly polarizable p electrons of the thiophene, which can take part to the electron cloud of the system. As stated in the introduction, in fact, the presence on the donor of an aromatic ring containing one heteroatom, such as thiophene, results in higher β values.[199]

2.3.1. Synthesis of the Pt(dpyb)Cl complexes

The synthetic procedure for the preparation of the complexes will be described in Chapter III. For the synthesis of the complexes with the double bond as a linker (**Pt-1** to **Pt-4**), diethyl 3,5-dibromobenzylphosphonate was prepared in the first time. Then, it reacted with the appropriate aldehyde reacted in a Horner-Wadsworth-Emmons reaction in order to form a *trans* double bond. Stille coupling with freshly prepared 2-(tri-*n*-butylstannyl)pyridine was performed in order to achieve the N^C^N ligand, which yielded the complexes upon reaction with K_2PtCl_4.

The complexes bearing a thiophene linker (**Pt-5** to **Pt-7**) were prepared starting from the appropriate bromo-derivative and 2-(tri-*n*-butylstannyl)thiophene through a series of Stille couplings. The obtained intermediate was turned into a stannyl derivative in order to react with 1,3,5-tribromobenzene to obtain a dibromo-derivative, which in turn reacted with 2-(tri-*n*-butylstannyl)pyridine to achieve the ligands. The complexes were obtained upon reaction of the ligands with K_2PtCl_4 at reflux in an $AcOH/H_2O$ or CH_3CN/H_2O mixture depending on the complex.

To obtain complex **Pt-8**, with an alkynyl bridge, 4-ethynyl-*N,N*-diphenylaniline was firstly prepared. Then, it reacted with 1,3,5-tribromobenzene through a Sonogashira coupling and the product reacted with 2-(tri-*n*-butylstannyl)pyridine assisted by microwaves to achieve the ligand. The complex was obtained upon reaction with K_2PtCl_4 in an $AcOH/H_2O$ mixture in a microwave reactor.

The complexation of the ligand to the platinum centres was confirmed by ^{1}H-NMR spectroscopy. The signal corresponding to the H in the position 6 of the pyridyl ring is shifted downfields and displays the typical coupling with [195]Pt. Furthermore, the signal corresponding to the proton 4' on the phenyl ring disappears. The complexes were also characterized by elemental analysis.

2.3.2. Second-order NLO properties of the Pt(dpyb)Cl complexes

The linear absorption spectra of the complexes were recorded (Table 11). Like other platinum(II) complexes with a cyclometallated 1,3-di(2-pyridyl)benzene ligand, they show a strong absorption band in the UV, which can be assigned to intraligand $^1\pi–\pi^*$ transitions of the cyclometallated 1,3-di(2-pyridyl)benzene, and less intense absorption bands at longer wavelengths in agreement with transitions of mixed CT/LC character.[256] The bands at longer wavelengths are particularly intense and can show a hint of the strength of charge-transfer transitions in such complexes.

All EFISH measurements were carried out working in CH_2Cl_2 solutions at a concentration of 10^{-3} M, with a non-resonant incident wavelength of 1.907 μm, obtained by Raman-shifting of the

fundamental 1.064 μm wavelength produced by a Q-switched, mode-locked Nd^{3+}:YAG laser. The μβ$_{EFISH}$ values for all complexes and some calculated β values[IV] are reported in Table 11:[266,267]

Complex	λ$_{abs}$ / nm ($\varepsilon \times 10^3$ / $M^{-1}cm^{-1}$)[a]	μβ$_{1907\ EFISH}$[b] (x10^{-48} esu)	μ$_{tot}$[c] (D)	β$_{EFISH}$[d] (x10^{-30} esu])
Pt-1	300 (18.9), 383 (2.7), 415 (3.0)	−660	9.5	−69
Pt-2	244 (65.9), 281 (46.9), 382 (41.2)	−820	9.4	−87
Pt-3	295 (21.0), 378 (15.7), 430sh (4.9)	−880	10.7	−82
Pt-4	235 (18.1), 284 (16.8), 378 (2.9)	−1540	–	–
Pt-5	242 (15.3), 280 (9.7), 375 (7.3)	−1078	–	–
Pt-6	237 (13.7), 285 (12.6), 379 (9.8)	−498	–	–
Pt-7	265 (4.5), 356 (6.0)	−945	–	–
Pt-8	240 (35.1), 292 (27.1), 338sh (18.2), 363 (22.8), 416sh (6.4)	−764	11.0	−69

Table 11. UV-vis absorption maxima, dipole moments and second-order NLO response. [a] In CH_2Cl_2 solution (10^{-5}M) at 298 K. [b] At 1.907 μm; estimated uncertainty in EFISH measurements is ±10%. [c] computed dipole moments in DMF solution using B3LYP//6-31g*/LANL2DZ// C-PCM level of theory. [d] β$_{EFISH}$ value was calculated using the μ value computed in solution.

All complexes are characterized by a negative value of μβ$_{EFISH}$, as determined by the EFISH technique working in DMF solution. This negative sign is in agreement with a decrease of the excited state dipole moment with respect to the ground state,[224a] suggesting that the second-order dipolar NLO response is dominated by the charge transfer from platinum to the cyclometalated ligand.[256] The complexes investigated here are characterized by better μβ$_{EFISH}$ values, than the platinum(II) complex bearing a cyclometallated 5-methyl-1,3-di(2-pyridyl)benzene ligand (μβ$_{EFISH}$ = −480 · 10^{-48} esu; β$_{EFISH}$ = −47 · 10^{-30} esu), previously reported by our group.[256] The highest μβ$_{EFISH}$ value was measured for **Pt-4**, bearing a strongly electron-rich guaiazulene moiety, while the lowest, as expected, was recorded for **Pt-1**, which has a simple styryl substituent. These considerations can lead to the observation of a trend: with the same tether between the π-conjugated substituent and the Pt(dpyb)Cl moiety, *i.e.* the double bond, the μβ$_{EFISH}$ values increase as the electron-richness of the substituent increases, in the order **Pt-1** < **Pt-2** < **Pt-3** < **Pt-4**. The presence of a more π-delocalized electron-rich group increases the intensity of the charge-transfer transitions leading to a higher μβ$_{EFISH}$ value. The μ and β$_{EFISH}$ values for **Pt-1,2,3** were also calculated. The complexes are characterized by a similar dipole moment, in particular the μ value

---

[IV] The β$_{EFISH}$ values were calculated in collaboration with Dr. S. Fantacci. The β$_{EFISH}$ values of the other platinum(II) complexes are currently under calculation.

of **Pt-2** is even lower than that of **Pt-1**, which lacks the triphenylamino or pyrene moiety. It can be noticed that **Pt-3** has the highest μ value, which leads to its higher $\mu\beta_{EFISH}$ value, while **Pt-2** has the highest hyperpolarizability value.

The trend observed for the first four Pt^{II} complexes is not well reproducible for the complexes bearing a thiophene as a linker, *i.e.* **Pt-4,5,6**. The thiophene, which is more rigid than the double bond and possesses delocalizable π-electrons thanks to the presence of the sulphur, is expected to increase the NLO properties of the Pt(dpyb)Cl complexes. Unfortunately, this was observed for **Pt-5** but not for **Pt-6**. In the first case, going from **Pt-2** to **Pt-5** the π-conjugation of the molecule is effectively enhanced and a planar system including the platinum, the thiophene linker and the pyrene can be envisaged. On the other hand, probably in **Pt-6** the triphenylamino substituent assumes a three-dimensional conformation and this lowers the π-conjugation and planarity of the molecule, consequently leading to an abrupt decrease in the $\mu\beta_{EFISH}$ value. **Pt-7** still has a fair $\mu\beta_{EFISH}$ value, considering that it has only two thiophene units as aromatic substituents, which is unexpectedly higher than that of **Pt-6**.

Finally, the complex with a triple bond as a tether was studied. The $\mu\beta_{EFISH}$ value of **Pt-8** is lower than that of **Pt-3** but higher than that of **Pt-6**, confirming the deleterious effect, in this case, of the presence of a thiophene as tether. Also, the β_{EFISH} value of **Pt-3** is quite similar to that of **Pt-8**, showing that the substitution of a double bond by a triple bond, as bridge between the triphenylamino moiety and the cyclometallated ring has a negligible NLO influence in this kind of complexes.

2.3.3. Conclusion

The second-order NLO properties of a series of Pt(dpyb)Cl complexes have been measured. It was observed that the $\mu\beta_{EFISH}$ values increase with the electron-richness of the aromatic pendants and by enhancing the planarity of the system. The observations made here indicate that it is not necessary to have a strong donor substituent on the styryl group in order to reach a high second-order NLO response. Remarkably, the simple platinum complex bearing a cyclometallated 5-styryl-1,3-di(2-pyridyl)benzene shows a good quadratic hyperpolarizability and has a great potential for application in photonics. Besides, it is worth pointing out that all the complexes investigated here are characterized by better $\mu\beta_{EFISH}$ values than the platinum(II) complex bearing a cyclometallated 5-methyl-1,3-di(2-pyridyl)benzene ligand.[256]

2.4. The first Platinum(II) dipyridylbenzene NLO switches

The second-order NLO properties of Pt(dpyb)Cl complexes bearing a photochrome (Figure 94), whose luminescent and photochromic behaviour was discussed in Chapter I, will be here presented. In Section 2.2.1, the NLO activity of Pt^{II} N^N^C complexes bearing a photochrome on the alkynyl co-ligand were reviewed, but, to date, no Pt^{II}(dpyb)Cl complexes bearing a photochrome are reported in literature.
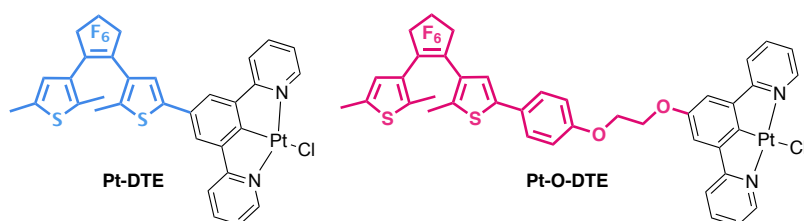
Figure 94. The Pt(dpyb)Cl complexes bearing a photochrome on the central phenyl ring of the cyclometalated ligand studied for second-order NLO.

2.4.1. Second-order NLO properties in solution

The complexes were investigated by the EFISH technique, which can provide direct information on the intrinsic molecular NLO properties through equation (10), discussed in Section 1.2.1:[187]

$$\gamma_{EFISH} = \frac{\mu\beta\,(-2\omega;\omega,\omega)}{5kT} + \gamma(-2\omega;\omega,\omega,0)$$

The $\mu\beta_{EFISH}$ values of all the investigated complexes, measured in DMF or CH$_2$Cl$_2$ solution with an incident wavelength of 1.907 μm, are reported in Table 12. To obtain $\beta_{1.907\,EFISH}$, the projection along the dipole moment axis of the vectorial component of the tensor of the quadratic hyperpolarizability, it is necessary to know the dipole moment, μ.

In agreement with the previously reported cyclometalated platinum(II) compounds,[256] all the investigated complexes are characterized by fair negative values of $\mu\beta_{EFISH}$, as expected for a negative value of $\Delta\mu_{eg}$ upon excitation and irrespective of the form of the DTE unit (open or closed).
Upon irradiation at 350 nm of the solution of **Pt-DTE(o)**, a 3-fold increase of the $\mu\beta_{EFISH}$ is readily observed due to the closing of the DTE bridge affording **Pt-DTE(c)**. This large enhancement of the quadratic NLO response upon ring-closing reflects the delocalization increase of the π-electron system in the closed form, accompanied by an important decrease of the HOMO-LUMO gap.

Complex	$\mu\beta_{1907\ \mathrm{EFISH}}$ [a] $[\mathrm{x}10^{-48}\ \mathrm{esu}]$
Pt-DTE(o)	-510
Pt-DTE(c)	-1450
Pt-O-DTE(o)	-575 [b]
Pt-O-DTE(c)	-1476 [b]

Table 12. Second-order NLO response and calculated dipole moments of **Pt-DTE** and **Pt-O-DTE** in their opened and closed forms. [a] Working in CH_2Cl_2 with an incident radiation wavelength of 1.907 μm; the error is ±10%. [b] Working in DMF, a $\mu\beta_{\mathrm{EFISH}}$ value of $-415 \cdot 10^{-48}$ and $-1170 \cdot 10^{-48}$ esu was obtained for **Pt-O-DTE(o)** and **Pt-O-DTE(c)**, respectively.

In order to investigate the influence on the second-order NLO properties of the connection mode between the DTE unit and the Pt(dpyb) fragment, complex **Pt-O-DTE** was investigated with the EFISH technique as well. Here the DTE moiety is separated from the N^C^N fragment by an insulator and flexible ethylene glycol bridge. It turned out that the open form of the complex is characterized by a $\mu\beta_{\mathrm{EFISH}}$ similar to that of **Pt-DTE(o)**, suggesting that the alcoxy group behaves as a thiophene from an NLO point of view in this kind of platinum complexes.

Remarkably, although the DTE moiety is separated from the platinum fragment in complex **Pt-O-DTE(o)**, the $\mu\beta_{\mathrm{EFISH}}$ value increases of 2.6 times upon ring-closing to form **Pt-O-DTE(c)**. This enhancement factor quite similar to that observed on going from the open to the closed form of **Pt-DTE** where the DTE and the metal moiety are directly connected.

This surprising NLO behavior of **Pt-O-DTE** is really fascinating. To our knowledge it represents the first example of an NLO switch based on a photochromic unit that is not directly linked to the NLO active moiety, opening new unexpected routes for the design of photoswitchable NLO compounds.

2.4.2. Second-order NLO properties in the solid state

The second-order NLO properties of **Pt-DTE** were studied in the solid state. Thin films of the chromophore dispersed in a PMMA or PS matrix were prepared.

The SHG signal of films in PMMA progressively faded due to a loss of orientation of the dyes (Figure 95). This behaviour, already reported in many other works, is not surprising if the β transition of PMMA, which has been attributed to rotation of the ester side group, is considered. A much better behaviour was obtained by using polystyrene as matrix.
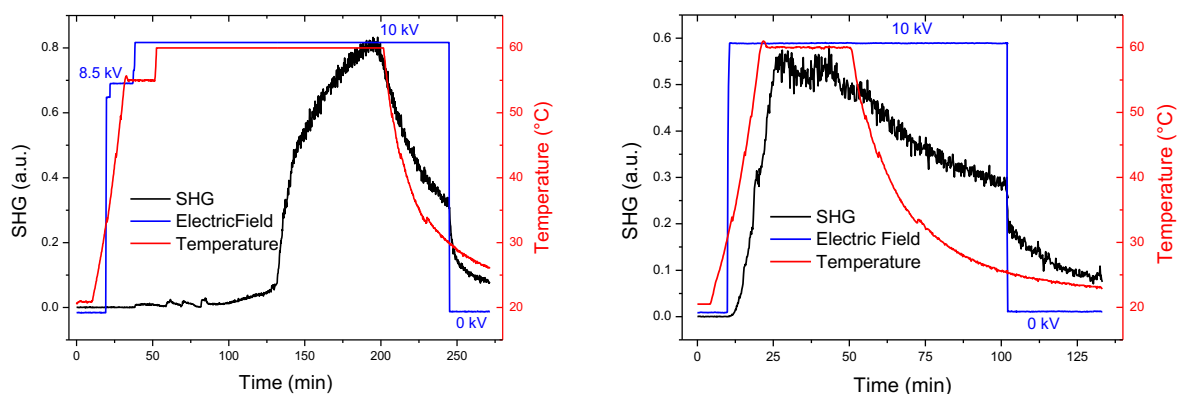
Figure 95. Poling of the **Pt-DTE**/PMMA films in the closed (left) and open (right) form.

Poling was done on polystyrene films of complex **Pt-DTE** either in the open or closed form (Figure 96). The SHG was negligible before applying the corona voltage and it quickly increased after application of the electric field. When the temperature was increased up to 50-60°C, a large increase of the SHG occurred, due to the decrease of the viscosity of the polymeric matrix which allowed an easier orientation of the NLO chromophores. When a stable SHG was reached, the sample was cooled at room temperature. The final switch off of the electric field caused the typical drop of the SHG.
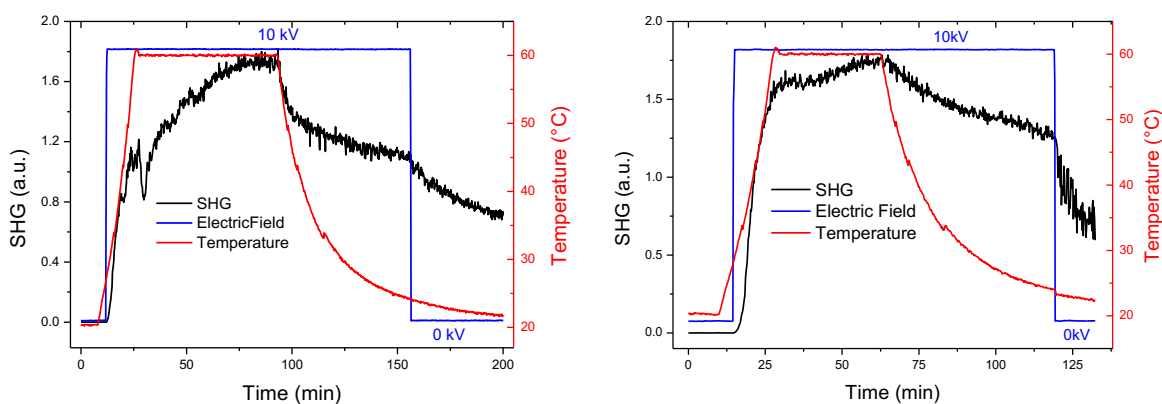
Figure 96. Poling of the **Pt-DTE**/PS films in the closed (left) and open (right) form.

After poling, both the open and the closed form of the **Pt-DTE**/PS film showed a decreasing of absorption peaks in comparison with that observed before poling (Figure 97). This is the characteristic so-called dichroic effect due to the partial orientation of molecules along the direction of the electric poling field (Z axis).[268] No appreciable Stark shift[268] of the absorption peaks was observed after poling.
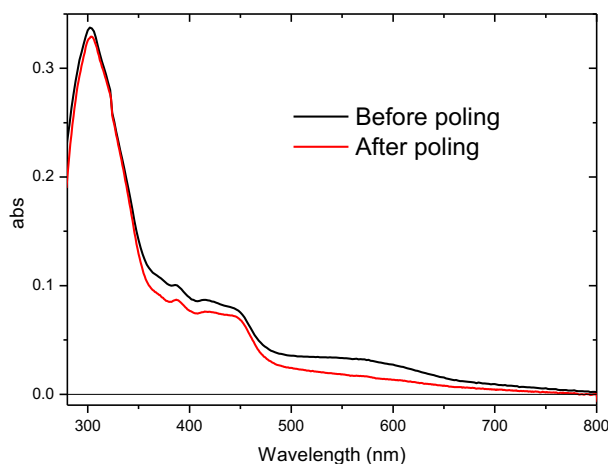
Figure 97. Absorption spectra of **Pt-DTE**/PS films in open form before and after poling.

By fitting the Maker fringe measurements with the standard expression presented in Section 1.5, three nonzero coefficients of the second-order susceptibility tensor $\chi_{33}^{(2)}$, $\chi_{31}^{(2)}$ and $\chi_{15}^{(2)}$ for a poled film have been evaluated. Their values are reported in Table 13, the error in these data can be estimated to be less than 20%.

Complex	$\chi_{33}^{(2)}$ (pm/V)	$\chi_{31}^{(2)}$ (pm/V)	$\chi_{15}^{(2)}$ (pm/V)	$\chi_{33}^{(2)}/\chi_{31}^{(2)}$	$\chi_{33}^{(2)}/\chi_{15}^{(2)}$
Pt-DTE(o)	0.56	0.58	0.15	0.96	3.73
Pt-DTE(c)	2.82	1.74	0.54	1.62	5.22

Table 13. Second-order susceptibility tensors of **Pt-DTE**/PS films in open and closed forms.

For **Pt-DTE**/PS films the $\chi_{33}^{(2)}$, $\chi_{31}^{(2)}$ and $\chi_{15}^{(2)}$ values increase going from the open to the closed form. Interestingly, the ratios of the components $\frac{\chi_{33}^{(2)}}{\chi_{31}^{(2)}}$ and $\frac{\chi_{33}^{(2)}}{\chi_{15}^{(2)}}$ for both forms are not close to 3, value expected for poled films in which the chromophores have a one dimensional first hyperpolarizability tensor.[269] This behaviour suggests that the charge transfer inside the chromophore is not only in the direction of the dipole moment but that other contributions are present in other directions,[270] and is the same as for the Pt(phbpy) complexes previously reported by our group.[265]

Polymeric films with second-order NLO properties and commutable NLO responses are of growing importance: recently the first examples of switchable NLO-polymer films based on Pt[II] 6-phenyl-2,2'-bipyridine complexes were reported,[265] opening new perspectives for the preparation of convenient reversible NLO switches. This is why, after poling, the SHG photoswitching of polystyrene films based on **Pt-DTE** was investigated (Figure 98).
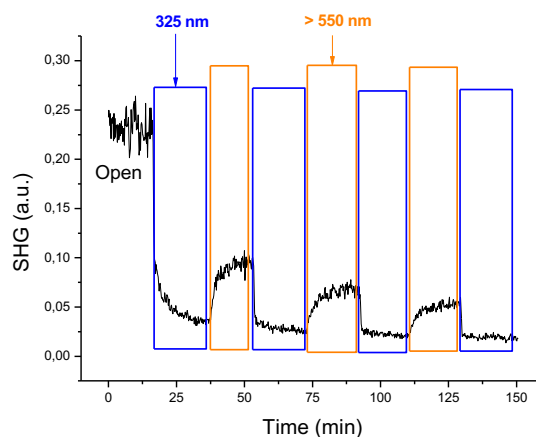
Figure 98. SHG photoswitch of the **Pt-DTE**/PS film starting from the open form.

We started from the open form with the fundamental and SH beams p-polarized. The intensity of the SHG signal decreases after UV irradiation, as the closed form is generated. Once a stable plateau is reached, if UV irradiation is stopped and visible light ($\lambda > 550$ nm) is turned on, the SHG intensity increases as the closed form converts back to the open form. As expected, exposure to visible light of a freshly prepared poled polystyrene film based on the closed form of **Pt-DTE** leads to an increase of the SHG intensity, due to the ring-opening of DTE (Figure 99).
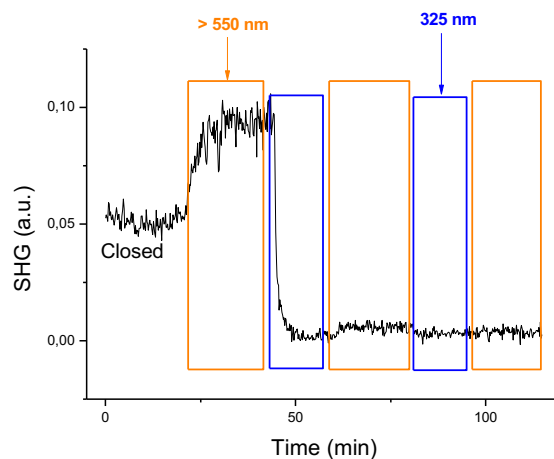
Figure 99. SHG photoswitch of the **Pt-DTE**/PS film starting from the closed form.

Unfortunately, SHG photoswitches of the **Pt-DTE**/PS films loose some SHG signal during the switches, due to the irreversible loss of orientation through the photoisomerization processes. However, it is worth pointing out how the SHG photoswitch starting from the freshly prepared poled polystyrene film based on the open form of **Pt-DTE** is more stable allowing to obtain at least four switches, whereas the SHG photoswitch starting from the related closed form did not shown any SHG signal after the second switch.

It is interesting to highlight that the closed form of **Pt-DTE** is more NLO-active than the related open form in solution, as determined by the EFISH technique, whereas the polymer film based on **Pt-DTE(o)** shows the highest SHG intensity. This difference between the molecular and macroscopic behavior has already been reported in a previous work on phenyl-substituted dithienylethene.[210]

In fact, in a SHG photoswitching experiment, the intensity of the SHG signal of the open and closed form depends on the effective nonlinear optical coefficient, d_{eff}, in particular from the combination of the nonzero coefficients of the second-order susceptibility tensor. These coefficients are in turn connected to the first hyperpolarizability tensor: the geometry and charge transfers inside the chromophores are important factors for the implementation of these complexes from a macroscopic point of view.

2.4.3. Conclusion

Complexes **Pt-DTE** and **Pt-O-DTE** possess a good second-order NLO response, which increases upon ring-closing of the photochromic moiety. Their $\mu\beta_{EFISH}$ values are of the same order of magnitude of those of the previously reported Pt(phbpy)(DTE) complexes, even though lower than the best performing of that family.[265] Remarkably, **Pt-O-DTE** shows a good NLO activity, even though the photochromic unit is not directly linked to the NLO active platinum moiety: it is the first time that such behaviour is observed.

The SHG signal in a polymeric film was measured for **Pt-DTE** and nonzero coefficients of the second-order susceptibility tensor were calculated: the values are fairly good, even though lower than those for the Pt(phbpy)(DTE) complexes previously studied by our group.[265] The values of $\chi^{(2)}_{33}/\chi^{(2)}_{31}$ and $\chi^{(2)}_{33}/\chi^{(2)}_{15}$ confirm that the charge transfer inside the chromophore is not only in the direction of the dipole moment but that other contributions are present in different directions.

Pt-DTE/PS polymeric films with commutable NLO response were prepared: unfortunately, they loose some SHG signal during the switches, due to the irreversible loss of orientation through the photoisomerization processes. In the future, stability improvement could be reasonably achieved by using the cross-linking technique for preparation of the polymer films in order to inhibit the reorientation of the chromophores during photoisomerization.

2.5. Iridium complexes with second-order NLO properties

The luminescent properties of Ir^{III} neutral and cationic complexes with cyclometalated ligands have been presented in the Chapter I. Some of these complexes also present high second-order NLO activity, extensively studied by our group. The NLO properties of some Ir^{III} complexes with terpyridyl ligands[271] and with monodentate pyridyl ligands[272] were studied with good results, but the attention of researchers mainly focused on cyclometalated Ir^{III} complexes.

An efficient class of NLO-phores are iridum(III) 1,10-phenantroline complexes:[273] they have large second-order NLO response and they do not show strong absorptions at longer wavelengths. This means that second harmonic generation can be obtained without any significant cost in transparency towards the strength of its emission (Figure 100).
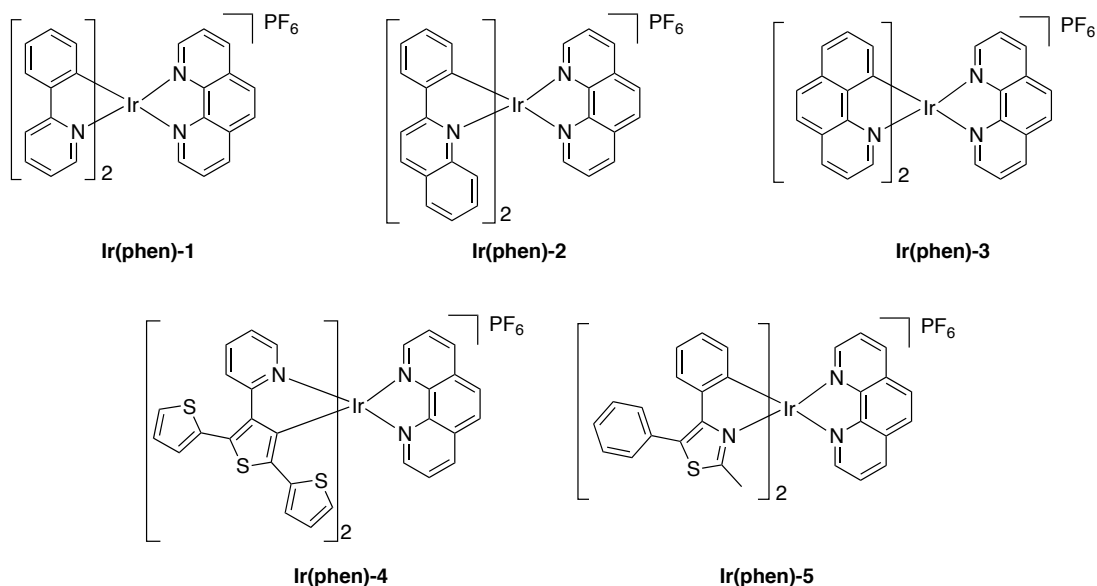
Figure 100. Schematic representation of the iridium(III) phenantroline complexes studied by our group.

Complexes **Ir(phen)-1** has also been functionnalized with substituents on the phenantroline[274] The better $\mu\beta_{EFISH}$ values were obtained for the complexes bearing a $-NO_2$ substituent on the position 5 of the 1,10-phenantroline ($-2230 \cdot 10^{-48}$ esu), higher than those of the complexes with dimethylamine, methyl or no substituents in this position. For these complexes, in fact, the HOMO is primarily composed of an antibonding combination of $Ir_{(t2g)}$ and π orbitals of the cyclometalated ligand, while the LUMO is the π^* antibonding orbital of the phenantroline. The $-NO_2$ antibonding orbital efficiently mixes with the phenantroline π^* orbital, with the effect of being stabilized and consequently lowering the HOMO-LUMO gap. In this case the resulting $\mu\beta$ value is issued by negative cooperating MLCT transitions. On the other hand, when the substituent is $-NMe_2$, large positive ILCT contributions must be considered: this is the origin of the much smaller $\mu\beta_{EFISH}$ absolute value for this complex. The

presence of π-conjugated groups, as phenyls, on the positions 4 and 7 of the phenatroline, can contribute to enhance the conjugation length of the system and also to increase the second-order NLO response. No special enhancement of the NLO response was reported if the cyclometalated ligand was changed.[275] Substitution of the 2,2'-phenylpyridine with the more π-delocalized cyclometallated benzo[h]quinoline (**Ir(phen)-2**) or 2-phenylquinoline (**Ir(phen)-3**) does not significantly affect the second-order NLO, whereas a slightly lower response was obtained for complexes with the cyclometallated 3'-(2-pyridil)-2,2':5',2''-terthiophene (**Ir(phen)-4**) and 4,5-diphenyl-2-methyl-thiazole (**Ir(phen)-5**). For these complexes, in summary, the NLO response is not strongly affected by the nature of the cyclometallated moiety whereas it is controlled and tuned by the nature of the R substituent on the phenanthroline ring. The effect of the ion pairing was also evaluated: it can affect the absolute value of $\mu\beta_{EFISH}$ and, when the ion pair is not too tight, like for PF_6^-, it can cause a significant increase of such absolute value upon dilution, because of the parallel decrease of the extent of ion pairing. This effect can be attributed to the decrease of the electronic perturbation induced by the counterion on the LUMO of the cyclometalated Ir^{III} complex.

Our group also studied the second-order NLO properties of some Ir(ppy)$_2$(acac) complexes (Figure 101).[253a] These complexes are more efficient that the cyclometalated Pt(ppy)(acac) complexes presented in Section 2.2.
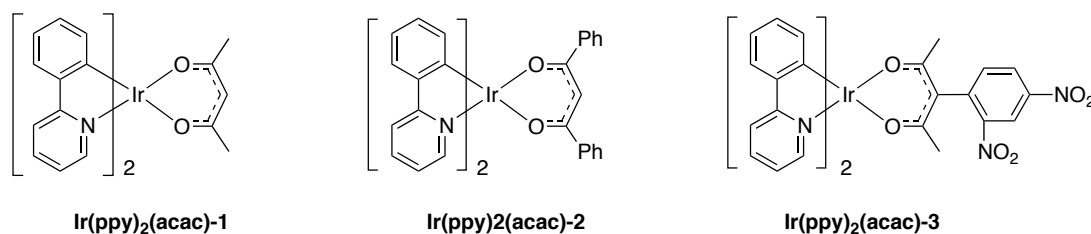
Figure 101. The Ir(ppy)$_2$(acac) complexes.

Complex **Ir(ppy)$_2$(acac)-2** shows the highest $\mu\beta_{EFISH}$ value ($-1340 \cdot 10^{-48}$ esu; $\beta_{EFISH} = -268 \cdot 10^{-30}$ esu), by virtue of the more π-delocalized β-diketonate. On the other hand, the $\mu\beta_{EFISH}$ value of the complex bearing the electron withdrawing 2,4-dinitrophenyl group, is much lower ($-975 \cdot 10^{-48}$ esu; $\beta_{EFISH} = -163 \cdot 10^{-30}$ esu). Indeed, for these complexes the HOMO is antibonding combination of $Ir(d_{xy})$ and $ppy(\pi)$ orbitals, while main contribution to the LUMO come from π* orbitals of the phenylpyridine ligands followed by π* orbitals on the acetylacetonate ligand. The largest positive contributions to the β_{EFISH} are originated from transitions with dominating MLCT character, whereas the strongest negative contributions are originated from a series of higher energy transitions involving mainly ppy-ILCT transitions, with a limited amount of metal character. So, transitions involving the only the acetylacetonate ligand are less important and weakly contribute to the EFISH hyperpolarizability.

More recently the second-order NLO properties of similar complexes with 4-styryl-2-phenylpyridine ligand were studied (Figure 102).[276]
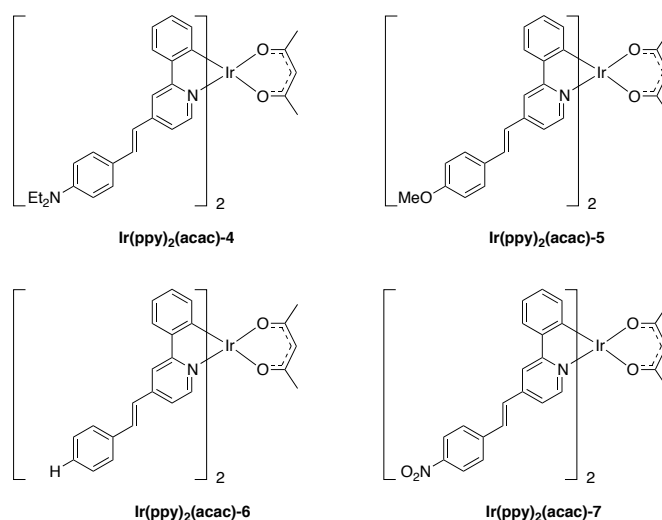
Figure 102. The Ir(ppy)(acac) complexes studier for second-order NLO.

The $\beta_{1.907\ EFISH}$ values of complexes **Ir(ppy)$_2$(acac)-4,5,6** are quite similar, whereas the absolute value of **Ir(ppy)$_2$(acac)-7** is higher and similar to that previously reported for Ir(ppy)$_2$(acac). In these Ir^{III} complexes the second-order NLO response is originated from the contribution of various positive and negative charge transfer transitions as for the complexes discussed above.

Recently, the second-order NLO response of the cationic [Ir(ppy)$_2$(4,5-diazafluorene)]$^+$ and [Ir(ppy)$_2$(9-fulleriden-4,5-diazafluorene)]$^+$, with PF6$^-$ or C$_{12}$H$_{25}$SO$_3^-$ as counterions, and the neutral [Ir(ppy)$_2$(9-fulleriden-4-monoazafluorene)] have been investigated.[277] They display high values of $\mu\beta_{EFISH}$, dominated by ILCT concerning the cyclometalated 2,2'-phenylpyridine. The presence of the fullerene group weakens the interaction between the counterion and the LUMO of the complex, enhancing the NLO activity. The neutral complex has, as expected from the absence of an ionic couple, a $\mu\beta_{EFISH}$ value comparable to that of other Ir^{III} bis-phenylpyridine complexes.

Ir(ppy)$_3$ complexes also demonstrated to be active NLO chromophores.[278] Our group studied a series of these complexes with differently substituted 2,2'-phenylpyridine ligands, in order to put in evidence the effect of the substituents on the NLO response (Figure 103). In these complexes, the HOMO is located on the iridium t$_{2g}$ orbitals together with the p orbitals of the phenyl (or thienyl) ligands. The contribution of the metal to the HOMO is smaller for complex **Ir(ppy)$_3$-7**. The LUMO is delocalized purely on the phenylpyridine ligands. Complexes **Ir(ppy)$_3$-2,3,4,5,9,10,12**, with electron-withdrawing or weak electron-donating substituents, have a positive value of $\mu\beta_{EFISH}$, dominated by MLCT transitions from the iridium centre to the phenylpyridine. The absolute value is smaller for those complexes whose ligands bear electron-acceptors, because of the contribution of ILCT transitions. On the other hand, the

remaining complexes have positive $\mu\beta_{EFISH}$ values, because ILCT prevail on MLCT. The NLO response is stronger for complexes with strong donors (**Ir(ppy)₃-7**: $\mu\beta_{EFISH} = 1430 \cdot 10^{-48}$ esu).
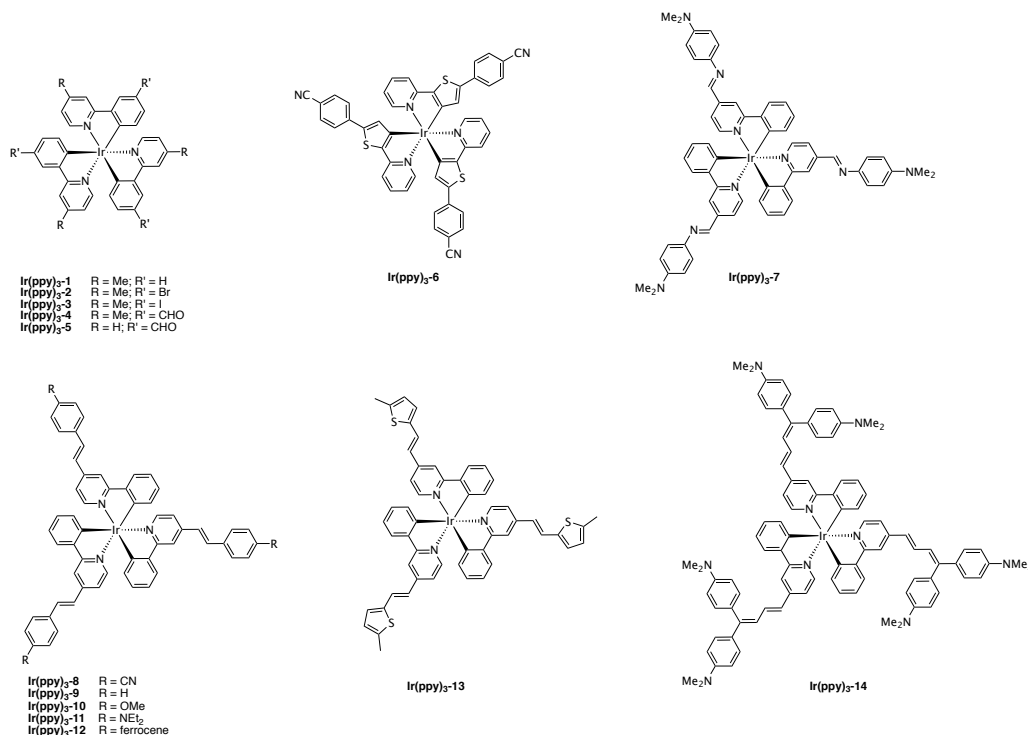
Figure 103. The Ir(ppy)₃ complexes studier for second-order NLO.

For complexes **Ir(ppy)₃-9** to **Ir(ppy)₃-14** the second-order NLO reponse was also studied with the HLS technique, in order to take into account both the dipolar and octupolar components. It was observed that the values of β_{HLS} are larger than β_{EFISH}, suggesting a much stronger octupolar contribution to the total quadratic hyperpolarizability of this family of complexes. The β_{HLS} increases with the electron-donating strength of the phenylpyridines, reaching a maximum for **Ir(ppy)₃-14**, with a noticeable value of $\beta_{HLS} = 460 \cdot 10^{-30}$ esu.

Finally, some cationic [Ir(ppy)(bpy)]⁺ complexes have been studied with both EFISH and HLS technique.[173]
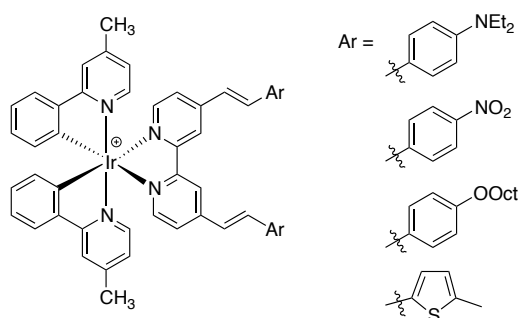
Figure 104. The [Ir(ppy)₂(bpy)]⁺ complexes.

The use of simply substituted bipyridines in place of phenanthrolines does not affect the second-order NLO response nor does the introduction of the methyl substituent on the phenylpyridine ligands. The absolute value of $\mu\beta_{1.907,EFISH}$ increases by enhancing the π-delocalization of the 2,2'-bipyridine with styryl substituents, reaching values even higher than that previously reported for the Ir^{III} complex with 5-nitro-1,10-phenanthroline discussed above. On the other hand, the nature of the substituents on the 2,2'-bipyridines does not affect significantly the global $\mu\beta_{1.907}$ values. The absolute value of $\mu\beta_{1.907,EFISH}$ is higher for the complex bearing two NO_2 groups on the 2,2'-bipyridine ($-2770 \cdot 10^{-48}$ esu, $\mu\beta_{HLS} = 432 \cdot 10^{-30}$ esu): this confirms an EFISH response controlled primarily by MLCT/L'LCT processes from the 2,2'-phenylpyridine Ir^{III} moiety to the π^* orbitals of the 2,2'-bipyridine. By doing the measurement with the HLS technique, it was found that the major contribution to the total quadratic hyperpolarizability is given mainly by the octupolar part, even though these complexes do not exhibit a classical octupolar structure.

2.6. A novel Iridium(III) NLO-phore

Iridium(III) complexes with π-conjugated substituents both on the 2-phenylpyridine and on the 2,2'-bipyridine ligands are not common in literature. In Chapter I, we presented the luminescent properties of a novel cationic $[Ir(ppy)_2(bpy)]PF_6$ complex, **Ir-5** (Figure 105), of which we studied the second-order NLO properties with the EFISH technique.[176]
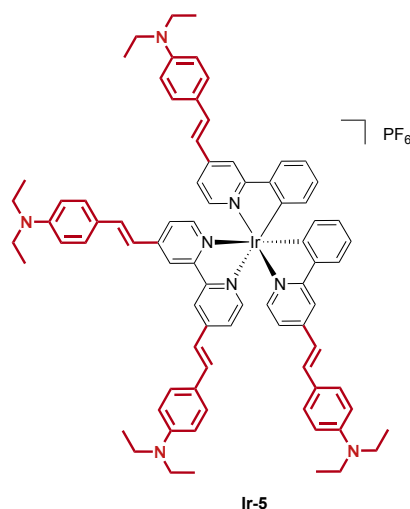
Figure 105. The novel $[Ir(ppy)_2(bpy)]PF_6$ complex.

Complex **Ir-5** is characterized by a negative value of $\mu\beta_{1.907} = -960 \cdot 10^{-48}$ esu. This value is in agreement with the observed solvatochromism of the complex. The absorption spectrum of **Ir-5** was registered both in dichloromethane and dimethyl sulfoxide (Figure 106), putting in evidence a pronounced solvatochromic behaviour, typical of electronic transitions with an appreciable degree of charge-transfer character.
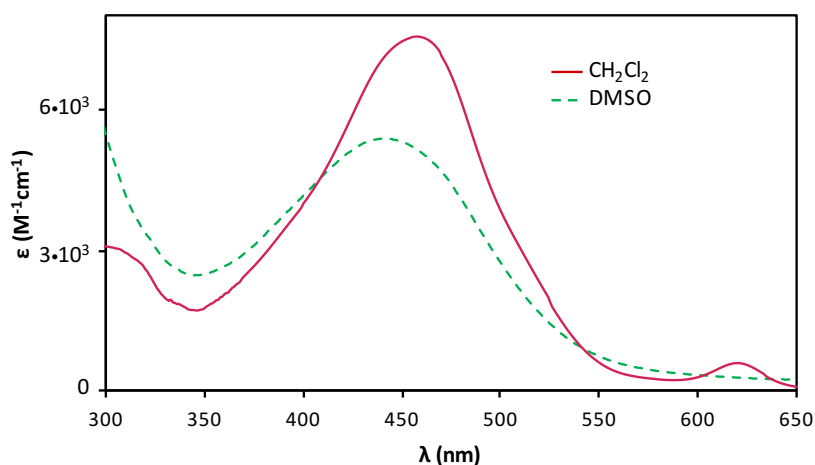
Figure 106. Superimposed absorption spectra of **Ir-5** in CH_2Cl_2 and DMSO.

The absorption bands are blue shifted with increasing solvent polarity, suggesting a lower dipole moment in the excited state than in the ground state, in agreement with a negative value of $\Delta\mu_{eg}$ (difference of the dipole moment between the excited and ground state) upon excitation.[279]

Unfortunately, the $\mu\beta_{EFISH}$ value of complex **Ir-5** is lower than those of the $[Ir(ppy)_2(bpy)]^+$ complexes previously studied by our group,[173] but it is worth pointing out that the absolute $\mu\beta_{1.907}$ value is almost twice that reported for **Ir(ppy)₂(acac)-4** presented in the previous paragraph.[276] This suggests that 4,4'-*p*-[(N,N-diethyl)aminostyryl]-2,2'-bipyridine is much better than acetylacetonate as ancillary ligand in this kind of cyclometallated Ir[III] complexes for second-order nonlinear optics.

2.6.1. Conclusion

In summary, we measured for the first time the second-order NLO properties with the EFISH technique of complex **Ir-5**, a $[Ir(ppy)_2(bpy)]PF_6$ complex with π-conjugated substituents both on the 2-phenylpyridine and 2,2'-bipyridine ligands. It revealed to have a negative $\mu\beta$ value, which can be considered moderately high for this class of complexes.

3. Third-order nonlinear optics

3.1. Principles of third-order nonlinear optics

The third-order NLO properties of a molecule or a material are related to the cubic hyperpolarizability term γ, that appears in the induced polarization equation if the molecule is subjected to a strong static electromagnetic field:

$$\vec{P} = \mu_0 + \alpha\vec{E} + \beta\vec{E}^2 + \gamma\vec{E}^3 + \cdots \qquad \text{Eq. (2)}$$

Cubic NLO processes are known as four-wave mixing processes, because they deal with three input fields and an output field, the latter being generated by the nonlinear component of the induced dipole moment:[280]

$$\mu_i^{(3)}(\omega_4) = \gamma_{ijkl}(\omega_4; \omega_1, \omega_2, \omega_3)E_j(\omega_1)E_k(\omega_2)E_l(\omega_3) \qquad \text{Eq. (11)}$$

The third-order nonlinear interaction has only two forms: either the frequencies of the three amplitudes sum to give the third-harmonic of the fundamental frequency, or the interaction involves one of the amplitudes taken with the reverse phase. The first case is third-harmonic generation, whether the second only introduces changes to the amplitude and phase of the existing electromagnetic field at ω, which can lead to self-focusing, soliton formation, all-optical switching, and nonlinear absorption processes such as two-photon absorption.

3.2. Introduction to two-photon absorption

Two-photon absorption theory was first proposed by Maria Goeppert-Mayer in her doctoral dissertation in 1931.[281] Nevertheless, the first observation of two-photon absorption dates back only to 1961, when Kaiser and Garrett reported the first observation of TPA-induced frequency upconversion fluorescence in CaF_2:Eu^{2+} crystals.[282] Two-photon absorption involves a transition from the ground state of a system to a higher-lying state by the simultaneous absorption of two photons from an incident radiation field, with different selection rules than those of single-photon absorption.
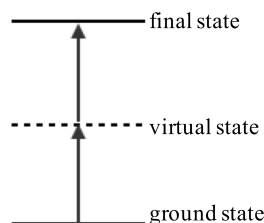
Figure 107. Energy levels for two-photon absorption from the ground to the excited state, the virtual state is a mixture of ground and final states wavefunction.

Linear absorption (one-photon) phenomena follow the Beer-Lambert law:

$$-\frac{dI}{dz} = \alpha I \qquad \text{Eq. (12)}$$

$$\frac{I}{I_0} = e^{-\alpha L} \qquad \text{Eq. (13)}$$

Where I is the light intensity after it passes through the sample, I_0 is the initial light intensity, α is the linear absorption coefficient and L is the optical path.

Two-photon absorption depends instead on the square of the intensity:

$$-\frac{dI}{dz} = \beta I^2 \qquad \text{Eq. (14)}$$

$$\frac{I}{I_0} = \frac{1}{1 + \beta I_0 L} \qquad \text{Eq. (15)}$$

Where β is the nonlinear absorption coefficient. This quadratic dependence improves spatial resolution respect to linear absorption. This and the very fast temporal response that characterizes TPA allow this process to be exploited in several technological applications, *e.g.* micro fabrication,[283] optical data storage,[284] two-photon fluorescence imaging.[285]

The individual molecular TPA property is described by the two-photon absorption cross-section σ_{TPA}. This value is related to the imaginary part of the cubic hyperpolarizability of a molecule, and can be expressed in terms of the nonlinear absorption coefficient β:[286]

$$\sigma_{TPA} = \frac{\hbar\omega}{N}\beta \qquad \text{Eq. (16)}$$

Where $\hbar\omega$ is the energy of photons of the incident optical field, N is the concentration of the absorbing molecules. The unit of measurement of σ_{TPA} is the Goeppert-Mayer:

$$1\ \text{GM} = 10^{-50}\,\frac{\text{cm}^4 \cdot \text{s}}{\text{photon} \cdot \text{molecule}}$$

σ_{TPA} can be expressed as:[287]

$$\sigma^{(2)}(\omega_p) = \frac{4\pi^3\omega_p^2}{n^2c^2}\left\langle\left|M_{fg}^{(2)}\right|^2\right\rangle g(2\omega_p) \qquad \text{Eq. (17)}$$

The last term is the line-width function, which gives the form of the spectrum:

$$g(2\omega_p) = \frac{1}{\pi} \frac{\Gamma_{fg}}{\pi(\omega_{fg} - 2\omega_p)^2 + \Gamma_{fg}^2}$$ Eq. (18)

The term $\langle \left| M_{fg}^{(2)} \right|^2 \rangle$ expresses the dependence of σ_{TPA} on the transition matrix element, the product of the transition dipole moment and the energy difference between the ground, intermediate and final states. It gives the propensity of a two-photon transition, since it is determined by the overlap of the electronic distribution before and after the transition.

1PA

$$\sigma \propto \langle |M_{fg}|^2 \rangle$$

transition dipole moment

2PA

$$\sigma_{TPA} \propto \langle \left| M_{fg}^{(2)} \right|^2 \rangle$$ Eq. (19)

transition matrix element
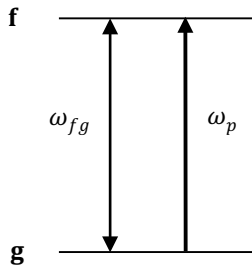
$$|M_{fg}| = \langle f|e \cdot \mu|g \rangle$$
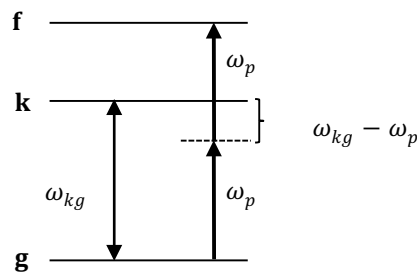
$$\left| M_{fg}^{(2)} \right| = \frac{2}{\hbar} \sum_k \frac{\langle f|e \cdot \mu|k \rangle \langle k|e \cdot \mu|g \rangle}{\omega_{kg} - \omega_p}$$ Eq. (20)

This last equation considers all the possible transitions of a system (with a summation over all the possible ground (g), intermediate (k) and final (f) states): this is the sum-over-states model. With the single intermediate state approximation, we consider only the lowest energy transition, which is the most relevant giving the largest contribution to the TPA phenomenon. We take into account only one intermediate state and simplify the sum in Eq. (20). The final equation for the TPA cross-section at the peak can be thus expressed as:

$$\sigma_{peak}^{(2)} = \frac{4\pi^2 \omega_{fg}^2}{5\hbar^2 c^2 n^2} \left[\frac{\left| \vec{\mu}_{fk} \right|^2 \left| \vec{\mu}_{kg} \right|^2}{\left(\omega_{kg} - \frac{1}{2}\omega_{fg} \right)^2} + \frac{\left| \Delta\vec{\mu}_{fg} \right|^2 \left| \vec{\mu}_{fg} \right|^2}{\frac{1}{4}\omega_{fg}^2} \right] \frac{1}{\Gamma_{fg}}$$ Eq. (21)

Where the first term is the three-states term, which is more important or the determination of σ_{TPA} for centrosymmetric molecules, while the second is the two-states term, more important for non-centrosymmetric molecules (Figure 108).

133

Centrosymmetric
Molecule

Non-centrosymmetric
Molecule
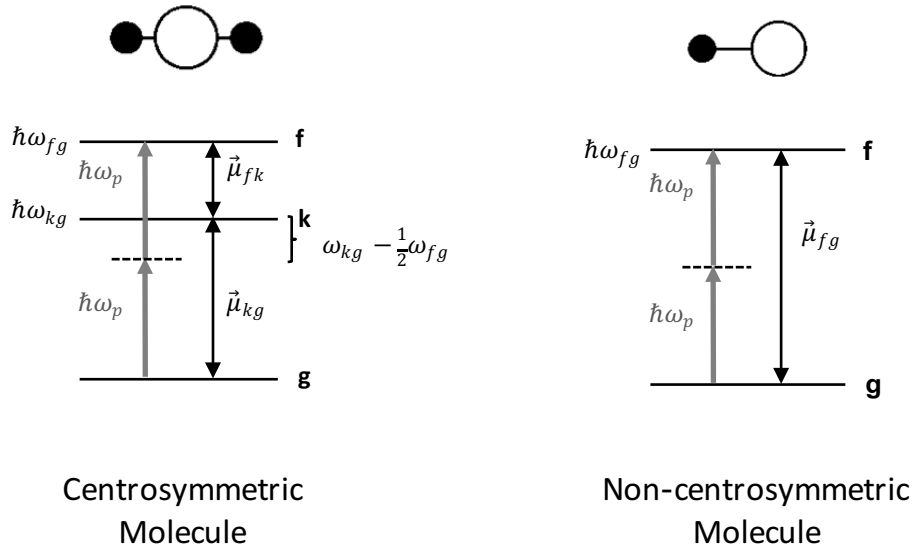
Figure 108. Energy level diagrams with the essential states for the lowest TPA transition in centrosymmetric and non-centrosymmetric chromophores.

For a centrosymmetric molecule:

$$\sigma_{peak}^{(2)} \propto \frac{\left|\vec{\mu}_{fk}\right|^2 \left|\vec{\mu}_{kg}\right|^2}{\left(\omega_{kg} - \frac{1}{2}\omega_{fg}\right)^2 \Gamma_{fg}}$$

Eq. (22)

Where $\vec{\mu}_{ij}$ is the transition dipole moment between the i and j states, $\omega_{kg} - \frac{1}{2}\omega_{fg}$ is the detuning energy and Γ_{fg} the spectral width. For a non-centrosymmetric molecule:

$$\sigma_{peak}^{(2)} \propto \frac{\left|\Delta\vec{\mu}_{fg}\right|^2 \left|\vec{\mu}_{fg}\right|^2}{\Gamma_{fg}}$$

Eq. (23)

Where $\Delta\vec{\mu}_{fg} = \vec{\mu}_f - \vec{\mu}_g$ is the difference in dipole moment between the ground and excited states.

These equations give us the selection rules for two-photon absorption, different from those for linear absorption:

1. For centrosymmetric molecules Laporte rule is valid and excited states allowed in OPA are not allowed in TPA: in two-photon absorption of centrosymmetric chromophores only $g \rightarrow g$ and $u \rightarrow u$ transitions are allowed;

2. For non-centrosymmetric molecules Laporte rule is not valid and excited states allowed in OPA are also allowed in TPA;

3. For centrosymmetric chromophores, TPA will probably not occur at $\lambda_{TPA} = 2\lambda_{OPA}$ and the spectral shapes will be different;

4. For non-centrosymmetric chromophores, TPA and OPA spectra will probably look alike ($\lambda_{TPA} = 2\lambda_{OPA}$).

These equations can also explain the phenomenon of resonance enhancement, situation in which the energy of the photons that allow TPA is similar to that necessary for OPA. When the detuning energy approaches 0 the 3-states term goes to ∞ and consequently σ_{TPA} can be overestimated. In such situation, the 3-states term should be taken into account also for understanding the spectra of non-centrosymmetric molecules otherwise this phenomenon can not be explained. Furthermore, since $\vec{\mu}_{k(f)g}/\Gamma_{fg}$ is the same term as in one-photon absorption, it can be expected that, when OPA is strong, TPA will be enhanced as well as a direct consequence.

The requirements to maximize σ_{TPA} of a chromophore can be articulated as:

a - Long π-conjugated systems with enforced co-planarity to ensure large conjugation lengths to have high transition dipole moments;

b - Donor and acceptor groups at the centre and end of a molecule to obtain push-pull systems;

c - Narrow one-photon and two-photon absorption bands to have small values of Γ;

d - Centrosymmetric chromophores should possess a strong OPA transition close to the TPA laser wavelength, in order to decrease the detuning energy.

e - For dendrimers, the Frenkel exciton model is valid: the properties of multibranched chromophores are connected with those of their single-branch counterparts to have a cooperative enhancement of two-photon absorption.

3.3. Measurement techniques for TPA

3.3.1. Two-photon excited fluorescence

The two-photon excited fluorescence method measures the fluorescence intensity given by two-photon excitation.[288] The easiest procedure is to compare the one and two-photon excited fluorescence spectra of the sample and a known reference. The setup uses a femtosecond pulsed laser and has the advantages of high detection sensitivity based on fluorescence measurements, a relatively simple experimental setup and less sensitivity to the pulse width of the laser beam. The value of σTPA can be calculated with the formula:

$$\sigma_s = \frac{F_s \cdot \eta_r \cdot N_r}{F_r \cdot \eta_s \cdot N_s} \sigma_r \qquad \text{Eq. (24)}$$

where F is the observed two-photon induced fluorescence signal, η is the fluorescence quantum yield, and N is the concentration of the chromophore. The subscript *s* is referred to the substrate, while the subscript *r* is referred to the reference.

The major disadvantages of this technique are that the sample must be luminescent, the linear absorption coefficient and luminescence quantum yield must be known and the technique assumes to have the same fluorescence quantum yields with one and two-photon excitation.

3.3.2.   Z-scan

The Z-scan technique allows to measure both the nonlinear refractive index and nonlinear absorption coefficient for a wide variety of materials.[289] The first can be measured with the closed-aperture setup, when the detector has a narrow aperture, while the latter can be measured with the open-aperture setup. In this case, the intensity-dependent transmission is collected and the two-photon absorption cross-section can be measured.

This is the technique that we used and the setup includes a laser system consisting of five interconnected laser devices (Figure 109). *Millennia-EV* generates continuous wave (CW) green laser beam that pumps *Tsunami* (oscillator), which generates high-repetition-rate (82 MHz) femtosecond pulses at 800 nm. Then, *Spitfire ACE* (amplifier) pumped by *Empower* laser amplifies selected pulses (at 1 kHz) from Tsunami. *TOPAS-Prime* allows to convert the wavelength of the amplified femtosecond pulses to the desired wavelength; thus, wavelength-tunable femtosecond pulses (typical pulsewidth oscillates between 90 and 140 fs in full width at half maximum) are obtained at the repetition rate of 1 kHz. Femtosecond pulses are needed in order to achieve high peak intensities at lower energy, and by consequence to increase sensitivity and minimize the sample's damages. They also have the advantage of avoiding excited state absorption and other NLO phenomena, which would cause overestimation of the TPA cross-section. By using low pulse repetition, sample's heating and consequent photophysical events that would cause an overestimation of the TPA cross-section are also avoided.[290]

The output laser beam is directed on the sample translated along the z-axis through the focused laser beam to measure the transmittance as a function of the sample position on the axis of the focused laser, that is, as a function of the incident power on the sample (Figure 109). Three photodiodes collect the radiation. The first, used as reference, is positioned before the sample, while the other two collect the beam after passing through the sample: the one situated in line behind the sample collects the closed-aperture trace, while the one that receives the outgoing beam at 90° respect to the sample collects the open-aperture trace, *i.e.* the signal we used for measuring TPA. For the present setup, thin samples (L ≤ 2 mm) are needed in order to fulfil the thin-sample condition,[289] which is the approximation assuming that the optical intensity in the sample is uniform along the Z-axis. It is necessary to make a measurement for every single wavelength for which the value of TPA cross-section is needed. σ_{TPA} is obtained directly

from the transmittance data and the peak intensity of the laser pulse or by using the reference sample whose TPA coefficient is known.
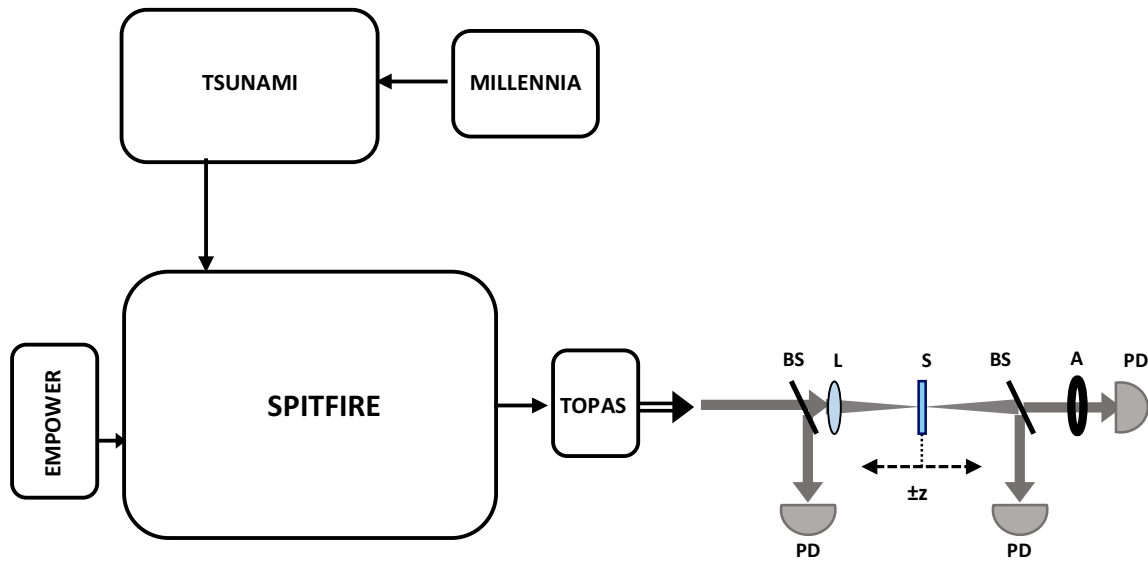
Figure 109. The femtosecond Z-scan setup. BS, beam splitter; L, lens; S, sample; A, aperture for the close-aperture measurement; PD, photodiode.

The main advantage of Z-scan is that it gives a direct measurement of the TPA cross-section, without the use of a reference. On the other hand, the laser parameters need to be attentively calibrated, other NLO phenomena can disturb the measurement, there are strong background signals and highly concentrated samples are needed.

The method we used to accurately measure the σ_{TPA} of our samples includes two steps:

1.   A fast wavelength scan at a fix incident laser power (0.4 mW) to obtain the overall shape of the nonlinear absorption spectrum was first performed, making one measurement every 20 or 10 nm. The simplified fixed-power procedure saves the measurement time, but assumes that the observed nonlinear absorption only arises from two-photon absorption.

2.   A power-dependence scan (0.1-0.5 mW) at some wavelengths of interest, corresponding principally to maxima, was made to obtain a more precise value of σ_{TPA} and confirm the values previously obtained with the faster wavelength scan. The power-dependence procedure can examine the nature of the observed nonlinear absorption but it is time-consuming.

Our method offers the advantage of being quicker than recording a power-dependence scan for every wavelength, but doesn't lack in reliability, since of σ_{TPA} at some interesting wavelengths is verified with a power-dependence scan. Since the lasers parameters can easily oscillate, we envisaged to use some standards, whose σ_{TPA} values are reported, to be sure to make precise measurements. We chose MMPBT

in dimethyl sulfoxide (2 mM)[291] for wavelengths shorter than 1020 nm and Rhodamine B in methanol (8.4 mM)[292] for the wavelengths longer than 1020 nm (Figure 110).
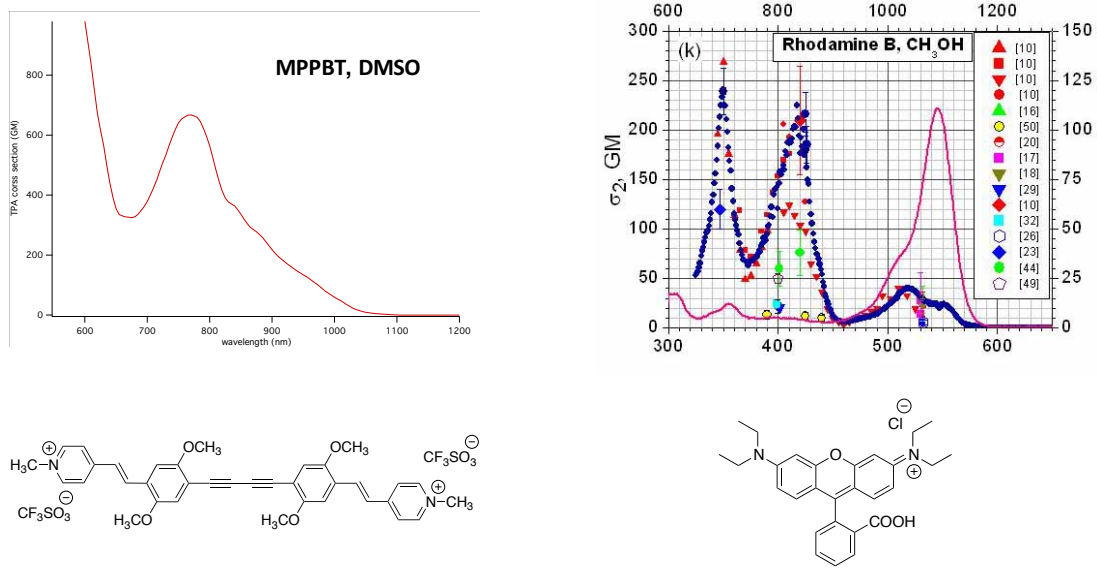
Figure 110. TPA spectra of the standard we used and relative chemical structures.

The relative magnitude of the two-photon absorption coefficient β from the fixed-power wavelength scan was obtained as:

$$\beta \propto q \cdot \lambda \cdot t_p \cdot z_r \qquad \text{Eq. (25)}$$

where q is the two-photon absorbance, λ the incident wavelength, t_p the pulse width and z_r the Rayleigh range. The relative TPA cross section was then calculated as:

$$\sigma_{TPA,\ rel} \propto \frac{\beta}{C \cdot \lambda} \qquad \text{Eq. (26)}$$

from the convention:

$$\sigma_{TPA} = \frac{h \cdot c \cdot \beta}{\lambda \cdot N} \qquad \text{Eq. (27)}$$

where h is Planck constant, c is the speed of light, and N is number density of molecule which is proportional to molar concentration C. The obtained values are in relative scale, but they can be rescaled to the standard spectrum of MPPBT or Rhodamine B (Figure 110), taken as a reference, to obtain the absolute value of the TPA cross section.

138

On the other hand, the value of TPA cross section can be obtained quantitatively from the fixed-wavelength power scan by using the equation:

$$\beta = \frac{q}{I_0(1-R)L_{eff}}$$

<div align="right">Eq. (28)</div>

where I_0 is the on-axis peak optical intensity of the irradiated laser pulse, R the Fresnel reflectance and L_{eff} the effective path length (which reduces to the physical path length of 2 mm when the absorption is absent), and then the absolute value of the TPA cross section is calculated from the same convention shown above (Eq. 26). By performing Z-scan measurements at different wavelengths followed by fitting the experimental results, it is possible to determine TPA cross-sections within a large spectral range.

In the area where tails of one-photon absorption persist, correction is needed:

$$L_{eff} = \frac{[1-e^{-\alpha L}]}{\alpha}$$

$$\alpha = \frac{-\ln T}{L}$$

$$\text{and} \quad \beta = \frac{q \cdot \lambda \cdot t_p \cdot z_r}{L_{eff}}$$

<div align="right">Eq. (29)</div>

4. TPA properties of organic chromophores

Organic chromophores with two-photon absorption properties have received considerable attentions due to the great application potentials in various fields, as fabrication of frequency upconversion lasers, optical limiting, high density data storage and micro fabrication.[293]

The TPA properties of some classes of compounds will be illustrated, in order to highlight design methods that have been generally applied to improve the performances of these chromophores.

4.1. Linear organic chromophores

The first demonstration of two-photon absorption by organic dies was in 1963, when Rieckhoff and co-workers reported the TPA cross-sections of phenantrene, anthracene, pyrene and benzopyrene powders.[294] The major part of the reported organic chromophores exhibiting TPA are centrosymmetric, even though examples of asymmetric chromophores have been given.[295] Among the first chromophores studied for a systematic research on structure-properties relationship were stilbene, as for second-order NLO. Perry et al. reported that, by substituting *trans*-stilbene with terminal donor substituents, as -NBu$_2$ or NPh$_2$, the σ_{TPA} values could be increased of 10 times, in the first case, and of 30 times, in the latter.[296] Going from *trans*-stilbene to 4,4-bis(dimethylamino)-*E*-stilbene, transition dipole moment is increased and the one-photon detuning term decreases. The enhancement in TPA cross-section results from the electron-donating properties of the terminal groups and is accentuated if the conjugation length is increased by inserting phenylene-vinylene (**St-3**, Figure 111) or phenylene-butadienylene groups and if electron-accepting groups are attached to the central ring of the bis(styryl)benzene backbone (**St-4**, **St-5**, Figure 111).
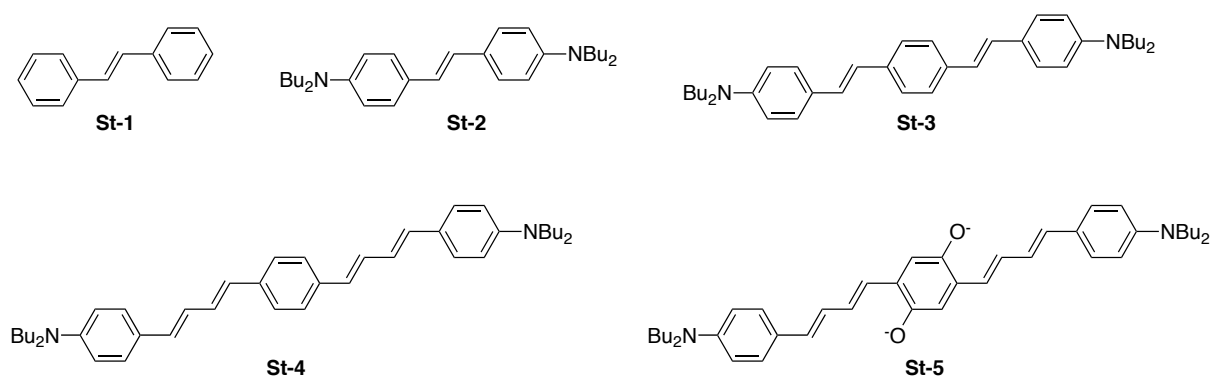
Figure 111. Some of the styryl derivatives studied for TPA.

The compound that gave the highest σ_{TPA} value is **St-5** (3670 GM), thanks to the presence of electron-donating and electron-withdrawing groups, and of an extended π-conjugated system. If the sense of the symmetric charge transfer is reversed by substituting electron-donating alkoxy donors on the central

rings and attaching electron-accepting terminal groups, good TPA cross-section values can still be obtained, even though lower, or with higher uncertainty, respect to the D-π-A-π-D compounds.

By substituting the double bonds with triple bonds, a decrease in the third-order NLO properties would be expected, because of the mismatching between sp and sp^2 orbitals. Nevertheless, Lambert et al. demonstrated that chromophores possessing a similar size of the conjugated system have similar σ_{TPA} even though the structural pattern connecting the terminal groups and the central core is different (double or triple bonds).[297] Furthermore, alkyne groups have the advantage of rigidifying the system, since they are not subject to *cis-trans* isomerization and cannot twist out of conjugation.

Considering that donor and acceptor substituents have a large impact on third-order nonlinearities, efforts have been made to investigate how they can improve the TPA response of chromophores. Dialkyl and diarylamino groups are among the most widely used, while alkoxy substituents demonstrated to be less effective.[298] The better performances of dyes with amino substituents can be attributed to their richness in π electrons. The best performing acceptor substituents, located on the central core of D-π-A-π-D compounds, resulted to be ciano groups[299] or carbocations.[300]

As for second-order NLO, increasing the length of the π-conjugated system is expected to impact positively on the TPA cross-section of organic compounds. If more chromophores are coupled together, the TPA cross-section of the resulting chromophore will strongly increase because of enhanced transition dipole moments.

Starting from these principles, a large variety of organic chromophores with different π-conjugated systems, substituents and geometry have been successfully synthesized and studied.

4.2. Branched and dendritic organic chromophores

An interesting class of molecules possessing good third-order NLO response are branched octupolar and dendritic chromophores, firstly developed by Prasad and co-workers.[301] They found that, as the number of arms increases, there is a non linear relative increase of the effective TPA cross-section, thanks to cooperative enhancement due to the multi-branched structures.

The group of Blanchard-Desce synthesized and studied a series of branched chromophores with a central triphenylbenzene core. This moiety was selected as ramification node because it maintains large distance between the conjugated connectors, thus preventing sterical hindrances which could diminish electronic conjugation.[302] TPA was measured and, as expected, the values increased by going from the quadrupolar to the octupolar to the dendritic analogue, with a maximum σ_{TPA} of 798 GM. Furthermore, increasing the branched character also improves the TPA-transparency,[303] a very important characteristic to consider for practical applications, as discussed in the previous paragraphs.

Cho et al. studied 1,3,5-tricyano-2,4,6-tris-(vinyl)benzene derivatives with a central electron-withdrawing core and electron-donating peripheral substituents (Figure 112).[304] They found that the TPA cross-section values increased with the length of the π-conjugated system of the branches, the electron-donating ability of the lateral groups and their π-delocalization (-NPh$_2$ is more effective than -NMe$_2$).

D = H, Me, OH, OMe, NH$_2$,
NMe$_2$, NEt$_2$, piperidyl, NPh$_2$

n = 2, 3
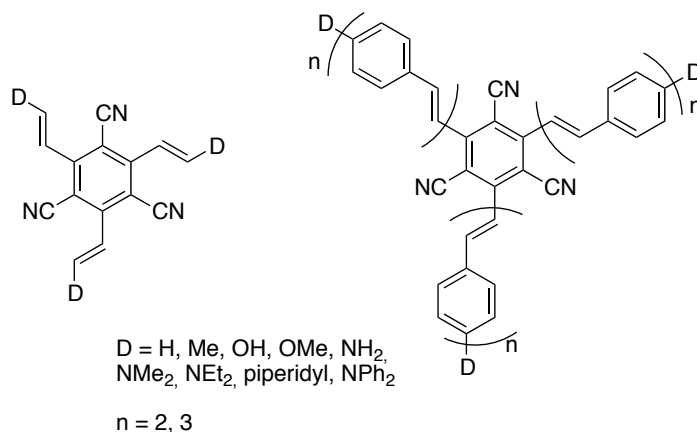
Figure 112. The first complexes studied by Cho et al.

The same group examined octupolar oligomers containing from 2 to 12 molecules of 1,3,5-tricyano-2,4,6-tris(styryl)benzene.[305] As the number of the repeating unit increases, the absorption maximum is shifted to shorter wavelengths and the TPA cross-section in enhanced but, more importantly, a linear relationship between the first hyperpolarizability and TPA cross-section of the octupolar oligomers was found experimentally. They also demonstrated that, for compounds of the same family, the third-order NLO properties of octupoles and quadrupoles are better than those of dipoles.[306]

Another way to increase the TPA response of organic compounds is to introduce a π-conjugated, planar and rigid central core. Wu and co-workers fabricated some chromophores with a central hexa-*peri*-hexabenzocoronene unit, possessing a large number of delocalized π electrons and a rigid planar structure, and strongly electron-withdrawing lateral groups.[307] They observed excellent TPA-cross section values, enhanced in polar solvent that can favour the intermolecular charge-transfers, dominating the photophysics of these molecules.

Branched chromophores with a central triphenylamino core had a great success. The group of Cho studied the effect of linking 1,4-(p-diphenylaminostryl)-2,5-dicyanobenzene units in multibranched systems, in order to obtain D-π-A-π-D structures.[308] They observed that the TPA cross-section values increase fast by increasing the number and size of branches and thus extending the π-conjugated system, reaching a maxiumum value of σ_{TPA} = 5030 GM. This effect is mainly caused by the vibronic coupling.[309] The electronic coupling is weak probably because the central amino group breaks the conjugation of the network. A useful figure of merit to consider when comparing the TPA response of different chromophores is σ_{TPA}/N_e (N_e : number of π electrons). It is desirable to have the biggest effect

with the smallest chromophore possible, because molecular weight can be a critical factor in *in vivo* applications. In this case, it was found that σ_{TPA}/N_e increased with the branching. The same group also demonstrated that, within this family of compounds, distortions can have a deleterious effect on TPA, even though the conjugation length is considerable.[310] Focusing the attention on small chromophores with a central triphenylamino core, it can be noticed that the TPA cross-section diminishes by lowering the acceptor strength of the substituent at the edge of the D-π-A branch (Figure 113),[311] still maintaining considerable TPA cross-section values.
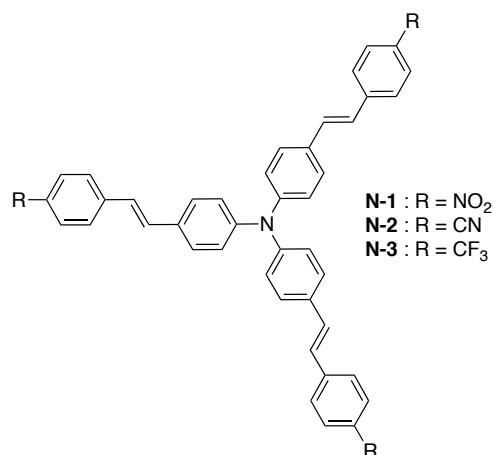
Figure 113. The small molecules with a central NPh_3 core studied by Cho et al.

The group of Blanchard-Desce studied similar compounds with triple bonds as linkers (Figure 114).[312] They noticed that the TPA response is highly affected by the nature of the end-groups. The octupolar chromophores with acceptor groups displayed higher σ_{TPA} values than the ones with donor groups, as already observed by Cho et al.,[311] because of enhanced charge transfers in the molecule. The TPA response increases also with the extension of the π-conjugated system, that is passing from compounds **N-5** and **N-6** to compounds **N-7** and **N-8**.
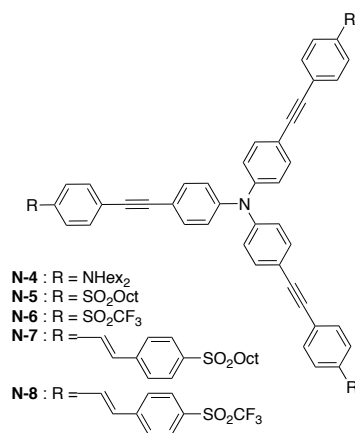
Figure 114. The compounds studied by the group of Blanchard-Desce.

The group of Jeon studied the TPA properties of chromophores with a central triphenylamino core and D-π-A-π-D branches.[313] In this case, the TPA cross-section values reported are not very high, and the authors attributed this to weak electronic coupling due to conjugation breaking ascribed to the central amino group. Many other similar compounds were studied in the same sense, and a correlation between the extension of the π-conjugated network and the σ_{TPA} values was confirmed.[314] Branched chromophores with fluorene groups as connectors have also been explored.[315] These compounds show good TPA properties and, in particular, they can absorb between 800 and 1000 nm, wavelengths that the other chromophores presented here cannot always reach. This renders them suitable for bioimaging applications, since they fit with the transparent window of tissues.[316]

4.3. Perylene derivatives: state of the art

Perylene tetracarboxylic derivatives are organic dyes and pigments often used in paints and coatings:[317] perylene-based materials are particularly attractive due to their thermal stability and chemical inertness. Their outstanding electrical and optical properties, in particular absorption and emission in the visible, make them suitable candidates for applications as organic semiconductors, photoconductors, photoreceptors and laser materials.[318] In recent years, the interest in the TPA properties of these molecules has rapidly grown.

4.3.1. Organic perylenes with TPA activity

The group of Mendonça first studied the two-photon absorption properties of a series of PTCDIs derivatives (Figure 115).[319]
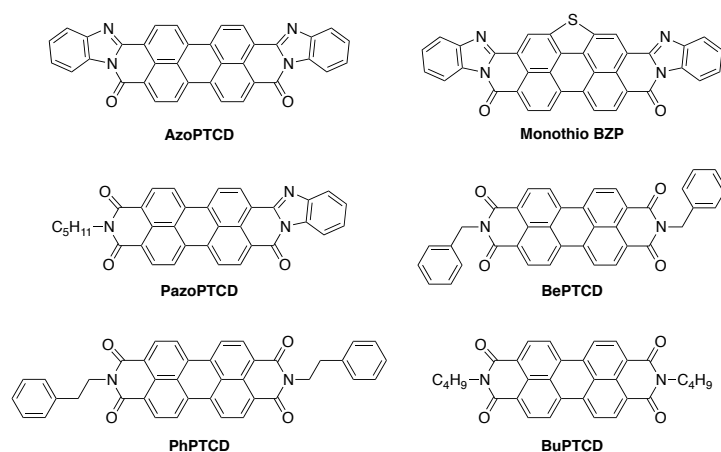
Figure 115. The PTCDI derivatives synthesized and studied by Mendonça et al.

The perylene core of these compounds remains unchanged, while different substitutions are made on the diimide moiety. The perylene moiety has electron-donating characteristics,[320] although by addition of lateral substituents the central core can play either the role of electron-acceptor or electron-donor.

The only issue of such compounds is the poor solubility: trifluoroacetic acid was needed in order to reach sufficient concentrations in dichloromethane for Z-scan measurements. The best TPA values were obtained with centrosymmetric compounds, especially with a benzimidazole group linked to one of the two lateral imide group: the A-D-A structure is expected to enhance the third order nonlinearity of molecules.

All the spectra show one-photon resonance enhancement effect near the OPA peak and then a shoulder at longer wavelengths, between 700 and 750 nm. Data in this range of wavelengths are the most reliable for this class of compounds, even though, below 800 nm, one-photon resonance enhancement interferes with the TPA measurements, becoming significant at shorter wavelengths and giving thus wrong estimations of σ_{TPA}. For four over six compounds have maximum σ_{TPA} values between 1500 and 500 GM in this range, being the value of **PhPTCD** and **BuTPCD** the lowest, while **AzoPTCD** and **PazoPTCD** reach σ_{TPA} values of about 3500 GM at the shoulder's wavelength. The values of σ_{TPA} reported by this group can change if different measurement techniques are used: more precisely, the peak's wavelengths are slightly shifted and there is no more trace of saturable absorption if white-light continuum (WLC) Z-scan is used.[321] Nevertheless, the use of different techniques does not considerably affect the profile of the TPA spectra. The studies on these compounds demonstrated that, in these cases, the TPA properties depend mostly on the central core, while the substituents can affect only the σ_{TPA} values at shorter wavelengths and the resonant enhancement. It was also demonstrated that the most planar PTCDIs and those with the most extended π-conjugated system can achieve better two-photon absorbing properties.

Przhonska et al. studied the effect of substituting the nitrogen of the imide of a PTCDI with a 7-benzothiazole-9,9-didecylfluoren-2-yl or a 7-diphenylamino-9,9-didecylfluoren-2-yl groups.[322] The found that the TPA cross-section is higher for the second derivative, especially at short wavelengths (up to 3500 GM around 650 nm), and that the two compounds have good optical power limiting properties. The high TPA cross-section values were explained by intermediate-state resonant enhancement, related to the decrease in detuning energy between incident photons and the lowest one-photon allowed state.

Some groups also focused on the two-photon absorption properties of PTDCI with substituents at the 1,6,7,12-bay positions. Marder et al. studied some PTDCI derivatives with phenylacetylide substituents (Figure 116).[323]
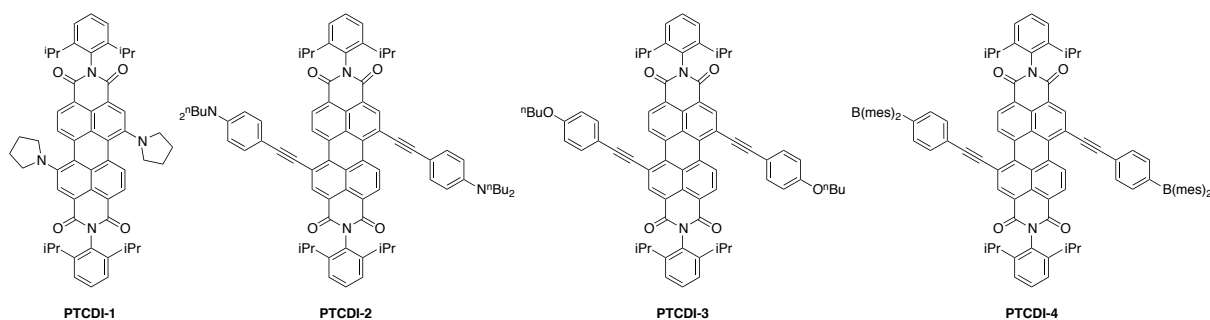
Figure 116. The PTCDI derivatives studied by Marder et al.

Compounds **PTCDI-1** and **PTCDI-2** show the best performances, with σ_{TPA} values in the order of 300-800 GM at long wavelengths, with **PTCDI-1** reaching 2800 GM in the resonance enhanced zone. **PTCDI-2** has a TPA cross-section of about 500 GM over a wide wavelength range, probably suggesting the presence of several 2PA states close in energy and broad TPA bands. **PTCDI-3** and **PTCDI-4** have a TPA spectral shape similar to **PTCDI-1**, but with lower cross-section values.

Lu et al. recently reported fair TPA cross-section values for PTCDI mono or bis-substituted with electron-donor triphenylamines at the bay positions, the central core performing the role of electron-acceptor.[324]

Few examples of 1,6,7,12(bay) substituted PTCDIs for TPA can be found in literature. Ponterini and co-workers discussed the TPA properties of a series of di- and tetrasubstituted PTDCI derivatives (Figure 117).[325]
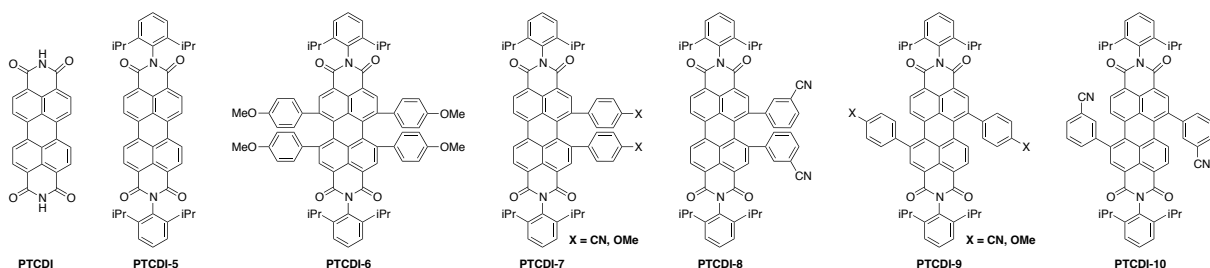
Figure 117. The molecules studied by Pagoaga et al.

The σ_{TPA} values of the tetrasubstituted compound **PTCDI-6**, between 800 and 900 nm, are one order of magnitude greater respect to the reference **PTCDI-5**, but still under 200 GM. These values are a lot smaller than the ones registered for the compounds reported above, probably because of the low extension of the π-conjugated system and the distorted geometry of the molecules. The asymmetric PTDCIs have TPA cross-sections in the order of some tens, with no particular difference if they bear −CN or −OME groups. The TPA spectra were also registered between 1000 and 1100 nm: at these longer wavelengths the values of σ_{TPA} do not exceed 2 GM for the reference and 20 GM for the tetrasubstituted **PTCDI-6**.

Interestingly, the group of De Schryver described a 1,6,7,12(bay) substituted PTDCI bearing four 4-methoxybenzenesulfonic acid substituents that make it water soluble and so suitable to be tested in cells (Figure 118).[326] Its TPA spectrum was measured in water with the two-photon excited fluorescence technique between 840 and 980 nm: the values of σ_{TPA} range between 10 and 50 GM in the scanned range. These values are considered very good respect to other fluorophores used in biology, which usually have TPA cross-sections up to 10 GM.
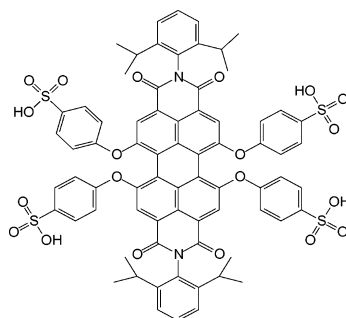
Figure 118. The water-soluble perylene dye studied by De Schryver et al.

This dye has an improved stability to photobleaching and can be successfully applied for single molecule studies, as well as for two-photon experiments: it represents an alternative to the other water-soluble dyes used in biology. Moreover, the low probability of triplet formation means that this compound can be used to follow the dynamics of the fluorescence energy transfer even on fast time scales.

Some PTCDI derivatives with thiophene-based dendrimeric substituents on the 1,6,7,12(bay) positions were studied by the group of Goodson.[327] Their TPA cross section are around 100-200 GM between 720 and 890 nm, but they don't increase with the increasing number of thiophene units in the dendrons. This is due to the fact that, in highly branched structure, the charge transfer character diminishes because of the twisting of the perylene core, interrupting the charge correlation between the perylene itself and the dendrons. This means that increasing the size and extension of the aromatic substituents is not an impeccable way to increase the TPA cross-section. In fact, many elements have to be taken into account in order to reach high σ_{TPA} values, as planarity and π-conjugation, that may contrast with the presence of bulky pendants.

Some examples exist of PTCDIs used as acceptors in an extended donor-acceptor system.[328] Such compounds have been studied mostly for the efficient photoinduced electron-transfer by which they are typically characterized. The TPA cross-section values do not exceed 1000 GM, despite the considerable size of the systems.

Tian and coworkers studied the TPA properties of some compounds bearing two PTDCI units linked by a conjugated bridge, reporting impressive σ_{TPA} values (up to 8735 GM).[329] The issue with those measurements is that they were performed with nanosecond pulsed laser, probably causing an overestimation of TPA due to the simultaneous occurring of excited-state absorption. Yu et al. also

investigated the TPA response of some donor-acceptor-donor PTDCI-thienoacene-PTDCI compounds:[330] they found moderate σ_{TPA} values. As expected, there is a proportional relationship between the TPA cross-section and the increase in the effective conjugation length of the thienoacenes bridge between the two perylenes in the molecule. The TPA cross-section of such compounds is strongly associated with their charge transfer character.

Considerably, perylenes have also been used in association with organometallic complexes, *e.g.* porphirines, to obtain molecules able to exhibit huge TPA at telecommunication wavelengths.[331]

4.4. New perylene derivatives for two-photon absorption

As reported in recent literature, appending the PTDCI core with π-conjugated substituents able to enhance charge-transfer transitions within the molecules is expected to increase the TPA response. So, we decided to study four new 3,4,9,10-perylenetetracarboxylic diimide derivatives substituted at the at the 1,6,7,12-bay positions with a highly π-conjugated structure (Figure 119). Their two-photon absorption spectra were measured in dichloromethane with the Z-scan technique.
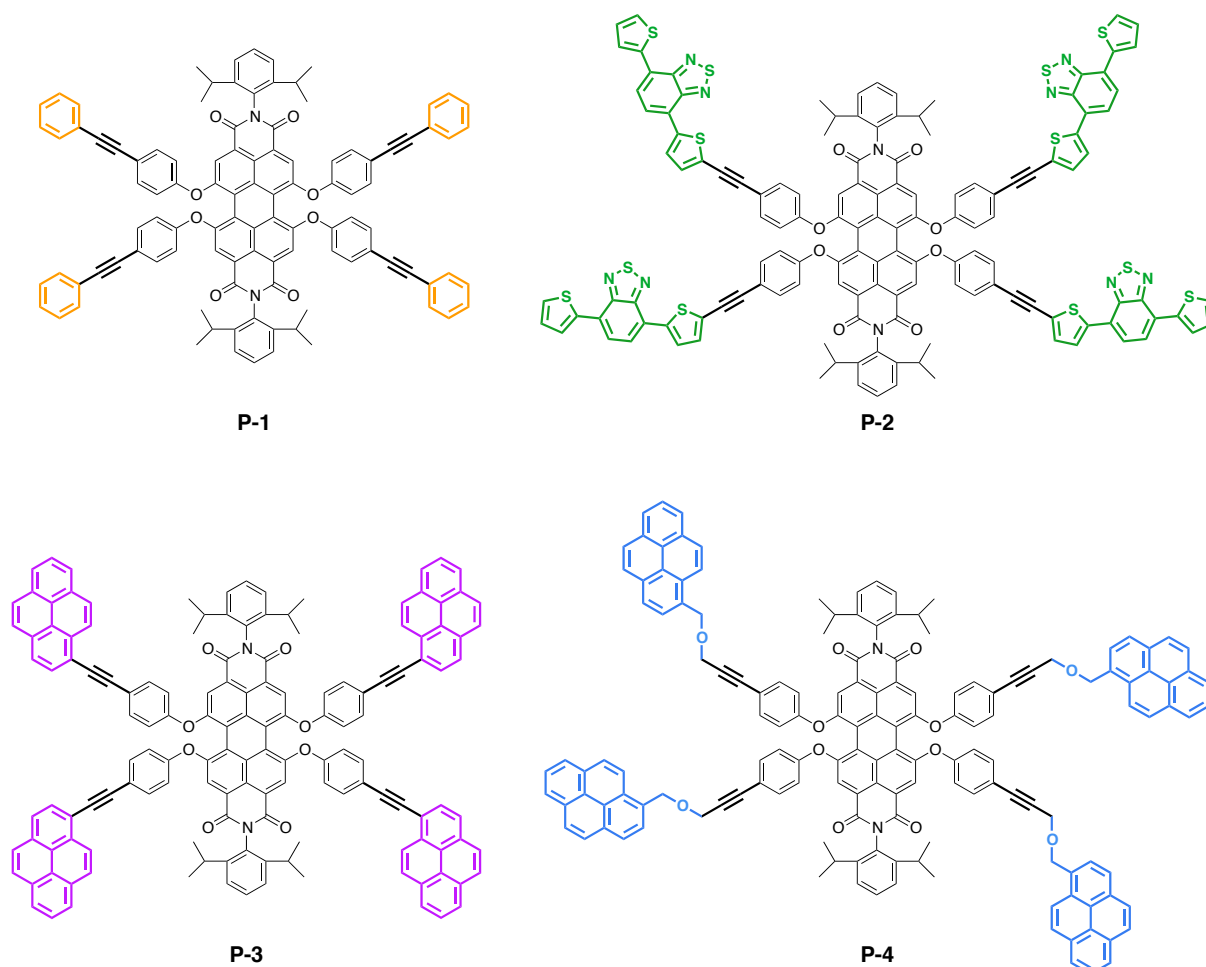
Figure 119. The new tetra-substituted PTCDI derivatives with aromatic pendants at the 1,6,7,12-bay positions.

As reported in the previous section, there are only few TPA studies concerning PTCDIs tetra-substituted with aromatic pendants at the 1,6,7,12-bay positions[323-327] and in all cases the σ_{TPA} values do not exceed few hundreds GM. We decided to substitute the 1,6,7,12-bay positions with some extended π-conjugated groups in order to have high charge delocalization and favour charge transfers from the substituents to the central core or vice-versa.

The substituents we chose are phenyl (**P-1**), pyrene (**P-3** and **P-4**) and 4,7-di(2-thienyl)benzo[c][1,2,5]thiadiazole (**P-2**). Compound **P-1** can be taken as reference to measure the effect of the more π-extended structures of pyrene and di(thienyl)benzothiadiazole. Furthermore, the electron-

149

donating effect of the first and the electron-withdrawing effect of the second can be compared. The pendants were connected to the phenolate groups on the central perylene core either with a simple triple bond (**P-1,2,3**) or with a more flexible and less conjugating ethynyl-alkoxy bridge (**P-4**). This will allow to study the effect of the linker between the lateral pendants and the PTCDI core, *i.e.* of the degree of conjugation between them.

4.4.1. Linear absorption

The UV-Vis spectra of the samples solution in dichloromethane were recorded by a *Shimadzu UV-3150* spectrometer using quartz cells. The spectral shapes are typical of this family of compounds with large ε values, showing high one-photon absorption (Figure 120).
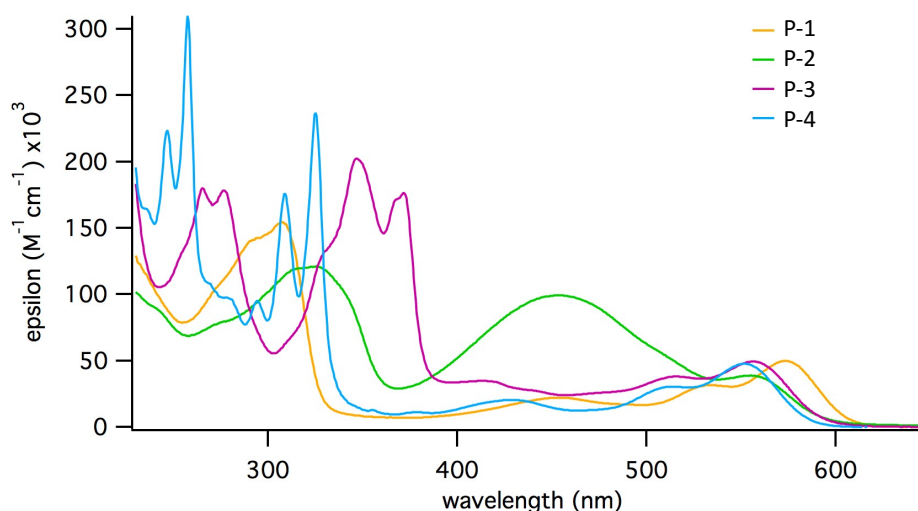
Figure 120. Absorption spectra of the perylene derivatives.

All spectra are characterized by a structured band in the visible, centred between 500 and 600 nm, typically assigned to $S_0 \rightarrow S_1$ π-π^* transitions with the vibronic progressions characteristic of the perylene core.[332] At shorter wavelengths, structured bands ascribed to absorption of the aromatic substituents (pyrene, phenyl, di(thienyl)benzothiadiazole) can be noticed. The presence of separate absorption bands for the central perylene unit and the substituents shows that there is limited ground-state electronic coupling between them.[333] Nevertheless, the PTCDI absorption band is less structured and more red-shifted that in the unsubstituted PTCDI, whose spectrum shows a highly structured band with maxima at 500 and 550 nm.[334] In the case of **P-2**, the absorption bands of the perylene core and the substituents are partially superimposed: the di(thienyl)benzothiadiazole moieties absorbs around 500 nm. At higher concentrations, the stacking between perylene molecules can take place causing the rise of long-wavelength shoulders,[333] but in this case the phenomenon was not observed.

Importantly, these compounds are transparent at wavelengths longer than 600 nm, which makes them suitable for the investigation of two-photon absorption in the near-IR spectral range, the most interesting for possible applications.

4.4.2. Two-photon absorption

To perform nonlinear absorption measurements, the samples were dissolved in dichloromethane and placed in 2 mm thick quartz cuvettes. The Z-scan technique requires highly concentrated samples, around 1 or 2 mM. Some of the studied perylenes had solubility problems, probably due to the highly planar structure of the molecules that favours π-stacking and aggregation at high concentrations: in particular, **P-3** and, less significantly, **P-2** had tendency to crystallize in 2-mm cells during the TPA measurement. Crystallization in the sample solution interferes with the measurements: the solution was thus filtered with membrane filters (pore size of 0.20 μm) and diluted until the formation of crystals stopped. In particular, it was necessary to reach concentrations equals or under 0.7 mM for **P-2** and 0.3 mM for **P-3**. In **P-1** sample, crystallisation stopped at a quite high concentration, about 1.3 mM, while the most soluble product was **P-4**, which had no solubility problems also at concentrations of 2.2 mM. Furthermore, in the most critical cases, the solution was stirred during the measurement in order to render aggregation more difficult.

The two-photon absorption spectra were recorded from 800 nm to 640 nm (Figure 121) and the TPA cross-section values are reported in Table 14 and Table 15.
All of the PTCDI derivatives show high σ_{TPA} values and two-photon absorption over a wide range of wavelengths, between 640 and 800 nm. The TPA properties have also been tested between 1100 and 1200 nm, but in this range of wavelengths the compounds response was under the detection limit of 3 GM. The relation between the molecules structures and σ_{TPA} maximum values can be explained taking into account the electronic properties of the substituents and the extension of the π-conjugation across the molecule. Planar compounds bearing aromatic groups connected by π-conjugated bridges that allow efficient charge delocalization have higher possibility to show strong two-photon absorption. All of the compounds here studied possess π-conjugated structures thanks to the presence of the phenylethnyl linker connecting the perylene core to the lateral aromatic pendants at 3,4,9,10-positions.

The TPA spectra of the four compounds show a similar feature: the maximum is at the shortest wavelength (640 nm), then the intensity decreases at longer wavelengths with a shoulder (**P-2**, **P-3**) or small peak (**P-1**, **P-4**) at around 720 nm.
The TPA magnitude differs considerably depending on the compound. This is ascribed to the different electronic properties of the aromatic substituents. **P-2** shows the highest σ_{TPA} value (3547 ± 291 GM at 639 nm) thanks to the di(thyenil)benzothiadiazole groups: they are electron-withdrawing, contribute to the planarity of the branches, extend the conjugation length and the delocalization of π-electron.[335]
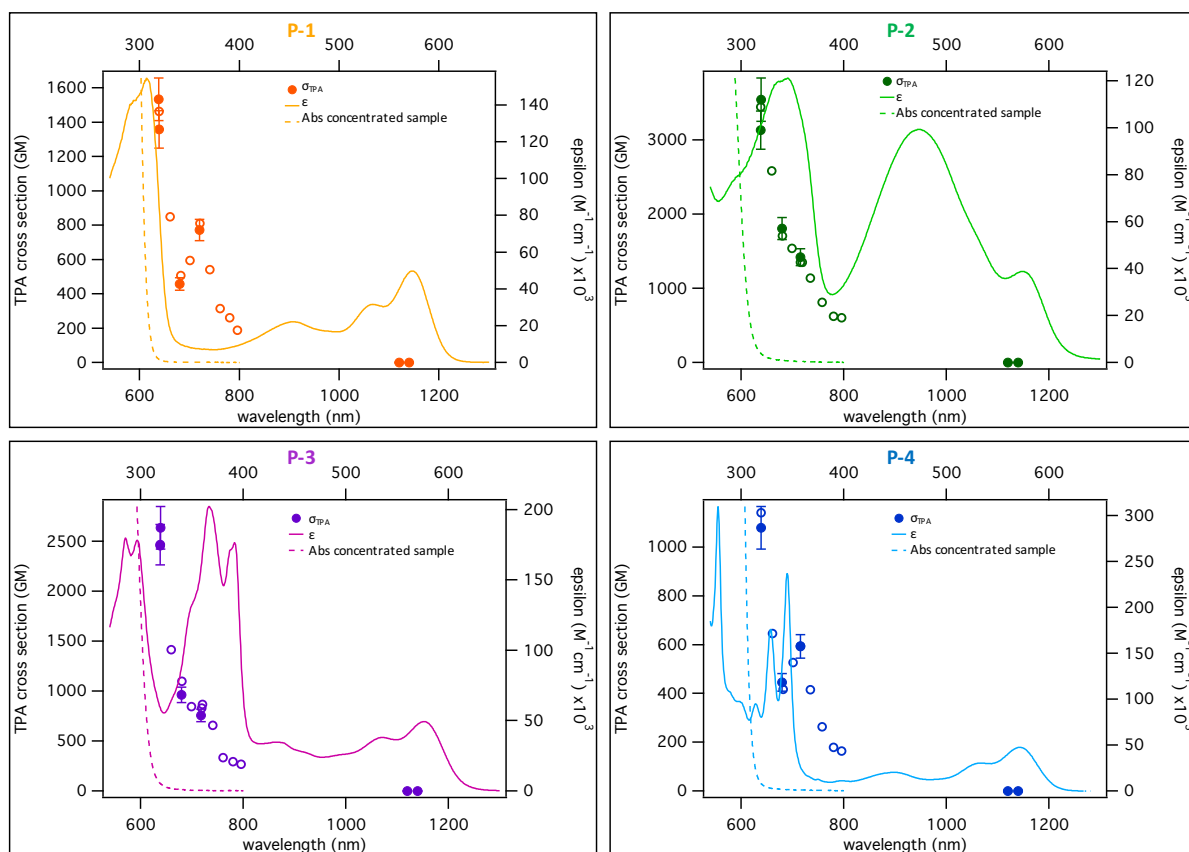
Figure 121. The OPA (continuous line), OPA at high concentration (dashed line) and TPA spectra of PTCDI derivatives: the empty markers are the values obtained with the wavelength scan at a fix power, while the full markers with error bars are the ones obtained with the power scan at a fixed wavelength.

Wavelength-scan measurements

P-1		P-2		P-3		P-4	
λ (nm)	σ$_{TPA}$ (GM)	λ (nm)	σ$_{TPA}$ (GM)	λ (nm)	σ$_{TPA}$ (GM)	λ (nm)	σ$_{TPA}$ (GM)
796	187	796	606	796	270	796	164
781	261	780	625	781	294	780	179
761	315	758	814	761	335	758	263
741	540	735	1138	741	657	735	416
721	812	719	1354	721	869	716	594
701	596	716	1352	719	829	701	526
682	506	699	1541	699	847	682	417
661	849	680	1708	680	1101	661	646
639	1463	660	2584	660	1415	639	1141
		638	3448	638	2457		

Table 14. TPA cross-section values obtained with the wavelength-scan at fix power.

Power-scan measurements

P-1			P-2		
λ (nm)	σ$_{TPA}$ (GM)	σ$_{TPA}$ error (GM)	λ (nm)	σ$_{TPA}$ (GM)	σ$_{TPA}$ error (GM)
720	773	62	716	1423	115
680	457	37	680	1809	148
639	1358	110	639	3547	291
638	1533	125	638	3133	257
P-3			P-4		
λ (nm)	σ$_{TPA}$ (GM)	σ$_{TPA}$ error (GM)	λ (nm)	σ$_{TPA}$ (GM)	σ$_{TPA}$ error (GM)
718	757	62	716	593	48
680	964	79	680	446	36
639	2635	215	639	1079	88
638	2468	204			

Table 15. TPA cross-section values and error obtained with the power-scan at fix wavelength.

P-3 has a lower but still high σ_{TPA} maximum (2635 ± 215 GM at 639 nm) thanks to the pyrene substituents that ensure high π-conjugation but, unlike the di(thienyl)benzothiadiazole, are electron-donating. Finally, **P-1** has the same π-conjugated backbone as the other two PTCDIs derivatives but bears phenyl pendants, smaller and weaker electron donors than the pyrene, which is the cause of its smaller σ_{TPA} maximum value (1533 ± 125 GM at 638 nm). **P-4** can be discussed in comparison to **P-3**: both of these two compounds possess pyrenes as pendant groups, but while in the first the substituents are linked to the central structure directly by rigid alkynyl tethers, in the second one the conjugation path is interrupted by a dimethylenether bridge. This not only breaks the π-conjugation in the molecule, but also allows rotations that reduce the planarity of the molecule and thus the π-delocalization: the σ_{TPA} maximum value for this compound (1079 ± 88 GM at 639 nm) is therefore about half that of the parent PTCDI derivative **P-3**, which has a far better π-conjugated structure.

The σ_{TPA} of the PTCDIs we studied is thus included between 500 and 1800 GM between 680 and 750 nm, depending on the substituents: these values exceed those reported for similarly substituted PTDCI compounds,[325] demonstrating that adding appropriate π-conjugated substituents to the central perylene can also contribute to a high enhancement of the TPA properties of PTCDIs derivatives. Furthermore, functionalising the perylene core offers a higher synthetic flexibility and a bigger choice of substituents and π-conjugated patterns than substitution of the diimide fragment.[319]

Concerning the shape of the spectra, some considerations are required.

At the shortest wavelength, one-photon absorption becomes predominant and saturable absorption interfered with the TPA measurement, too. In Figure 121 the TPA and the OPA spectrum at high concentrations are overlaid (same wavelength scale): it can be noticed how, below 600 nm, the linear absorption becomes the predominant phenomenon. Since two-photon absorption is a weaker phenomenon, due to its third-order nonlinearity, it is not possible to measure it reliably when stronger phenomena occur at the same time.

To explain saturable absorption, we must consider that, as photons from the incident light pump electrons into the upper energy level, the ground state becomes depleted. If the electrons in the upper state do not relax to the lower state fast enough, the net result is that the system cannot absorb a large fraction of the incident light that is investing the sample. Especially at lower wavelengths, higher energy photons hit the sample and this can lead to almost complete depopulation of the ground state. Furthermore, other phenomena, as linear absorption, can contribute to depletion of the ground state. In practice, regular Z-scan signatures present a decrease in the normalized transmittance *vs* Z position, indicating a 2PA process. On the other hand, during the measurement, a distorted transmittance *vs* Z trace is recorded (Figure 122), which does not allow elaboration to obtain a reliable σ_{TPA} value. In such cases, two-photon absorption at short wavelengths cannot be measured for the sample.
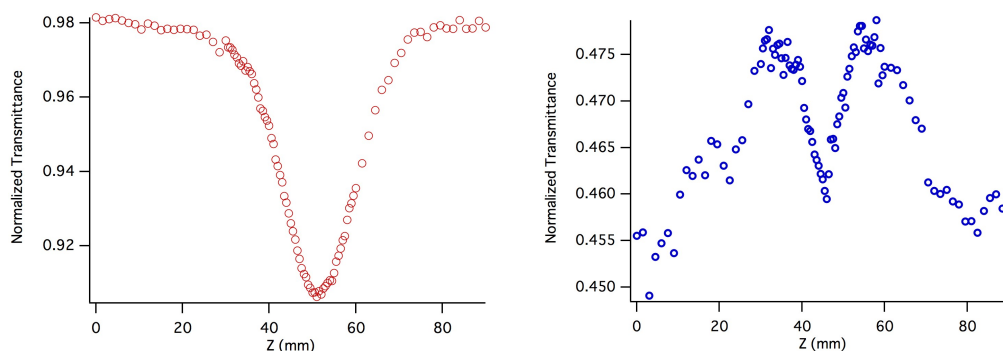
Figure 122. Regular Z-scan trace (left) and evidence of saturable absorption (right).

The monotonic increase of the TPA values at shorter wavelengths, namely while approaching the one-photon absorption band, is caused by one-photon absorption resonance enhancement of nonlinearity,[291,319c] which can be explained with the sum-over states model (Section 3.2.). The theoretical equation of σ_{TPA} based on the SOS model depends not only on μ_{fk}, the transition dipole moment between the final (f) and intermediate (k) states, and the detuning energy, but also on μ_{kg}, the transition dipole moment between the ground (g) and intermediate (k) states, and Γ_{fg}, the relaxation term. The last two terms arise directly from one-photon absorption, in such way that it influences TPA when the two phenomena happen together. So, when irradiating at an optical frequency ω near to those at which OPA takes place, resonance enhancement of TPA occurs: the detuning energy $\omega_{kg} - \frac{1}{2}\omega_{fg}$ is small and σ is highly increased.

$$\sigma_{peak}^{(2)} \propto \frac{\left|\vec{\mu}_{fk}\right|^2 \left|\vec{\mu}_{kg}\right|^2}{\left(\omega_{kg} - \frac{1}{2}\omega_{fg}\right)^2 \Gamma_{fg}} \qquad \text{Eq. (22)}$$

Another interesting feature of the TPA spectra of these PTCDI derivatives, as anticipated above, is the presence of a shoulder around 720 nm, more or less evident depending on the compound. In the spectra of **P-1** and **P-4** it appears as a peak, while it is less noticeable in the spectra of **P-2** and **P-3**. The spectral shape can be satisfactorily explained with the four-state model with two final states. The σ_{TPA} dependence on the frequency of the exciting laser can be expressed as:[291]

$$\sigma^{(2)}(\nu_p) \propto \frac{\nu_p{}^2}{(\nu_{j0}-\nu_p)^2 \Gamma_{j0}^2} \times \left[\frac{A_1}{(\nu_{f_10}-2\nu_p)^2 \Gamma_{f_10}^2} + \frac{A_2}{(\nu_{f_20}-2\nu_p)^2 \Gamma_{f_20}^2}\right] \qquad \text{Eq. (30)}$$

This model fits well the observed spectrum: the shoulder can be assigned to the transition to the final state at lower energy, while the transition to the final state at higher energy contributes to the enhancement of the TPA cross-section at shorter wavelength. Also, while approaching the one-photon transition frequency, the first term increases giving one-photon resonance enhancement effect. Observing the spectra, it is clear that the position of the resonant enhanced band doesn't depend on the different substituents. The aromatic substituents instead influence the its magnitude as well as the shape and intensity of the shoulder at lower wavelength.

4.4.3. Calculated absorption spectra

The calculated absorption spectrum of 3,4,9,10-perylenetetracarboxylic diimide[332] can give an idea of which transitions are involved in the two-photon absorption of the here studied PTCI derivatives.

Transition properties[a]		λ_{max} (nm)	f^{b}
B_{2u} (y)	(π-π*)	441	1.258
B_{1u} (z)	(n-π*)	373	0.001
B_{3g}	(n-π*)	373	0.000
A_{u}	(n-π*)	355	0.000
B_{2g}	(n-π*)	355	0.000
B_{1g}	(π-π*)	347	0.000
B_{3u}	(x) (π-π*)	344	0.022

Table 16. Calculated absorption spectra. [a] Transition symmetries assigned in the D_{2h} point group. [b] Oscillator strength for OPA.

The allowed levels for one and two-photon absorption are decided by the symmetry group D_{2h}: the transitions allowed in OPA will be towards ungerade states (B_{2u}, B_{1u}, B_{3u}), while the transitions allowed in TPA will be towards gerade states (B_{1g}, B_{2g}, B_{3g}). A_{u} is a dark state both in one- and two-photon absorption (Table 16). It is possible to obtain the transitions energies of the studied PTDCIs from the OPA and TPA spectra and to compare them with the calculated energies of the reference PTDCI (Table 17).

Transition properties[a]		Energy (cm^{-1})[b]		Relative energy (cm^{-1})[c]	
		PTCDI ref	P-1	PTCDI ref	P-1
B_{2u} (y)	(π-π*)	22676	17452	1	1
B_{1u} (z)	(n-π*)	26810	18416	1.18	1.05
B_{3g}	(n-π*)	26810	25641	1.18	1.46
A_u	(n-π*)	28169	22026	1.24	1.26
B_{2g}	(n-π*)	28169	27778	1.24	1.59
B_{1g}	(π-π*)	28818	31250	1.27	1.79
B_{3u}	(x) (π-π*)	29070	32573	1.28	1.86

Table 17. Transitions energies. [a] Transition symmetries assigned in the D_{2h} point group. [b] Energy of the different transitions. [c] Relative energy calculated assigning the value of 1 to the lowest transition.

This study was done only on one sample (**P-1**) because the OPA and TPA spectra of the PTCDIs derivatives are similar to each other. The comparison is easier if the value of 1 is assigned to the lowest transition and the other values are consequently scaled (Figure 123). By extending the molecule's π-conjugate system (**P-1**), the transitions are spread over a wider energy range: from lower energies, due to the red shift caused by extended π-conjugation, to higher energies, due to the presence of the phenyl substituents (Figure 119a). Experimentally there are no degenerate OPA and TPA levels but the transitions' levels distribution follows an overall similar pattern. The main difference consists in the fact that in **P-1** the OPA allowed transition B_{1u} and the dark A_u lie under the TPA allowed transitions.
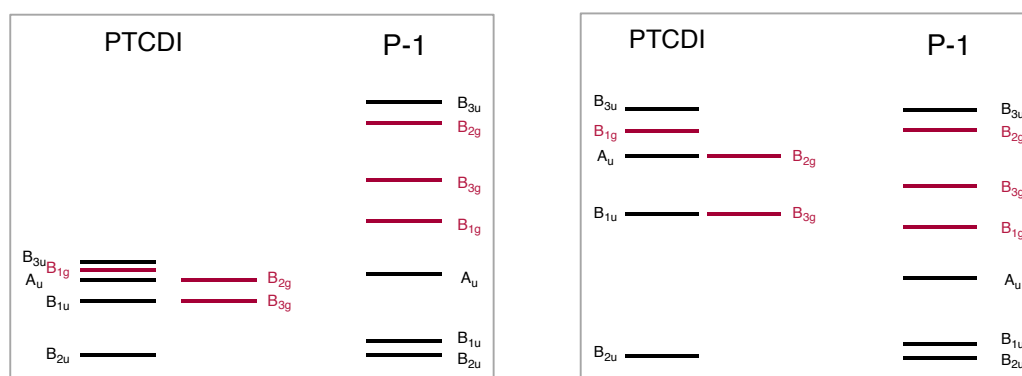
Figure 123. Left: Transitions levels. Right: Scaled transitions, distributed in a way so that the highest and the lowest have the same height in both molecules.

4.4.4. Perylene as ligand of a ruthenium(II) complex

We discussed above the TPA activity of some purely organic PTDCIs. In literature, perylenes used as ligands for some metal complexes have been reported.[336] In particular, Ru(II) complexes containing perylene units have been studied for their interesting photophysical properties[337] and applications, especially in solar cells.[338]

There are no reports of Ru(II)-PTDCI complexes for applications in two-photon absorption in literature. This prompted us to synthesize a novel ruthenium(II) complex with a 3,4,9,10-perylenetetracarboxylic diimide core substituted at the at the 1,6,7,12-bay positions with four ruthenium σ-acetylide units (Figure 124).

P-5
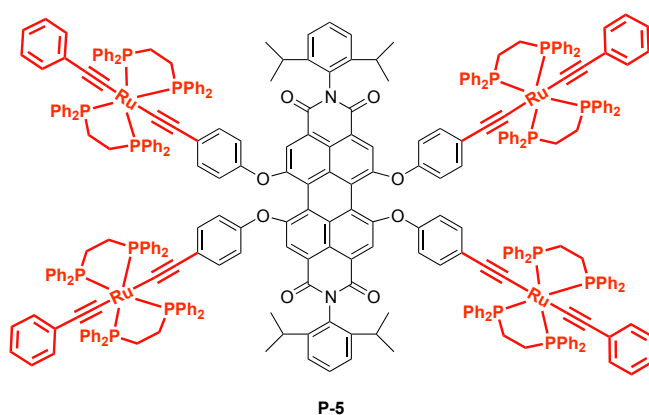
Figure 124. The novel Ru(II)-PTDCI complex.

This complex was synthesized starting from perylene-3,4,9,10-tetracarboxylic dianhydride, which was chlorinated with the use of $HClSO_3$ and then aminated with 2,6-diisopropylaniline in order to obtain N, N'-bis(2,6-diisopropylphenyl)-1,6,7,12-tetrachloro-3,4,9,10-perylenetetracarboxylic diimide. This derivative reacted with iodophenol to obtain a precursor suitable for Sonogashira coupling, in order to insert the alkynyl functions in the structures.[339] *Trans*-[(dppe)$_2$(Cl)Ru-C≡C-Ph] was synthesized[340] and then reacted with the appropriate alkynyl-substituted PTDCI in basic conditions to obtain compound **P-5**. The detailed synthetic procedure is reported in Chapter III.

Unfortunately, the TPA properties of this complex could not be measured during my PhD due to lack of time, but they will in collaboration with the group of Dr. Kamada. We expect a considerable increase of the TPA activity, thanks to the presence of the four metal units in the "arms" of the PTCDI, as part of a highly π-conjugated structure.

4.4.5. Conclusion

To summarize, four new 3,4,9,10-perylenetetracarboxylic diimide derivatives substituted at the 1,6,7,12-bay positions with highly conjugated groups have been studied. The TPA cross-section values were measured with the Z-scan technique using femtosecond laser pulses in order to avoid other concomitant NLO phenomena (as excited state absorption).

The compounds demonstrated a good TPA response, in line with the best performing PTDCIs reported to date and higher than all the other 3,4,9,10-perylenetetracarboxylic diimides with bay substituents. The TPA activity could be increased thanks to the electron-donating or electron-withdrawing activity of the substituents on the 1,6,7,12-bay positions and to the degree of π-conjugation of the entire system. The best TPA cross-section values were thus found for **P-2**, with di(thienyl)benzothiadiazole electron-withdrawing substituents: a σ_{TPA} value over 3100 GM was obtained at 639 nm.

A novel metal complex composed by a central PTDCI core and four Ru(II) σ-acetylide units on the 1,6,7,12-bay positions was successfully synthesized and characterized. We thus demonstrated that, even though PTDCI already show outstanding performances as purely organic dyes, we can envisage to improve their NLO characteristics by inserting metals in their structure. Compound **P-5** is thus expected to possess a remarkably high TPA activity, which will be studied soon.

5. TPA properties of organometallic chromophores

The third-order optical nonlinearities of a large number of coordination compounds have been reported: transition metal complexes are attractive, as already stressed for second-order NLO, because of the different coordination geometries they offer and the flexibility in tuning the nonlinear optical properties by modification of the ligands or the oxidation state of the metal. Various organometallic complexes with different transition metal centres, as copper,[341] nickel,[342] iridium,[343] iron,[344] ruthenium,[345] zinc,[346] cadmium,[347] mercury,[348] platinum,[349] palladium,[350] cobalt[342] (...) have been explored with good results for many applications. In the following paragraphs we will focus on the two-photon absorption properties of ruthenium(II) and iridium(III) complexes.

5.1. Two-photon absorption of ruthenium alkynyl complexes

In the last decades, the TPA properties of various ruthenium complexes have been explored. The groups of Shuai[351] and Humphrey[352] reported the TPA properties of some $Ru^{II}(bpy)_3$ complexes with electron-withdrawing cationic or electron-donating neutral substituents, respectively. Complexes bearing π-conjugated donor groups show higher σ_{TPA} values than complexes with electron-withdrawing groups, stressing the importance of π-donor-conjugated substituents and of ILCT vs MLCT transitions, and ruthenium complexes have better performances than other metal complexes. In particular, complex **Ru-A** (Figure 125) exhibits a maximum σ_{TPA} value of 2200 ± 300 GM at 765 nm.
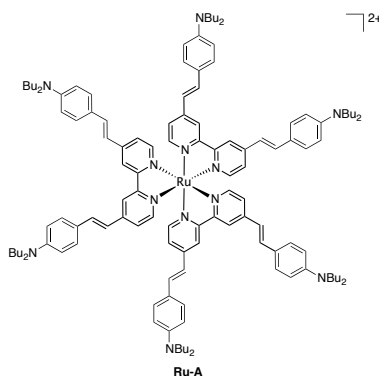
Figure 125. The $Ru(bpy)_3^{2+}$ complex studied by the group of Humphrey.

The group of Lemercier reported the TPA properties of a series of fluorene-substituted Ru(1,10-penantroline)$_3^{2+}$ complexes.[353] As a general trend, they observed that if the number of connected fluorene units increases the TPA values increase as well and if triple bonds are introduced as linkers absorption spectra are bathochromically shifted because of a more π-conjugated character of the ligands. These complexes show good TPA cross-section values ($\sigma_{TPA,max}$ around 500 GM) and by virtue of the simultaneous excited-state absorption they have been tested as efficient optical power limiters.

Ruthenium(II) tris-phenantroline complexes have also been tested as DNA probes by the group of Samoc.[354] They studied a monomeric and two dimeric complexes: the σ_{TPA} values are enhanced as the number of metal centres in the molecules increases, but the linker between the two Ru^{II} centres is important in determining the value of the TPA cross-section: it will be lower if the bridging ligands do not provide a well conjugated π-electron system. These complexes are still promising for DNA binding and related multiphoton fluorescence properties since they can reach a huge maximum σ_{TPA} of 4900 ± 600 GM (Figure 126) in the absorption band sensitive to intercalation (560 nm).
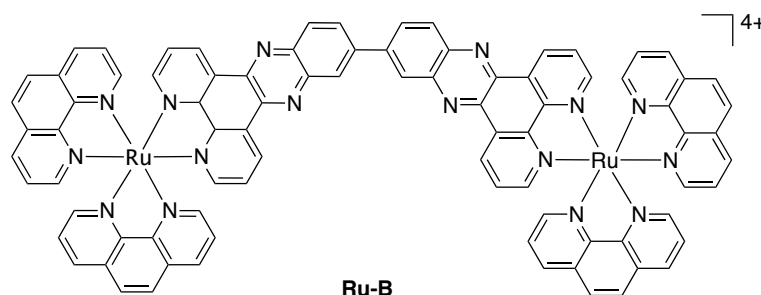
Figure 126. The binuclear Ru^{II} complex for DNA binding.

The group of Chao used four $Ru(1,10\text{-penantroline})_3^{2+}$ complexes as mitochondria- targeted two-photon photodynamic anticancer agents.[355] These complexes possess high singlet oxygen quantum yields (0.74-0.81), moderate TPA cross-sections ($\sigma_{TPA,max} = 198$ GM) and remarkable mitochondria-targeting for which they were specifically designed, demonstrating a potential for two-photon photodynamic therapy.

Recently, the group of Xu also reported nanoparticles with cross-linked Ru^{II} terpyridine complexes as the core and glycopolymers as the corona to be used as cellular labelling agents for one- and two-photon excited fluorescence imaging.[356] Such complexes have low TPA cross-sections (0.2-22.4 GM at excitation wavelengths between 720 nm and 880 nm): this performance is anyway sufficient for two-photon excited fluorescence imaging applications.

In literature there are, though, many more examples of ruthenium σ-acetylide complexes, and dendrimers, for third-order NLO: almost all the research on this subject has been performed by the group of Humphrey.[357] In 1999 they reported for the first time the third-order NLO properties of a ruthenium σ-acetylide dendrimer at a single wavelength (Figure 127).[358]
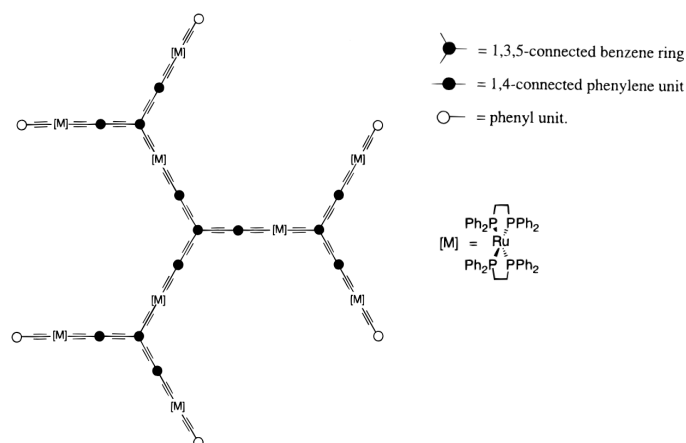
Figure 127. Example of a dendrimer synthesized by Humphrey et al.

They noticed that, going from the constituent molecules to the dendrimer, there is no loss of optical transparency, an increase in the second hyperpolarizability γ and a dramatic enhancement of two-photon absorption. They observed a maximum value of σ_{TPA} of 4800 GM for the compound reported in Figure 127: they concluded that size and two-dimensional nature of the π-delocalized system combined with the strong MLCT transition contribute to the large TPA response of the complex.

Later on, they studied the properties of some linear ruthenium alkynyl complexes in relation to the corresponding dendrimers (Figure 128).[359] First of all, remembering that organic compounds with *E*-configured alkene linkers afforded more efficient organic NLO materials than those linked by alkynes,[360] they synthesized and studied some Ru-acetylide complexes with *E*-phenylethenyl spacers. They obtained a maximum TPA cross-section of 170±100 GM at 800 nm for the linear complexes, while they reached 2100±500 GM for branched octupolar complexes. Clearly, the TPA response is enhanced by increasing the extension of the π-conjugated system and the number of metal units in the molecules, as a consequence of the major number of mobile delocalized electrons. Interestingly, they also observed some trends, useful as future guidelines: *(i)* by replacing 1,1-bis(diphenylphosphino)methane with 1,1-bis(diphenylphosphino)ethane on the ruthenium centre, *(ii)* by replacing -ene with -yne linkages and *(iii)* by replacing a chloride with a phenylacetylene end-capping ligand, the TPA cross-section can be enhanced.
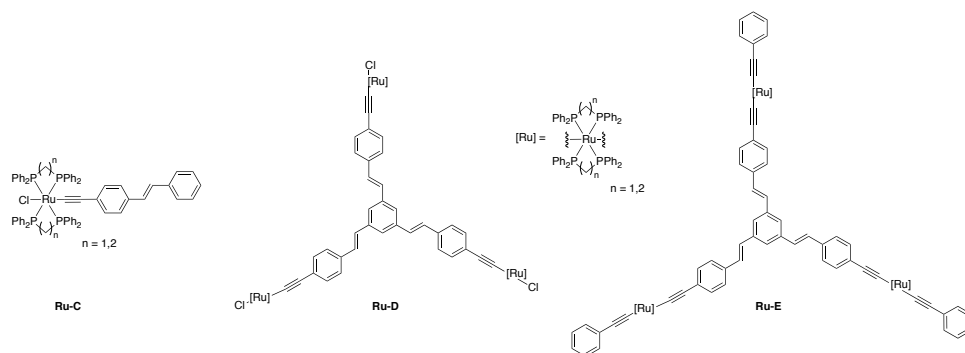
Figure 128. Some examples of linear and octupolar complexes studied by Humphrey et al.

High values of TPA cross-section were also obtained with ruthenium dendrimers having a central 1,3,5-tris(phenylethynyl)benzene[361] or tris(4-ethynylphenyl)amine core.[362] In the first case, both two- ad three-photon absorption were observed, with significantly different profiles from the linear absorption spectrum, with no evidence of MLCT transitions. The maximum σ_{TPA} is between 3000 and 4000 GM at 740 nm. Interestingly, the maxima of twice the two-photon and three-times the three-photon absorption profiles are blue-shifted relative to the maxima of the one-photon absorption spectrum. This difference may arise from the transition symmetry requirements for two-photon and three-photon absorption, which do not correspond to those for one-photon absorption. The tris(4-ethynylphenyl)amine containing complexes (Figure 129) demonstrated a dendrimer enhancement effect when **Ru-H** is compared to its smaller counterparts **Ru-F** and **Ru-G**. This comparison is made by normalizing the data for molecular-weight variations, *e.g.* by comparing σ_{TPA}/MW or σ_{TPA}/V_m (*i.e.* molecular volume) values.[363] These data reveal an approximately two-fold enhancement of the cross-section at the TPA peak by increasing the size of the dendrimer.
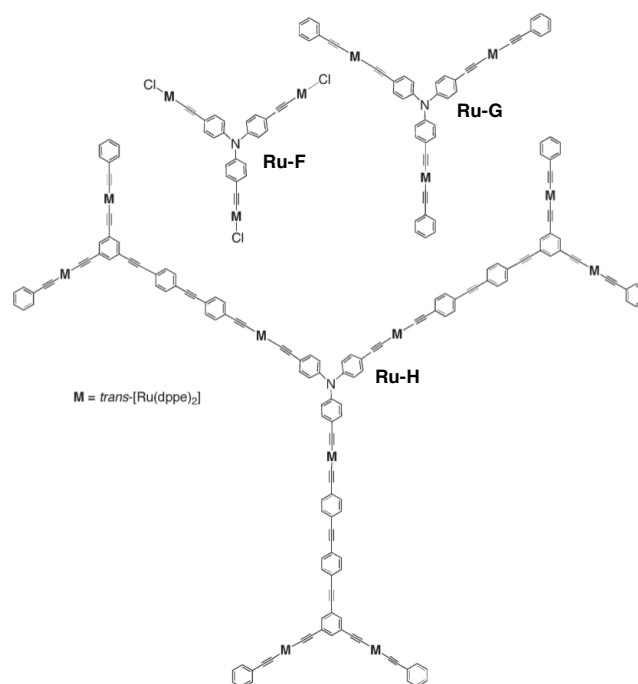
Figure 129. The ruthenium dendrimers with a tris(4-ethynylphenyl)amine core.

The open-aperture TPA-trace for these complexes, in the range 532-1600 nm, reveals to be asymmetric: this can be probably due to the production of photochemical products that absorbs light at the positions of the cell close to z = 0, that persist in solution long enough to give an increased absorption effect going on with the measurement. So, the effective TPA cross-sections do not only derive from two-photon processes, but rather from a combination TPA and higher order nonlinear phenomena as three-photon absorption, excited-state absorption, photochemical transformations, and absorption by photochemical intermediates and products.

More recently, even bigger dendrimers, the so-called second generation dendrimers, have been reported with huge TPA cross-sections reaching 28000 GM.[364] This enhancement is due both to the large extension of the π-conjugated system and to the dendrimer enhancement effect mentioned before. This means that the TPA cross-section values do not increase linearly by extending the size of the dendrimer, but they result even more enhanced by effect of the cooperation between different branches to the TPA. Moreover, these second-generation dendrimers were found to be efficient three- and four-photon absorbers with exceptionally large cross-sections.[365]

Centrosymmetric ruthenium-functionalized linear oligo(*para*-phenyleneethynylene)s also have a moderately good TPA response in the range 520-1500 nm (Figure 130).[366] The σ_{TPA} maximum wavelength does not depend on modifications of the OPE length or on the end-capping substituents. On the other hand, even though maxima σ_{TPA} values are reported for those complexes that possess the longest OPE bridge (up to 1050 GM), there is not a rational dependence of the magnitude of the TPA cross-section on OPE bridge length.
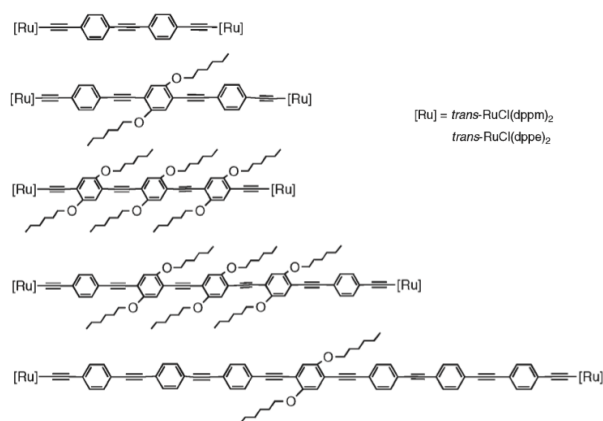
Figure 130. Some of the binuclear ruthenium-functionalized linear oligo(*para*-phenyleneethynylene) complexes synthesized by the group of Humphrey.

When ruthenium-functionalized oligo(*para*-phenyleneethynylene)s are combined in a branched structure, the σ_{TPA} values, measured at 750 nm, become immediately bigger ($\sigma_{TPA,max}$ = 4020±1640 GM for complexes with electron-withdrawing nitro substituents).[367] As observed in previous studies, the TPA response is enhanced by increasing the size of the dendrimer and by substituting triple bonds with double bonds. Curiously, for the *E*-ene-linked dendrimers, the nonlinearity decreases by increasing the size of the molecules, probably because of planarity loss.

The group of Paul recently studied the TPA properties of a mononuclear and a dinuclear Ru[II] compounds (Figure 131).[368]
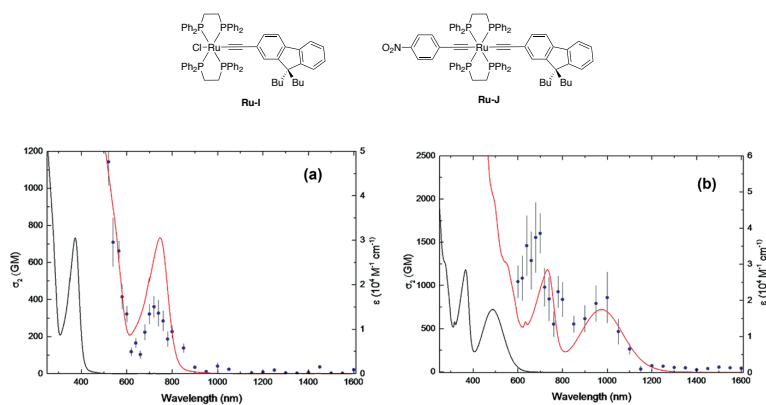
Figure 131. The Ru^{II} alkynyl complexes studied by the group of Paul and their TPA spectra.

The molecules being asymmetric, TPA peaks arise from the same transitions as for linear absorption, and the OPA and TPA spectra are superimposable: the allowed excited states at lowest energy are those that give rise to two-photon absorption. The first TPA band of **Ru-J** has an apparent TPA cross-section twice as strong as that of compound **Ru-I**, because are ascribed to different charge transfers. In compound **Ru-J** it is directed from the metal toward the nitroaryl group ($\pi_{C\equiv CPh/dRu} \rightarrow \pi^*_{C6H4NO2}$), while in **Ru-I** it is directed from the metal toward the fluorenyl group ($\pi_{C\equiv CFluo/dRu} \rightarrow \pi^*_{Fluo}$). The second band of **Ru-J** corresponds instead to the first band of **Ru-I**: substitution of the chlorine with a more acceptor nitrophenylalkynyl group causes an important increase of the TPA cross-section of the complex around 700 nm. As for other ruthenium complexes discussed above, the strong linear absorptivity at short wavelengths gives rise to saturable absorption phenomena, which results in larger uncertainty and experimental errors.

5.2. New ruthenium alkynyl complexes for two-photon absorption

While the TPA properties of ruthenium dendrimers have been widely studied, there are few examples of mononuclear and dinuclear ruthenium complexes for TPA applications. So, the two-photon absorption of two new ruthenium(II) σ-acetylide complexes (Figure 132) was measured. This class of complexes, of which many examples have been discussed above, is interesting for their facile high-yielding syntheses,[340a] reversible redox properties[369] and high third-order NLO response.[370] In our compounds, the metal centres act as donor groups of a donor-acceptor system, where the acceptor is the organic fragment 4,7-di(2-thienyl)benzo[c][1,2,5]thiadiazole. In complex **Ru-1** two 4,7-di(2-thienyl)benzo[c][1,2,5]thiadiazole units are linked by a Ru(II) σ-acetylide bridge, while in **Ru-2** the two Ru[II] σ-acetylide units are linked through a 4,7-di(2-thienyl)benzo[c] [1,2,5]thiadiazole. The almost linear metal-alkynyl structure allows a good coupling between the π system of the σ-acetilydes and the d orbitals of the metal. Furthermore, the phenylalkynyl ancillary ligands in compound **Ru-2** are meant to increase the donor properties of the ruthenium centre[371].

Ru-1   **Ru-2**
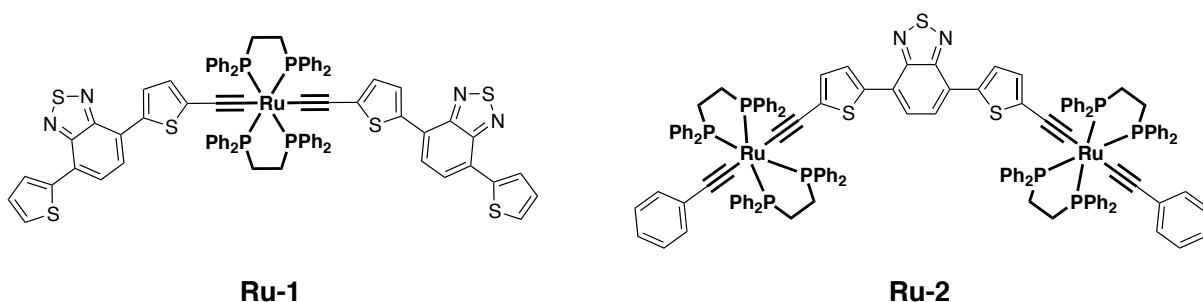
Figure 132. The two newly studied Ru[II] complexes.

Complex **Ru-2** has already been studied in our group as a material for bulk heterojunction solar cells[372] and for its second-order nonlinear optical properties.[251] In solar cells, it was investigated as a donor material combined with an electron-withdrawing methanofullerene derivative (as [6,6]-phenyl-C61-butyric acid methyl ester, PCBM) with good performances: the absorption spectrum is red-shifted because of the presence of the Ru and thus gives better solar light harvesting, and also the photoinduced electron transfer process to PCBM is efficient. As for second-order NLO properties, it demonstrated good β_{EFISH} values ($\beta_{EFISH} = -566 \cdot 10^{-30}$esu, $\mu\beta_{EFISH} = -900 \cdot 10^{-48}$esu) and to be an efficient building block for active polymeric films with second-order NLO response.

5.2.1. Linear absorption

The UV-Vis spectra of the samples solution in dichloromethane shown in Figure 133 were recorded by a *Shimadzu UV-3150* spectrometer using 1 cm quartz cells, at a concentration of about 10^{-6} M. The intense absorption band between 300 and 450 nm can be attributed to MLCT $d_{Ru} \rightarrow \pi^*_{acetilyde}$

transitions, while the bands at longer wavelengths can be attributed to charge-transfer transitions within the di(thienyl)benzothiadiazole ligand. The epsilon values are good and similar between the two complexes, even though the maxima are at different wavelengths, and in particular red shifted for the binuclear ruthenium complex, as expected from the presence of two metals.
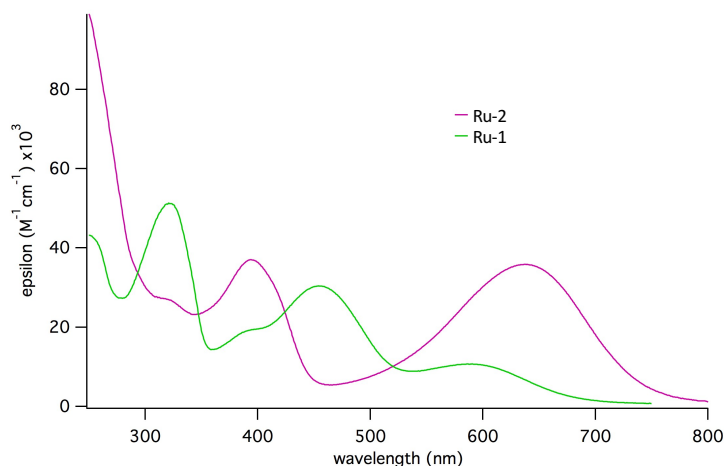
Figure 133. Linear absorption spectra of **Ru-1** and **Ru-2** in CH_2Cl_2.

The spectra recorded in DMSO (Figure 134), a more polar solvent, are similar to those recorded in CH_2Cl_2. Being the transition of charge-transfer character, a red shift was expected in DMSO because the excited state would have been more stabilised in a polar solvent. Nevertheless, there are no evident changes in the absorption bands. The only difference is that the magnitude of the bands centred at 600-700 nm is smaller in DMSO than in CH_2Cl_2, probably because these transitions are less favoured in a polar solvent.
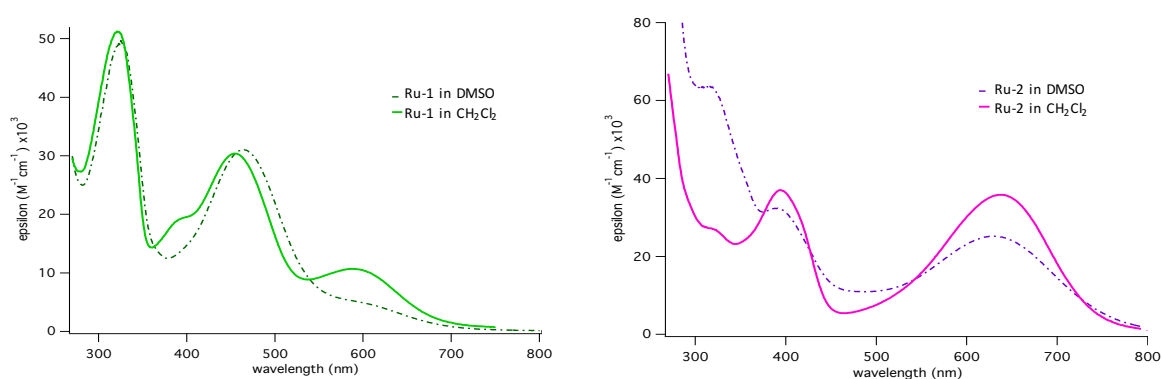
Figure 134. Superimposed linear absorption spectra in DMSO and DCM.

In an extreme case, some bands can even disappear in polar solvents due to a complete charge separation: if the ground and excited states have completely opposite distribution of charge, it can happen that the orbital concerned in the transition don't overlap. In these particular cases there is a difference in charge and dipole moment between the ground and excited state, but it is so large that the optical transition does not occur anymore.

5.2.2. Two-photon absorption

The complexes were dissolved in dichloromethane and placed in 2-mm cuvettes. The solubility was quite good: complex **Ru-2** was stable in an 0.8 mM solution, while for complex **Ru-1** a concentration of 1.5 mM could be reached. The two-photon absorption spectra of **Ru-1** and **Ru-2** were recorded from 960 nm to 800 nm.

To measure properly the nonlinear absorption of these samples the solutions needed to be stirred, in order to avoid overestimation of the TPA cross-section. In fact, apparently the two complexes undergo photochemical reaction under irradiation of the laser beam, giving rise to the formation of a new product that absorbs linearly at the irradiation wavelength, thus enormously decreasing the registered transmittance and somehow falsifying the real value of the TPA cross-section. We could reach this conclusion by observing the transmittance *vs* Z graphics as long as the measurements were being performed (Figure 135).
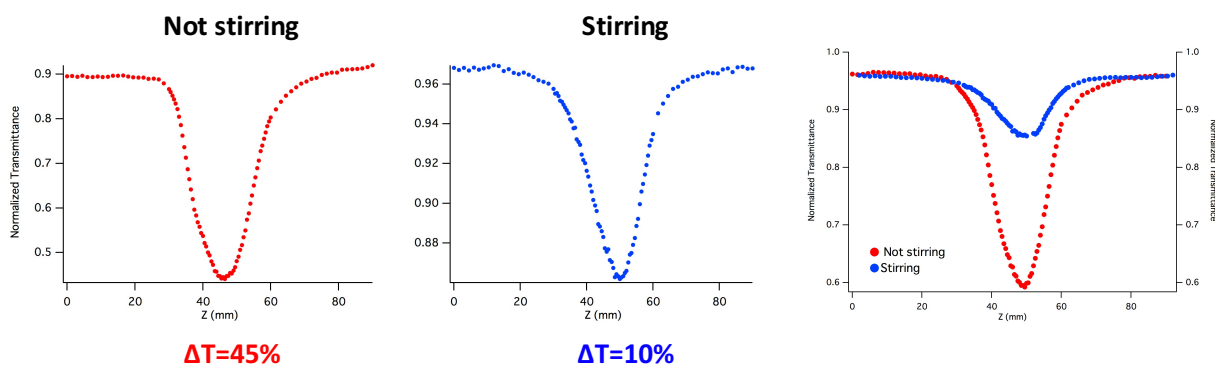
Figure 135. Comparison of the Z-scan traces without and with stirring.

When the sample is not stirred, the Z-scan trace, recorded from left to right, is not symmetric and deeper than it appears while stirring the sample, because under irradiation a photochemical product forms and linearly absorbs. The fact that the Z-scan trace without stirring the sample is not symmetric confirms that we are not observing excited-state absorption. The transmittance decreases abruptly by approaching to the focal point because the photochemical product suddenly forms, and then by moving away it increases gradually because the product formed already and is just absorbing light. If excited-state absorption occurs, the curve remains symmetric and is just deeper.

By stirring, fresh solution is continuously brought to the focal point of the laser beam, not allowing accumulation of the newly formed photochemical product to be detected (Figure 136).

This phenomenon was observed also for other ruthenium (II) dendritic σ-acetylide complexes reported in literature and could possibly be exploited to initiate polymerisation reactions, since the product forming is probably a radical.[362]
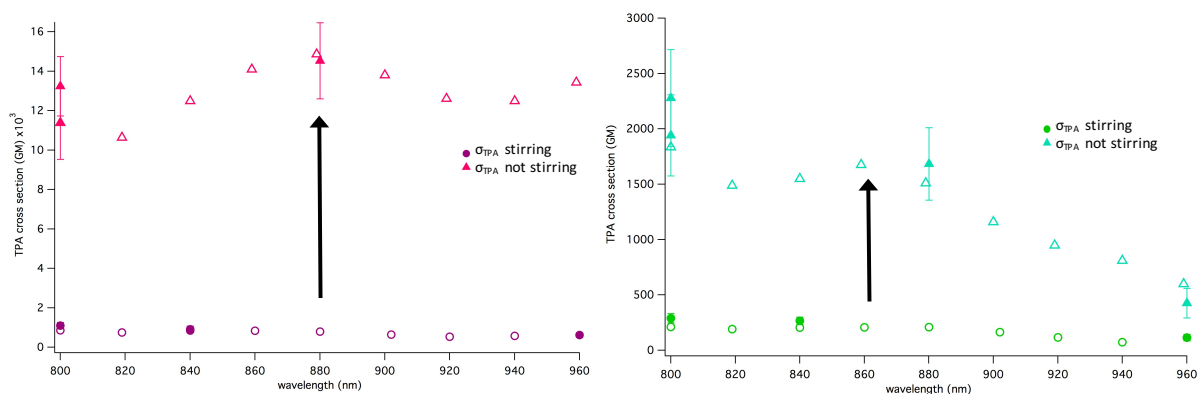
Figure 136. Comparison of the TPA spectra registered with or without stirring the solution.

The two-photon absorption spectra of **Ru-1** and **Ru-2** are shown in Figure 137 and the TPA cross-section values are reported in Table 18 and Table 19. The two-photon allowed transitions occur in correspondence of the MLCT bands of the complexes and the one and two-photon absorption spectra are almost superimposable, due to the lack of central symmetry of the molecules. It was not possible to measure the TPA response at shorter wavelength because linear absorption occurs, preventing the measurements.

The TPA cross-section values are moderately good for both complexes, with maxima of 1200 GM for **Ru-2** and 300 GM for **Ru-1**. The σ_{TPA} values of the binuclear complex **Ru-2** are almost 4 times larger than those of the mononuclear complex **Ru-1**. This can be explained with different motivations:

1.   First of all, the presence of two metal centres is expected to naturally increase the TPA properties of the molecule because of the major number of highly polarizable d-electrons in the metal orbitals. These electrons are numerous and less strictly bound to the atomic nucleus, which means that they are more mobile within the molecule when excitation occurs.[V]

2.   Furthermore,   the   structure   of   the   considered   molecules   is   almost   flat: the di(thienyl)benzothiadiazole units, electron-withdrawing, contribute to the planarity of the branches, extend the conjugation length and the delocalization of π-electrons, as already noticed for the PTDCI derivatives discussed before.[335]

[V] In a previous paper about complex **Ru-2**, it was proved that the two ruthenium units do not communicate through the di(thienyl)benzothiadiazole bridge.[372] So, the enhanced TPA cross-section is most probably due to the presence of two metals, without a significant synergic effect (a sort of "dendrimeric effect", like for complexes described in the previous section). Such statements need in any case to be proved by theoretical calculations.
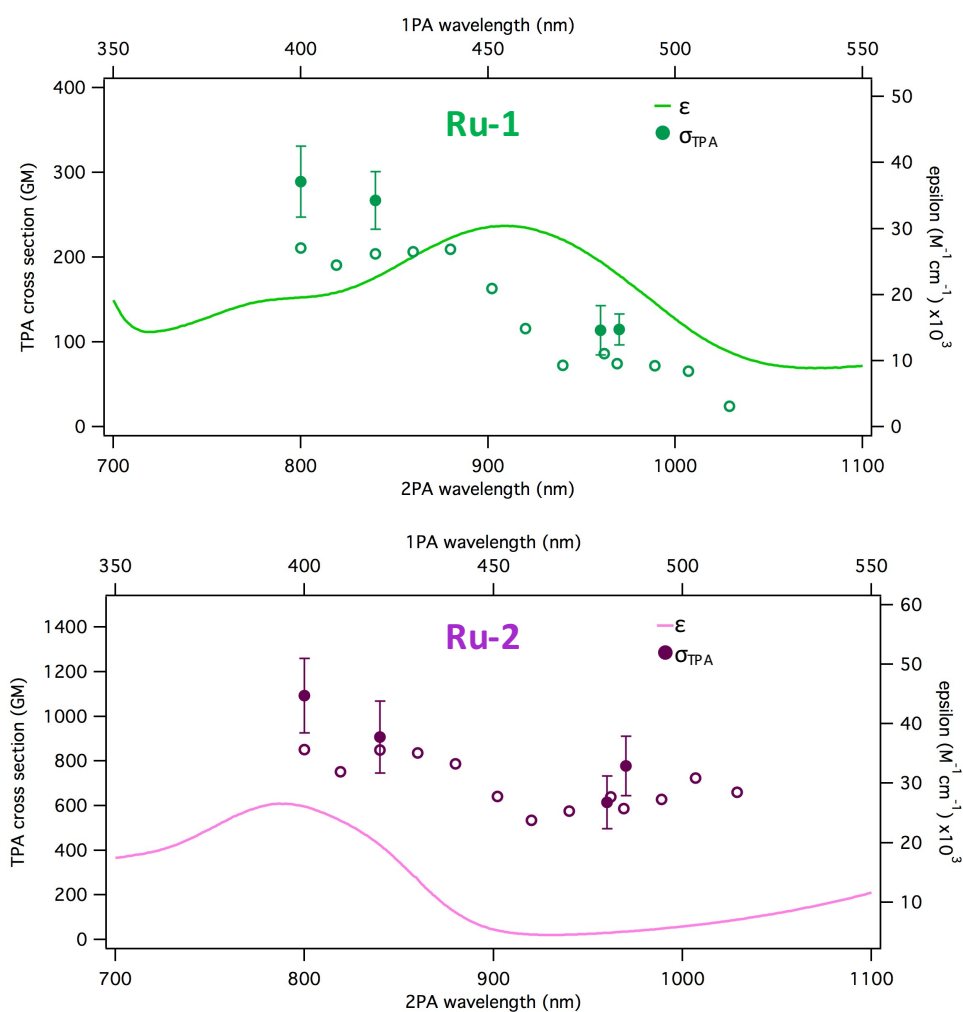
Figure 137. One-photon (plain line) and two-photon absorption spectra of **Ru-1** (top) and **Ru-2** (bottom). The empty markers are the values obtained with the wavelength scan at a fix power, while the full markers with error bars are the ones obtained with the power scan at a fixed wavelength.

Wavelength-scan measurements

Ru-1		Ru-2	
λ (nm)	σ_{TPA} (GM)	λ (nm)	σ_{TPA} (GM)
800	193	800	749
819	175	819	690
840	189	840	792
860	191	860	789
880	194	880	755
902	153	902	616
920	109	920	516
940	91	940	552
962	81	962	616
969	74	969	586
989	72	989	629
1007	65	1007	723
1029	24	1029	659

Table 18. TPA cross-section values obtained with the wavelength-scan at fix power.

Power-scan measurements

Ru-1			Ru-2		
λ (nm)	σ_{TPA} (GM)	σ_{TPA} error (GM)	λ (nm)	σ_{TPA} (GM)	σ_{TPA} error (GM)
800	281	41	800	1094	167
840	260	34	840	907	161
960	211	28	960	615	118
970	115	18	970	779	131

Table 19. TPA cross-section values obtained with the power-scan at fix wavelength.

Anyway, the presence of some rotational isomers in solution should not be excluded. Considering the monometallic **Ru-1** complex, if the flat lateral di(thienyl)benzothiadiazole substituents rotate of some degrees, the π-conjugation in the molecule would be abruptly interrupted, because the p orbitals would not result anymore coplanar to the rest of the molecule. The situation is different for the bimetallic complex **Ru-2**: even though rotation occurs, d orbitals are less strictly directional than the p orbitals and some degree of conjugation can be maintained, explaining so the bigger TPA cross sections of compound **Ru-2**.

This second explanation is only tentative, and should be supported by theoretical calculations that will soon be performed.

3.   Also, the difference in the TPA response of the two complexes can be explained by considering the strength of the charge transfer transitions inside the molecule. Charge transfers will be more effective between a strong donor and a strong acceptor, and so the magnitude of σ_{TPA} will be enhanced. On the other hand, if the different fragments in the molecule are weaker donor or acceptor, the charge transfers will be less strong. In the case of the two complexes **Ru-1** and **Ru-2**, by observing the experimental data and the structure of the molecules, it is possible to suppose that the charge transfers are more effective in the bimetallic complex (Figure 138). The two metal centres act as good donors towards the di(thienyl)benzothiadiazole moiety: this could be a reason why the magnitude of σ_{TPA} is bigger for **Ru-2** than for **Ru-1**, which possesses only one metal centre.

This kind of comparison is anyway difficult without theoretical studies that can give information on the strength of the transitions between donor and acceptor groups.
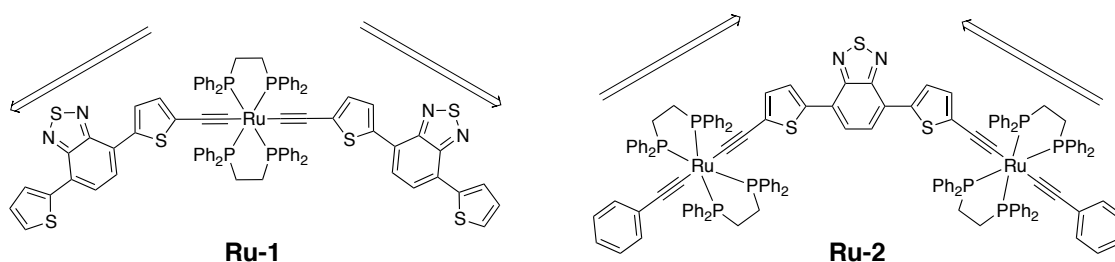
Figure 138. The two Ru[II] complexes with, in evidence, the direction of the charge transfers transitions between the donor metal and the acceptor organic fragments.

5.2.3. Conclusion

In summary, the TPA cross-sections of one mononuclear and one dinuclear Ru^{II} complexes were measured. The TPA cross-sections of these complexes are moderately good, even though somehow lower than those of recently reported Ru^{II} alkynyl complexes.[367] As expected by the presence of two metal units, the binuclear complex **Ru-2** displays better nonlinear absorption, even though communication between the two metal units was proven to be weak.

Interestingly, through a photochemical reaction induced by the laser, a new product forms upon irradiation. This was confirmed by noticing the absorption of this newly formed compound during the Z-scan measurements. This phenomenon previously caused difficulties in the measurement of the TPA response of some ruthenium dendrimers. We managed to overcome this problem by stirring the solution with a small magnetic stirrer and we succeeded in measuring the TPA cross-section of these complexes with a sufficiently small uncertainty.

As soon as the setup will be ready, in the near future, these complexes will be tested as promising initiators for two-photon induced polymerization.

5.3. Two-photon absorption of iridium complexes

Iridium complexes have recently attracted attention for their third-order NLO properties. In section 2 we have already considered iridium complexes for their outstanding optical properties, tunable over the entire visible region, their robustness and their intriguing NLO properties.

The group of Beeby reported a series of iridium(III) tris(2-phenylpyridine) or bis(2-phenylpyridine)(acetylacetonate) complexes (Figure 139).[373]
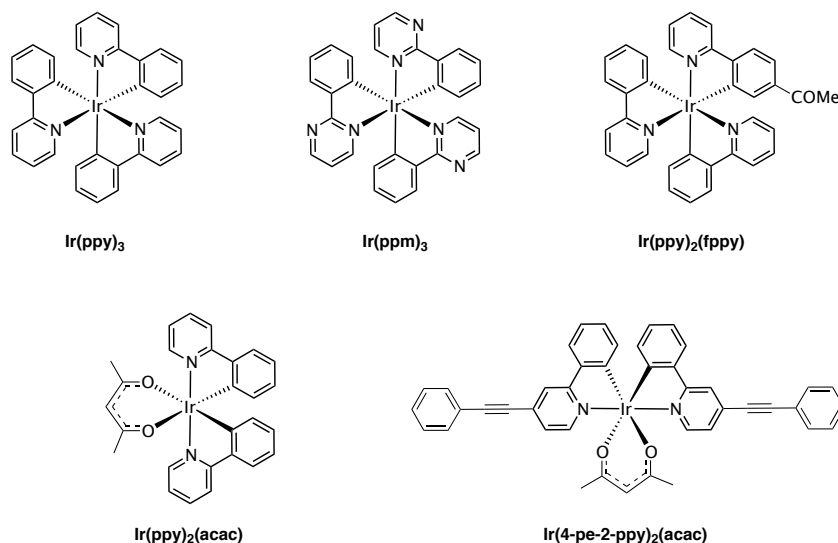
Figure 139. The complexes studied by the group of Beeby.

They found moderate TPA cross-section values (maximum 60 GM for Ir(4-pe-2-ppy)$_2$(acac)) in the range between 760 and 880 nm. They observed better TPA response for the complexes bearing an acetylacetonate ligand, while substitution of 2-phenylpyridine with 2-phenylpyrimidine has a strong negative effect of TPA values.

The group of Wong also studied some Ir(ppy)$_3$ complexes with more extended ligands (Figure 140).[374]
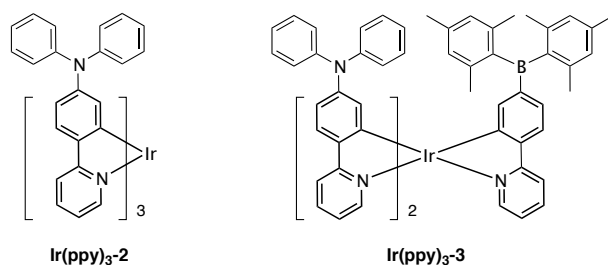
Figure 140. The complexes studied by Wong and co-workers.

Complex **Ir(ppy)$_3$-3** demonstrated larger TPA cross sections than **Ir(ppy)$_3$-2** (340 GM at 750 nm), but both complexes revealed very strong two-photon induced emission in solution. The complexes have

been tested in vivo and they demonstrate high target-specificity to the Golgi apparatus with long residential lifetime, low cytotoxicity and highly induced two-photon emission.

Zhao et al reported some symmetrically and unsymmetrically, *para-* or *ortho-* substituted Ir(ppy)$_3$ complexes with oligofluorene-substituted phenylpyridines.[375] These iridium complexes (Figure 141) are among those with the largest TPA cross-sections reported in literature.
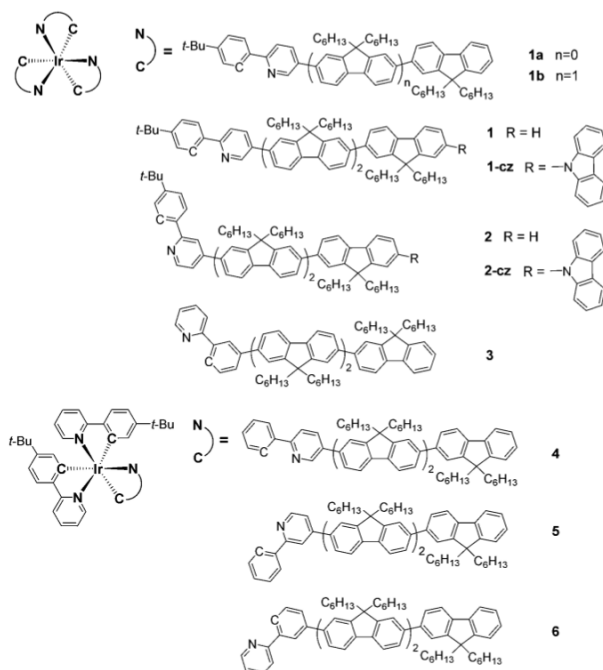
Figure 141. The iridium complexes with fluorenyl substituents.

They demonstrated that the TPA response is proportional to the size of the conjugated ligand. When they extend from one to three fluorene units, σ_{TPA} values are enhanced fourfold. Furthermore, if a donor carbazole group is added at the end of the ligand, TPA is further improved due to increased donor-acceptor electronic effects, reaching maxima values slightly lower than 1200 GM for complexes **1-cz** and **2-cz**. The complexes also demonstrated to have three-photon absorption and two-photon excited emission properties.

Our group studied the TPA properties of a neutral *cis*-[Ir(CO)$_2$Cl(4-(para-di-*n*-butylaminostyryl)pyridine)] complex.[376] The TPA cross-section maximum was found to be 779 ± 61 GM at 910 nm. This value is four times higher than that reported for 4-(para-di-*n*-butylaminostyryl)pyridine (190 ± 34 GM), demonstrating how the σ_{TPA} can be highly enhanced upon coordination to the Ir^{I} metal centre.

Some examples of neutral iridium(III) complexes with TPA properties and direct applications in vivo were also recently reported by the groups of Kawamata[377] and Monnereau.[378] The complexes they studied exhibit TPA in the near-infrared, at wavelengths suitable for biological applications, with quite

low TPA cross-section values (around 20-40 GM), which are enough to allow recognition of two-photon induced emission in cells.

The TPA response of several cationic iridium complexes was also explored. Magennis et al. firstly studied $Ir(trpy)_2^+$ complexes, reporting fair TPA cross-section values with maxima of 70 GM.[379] The group of Huang synthesized and studied a binuclear Ir^{III} cationic complex bearing dimesitylboryl groups on the cyclometalated 2-phenylquinoline ligands and a push-pull conjugated bipyridine oligomer.[380] The TPA spectra of the complex was determined between 730 and 840 nm in THF obtaining a maximum value of 500 GM at 750 nm. This value is considerably high and can be explained by the long π-extension of the bipyridyl ligand and the presence of two metal centres instead of one as in the complexes considered before. The complex bearing boron-based substituents, it can be used as a one- and two-photon-excited switchable phosphorescent probe for F^- ions, thanks to the strong B-F interactions.

The group of Das studied a series of $[Ir(ppy)_2(bpy)]PF_6$ complexes with extended π-conjugated styrene substituents on the bipyridine ligand.[381] The TPA cross-sections were reported at 800 nm with ps pulses and at 680 nm with fs pulses and values as high as 900 GM were reached. Nevertheless, the reported Z-scan traces reveal that two-photon absorption is not the only phenomenon that these molecules undergo when irradiated with laser pulses. The very sharp curves reveal the presence of contemporaneous three-photon absorption and some distorted TPA traces indicate saturable absorption. So, probably, the reported TPA values are not always completely reliable, especially at 680 nm.

The group of Chao extensively studied the TPA response of some cationic iridium complexes with chelating ligands for applications as probes is cells, especially in mitochondria.[382] The complexes they reported have moderate TPA cross-section values, but they can enter cells, localize in mitochondria and signal the excessive presence of ClO^- (Figure 142) or track mitochondrial morphological changes during the early stages of cells apoptosis even under hypoxia, highlighting the potential of such complexes for applications in biomedical research.
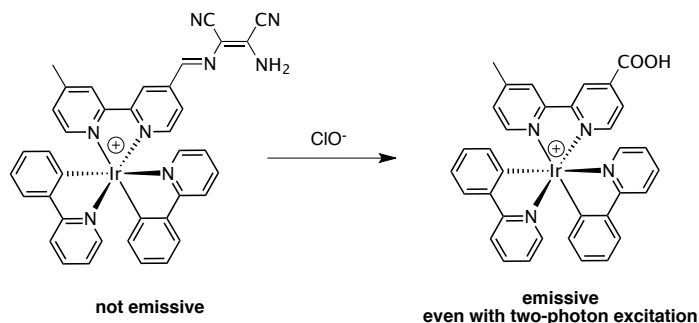
Figure 142. A complex studied by Chao et al. and its reaction with ClO^-.

5.4. New neutral and cationic iridium complexes for two-photon absorption

The two-photon absorption properties of four neutral Ir(2-phenylpyridine)$_3$ neutral derivatives and one [Ir(2-phenylpyridine)$_2$(2,2'-bipyridine)]PF$_6$ cationic derivative (Figure 143) were studied with the Z-scan technique. All of these compounds are substituted on the *para*-position of the pyridyl ligands with a π-conjugated substituent possessing different donor abilities. The last compound, **Ir-5**, is cationic and bears two 2-phenylpyridine substituents and a 2,2'-bipyridine substituent doubly functionalized with donating π-conjugated groups.
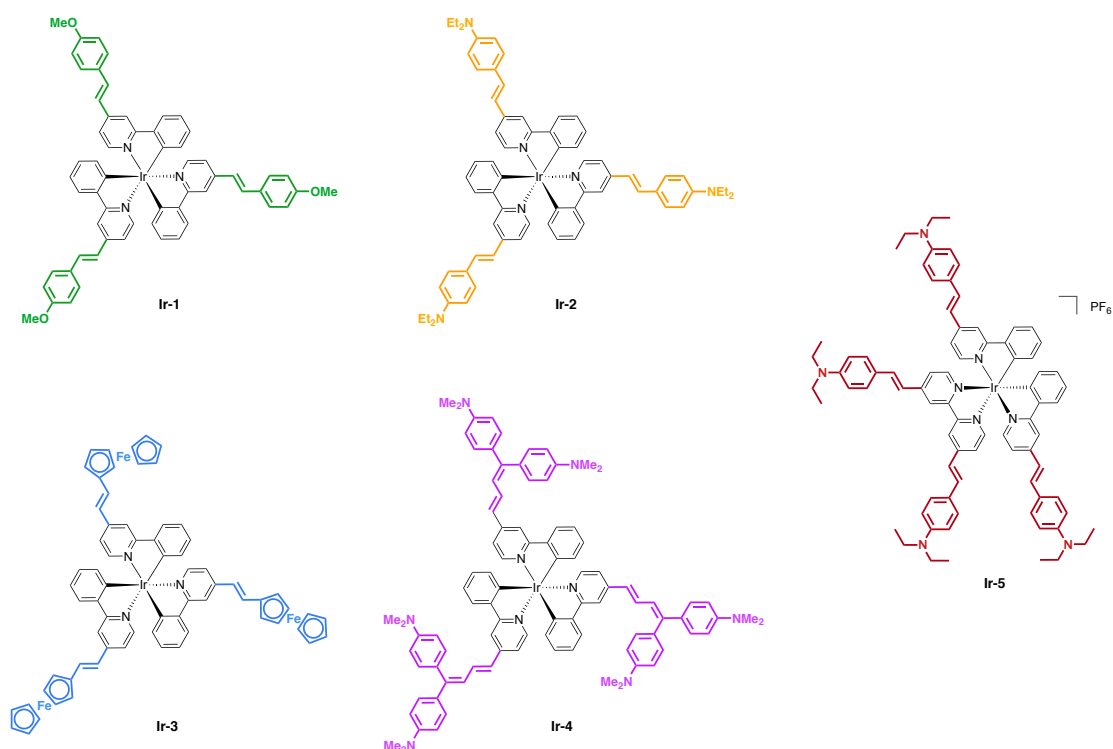
Figure 143. The Ir^{III} complexes for TPA.

The neutral complexes were already studied by our group for their second-order NLO properties: they are characterised by high absolute values of μβ$_{EFISH}$, dependent on the substituent on the position 4 of the pyridyl ring (Table 20).[175]

	μβ$_{EFISH}$ · 10^{-48} esu	μ · 10^{-18} esu	β$_{EFISH}$ · 10^{-30} esu	⟨β$_{HLS}$⟩ · 10^{-30} esu
Ir-1	−700	12.8	−54	290
Ir-2	480	14.5	33	400
Ir-3	−430	8.5	−51	330
Ir-4	620	17.1	36	460

Table 20. Second-order hyperpolarizabilities of the neutral Ir^{III} complexes.

β$_{EFISH}$ of the complexes bearing a weakly donor substituent has a negative value because of the negative value of Δμ$_{eg}$ due to the decreased dipole moment of the excited state. This is caused by the fact that the

MLCT directed from the iridium to the pyridine are stronger than the vectorially opposed ILCT from the donor. When the donor is stronger, the ILCT transitions prevail on the MLCT and the sign of β_{EFISH} becomes positive. The value of β_{HLS} instead takes into account also the octupolar contribution along with the dipolar ones and increases with the increasing electron-donating ability of the substituents.

The luminescent properties of **Ir-5** were discussed in the Chapter I and its second-order NLO properties of were discussed in section 2.6 of this chapter. **Ir-5** has a good $\mu\beta_{EFISH,1.907}$ of $-960 \cdot 10^{-48}$ esu, higher than those of the Ir(ppy)$_3$ neutral complexes.

5.4.1. Synthesis of the complexes

The neutral iridium complexes were prepared following a reported procedure.[175] The bis-cyclometalated chloro-bridged dimers were first obtained by reaction of IrCl$_3 \cdot$ nH$_2$O with 4-methyl-2-phenylpyridine. Upon reaction of the dimers with 4-methyl-2-phenylpyridine in glycerol at 200°C, the tris-chelate methyl complex *fac*-Ir(4-methyl-2-phenylpyridine)$_3$ was achieved. It was then treated at room temperature with the appropriate *para*-R-benzaldehyde in the presence of *t*-BuOK to obtain the desired complexes with a "chemistry-on-the-complex" approach. It is not possible to synthesize the complexes directly from the styryl-substituted dimer, because in the required conditions the double bonds would be hydrogenated.[383] The cationic complex was prepared as described in section 5.2.1 of Chapter I. The detailed synthetic procedure for the preparation of the iridium complexes will be described in Chapter III. All the complexes were characterized by standard techniques.

5.4.2. Linear absorption

The UV-Vis spectra of the samples solution in dichloromethane were recorded by a *Shimadzu UV-3150* spectrometer using 1 cm quartz cells, at a concentration of about 10^{-6} mM (Figure 144).
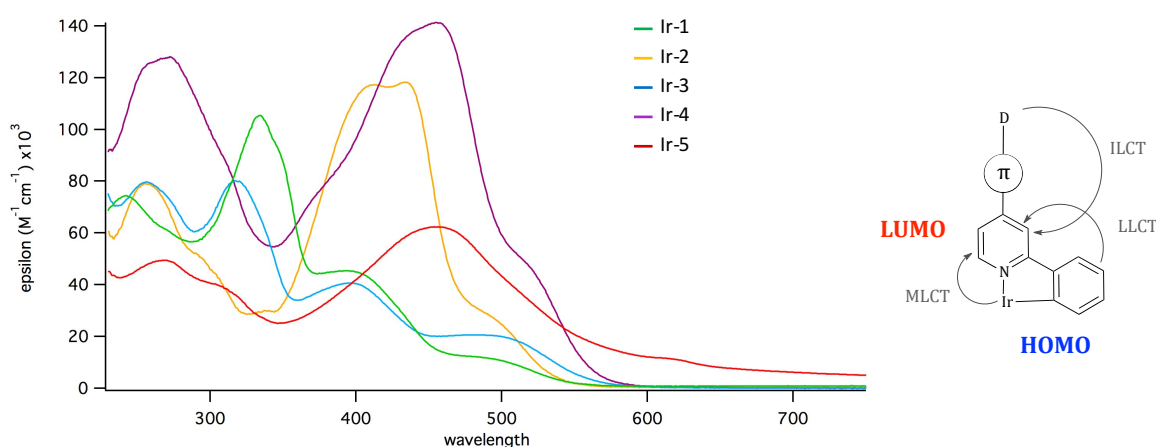
Figure 144. The linear absorption spectra of the iridium complexes in dichloromethane (left) and a schematic representation of charge transfers within the 2-phenylpyridyl ligands and the metal centre (right).

Complexes **Ir-1** and **Ir-3** show similar spectra: the more intense absorption band at 310-350 nm can be attributed to ILCT π-π* transitions of the styryl-phenylpyridine ligands, while the absorption bands at lower energy, about 370-450 nm, can be assigned to MLCT transitions and the band tailing up to 560 nm could be due to excitation to triplet charge transfer states.[175] Complexes **Ir-2** and **Ir-4**, bearing the amino substituents, which is strong electron-donating, show an intense band at 400-550 nm hiding the MLCT band: this is assigned to a ILCT transition in which the pyridyl ligand acts as a π*-acceptor group. The absorption spectrum of complex **Ir-5** was registered both in dichloromethane and dimethyl sulfoxide (Figure 106): the solubility in dichloromethane is low and not enough to record a proper TPA spectrum. Interestingly, in DMSO, a negative solvatochromism with subsequent hypsochromic shift can be observed. This behaviour was already discussed in paragraph 2.6.

5.4.3. Two-photon absorption of the neutral iridium complexes

The neutral Ir[III] complexes were dissolved in DCM, while the cationic complex **Ir-5** was dissolved in DMSO, and placed in 2 mm quartz cuvettes. The solubility of the neutral complexes was good, ranging from 1.3 to 2 mM, while the maximum solubility of **Ir-5** was 0.55 mM in DMSO, and even lower in dichloromethane, explaining thus the choice for the more polar solvent for the measurements.

Some expedients were necessary in order to measure properly the nonlinear absorption of these samples. Complexes **Ir-2** and **Ir-4** apparently undergo photochemical reactions under irradiation of the laser beam. This can be understood by looking at the shape of the Z-scan trace, which looks like the one observed for the ruthenium complexes discussed before without stirring: the Z-scan trace is not symmetric and deeper than normal.

From 700 nm to shorter wavelength, most of the samples also absorbed linearly: in this case the correction was taken into account while calculating the TPA cross section value (Eq. 29). When linear absorption occurs, the transmittance value at Z = 0 mm is smaller than one (Figure 145): at this distance from the focal point, TPA should not occur, so eventual decreases in transmittance are surely due to linear absorption phenomena.

The two-photon absorption spectra of the four neutral iridium complexes **Ir-1,2,3,4** are shown in Figure 146 and the σ_{TPA} values are reported in Table 22 and Table 23.
The σ_{TPA} values are very high especially if compared with those of the unsubstituted Ir(2-phenylpyridine)$_3$:[373] the reported values range from 35 to 5 GM between 760 and 800 nm. By adding various donating substituents, the TPA response is increased more than tenfold, depending on the strength of the donor. The complexes bearing the methoxyphenyl and ferrocenyl groups have the lowest TPA cross-section (**Ir-1**: $\sigma_{TPA,max}$ = 169 ± 29 GM, **Ir-3**: $\sigma_{TPA,max}$ = 439 GM at 620 nm), demonstrating

the similar effect of these substituents, already observed for compounds studied for second-order NLO.[212]
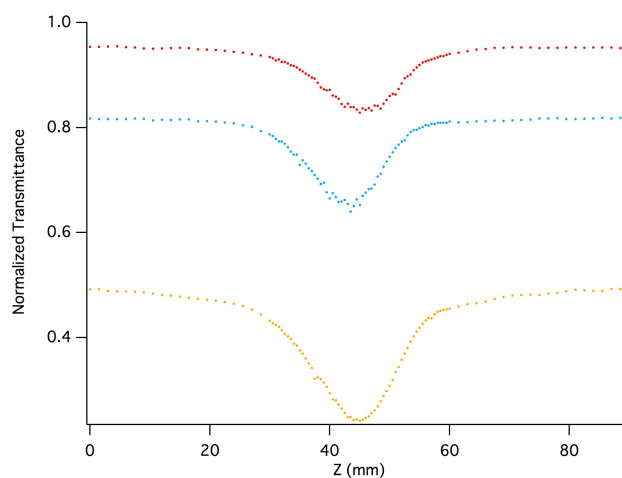
Figure 145. Z-scan traces of **Ir-5** at wavelengths at which linear absorption increases (from the red to the yellow).

The TPA becomes even more intense if the substituents are aminophenyl groups (**Ir-2**: $\sigma_{TPA,max}$ = 536 GM at 780 nm, **Ir-4**: $\sigma_{TPA,max}$ = 748 ± 130 GM at 800 nm) reaching values of several hundreds of GM. The minimum values we recorded, for complex **Ir-1**, are still much higher that for the unsubstituted complex. This behaviour is interesting, because it demonstrates that by a careful design of the complexes and with overall small changes in the molecules' structure, *i.e.* by simply changing the donating substituents, the TPA magnitude can be modulated over a wide range reaching high values. The largest TPA cross-sections have been obtained for **Ir-4**, bearing strongly electron-donating substituents, with mobile electrons on the p orbitals of the nitrogen, and with a longer π-conjugated system, due to the presence of two double bonds and two N,N-dimethylaniline groups. The highest TPA cross-section values for some neutral Ir(ppy)₃ complexes were reported by Zhao and co-workers.[375] Nevertheless, they used very large and extended substituents to obtain a result that we reached with smaller complexes, using more simple ligands and thus reducing the synthetic steps.

The monotonic increase of the TPA values at shorter wavelengths, namely while approaching the one-photon absorption band at 600 or 620 nm, depending on the sample, is caused by one-photon absorption resonance enhancement of nonlinearity which is explained considering the theoretical equation of σ_{TPA} based on the SOS model. It is quite uncommon to observe resonance enhancement for non-centrosymmetric molecules like these, because this phenomenon is usually explained with the diminishing of the detuning factor, present in the three-states model for centrosymmetric molecules. For non-centrosymmetric molecules, on the other hand, the two-states model is considered good in predicting the shape of the spectrum, but the detuning factor does not appear in its equation (Eq. 23). Nevertheless, these complexes have some degrees of rotational symmetry, which justify their behaviour as centrosymmetric at shorter wavelengths.

The shape of the TPA spectrum for our neutral iridium complexes, so, cannot be easily predicted with only one model. Being the complexes of C_3 symmetry and thus non-centrosymmetric, according to theory, Laporte selection rule is not valid and so excited states allowed in one-photon absorption are also allowed in two-photon absorption. TPA is expected to take place at a double wavelength respect to the one of OPA. Nevertheless, since molecules possess come degree of symmetry, this complicates the theoretical approach to the explanation of the TPA spectrum. A good approximation can be done by considering the point group symmetry character table for C_3 point group (Table 21): some transitions are stronger for OPA, while other are stronger for TPA. So, even if the peak wavelength should be in theory the same in OPA and TPA spectra, the bands don't have exactly the same shape because different transitions are favoured.

C_3	Linear functions	Quadratic functions
A	z, R_z	$x^2 + y^2, z^2$
E	(x,y), (R_x,R_y)	$(x^2 - y^2, xy)(yz, xz)$

Table 21. Character table for point group C_3.

So, to try to easily predict and explain the spectral shape of these compounds, we should basically consider both the two- and three-state models, with some relaxation. The first can be applied at longer wavelengths, while at short wavelengths the three-states model results more appropriate since it takes into account the detuning energy that justifies the resonance enhancement of the TPA cross-section.

TPA spectra of **Ir-1** and **Ir-3** are almost superimposable to the respective OPA spectra at half wavelength but the situation is different for **Ir-2** and **Ir-4**.

First of all, it should be considered that OPA spectra of **Ir-2** and **Ir-4** have very similar shapes, just the absorption of **Ir-4** is red shifted because of is more extended π-conjugation. Both TPA spectra are slightly blue shifted respect to the relative OPA spectra and also quite different between them. The spectrum of **Ir-4** presents a sharp outstanding peak centred at 780 nm with a shoulder at about 900 nm, while the spectrum of **Ir-2** presents an unexpectedly broad and structureless red-shifted band from 700 nm to 1000 nm. Also, the magnitude of the TPA cross section of **Ir-4** between 700 and 900 nm is of about 200 GM higher than **Ir-2**. This changes are noteworthy considering the similar structure of the two complexes: both complexes possess electron-donating groups of the same nature and in **Ir-4** π-conjugation is increased to a small extent respect to **Ir-2**. Nevertheless, this difference is still enough to achieve a quite large increase of σ_{TPA} and to change the energy of the excited states for the two complexes.
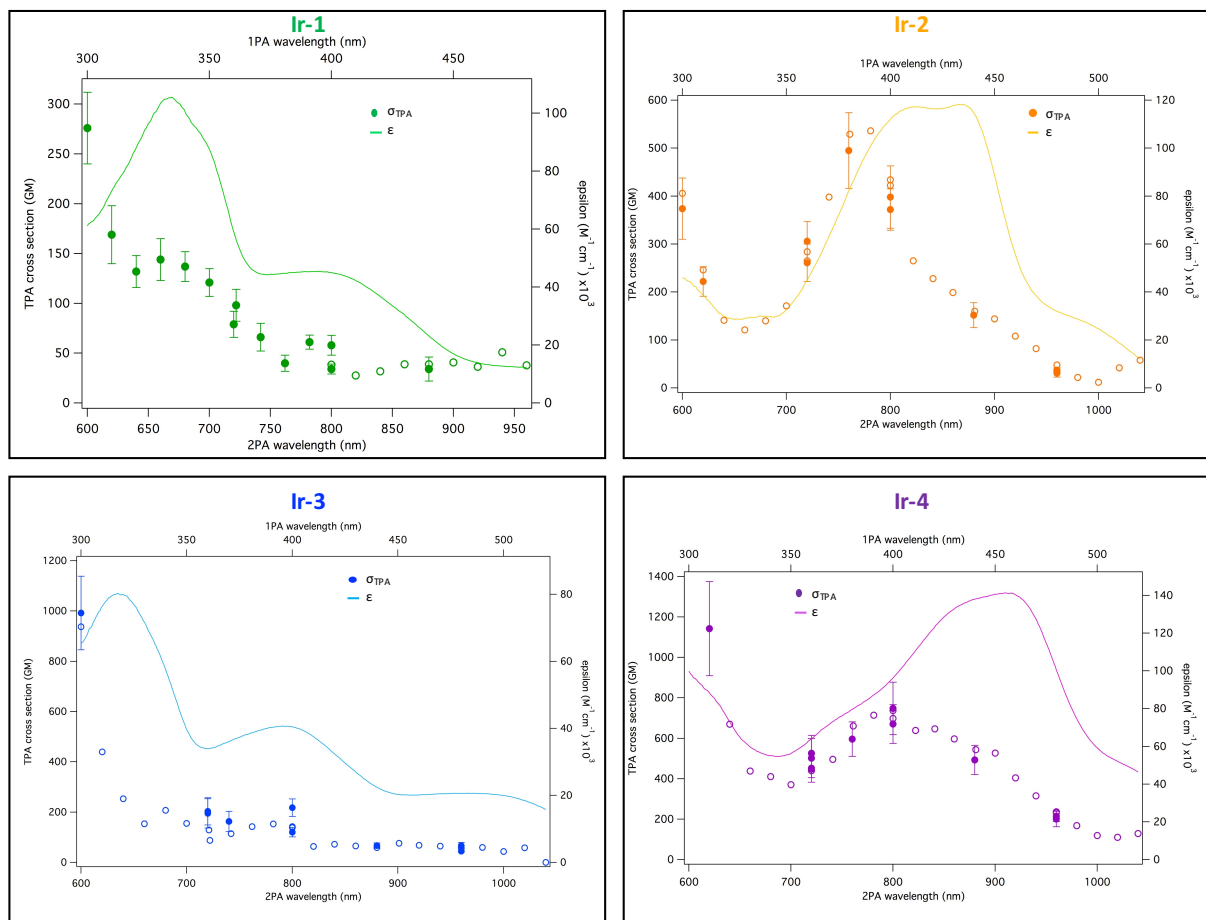
Figure 146. The one-photon absorption (plain line) and two-photon absorption (circles) spectra of the neutral Ir(ppy)$_3$ complexes: the empty circles are the values obtained with the wavelength scan at a fix power, while the full markers with error bars are the ones obtained with the power scan at a fixed wavelength.

Wavelength-scan measurements

Ir-1		Ir-2		Ir-3		Ir-4	
λ (nm)	σ_{TPA} (GM)	λ (nm)	σ_{TPA} (GM)	λ (nm)	σ_{TPA} (GM)	λ (nm)	σ_{TPA} (GM)
800	38	600	406	600	937	620	1367
820	28	620	246	620	439	640	670
840	32	640	141	640	253	660	438
860	39	660	121	660	153	680	410
880	39	680	140	680	207	700	370
900	41	700	171	700	155	720	448
920	36	720	265	721	129	720	440
940	51	720	284	722	86	741	496
960	38	741	398	742	113	761	661
		761	529	762	142	781	714
		781	536	782	154	800	698
		800	422	800	143	800	737
		800	434	800	138	822	639
		822	265	820	64	841	647
		841	228	840	72	860	597
		860	199	860	66	881	544
		881	160	880	59	900	527
		900	144	901	76	920	404
		920	108	920	68	940	315
		940	82	940	65	960	236
		960	48	960	59	960	231
		960	34	960	60	980	168
		980	22	980	60	1000	119
		1000	12	1000	44	1020	110
		1020	42	1020	59	1040	129
		1040	58				

Table 22. TPA cross-section values obtained with the wavelength-scan at fix power.

Power-scan measurements

Ir-1			Ir-2		
λ (nm)	σ_{TPA} (GM)	σ_{TPA} error (GM)	λ (nm)	σ_{TPA} (GM)	σ_{TPA} error (GM)
600	276	36	600	374	64
620	169	29	620	222	31
640	132	16	720	306	41
660	144	21	720	261	39
680	137	15	760	495	79
700	121	14	800	372	43
720	79	13	800	398	65
722	98	16	880	152	26
742	66	14	960	37	5
762	40	8	960	31	8
782	61	7			
800	58	10			
800	34	5			
880	34	12			
Ir-3			**Ir-4**		
λ (nm)	σ_{TPA} (GM)	σ_{TPA} error (GM)	λ (nm)	σ_{TPA} (GM)	σ_{TPA} error (GM)
600	992	146	620	1142	233
720	195	58	720	452	69
720	203	54	720	526	89
740	163	40	720	502	97
800	218	35	760	596	85
800	120	19	800	671	96
880	67	11	800	748	130
960	67	13	880	493	72
960	45	4	960	214	26
			960	201	38

Table 23. TPA cross-section values obtained with the power-scan at fix wavelength.

5.4.4. Two-photon absorption of the cationic iridium complex

The TPA spectrum of **Ir-5** has different characteristics respect to those of other iridium complexes (Figure 148, Table 24).[176] First, it was registered in DMSO, because of its low solubility in DCM, used for the other complexes. The degree of symmetry is diminished because two ligands are phenylpyridines, while one is a bipyridine: this increases the possibilities for OPA excited states to be allowed also for TPA transitions. In fact, the TPA spectra can be almost exactly superposed with the OPA spectra at half wavelength.

During the measures of sample **Ir-5** in dichloromethane another artefact caused by the solvent was observed (Figure 147). The shape of the Z-scan trace is sharper than if only TPA occurred, because of a sudden change in the normalized transmittance against the optical intensity, and deformed. Such behaviour cannot be explained by three-photon absorption, because the trace would be smooth even though narrower than the two-photon absorption trace. The irregular peak is due to stimulated Raman scattering of the solvent, *i.e.* the solvent itself absorbs photons and emits them in an inelastic way. This phenomenon tends to be observable when the signal from the solute molecule is weak because of small TPA activity or low concentration of the complex in solution. So, even though the Raman scattering efficiency of the solvent is low, the solvent molecules are in large excess respect to the solute molecules, leading to a significant observability of the effect. This is why the TPA spectrum of **Ir-5** was later measured in DMSO: the solubility of the sample is higher in this solvent and no solvent artefacts interfere.
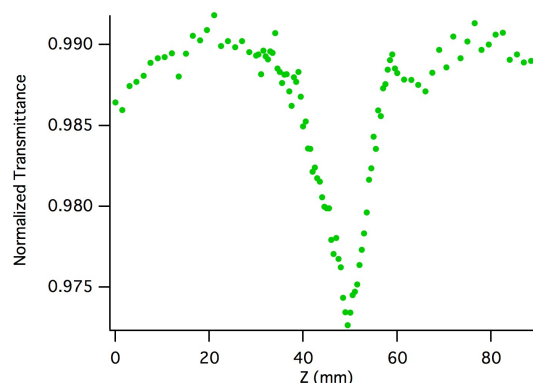
Figure 147. The Z-scan trace with solvent Raman scattering.

Remarkably, the TPA cross-sections are quite high, between 100-250 GM in the range 600-1000 nm, even though lower than the other two complexes with amine as substituents reported above (**Ir-2** and **Ir-4**). This effect could be due to the different charge distribution within the molecule, which does not belong to C_3 symmetry point group anymore.
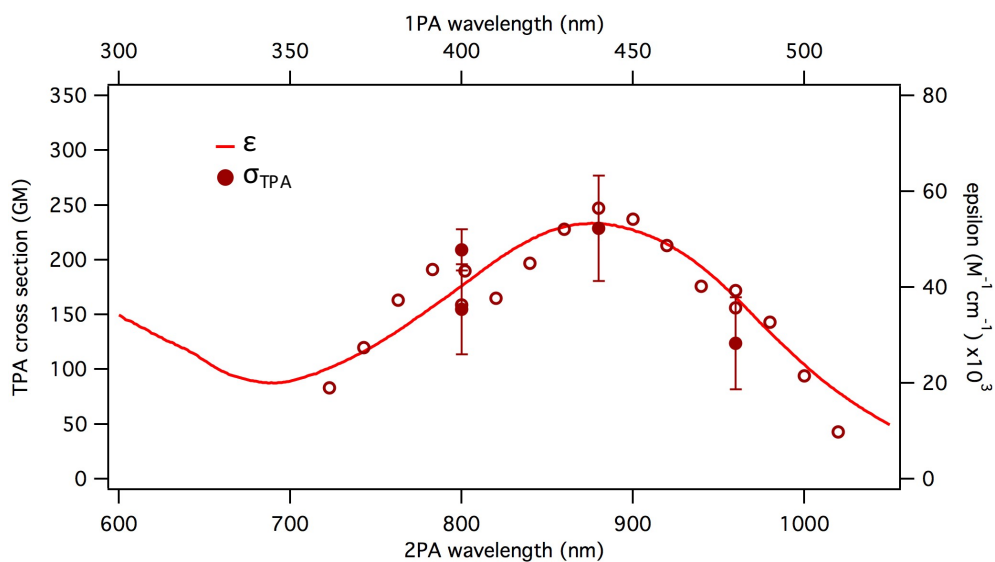
Figure 148. The one-photon absorption (plain line) and two-photon absorption (circles) spectra of **Ir-5**: the empty circles are the values obtained with the wavelength scan at a fix power, while the full markers with error bars are the ones obtained with the power scan at a fixed wavelength

Ir-5				
Wavelength scan		**Power-scan**		
λ (nm)	**σ_{TPA} (GM)**	**λ (nm)**	**σ_{TPA} (GM)**	**σ_{TPA} error (GM)**
722	96	800	209	19
742	104	800	155	41
762	179	880	229	48
783	191	960	124	42
800	159			
800	226			
802	190			
820	165			
840	197			
860	228			
880	247			
900	237			
920	213			
940	176			
960	172			
960	156			
980	143			
1000	94			
1020	43			

Table 24. TPA cross-section values obtained with the wavelength-scan at fix power (left) and TPA cross-section values obtained with the power-scan at fix wavelength (right).

Contrarily to previously reported TPA active cationic Ir^{III} complexes having two cyclometallated unsubstituted 2-phenylpyridines and a 2,2'-bipyridine bearing highly π-delocalized substituents,[381] **Ir-5** has less extended substituents on the bipyridine but it bears the same groups also on the 2-phenylpyridine ligands. In this way the π-conjugated system results more extended through all the molecule leading to good TPA properties.

5.4.5. Conclusion

In summary we studied the two-photon absorption activity of a series of neutral and cationic iridium(III) complexes with cyclometalated ligands.

The TPA activity of the neutral complexes is high on a wide range of wavelengths and better than that of the unsubstituted Ir(ppy)$_3$ complex reported in literature. They have good TPA cross-section values, comparable to the best results in literature. Furthermore, it should be considered that this high activity is reached with relatively small molecules with simple substituents. This demonstrates that an accurate molecular design is decisive in managing to enhance the third-order NLO properties of such compounds. The highest σ_{TPA} values were measured for complex **Ir-4**, as expected, which bears the most electron-donating substituents and has the most extended π-conjugated system.

Ir-5 also has a very good TPA activity, higher than that of reported compounds of the same class. Similarly to them, it could find application in biomedical research.

III. EXPERIMENTAL SECTION

1. General comments

Solvents and reagents:

Commercial products were purchased from Alfa Aesar, Acros and Sigma Aldrich and were used without further purification. All reactions were carried out using standard Schlenk techniques under inert (Ar) atmosphere with reagent-grade solvents. Anhydrous CH_2Cl_2, Et_2O and toluene were obtained from a MB SPS-800 M-Braun solvent purification system (Innovative Technologies). Triethylamine, diisopropylamine and pyridine were distilled over CaH_2, THF over sodium/benzophenone under argon using standard procedures. Column chromatography was performed using silica gel (Silica-P from Silicycle, 60 Å, 40-63 μm).

Nuclear Magnetic Resonance

NMR spectra were recorded on a Brucker AVANCE III 400 MHz spectrometer (400 MHz for H and 101 MHz for C, 376.5 MHz for F) or a Brucker AVANCE I 500 MHz spectrometer (500 MHz for H and 126 MHz for C). Chemicals shifts are given in ppm (part per million) and relative to the residual solvent peaks ($CHCl_3$ or CH_2Cl_2) for H and C NMR.

Elemental analysis and mass spectrometry

Measurements performed in Rennes: Elemental analysis was performed in the laboratory of CNRS for microanalysis in CRMPO (Centre régional de mesures physiques de l'Ouest). High resolution mass spectra (HRMS) were recorded on a ZabSpec TOF (LSIMS at 4 kV) spectrometer Bruker MicroTof-Q II in CRMPO.

Measurements performed in Milan: Mass spectra were obtained with a FT-ICR Mass Spectrometer APEX II & Xmass software (Cruker Daltonics) - 4.7 Magnet and Autospec Fission Spectrometer (Fast Atom Bombardment - FAB - ionisation).

X-ray diffraction

Data were collected at 150 K in a D8 VENTURE Bruker AXS diffractometer with Mo-Kα radiation (λ = 0.71073 Å).

UV-Visible spectroscopy

Measurements performed in Rennes: UV-Vis absorption spectra were recorded in pure CH_2Cl_2, CH_3CN, THF, or DMSO using Specord 205 UV-Vis-NIR spectrophotometer in quartz cuvettes of 1 cm pathlength, against a reference of, respectively, pure CH_2Cl_2, CH_3CN, THF, or DMSO contained within a matched cuvette. Molar absorptivity determination was verified by linear least-squares fit of values obtained from independent solutions at varying concentrations ranging from 10^{-4} to 10^{-5} M.

Measurements performed in Milan: UV-Vis absorption spectra were recorded in pure CH_2Cl_2 with JASCO V530 spectrometer in quartz cuvettes of 1 cm pathlength, against a reference of pure CH_2Cl_2

contained within a matched cuvette. Molar absorptivity determination was verified by linear least-squares fit of values obtained from independent solutions at varying concentrations ranging from 10^{-4} to 10^{-5} M.

UV-Visible irradiation

UV-Vis irradiation in CH_2Cl_2 solution was performed with a LS series Light Source of ABET technologies, Inc (150W xenon lamp), with single wavelength light filters '350FS 10-25" and "450FS 20−25" for cyclization, and "580FS 40-25" for photocycloreversion.

Photophysical measurements

The sample solutions for the emission spectra were prepared in HPLC grade solvents (CH_2Cl_2, THF, CH_3CN, DMSO) and degassed via three freeze-pump-thaw cycles using an in-house designed quartz cuvette. Steady-state luminescence spectra were measured using an Edinburgh FS920 Steady State Fluorimeter combined with a FL920 Fluorescence Lifetime Spectrometer. All samples for steady-state measurements were excited at 400, 440, or 460 nm depending on the compound. The spectra were corrected for the wavelength dependence of the detector, and the quoted emission maxima refer to the values after correction. Luminescence quantum yields were determined using $[Ru(bpy)_3]Cl_2$ ($\Phi = 0.028$ in air-equilibrated aqueous solution)[384] as standard. Life-times measurements were conducted with 375 nm diode laser excitation (EPL-series).

EFISH measurements

All EFISH measurements[385] were carried out at the Dipartimento di Chimica of the Università degli Studi di Milano, in DMF (Pt complexes) solutions at a concentration of 1 x 10^{-3} M, working with a non-resonant incident wavelength of 1.907 μm, obtained by Raman-shifting the fundamental 1.064 μm wavelength produced by a Q-switched, mode-locked Nd^{3+}:YAG laser manufactured by Atalaser. The apparatus for the EFISH measurements is a prototype made by SOPRA (France). The $\mu\beta_{EFISH}$ values reported are the mean values of 16 successive measurements performed on the same sample. The sign of μ is determined by comparison with the reference solvent (DMF or CH_2Cl_2).

2. Synthesis of the Platinum (II) complexes

2.1. General synthetic methods

Diethyl 3,5-dibromobenzylphosphonate was prepared according to the literature[386]. Stille couplings were performed following a reported procedure[387], using 2-(tri-*n*-butylstannyl)pyridine freshly prepared according to the literature[388]. Compounds **1**,[389] **1-azulenecarboxaldehyde**,[390] **19**,[391] **22**,[392] **Pt-8** and its precursors were prepared according to the literature.[393] Pt(dpyb)Cl[394] and 4,4'-(tetraethylene glycol)bis(ethynylbenzene)[395] used as precursor for the synthesis of **Pt$_2$(dpyb)$_2$(C≡Cteg)**, were prepared as reported. Compounds **33**,[58,396] **39**,[397] **44**,[149] **45**[32] and their precursors were prepared following a reported procedure. Sonogashira couplings were performed as previously reported.[398] Platinum complexes, except for **Pt-8**, were synthesized by reaction of K$_2$PtCl$_4$ with the corresponding ligands, in acetic acid heated at reflux, as previously described for other Pt(dpyb) complexes.[397]

General Horner-Wadsworth-Emmons procedure (I)

The chosen aromatic aldehyde and diethyl 3,5-dibromobenzylphosphonate were dissolved in THF under Ar atmosphere at 0°C. *t*-BuOK was added in small portions to the solution over 20 minutes, keeping the mixture under stirring. The mixture was then allowed to warm gradually at room temperature and stirred overnight. Afterwards, H$_2$O was added causing the formation of a precipitate and the mixture was stirred for 30 minutes. The solvent was partially removed under reduced pressure, the residue was extracted into CH$_2$Cl$_2$, the organic layer was dried over MgSO$_4$ and removed under reduced pressure. The crude product was purified by flash chromatography.

General procedure for Stille coupling (II)

A mixture of the bromo derivative, the tri-*n*-butylstannyl derivative, PdCl$_2$(PPh$_3$)$_2$ and LiCl was suspended in toluene and heated at reflux under argon atmosphere for 48 hours. After cooling to room temperature, an aqueous solution of NaOH 1 M was added. The resulting solution was extracted with AcOEt and the organic layer was dried over MgSO$_4$ and removed under reduced pressure.

General procedure for the synthesis of a 2-(tri-*n*-butylstannyl)thiophene derivative (III)

A solution of the aromatic thiophene derivative in THF was placed in a dried two-necked-round-bottomed flask under argon atmosphere. The mixture was cooled to -50°C and degassed, *n*-BuLi was added, then the mixture was allowed to warm gradually at -10°C and stirred for 30 minutes. The mixture was cooled to -40°C, *n*-Bu$_3$SnCl was added, then the mixture was allowed to warm gradually at room temperature and stirred overnight. H$_2$O was added to quench the reaction, the mixture was stirred for 15 minutes and extracted into Et$_2$O. The organic layer was dried over MgSO$_4$, filtered and the solvent was removed under reduced pressure. ^{1}H-NMR was used to assess the purity of the stannane, and the crude product was used directly for the following Stille coupling.

2.2. Synthesis of the mononuclear Pt(dpyb)Cl complexes Pt-1 to Pt-8
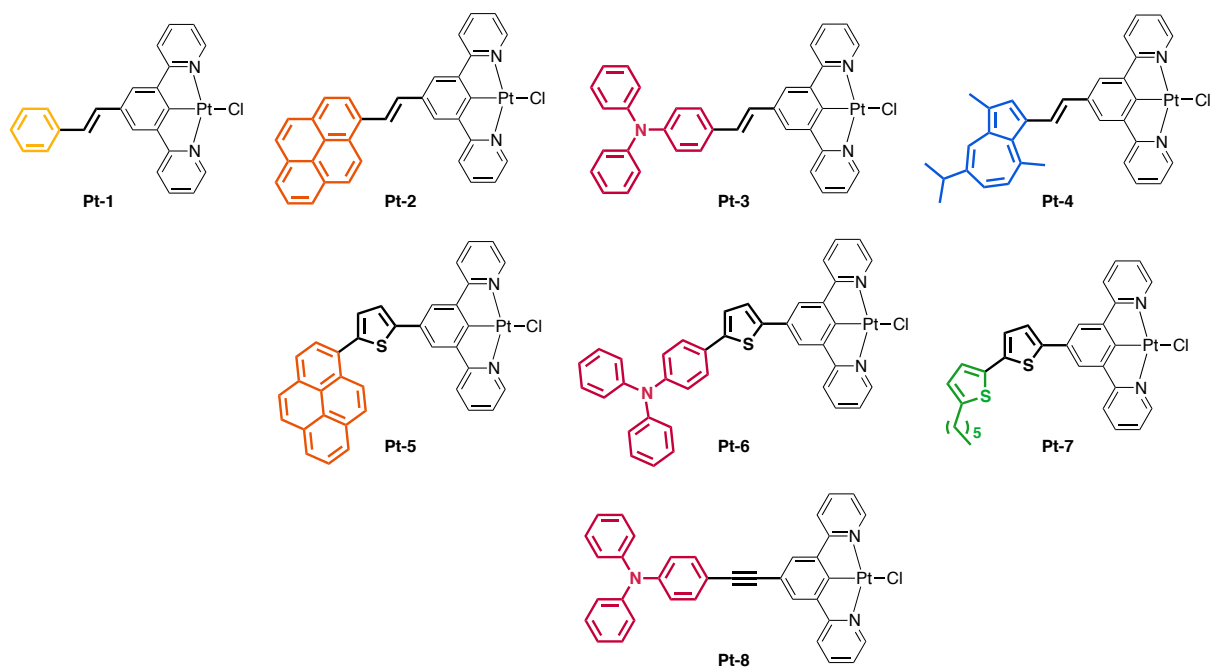
Figure 149. The Pt(dpyb)Cl complexes for NLO.

2.2.1. Synthesis of Pt-1
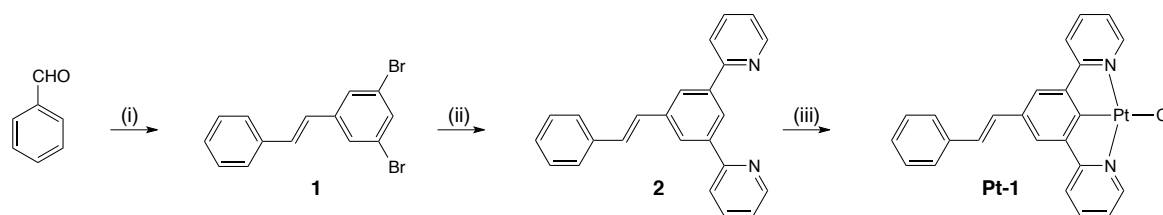
Scheme 1. Reagents and conditions: (i) Diethyl 3,5-dibromobenzylphosphonate, *t*-BuOK, THF, Ar, 0°C, then rt, 15 h; (ii) 2-(tri-*n*-butylstannyl)pyridine, LiCl, PdCl$_2$(PPh$_3$)$_2$, toluene, 110°C, 48 h; (iii) K$_2$PtCl$_4$, AcOH, 118°C, 48 h.

1. Procedure (I). Reactants: Diethyl 3,5-dibromobenzylphosphonate (698 mg, 1.80 mmol), benzaldehyde (230 mg, 2.10 mmol), *t*-BuOK (808 mg, 72 mmol). Solvents: THF (20 mL). Purification: The crude product was purified by flash chromatography (silica, hexane:CH$_2$Cl$_2$, 7:3). The pure compound was obtained as yellow solid (412 mg). **Yield:** 58%. **^{1}H-NMR** (400 MHz, CDCl$_3$) δ (ppm): 7.56 (2H, d, *J* = 1.6 Hz), 7.53 (1H, t, *J* = 1.7 Hz), 6.49 (2H, d, *J* = 8.0 Hz), 7.38 (2H, t, *J* = 7.8 Hz), 7.30 (1H, m), 7.09 (1H, d, *J* = 16.2 Hz), 6.92 (1H, d, *J* = 16.2 Hz). **^{13}C-NMR** (101 MHz, CDCl$_3$) δ (ppm): 141.0, 136.3, 132.6, 131.5, 128.8, 128.4, 128.8, 126.8, 125.6, 123.2.

2. Procedure (II). Reactants: **1** (410 mg, 1.06 mmol), 2-(tri-*n*-butylstannyl)pyridine (858 mg, 2.33 mmol), PdCl$_2$(PPh$_3$)$_2$ (37 mg, 0.05 mmol), LiCl (360 mg, 8.48 mmol). Solvents: Toluene (10 mL). Purification: The crude product was purified by flash chromatography (silica, petroleum ether/Et$_2$O, 1:1). The desired product was obtained as a white solid (160 mg). **Yield:** 45%. **^{1}H NMR** (400 MHz, CD$_2$Cl$_2$) δ (ppm): 8.76 (2H, d, *J* = 4.2 Hz), 8.51 (1H, s), 8.26 (2H, s), 7.89 (2H, d, *J* = 7.8 Hz), 7.80 (2H, t, *J* = 7.6 Hz), 7.58 (2H, d, *J* = 7.4 Hz), 7.40, (2H, t, *J* = 7.5 Hz), 7.29 (5H, m). **^{13}C-NMR** (101 MHz, CD$_2$Cl$_2$) δ (ppm): 157.1, 149.7, 140.3, 138.5, 137.3, 136.8, 129.6, 128.8, 128.4, 127.8, 126.6, 125.7, 124.7, 122.4, 120.8. **Elem. Anal.** calcd for C$_{24}$H$_{18}$N$_2$: C, 86.20; H, 5.43; N, 8.38. Found: C, 84.30; H, 5.45; N, 7.99.

Pt-1. Compound **2** (100 mg, 0.30 mmol) was dissolved in acetic acid (5 ml). The solution was degassed through freeze-pump-thaw cycles. K$_2$PtCl$_4$ (149 mg, 0.36 mmol) was added and the mixture was heated at reflux for 2 days. A yellow precipitate formed: it was filtered, washed with MeOH, H$_2$O, EtOH and Et$_2$O and dried under vacuum to obtain pure **5** as a yellow powder (130 mg). **Yield:** 77%. **^{1}H-NMR** (400 MHz, CD$_2$Cl$_2$) δ (ppm): 9.33 (2H, dt, *J* = 16.1 Hz, 6.6 Hz), 8.05 (2H, t, *J* = 7.7 Hz), 7.71 (2H, s), 7.62 (2H, d, *J* = 7.9 Hz), 7.36 (8H, m), 7.21 (1H, d, *J* =16.2 Hz). **Elem. Anal.** calcd for C$_{24}$H$_{17}$ClN$_2$Pt: C, 51.11; H, 3.04; N, 4.97. Found: C, 51.04; H, 2.90; N, 4.55. **MS (FAB$^+$), calculated:** (C$_{24}$H$_{17}$N$_2$Pt): m/z 528.10 [M-Cl]. **Found:** m/z 528 [M-Cl].

2.2.2. Synthesis of Pt-2

Scheme 2. Reagents and conditions: (i) Diethyl 3,5-dibromobenzylphosphonate, *t*-BuOK, THF, Ar, 0°C, then rt, 15 h; (ii) 2-(tri-*n*-butylstannyl)pyridine, LiCl, PdCl$_2$(PPh$_3$)$_2$, toluene, 110°C, 48 h; (iii) K$_2$PtCl$_4$, CH$_3$CN/H$_2$O, 90°C, 24 h.

3. Procedure (I). Reactants: Diethyl 3,5-dibromobenzylphosphonate (320 mg, 0.83 mmol), 1-pyrenecarboxaldehyde (173 mg, 0.75 mmol), *t*-BuOK (222 mg, 1.96 mmol). Solvents: THF (7.5 mL). Purification: The crude product was purified by flash chromatography (silica, hexane:CH$_2$Cl$_2$, 7:3). The pure compound was obtained as yellow solid (284 mg). **Yield:** 92%. **¹H-NMR** (400 MHz, CDCl$_3$) δ (ppm): 8.47 (1H, d, J = 9.2 Hz), 8.27 (1H, d, *J* = 8 Hz), 8.19 (4H, m), 8.10-8.00 (3H, m), 7.74 (2H, d, *J* = 1.6 Hz), 7.60 (2H, t, *J* = 1.6 Hz), 7.18 (1H, d, *J* = 16 Hz). **¹³C-NMR** (101 MHz, CDCl$_3$) δ (ppm): 141.5, 132.9, 131.6, 130.9, 130.7, 128.7, 128.4, 128.1, 127.9, 127.5, 126.3, 125.7, 125.5, 125.3, 125.1, 124.9, 123.8, 123.5, 122.9.

4. Procedure (II). Reactants: **3** (164 mg, 0.36 mmol), 2-(tri-*n*-butylstannyl)pyridine (359 μL, 0.90 mmol), PdCl$_2$(PPh$_3$)$_2$ (13 mg, 0.02 mmol), LiCl (136 mg, 3.24 mmol). Solvents: Toluene (4 mL). Purification: The crude product was purified by flash chromatography (silica, hexane:CH$_2$Cl$_2$, 1:9 to 2:8). The desired product was obtained as a yellow solid (101 mg). **Yield:** 60%. **¹H-NMR** (400 MHz, CDCl$_3$) δ (ppm): 8.56 (1H, d, *J* = 9.3 Hz), 8.38 (1H, d, *J* = 8.01 Hz), 8.31 (1H, d, *J* = 16.1 Hz), 8.22 (3H, d, *J* = 8.01 Hz), 8.19 (1H, d, *J* = 9.3 Hz), 8.13 (3H, s), 8.04 (2H, t, *J* = 7.6 Hz), 7.85 (2H, s), 7.82 (1H, s), 7.49 (2H, d, *J* = 3.6 Hz), 7.43 (1H, d, *J* = 16.1 Hz), 7.39 (2H, d, *J* = 4.3 Hz), 7.17 (2H, t, *J* = 3.6 Hz). **Elem. Anal**. Calcd for C$_{34}$H$_{22}$N$_2$: C, 89.06; H, 4.84; N, 6.11. **Found:** C, 89.01; H, 4.87; N, 6.00.

Pt-2. Compound **4** (170 mg, 0.36 mmol) was dissolved in acetonitrile (5 mL), and an aqueous solution of K$_2$PtCl$_4$ (165 mg, 0.40 mmol, in 5 mL water) was added. The solution was degassed through freeze-pump-thaw cycles. The mixture was heated at reflux under argon for 2 days. A precipitate formed: it was filtered, washed with H$_2$O, MeOH, EtOH and Et$_2$O and dried in vacuo. The desired product was obtained as a yellow solid (80 mg). **Yield:** 32%. **¹H-NMR** (400 MHz, CD$_2$Cl$_2$) δ (ppm): 8.78 (2H, m), 8.56 (1H, t, *J* = 1.6 Hz), 8.42 (3H, m), 8.35 (1H, d, *J* = 8.4 Hz), 8.18 (4H, m), 8.07 (2H, s), 8.01 (3H, m), 7.86 (2H, dt, *J* = 7.6 Hz, 2 Hz), 7.51 (1H, d, *J* = 16 Hz), 7.32 (1H, dd, *J* = 1.2 Hz, 4.8 Hz), 7.32 (1H, dd, *J* = 0.8 Hz, 4.8 Hz). **¹³C-NMR** (101 MHz, CD$_2$Cl$_2$) δ (ppm): 156.7, 149.1, 139.7, 139.2, 137.8, 131.9, 131.6, 131.3, 131.1, 128.7, 127.8, 127.8, 127.6, 127.5, 127.1, 126.4, 126.1, 125.4, 125.3, 125.2, 123.9, 123.5, 122.8, 121.5. **Elem. Anal**. Calcd for C$_{34}$H$_{21}$ClN$_2$Pt: C, 59.35; H, 3.08; N, 4.07. **Found:** C, 59.64; H, 3.10; N, 4.05.
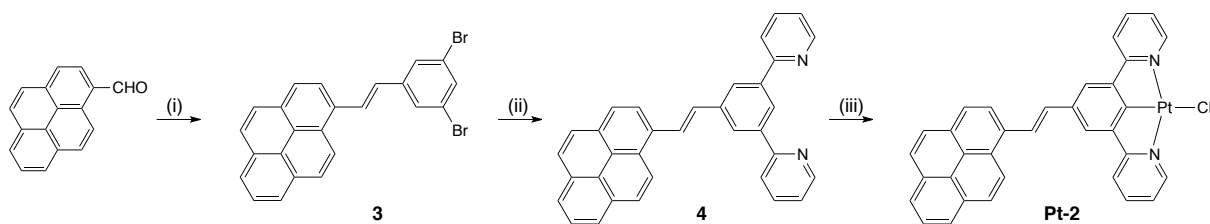
2.2.3. Synthesis of Pt-3

Scheme 3. Reagents and conditions: (i) Diethyl 3,5-dibromobenzylphosphonate, *t*-BuOK, THF, Ar, 0°C, then rt, 15 h; (ii) 2-(tri-*n*-butylstannyl)pyridine, LiCl, PdCl$_2$(PPh$_3$)$_2$, toluene, 110°C, 48 h; (iii) K$_2$PtCl$_4$, AcOH/H$_2$O, 118°C, 48 h.

5. Procedure (I). Reactants: 3,5-dibromobenzylphosphonate (320 mg, 0.83 mmol), 4-(diphenylamino)benzaldehyde (305 mg, 1.10 mmol), *t*-BuOK (323 mg, 2.87 mmol). Solvents: THF (9 mL). Purification: The crude product was purified by flash chromatography (silica, hexane:CH$_2$Cl$_2$, 8:2). The desired product was obtained as a pale yellow solid (444 mg). **Yield:** 88%. **^{1}H-NMR** (400 MHz, CDCl$_3$) δ (ppm): 7.56 (2H, d, *J* = 1.6Hz), 7.52 (1H, t, *J* = 1.6Hz), 7.37 (2H, d, *J* = 8.8Hz), 7.31 (4H, m), 7.14 (4H, d, *J* = 7.6 Hz), 7.07 (5H, m), 6.83 (1H, d, *J* = 16 Hz). **^{13}C-NMR** (101 MHz, CDCl$_3$) δ (ppm): 148.3, 147.4, 141.5, 132.3, 131.1, 130.1, 129.4, 127.9, 127.8, 127.6, 124.7, 123.7, 123.5, 123.3, 123.1.

6. Procedure (II). Reactants: **5** (304 mg, 0.60 mmol), 2-(tri-*n*-butylstannyl)pyridine (427 μL, 1.32 mmol), PdCl$_2$(PPh$_3$)$_2$ (25 mg, 0.03 mmol), LiCl (453 mg, 10.8 mmol). Solvents: Toluene (7.5 mL). Purification: The crude product was purified by flash chromatography (silica, hexane:AcOEt, 8:2). The desired product was obtained as a yellow solid (69 mg). **Yield:** 23%. **^{1}H-NMR** (400 MHz, CDCl$_3$) δ (ppm): 8.76 (2H, d, *J* = 4.8 Hz), 8.46 (1H, s), 8.23 (2H, s), 7.92 (2H, d, *J* = 7.6 Hz), 7.83 (2H, dt, *J* = 7.6 Hz, 3.6 Hz), 7.43 (2H, d, *J* = 8.4 Hz), 7.29 (7H, m), 7.15 (5H, m), 7.06 (4H, m). **^{13}C-NMR** (101 MHz, CDCl$_3$) δ (ppm): 156.9, 149.4, 147.5, 139.9, 138.9, 137.2, 131.3, 129.3, 129.2, 127.5, 126.4, 125.6, 124.6, 124.4, 123.4, 123.1, 122.5, 121.1. **Elem. Anal. Calcd** for C$_{36}$H$_{27}$N$_3$: C, 86.20; H, 5.43; N, 8.38. **Found:** C, 86.23; H, 5.41; N, 8.35.

Pt-3. Compound **6** (130 mg, 0.26 mmol) and K$_2$PtCl$_4$ (108 mg, 0.26 mmol) were dissolved in a mixture of AcOH/H$_2$O 9:1 (3 mL). The solution was degassed through freeze-pump-thaw cycles. The mixture was heated at reflux under argon for 2 days. A precipitate formed: it was filtered, washed with H$_2$O, MeOH, EtOH and Et$_2$O and dried in vacuo. The desired product was obtained as a yellow solid (90 mg). **Yield:** 47%. **^{1}H-NMR** (400 MHz, CD$_2$Cl$_2$) δ (ppm): 9.31 (2H, dd, *J* = 4.2 Hz, 2.2 Hz), 8.03 (2H, t, *J* = 7.6 Hz), 7.82 (2H, d, *J* = 7.6 Hz), 7.67 (2H, s), 7.49 (2H, d, *J* = 8.8 Hz), 7.33 (6H, m), 7.23 (1H, d, *J* = 16.4 Hz), 7.12 (9H, m). **^{13}C-NMR** (101 MHz, CDCl$_3$) δ (ppm): 152.6, 139.9, 129.9, 127.7, 125.1, 124.1, 123.7, 122.6, 120.1. **Elem. Anal. Calcd** for C$_{36}$H$_{26}$ClN$_3$Pt: C, 59.14; H, 3.58; N, 5.75. **Found:** C, 59.08; H, 3.57; N, 5.83.
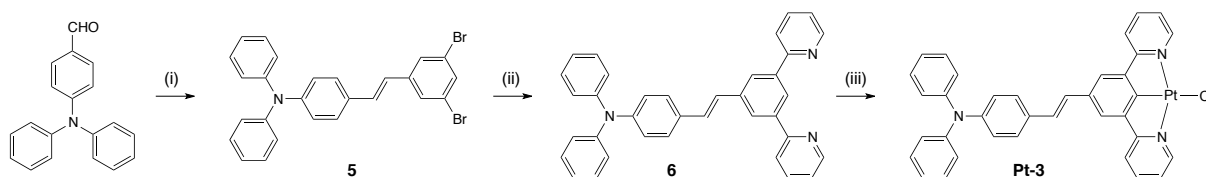
2.2.4. Synthesis of Pt-4
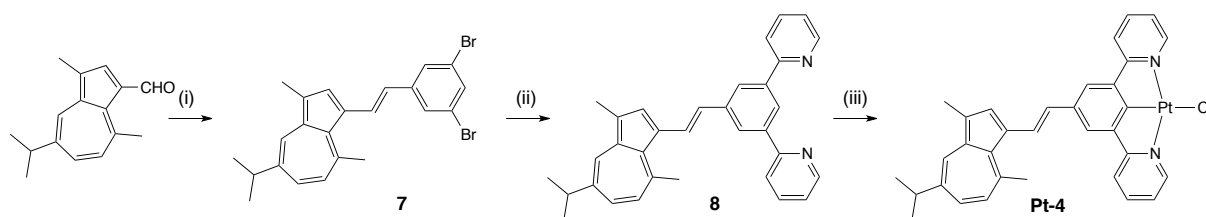
Scheme 4. Reagents and conditions: (i) Diethyl 3,5-dibromobenzylphosphonate, *t*-BuOK, THF, Ar, 0°C, then rt, 15 h; (ii) 2-(tri-*n*-butylstannyl)pyridine, LiCl, PdCl$_2$(PPh$_3$)$_2$, toluene, 110°C, 48 h; (iii) K$_2$PtCl$_4$, AcOH/H$_2$O, 118°C, 48 h.

1-azulenecarboxaldehyde. Guaiazulene (500 mg, 3.16 mmol) and DMF (5 mL) were degssed in a two-necked-round-bottomed flask, then a mixture of phosphoryl chloride (324 µL, 3.47 mmol) in DMF (1 mL) was slowly added. A brownish solid formed. After stirring for 5 minutes at room temperature, the mixture was heated at 80°C for 20 minutes, until the solid dissolved. NaOH 1.25 M (20 mL) was added to break the aggregate. Purification: The mixture was extracted into CH$_2$Cl$_2$, the organic layer was dried over Na$_2$SO$_4$, filtered and the solvent removed under reduced pressure. The crude product was purified by flash chromatography (silica, hexane:Et$_2$O, 6:4 to 1:1). The desired product was obtained as a blue oil (430 mg). **Yield:** 60% yield. **^{1}H-NMR** (400 MHz, CDCl$_3$) δ (ppm): 10.65 (1H, s), 8.31 (1H, d, J = 2 Hz), 8.24 (1H, s), 7.60 (1H, dd, J = 2 Hz, 10.8 Hz), 7.43 (1H, d, J = 10.8 Hz), 3.19 (1H, d, J = 6.9 Hz), 3.17 (3H, s), 2.60 (3H, s), 1.41 (6H, d, J = 6.9 Hz)

7. Procedure (I). Reactants: guaiazulene-1-carboxaldehyde (453 mg, 1.17 mmol), 22 (240 mg, 1.07 mmol), t-BuOK (315 mg, 2.78 mmol). Solvents: THF (10 mL). Purification: Column chromatography (silica, hexane:CH$_2$Cl$_2$, 6:4). The desired product was obtained as a bluish green laque (115 mg). **Yield:** 23%. **^{1}H-NMR** (400 MHz, CDCl$_3$) δ (ppm): 8.07 (1H, d, J = 1.7 Hz), 8.01 (1H, d, J = 15.7 Hz), 7.88 (1H, s), 7.53 (1H, s), 7.50 (1H, d, J = 11.4 Hz), 7.30 (2H, m), 6.93 (1H, d, J = 10.6 Hz), 6.69 (1H, d, J = 15.7 Hz), 3.05 (4H, m), 2.65 (3H, m), 1.39 (6H, d, J = 6.9 Hz).

8. Procedure (II). Reactants: **7** (115 mg, 0.25 mmol), 2-(tri-*n*-butylstannyl)pyridine (237 µL, 0.63 mmol), PdCl$_2$(PPh$_3$)$_2$ (57 mg, 0.08 mmol), LiCl (95 mg, 2.25 mmol). Solvents: Toluene (3 mL). Purification: The crude product was purified by flash chromatography (silica, hexane:AcOEt, 2:8 to 7:3). The desired product was obtained as a green laque 64 mg. **Yield:** 56%. **^{1}H-NMR** (400 MHz, CDCl$_3$) δ (ppm): 8.70 (2H, m), 8.41 (2H, m), 8.21 (2H, m), 8.03 (1H, m), 7.97 (3H, m), 7.80 (3H, m), 7.28 (2H, m), 7.11 (1H, d, J = 15.8 Hz), 6.88 (1H, d, J = 10.9 Hz), 3.10 (3H, s), 3.02 (1H, d, J = 6.8 Hz), 2.65 (3H, s), 1.36 (6H, d, J = 6.8 Hz). **Elem. Anal. Calcd** for C$_{33}$H$_{30}$N$_2$: C, 87.19; H, 6.65; N, 6.16. **Found:** C, 87.21; H, 6.64; N, 6.18.

Pt-4. Compound **8** (23 mg, 0.05 mmol) and K$_2$PtCl$_4$ (19 mg, 0.05 mmol) were dissolved in a mixture of AcOH/H$_2$O 9:1 (1 mL). The mixture was degassed through freeze-pump-thaw cycles and heated at reflux under argon for 2 days. A precipitate formed: it was filtered, washed with H$_2$O, MeOH, EtOH

and Et$_2$O and dried in vacuo. The desired product was obtained as a dark green solid (25 mg). **Yield:** 74%. **^{1}H-NMR** (400 MHz, CD$_2$Cl$_2$) δ (ppm): 9.83 (1H, d, J = 5.9 Hz), 9.30 (1H, d, J = 5.6 Hz), 8.22 (2H, t, J = 7.6 Hz), 8.02 (4H, m), 7.77 (2H, m), 7.69 (2H, t, J = 6.9 Hz), 7.41 (2H, s), 7.35 (2H, d, J = 5.5 Hz), 3.10 (3H, s), 3.02 (1H, d, J = 6.8 Hz), 2.65 (3H, s), 1.36 (6H, d, J = 6.8 Hz). **Elem. Anal. Calcd** for C$_{33}$H$_{29}$ClN$_2$Pt: C, 57.94; H, 4.27; N, 4.09. **Found:** C, 57.97; H, 4.28; N, 4.13.

2.2.5. Synthesis of Pt-5
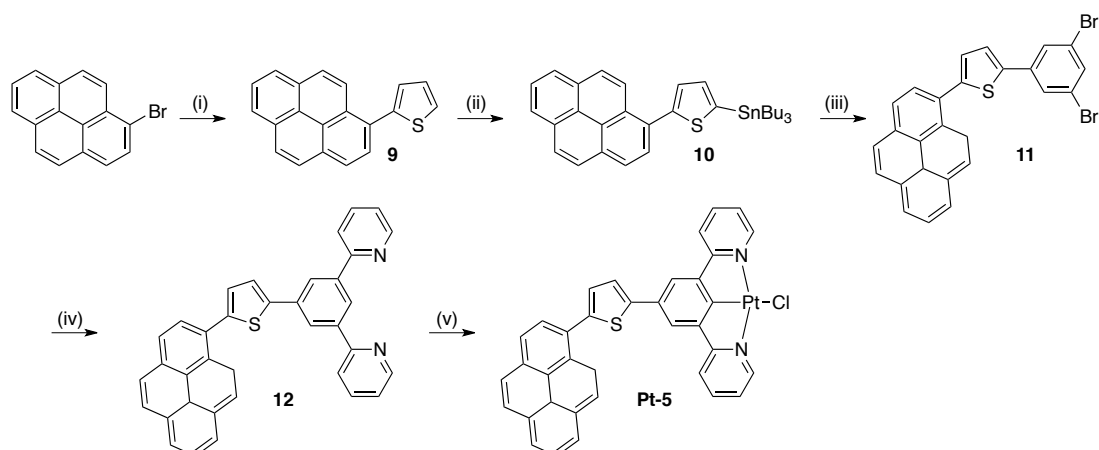
Scheme 5. Reagents and conditions: (i) 2-(tri-*n*-butylstannyl)thiophene, Pd(PPh$_3$)$_4$, toluene, 110°C, 24 h; (ii) *n*-BuLi, *n*-Bu$_3$SnCl, THF, Ar, -50°C to rt, 15 h; (iii) 1,3,5-tribromobenzene, Pd(PPh$_3$)$_4$, toluene, 110°C, 4 days; (iv) 2-(tri-*n*-butylstannyl)pyridine, LiCl, PdCl$_2$(PPh$_3$)$_2$, toluene, 110°C, 48 h; (v) K$_2$PtCl$_4$, AcOH/H$_2$O, 118°C, 48 h.

9. Procedure (II). Reactants: 1-bromopyrene (200 mg, 0.71 mmol), 2-(tri-*n*-butylstannyl)thiophene (339 μL, 1.07 mmol), Pd(PPh$_3$)$_4$ (41 mg, 0.035 mmol). Solvents: Toluene (10 mL), reflux 24 hours. Purification: The crude product was purified by flash chromatography (silica, hexane:CH$_2$Cl$_2$, 1:9 to 7:3). The desired product was obtained as a yellow laque (176 mg). **Yield:** quantitative. **¹H-NMR** (400 MHz, CDCl$_3$) δ (ppm): 8.60 (1H, d, *J* = 9.2 Hz), 8.20 (4H, m), 8.08 (4H, m), 7.61(1H, d, *J* = 5.1 Hz), 7.48 (1H, d, *J* = 3.4 Hz), 7.28 (1H, t, *J* = 5.1 Hz).

10. Procedure (III). Reactants: **9** (176 mg, 0.71 mmol), *n*-BuLi 1.6M (530 μL, 0.85 mmol), *n*-Bu$_3$SnCl (229 μL, 0.85 mmol). Solvents: THF (14 mL). The desired product was obtained as a brownish oil (407 mg). **Yield:** quantitative. **¹H-NMR** (400 MHz, CDCl$_3$) δ (ppm): 8.69 (1H, d, *J* = 9.3 Hz), 8.23 (1H, d, *J* = 7.9 Hz), 8.17 (3H, d, *J* = 7.8 Hz), 8.10 (1H, d, *J* = 9.3Hz), 8.05 (2H, s), 8.01(1H, t, *J* = 7.6 Hz), 7.64 (1H, d, *J* = 3.1 Hz), 7.47 (1H, d, *J* = 3.1 Hz), 1.84 (6H, m), 1.58 (6H, m), 1.36 (6H, m), 1.12 (9H, m).

11. Procedure (II). Reactants: **10** (407 mg, 0.71 mmol), 1,3,5-tribromobenzene (302 mg, 0.47 mmol), Pd(PPh$_3$)$_4$ (28 mg, 0.024 mmol). Solvents: Toluene (10 mL), reflux for 4 days. Purification: The crude product was purified by flash chromatography (silica, hexane:CH$_2$Cl$_2$, 1:9). The desired product was obtained as a yellow laque (74 mg). **Yield:** 20%. **¹H-NMR** (400 MHz, CDCl$_3$) δ (ppm): 8.57 (1H, m), 8.23 (3H, m), 8.13 (5H, m), 8.06 (1H, t, *J* = 7.5 Hz), 7.80 (1H, d, *J* = 1.3Hz), 7.63 (1H, d, *J* = 4.0 Hz), 7.48 (1H, d, *J* = 3.6 Hz), 7.38 (1H, d, *J* = 3.5 Hz).

12. Procedure (II). Reactants: **11** (74 mg, 0.14 mmol), 2-(tri-*n*-butylstannyl)pyridine (133 μL, 0.35 mmol), PdCl$_2$(PPh$_3$)$_2$ (29 mg, 0.04 mmol), LiCl (53 mg, 1.26 mmol). Solvents: Toluene (5 mL). Purification: The crude product was purified by flash chromatography (silica, AcOEt:CH$_2$Cl$_2$, 1:4). The desired product was obtained as a yellow laque (23 mg). **Yield:** 32%. **¹H-NMR** (400 MHz, CDCl$_3$) δ (ppm): 8.78 (2H, d, *J* = 4.7 Hz), 8.65 (1H, d, *J* = 9.3 Hz), 8.59 (1H, s), 8.45 (2H, d, *J* = 1.5 Hz), 8.22

(4H, m), 8.16 (2H, m), 8.12, (1H, d, J = 1.8 Hz), 8.05 (1H, t, J = 7.6 Hz), 7.95 (4H, d, J = 7.9 Hz), 7.83 (2H, dt, J = 1.7 Hz, 7.8 Hz), 7.70 (1H, d, J = 3.6 Hz), 7.43 (1H, d, J = 3.6 Hz), 7.31 (2H, m). **Elem. Anal. Calcd** for $C_{36}H_{22}N_2S$: C, 84.02; H, 4.31; N, 5.44. **Found:** C, 83.93; H, 4.60; N, 5.57.

Pt-5. Compound **12** (23 mg, 0.04 mmol) and K_2PtCl_4 (18 mg, 0.04 mmol) were dissolved in a mixture of $AcOH/H_2O$ 9:1 (1 mL). The solution was degassed through freeze-pump-thaw cycles. The mixture was heated at reflux under argon for 2 days. The precipitate was filtered, washed with H_2O, MeOH, EtOH and Et_2O and dried in vacuo. The desired product was obtained as a dark green solid (19 mg). **Yield:** 61%. **^{1}H-NMR** (400 MHz, CD_2Cl_2) δ (ppm): 9.38 (2H, d, J = 5.6 Hz), 8.70 (1H, d, J = 9.2 Hz), 8.28 (3H, t, J = 6.4 Hz), 8.23 (3H, m), 8.19 (2H, d, J = 2.7 Hz), 8.10 (3H, m), 7.92 (3H, s), 7.65 (1H, d, J = 3.7 Hz), 7.48 (1H, d, J = 3.7 Hz), 7.43 (2H, t, J = 6.47 Hz). **Elem. Anal. Calcd** for $C_{36}H_{21}ClN_2SPt$: C, 58.10; H, 2.84; N, 3.76. **Found:** C, 57.98; H, 3.15; N, 3.78.

2.2.6. Synthesis of Pt-6
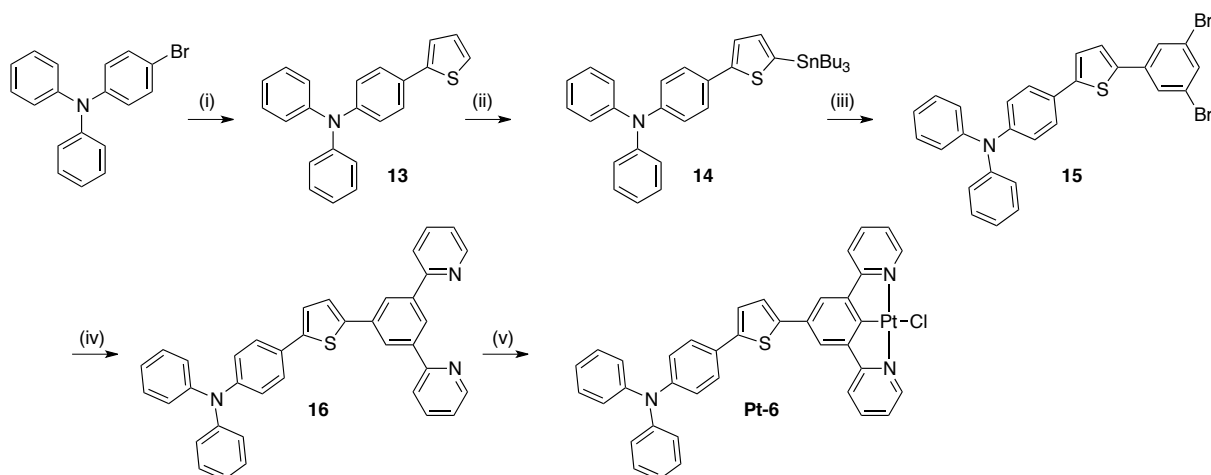
Scheme 6. Reagents and conditions: (i) 2-(tri-*n*-butylstannyl)thiophene, Pd(PPh$_3$)$_4$, toluene, 110°C, 24 h; (ii) *n*-BuLi, *n*-Bu$_3$SnCl, THF, Ar, -50°C to rt, 15 h; (iii) 1,3,5-tribromobenzene, Pd(PPh$_3$)$_4$, toluene, 110°C, 4 days; (iv) 2-(tri-*n*-butylstannyl)pyridine, LiCl, PdCl$_2$(PPh$_3$)$_2$, toluene, 110°C, 48 h; (v) K$_2$PtCl$_4$, AcOH/H$_2$O, 118°C, 48 h.

13. Procedure (II). Reactants: 4-bromo-N,N-diphenylamine (750 mg, 2.3 mmol), 2-(tri-*n*-butylstannyl)thiophene (1.10 mL, 3.4 mmol), Pd(PPh$_3$)$_4$ (150 mg, 0.13 mmol). Solvents: Toluene (40 mL), reflux 24 hours. Purification: The crude product was purified by flash chromatography (silica, hexane:CH$_2$Cl$_2$, 9:1). The desired product was obtained as a pale yellow solid (753 mg). **Yield:** quantitative. **^{1}H-NMR** (400 MHz, CDCl$_3$) δ (ppm): 7.53 (2H, d, *J* = 6.7 Hz), 7.30 (6H, m), 7.13 (2H, d, *J* = 7.6 Hz), 7.08 (7H, m).

14. Procedure (III). Reactants: **13** (753 mg, 2.3 mmol), *n*-BuLi 1.6M (1.6 mL, 2.73 mmol), *n*-Bu$_3$SnCl (736 µL, 2.73 mmol). Solvents: THF (50 mL). The product was obtained as a brown oil (1.42 g). **Yield:** quantitative. **^{1}H-NMR** (400 MHz, CDCl$_3$) δ (ppm): 7.71 (1H, m), 7.53 (1H, m), 7.48 (1H, d, *J* = 8.5 Hz), 7.26 (5H, m), 7.12 (3H, d, *J* = 7.8 Hz), 7.02 (5H, m), 1.76-0.93 (36H, m).

15. Procedure (II). Reactants: **14** (277 mg, 0.45 mmol), Pd(PPh$_3$)$_4$ (24 mg, 0.02 mmol), 1,3,5-tribromobenzene (130 mg, 0.41 mmol). Solvents: Toluene (0.5 mL), reflux 4 days. Purification: The crude product was purified by flash chromatography (silica, hexane: CH$_2$Cl$_2$, 9:1 to 8:2). The desired product was obtained as a yellow solid (167 mg). **Yield:** 67%. **^{1}H-NMR** (400 MHz, CDCl$_3$) δ (ppm): 7.69 (2H, d, *J* = 1.5), 7.56 (1H, s, *J* = 1.5 Hz), 7.49 (2H, d, *J* = 8.6 Hz), 7.32 (2H, d, *J* = 8.3 Hz), 7.28 (2H, m), 7.21 (1H, d, *J* = 3.8 Hz), 7.16 (4H, d, *J* = 7.6 Hz), 7.09 (5H, m).

16. Procedure (III). Reactants: **15** (167 mg, 0.30 mmol), 2-(tri-*n*-butylstannyl)pyridine (359 µL, 0.90 mmol), PdCl$_2$(PPh$_3$)$_2$ (63 mg, 0.09 mmol), LiCl (113 mg, 2.7 mmol). Solvents: Toluene (4 mL). Purification: The crude product was purified by flash chromatography (silica, hexane:AcOEt, 7:3). The desired product was obtained as a yellow solid (138 mg). **Yield:** 82%. **^{1}H-NMR** (400 MHz, CDCl$_3$) δ (ppm): 8.77 (2H, d, *J* = 4.8 Hz), 8.51 (1H, s), 8.33 (2H, d, *J* = 1.5 Hz), 7.9 (2H, d, *J* = 7.9 Hz), 7.81 (2H, dt, *J* = 1.7 Hz, 7.9 Hz), 7.54 (2H, d, *J* = 8.6 Hz), 7.49 (1H, d, *J* = 3.8 Hz), 7.29 (7H, m), 7.14 (4H, d, *J*

= 7.6 Hz), 7.10 (2H, d, J = 8.6 Hz), 7.06 (2H, d, J = 7.3 Hz). **Elem. Anal. Calcd** for $C_{38}H_{27}N_3S$: C, 81.84; H, 4.88; N, 7.53. **Found:** C, 81.82; H, 4.85; N, 7.49.

Pt-6. Compound **16** (138 mg, 0.25 mmol) and K_2PtCl_4 (114 mg, 0.28 mmol) were dissolved in a mixture of $AcOH/H_2O$ 1:1 (8 mL). The solution was degassed through freeze-pump-thaw cycles. The mixture was heated at reflux under argon for 2 days. The precipitate was filtered, washed with H_2O, MeOH, EtOH and Et_2O and dried in vacuo. The desired product was obtained as an ochre solid (87 mg). **Yield:** 44%. **^{1}H-NMR** (400 MHz, CD_2Cl_2) δ (ppm): 9.82 (1H, d, J = 5.9 Hz), 9.34 (1H, d, J = 4.9 Hz), 8.22 (2H, t, J = 7.7 Hz), 8.06 (3H, m), 7.87 (2H, d, J = 7.7 Hz), 7.79 (1H, s), 7.76 (1H, t, J = 7.7 Hz), 7.58 (2H, d, J = 8.5 Hz), 7.43 (1H, d, J = 3.8 Hz), 7.40 (2H, m), 7.32 (4H, m), 7.17 (3H, d, J = 7.7 Hz), 7.12 (3H, m). **Elem. Anal. Calcd** for $C_{38}H_{26}ClN_3PtS$: C, 57.98; H, 3.33; N, 5.34. **Found:** C, 57.95; H, 3.30; N, 5.29.

2.2.7 Synthesis of Pt-7
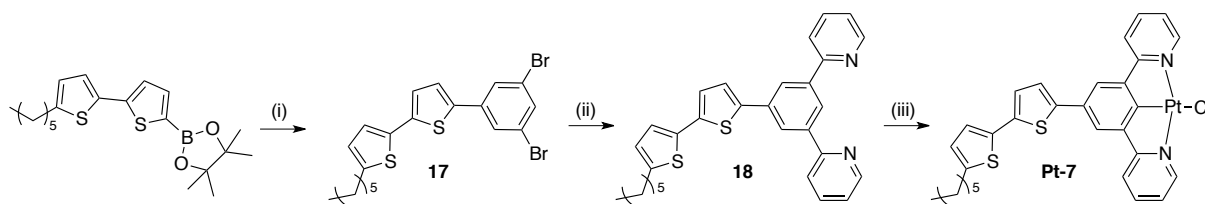
Scheme 7. Reagents and conditions: (i) 1,3,5-tribromobenzene, Pd(PPh$_3$)$_4$, Na$_2$CO$_3$, THF/H$_2$O, 90°C, 24 h; (ii) 2-(tri-n-butylstannyl)pyridine, LiCl, PdCl$_2$(PPh$_3$)$_2$, toluene, 110°C, 48 h; (iii) K$_2$PtCl$_4$, CH$_3$CN/H$_2$O, 90°C, 24 h.

17. A suspension of 1,3,5-tribromobenzene (150 mg, 0.47 mmol), 5'-Hexyl-2,2'-bithiophene-5-boronic acid pinacol ester (175 mg, 0.47 mmol), Pd(PPh$_3$)$_4$ (81 mg, 0.07 mmol) and Na$_2$CO$_3$ (7.5 mg, 0.07 mmol) in a mixture of THF/H$_2$O 1:1 (16 mL) was heated at 90°C for 24 hours. The mixture was then allowed to cool to room temperature, extracted in CH$_2$Cl$_2$/H$_2$O. The organic phase was dried over Na$_2$SO$_4$, the solvent removed under reduced pressure, and the crude was purified by flash chromatography (silica, hexane:CH$_2$Cl$_2$, 1:1). The desired product was obtained as a yellowish oil (150 mg). **Yield:** 66%. **^{1}H-NMR** (400 MHz, CDCl$_3$) δ (ppm): 7.66 (1H, s), 7.50 (2H, d, J = 4.5 Hz) 7.48 (2H, bs), 7.45 (2H, s) 6.83 (1H, d, J = 4.5 Hz), 2.84 (2H, m), 2.11 (2H, m), 1.57 (6H, m), 0.88 (3H, t).

18. Procedure (II). Reactants: **15** (103 mg, 0.20 mmol), 2-(tri-n-butylstannyl)pyridine (214 μL, 0.60 mmol), PdCl$_2$(PPh$_3$)$_2$ (29 mg, 0.04 mmol), LiCl (54 mg, 1.26 mmol). Solvents: Toluene (5 mL). Purification: The crude product was purified by flash chromatography (silica, AcOEt:hexane, 1:9). The desired product was obtained as a yellowish oil (50 mg). **Yield:** 52%. **^{1}H-NMR** (400 MHz, CDCl$_3$) δ (ppm): 8.68 (1H, s), 8.50 (2H, d, J = 4.3 Hz), 8.23 (2H, s), 7.49 (2H, m) 7.25 (2H, d, J = 4.3 Hz), 7.14 (2H, m), 7.04 (4H, m), 2.84 (2H, m), 2.11 (2H, m), 1.57 (6H, m), 0.88 (t, 3H). **Elem. Anal. Calcd** for C$_{30}$H$_{28}$N$_2$S$_2$: C, 74.96; H, 5.87; N, 5.83. **Found:** C, 80.01; H, 5.85; N, 5.81.

Pt-7. Compound **16** (32 mg, 0.07 mmol) and K$_2$PtCl$_4$ (26 mg, 0.06 mmol) were dissolved in a mixture of CH$_3$CN/H$_2$O 1:1 (2.5 mL) under argon atmosphere. The solution was degassed through freeze-pump-thaw cycles. The mixture was heated at 90°C under argon for 24 hours. The precipitate was filtered, washed with H$_2$O, MeOH, EtOH and Et$_2$O, recrystallised from CH$_2$Cl$_2$/pentane and dried in vacuo. The desired product was obtained as a brownish solid (21 mg). **Yield:** 50%. **^{1}H-NMR** (400 MHz, CD$_2$Cl$_2$) δ (ppm): δ 8.75 (2H, d, J = 4.1 Hz), 8.21 (2H, s), 7.84 (2H, m) 7.53 (2H, d, J = 4.3 Hz), 7.45 (2H, m), 7.13 (4H, m), 2.84 (2H, m), 2.11 (2H, m), 1.55 (6H, m), 0.94 (3H, t). **Elem. Anal. Calcd** for C$_{30}$H$_{27}$ClN$_2$PtS$_2$: C, 50.73; H, 3.83; N, 3.94. **Found:** C, 50.80; H, 3.88; N, 3.87.

2.2.8. Synthesis of Pt-8
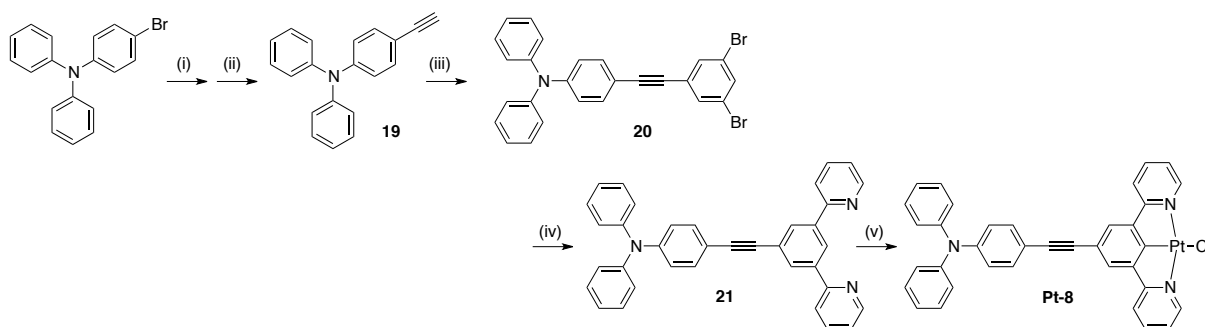
Scheme 8. Reagents and conditions: (i) TMSA, PdCl$_2$(PPh$_3$)$_2$, PPh$_3$, CuI, Et$_3$N, 75°C, 12 h; (ii) K$_2$CO$_3$, MeOH, rt, 12 h; (iii) 1,3,5-tribromobenzene, PdCl$_2$(PPh$_3$)$_2$, CuI, PPh$_3$, Et$_3$N, 70°C, 18 h; (iv) 2-(tri-*n*-butylstannyl)pyridine, CuO, PdCl$_2$(PPh$_3$)$_2$, DMF, 160°C, 45 min (MW); (v) K$_2$PtCl$_4$, AcOH/H$_2$O, 160°C, 45 min (MW).

19. (a) 4-bromo-*N,N*-diphenylamine (500 mg, 1.54 mmol), PdCl$_2$(PPh$_3$)$_2$ (65 mg, 0.09 mmol), CuI (190 mg, 0.04 mmol) and PPh$_3$ (262 mg, 0.04 mmol) were inserted in a Schlenk tube under argon. The mixture was degassed, trimethylsilylacetylene (326 μL mL, 2.31 mmol) and Et$_3$N (15 mL) were added. The mixture was heated at 70°C for 12 hours, then CH$_2$Cl$_2$ and H$_2$O were added, the organic layer was separated, dried over Na$_2$SO$_4$, the solvent removed under reduced pressure. The crude product was purified by column cromathography (silica, hexane:CH$_2$Cl$_2$, 9:1). The desired product was obtained as a yellow solid (422 mg) that was used directly for the following reaction. **Yield:** 80%.

(b) K$_2$CO$_3$ (500 mg, 3.6 mmol) was added to a methanol solution (20 mL) of **17** (422 mg, 1.23 mmol) and the mixture was stirred for 12 hours at room temperature. The solvent was then removed under reduced pressure, H$_2$O was added and then the mixture was extracted with CH$_2$Cl$_2$. The organic layer was dried over Na$_2$SO$_4$ and the solvent removed under reduced pressure. The crude product was purified by column cromathography (silica, hexane:CH$_2$Cl$_2$, 8:2). The desired product was obtained as a yellow solid (241 mg). **Yield:** 73%.**^{1}H-NMR** (400 MHz, CDCl$_3$) δ (ppm): 7.32 (2H, d, *J* = 8.8 Hz), 7.27 (4H, t, *J* = 8.4 Hz), 7.07 (6H, m), 6.95 (2H, d, *J* = 8.4 Hz), 3.01 (1H, s).

20. To a solution of 4-ethynyl-*N,N*-diphenylaniline (196 mg, 0.73 mmol) and 1,3,5-tribromobenzene (253 mg, 0.80 mmol) in degassed triethylamine (7.5 mL), PdCl$_2$(PPh$_3$)$_2$ (30.7 mg, 0.04 mmol), CuI (3.8 mg, 0.02 mmol) and PPh$_3$ (5.2 mg, 0.02 mmol) were added under argon flux. The reaction mixture was stirred at 70°C for 18 hours. The solvent was removed under reduced pressure and the residue was purifed by flash chromatography, (silica, hexane:CH$_2$Cl$_2$, 9:1). The desired product was obtained as a pale yellow solid (220 mg). **Yield:** 60%. **^{1}H-NMR** (400 MHz, CDCl$_3$) δ (ppm): 7.59 (1H, t, *J* = 1.6 Hz), 7.57 (2H, d, *J* = 1.6 Hz), 7.33 (2H, d, *J* = 8.8 Hz), 7.29 (4H, t, *J* = 7.2 Hz, 8.4 Hz), 7.12 (4H, d, *J* = 8.4 Hz), 7.08 (2H, t, *J* = 7.2 Hz, 8.4 Hz), 6.98 (2H, d, *J* = 8.8 Hz). **^{13}C-NMR** (101 MHz, CDCl$_3$) δ (ppm): 148.7, 147.1, 133.6, 132.9, 132.8, 129.6, 127.3, 125.4, 123.9, 122.7, 121.9, 114.8, 92.6, 85.8. **Elem. Anal. Calcd** for C$_{26}$H$_{17}$Br$_2$N: C, 62.06; H, 3.41; N, 2.78. **Found:** C, 62.04; H, 3.43; N, 2.75.

21. A mixture of **20** (407 mg, 0.81 mmol), 2-(tri-*n*-butylstannyl)pyridine (898 mg, 2.44 mmol),

PdCl$_2$(PPh$_3$)$_2$ (56 mg, 0.08 mmol), CuO (194 mg, 2.44 mmol) and DMF (8 mL) was placed in a microwave reactor at 160°C (250 W) for 45 min under nitrogen atmosphere, controlling the flow rate of cooling air. After cooling to room temperature, the reaction mixture was poured into ethyl acetate and filtered. The filtrate was washed with water, the organic layer was dried over anhydrous Na$_2$SO$_4$ and concentrated under reduced pressure. The crude product was purified by column chromatography, using (silica, hexane:AcOEt, 8:2). The desired product was obtained as a yellow solid (252 mg). **Yield:** 62%. **^{1}H-NMR** (400 MHz, CDCl$_3$) δ (ppm): 8.73 (2H, ddd, J = 4.8 Hz, 1.6 Hz, 0.8 Hz), 8.59 (1H, t, J = 1.6 Hz), 8.21 (2H, d, J = 1.6 Hz), 7.87 (2H, dt, J = 8.0 Hz, 2.0 Hz), 7.79 (2H, dt, J = 8.0 Hz, 3.6 Hz), 7.41 (2H, d, J = 8.8 Hz), 7.30 (6H, m), 7.13 (4H, dd, J = 7.6 Hz, 1.2 Hz), 7.07 (2H, tt, J = 7.2 Hz, 1.2 Hz), 7.01 (2H, d, J =8.8 Hz). **^{13}C-NMR** (101 MHz, CDCl$_3$) δ (ppm): 156.6, 149.7, 148.1, 147.3, 140.2, 136.9, 132.7, 130.4, 129.5, 125.2, 124.9, 123.7, 122.7, 122.4, 120.9, 116.1, 90.3, 88.6. **MS(FAB$^+$), calculated** (C$_{36}$H$_{25}$N$_3$): m/z 502.97. **Found:** m/z 499. **Elem. Anal. Calcd** for C$_{26}$H$_{25}$N$_3$: C, 86.55; H, 5.04; N, 8.41. **Found:** C, 86.61; H, 5.03; N, 8.37.

Pt-8. Compound **21** (119 mg, 0.24 mmol) was dissolved in a degassed mixture of AcOH/H$_2$O (1 mL) and K$_2$PtCl$_4$ (99 mg, 0.24 mmol) was added. The mixture was placed in a microwave reactor at 160°C (250 W) for 45 min under nitrogen atmosphere controlling the flow rate of cooling air. After cooling to room temperature, the reaction mixture was filtered. The precipitate was washed successively with MeOH, H$_2$O, EtOH and Et$_2$O, to obtain the desired product as a yellow powder (87 mg). **Yield:** 50%. **^{1}H-NMR** (400 MHz, CD$_2$Cl$_2$) δ (ppm): 9.34 (2H, bs), 8.04 (2H, t, J = 7.6 Hz), 7.92 (2H, d, J = 8.8 Hz), 7.75 (2H, d, J = 7.6 Hz), 7.44 (2H, s), 7.35 (6H, m), 7.20 (6H, m), 7.01 (2H, d, J = 8.8 Hz). **MS(FAB$^+$), calculated** (C$_{26}$H$_{24}$ClN$_3$Pt): m/z 693.16 [M-Cl]. **Found:** m/z 693 [M-Cl]. **Elem. Anal. Calcd** for C$_{36}$H$_{24}$ClN$_3$Pt: C, 59.30; H, 3.32; N, 5.76. **Found:** C, 59.43; H, 3.33; N, 5.68.

2.3. Synthesis of the binuclear Pt(dpyb)X complexes and the reference
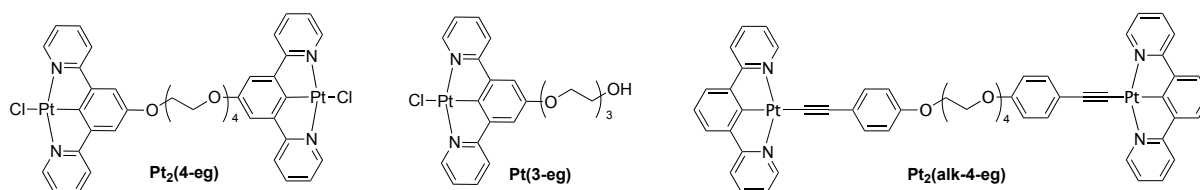
Figure 150. The Pt(II) complexes with a flexible chain.

2.3.1. Synthesis of Pt₂(4-eg) and Pt(3-eg)
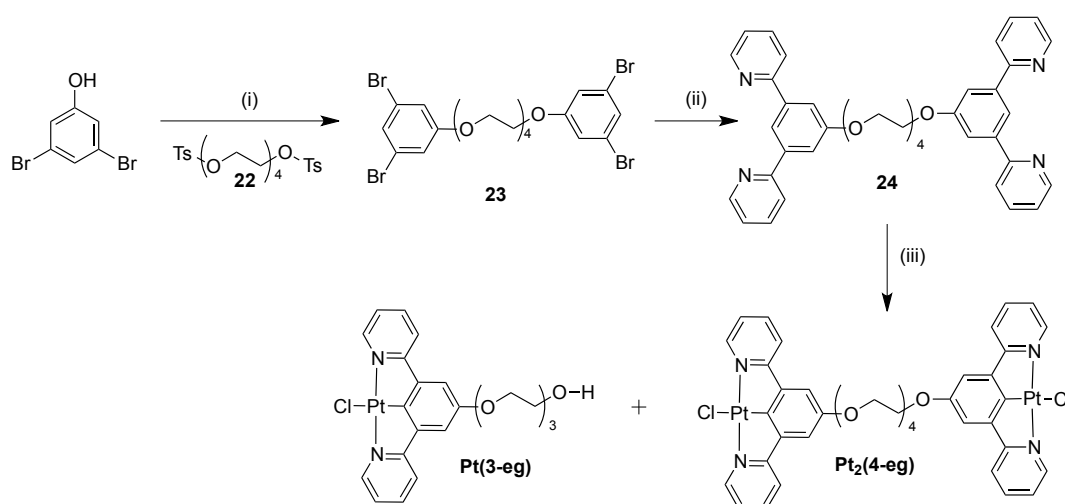
Scheme 9. Reagents and conditions: (i) K_2CO_3, acetonitrile, 90°C, 12 h; (ii) 2-(tri-*n*-butylstannyl)pyridine, LiCl, $PdCl_2(PPh_3)_2$, toluene, reflux, 48 h; (iii) K_2PtCl_4, $CH_3CN:H_2O$ 1:1, reflux, 48 h.

22. Tetraethylene glycol (1.00 mL, 5.8 mmol) was dissolved in anhydrous CHCl₃ (8 ml). The solution was cooled to −20°C in a NaCl ice bath. Tosyl chloride (3.32 g, 17.4 mmol) and anhydrous pyridine (6 mL) were added sequentially while keeping the temperature of the solution below 0°C. After 5 hours reaction at −20°C, chloroform and pyridine were removed under reduced pressure. Ice water (60 mL) was added and the solution was extracted with CH_2Cl_2 three times (50 mL each). The combined organic phase was washed twice with HCl (2N, 65 mL), saturated $NaHCO_3$ solution (50 mL) and water (50 mL) sequentially. Then the organic layer was dried over $MgSO_4$ and the solvent was removed under reduced pressure. The residue was purified by column chromatography (silica, AcOEt:petroleum ether, 1:1) to give **1** as a colorless oil (2.31 g). **Yield:** 79%. **¹H-NMR** (400 MHz, CDCl₃) δ (ppm): 7.75 (4H, d, J = 8.3 Hz), 7.31 (4H, d, J = 8.1 Hz), 4.12 (4H, t, J = 4.6 Hz), 3.64 (4H, t, J = 4.9 Hz), 3.52 (8H, m), 2.41 (6H, s).

23. To a solution of 3,5-dibromophenol (1.00 g, 2 mmol) in 40 mL CH_3CN, **22** (1.00 g, 4 mmol) and anhydrous K_2CO_3 (825 mg, 6 mmol) were added. The reaction mixture was refluxed under argon atmosphere for 12 hours. After cooling to room temperature, the resulting suspension was extracted with

water and CH_2Cl_2 (3 x 40 mL). The organic layer was dried over $MgSO_4$ and concentrated in vacuo. Compound **23** was obtained as an orange oil (1.32 g). **Yield:** 99%. **^{1}H-NMR** (400 MHz, $CDCl_3$) δ (ppm): 7.15 (2H, t, J = 1.5 Hz), 6.92 (4H, d, J = 1.5 Hz), 3.99 (4H, t, J = 4.6 Hz), 3.74 (4H, t, J = 4.5 Hz), 3.61 (8H, m). **^{13}C-NMR** (101 MHz, $CDCl_3$) δ (ppm): 159.9, 126.6, 123.0, 117.1, 70.9, 70.7, 69.4, 68.1. **Elem. Anal**. **Calcd** for $C_{20}H_{22}Br_4O_5$: C, 36.29; H, 3.35. **Found:** C, 36.85; H, 3.48.

24. Procedure (II). Reactants: **23** (827 mg, 1.3 mmol), 2-(tri-*n*-butylstannyl)pyridine (3.68 g, 10.0 mmol), $PdCl_2(PPh_3)_2$ (84 mg, 0.1 mmol), LiCl (954 mg, 22.5 mmol). Solvents: Toluene (12 mL). Purification: The crude product was purified by column chromatography (silica, from AcOEt to AcOEt:MeOH, 96:4) to obtain **24** as a white solid (379 mg). **Yield:** 46%. **^{1}H-NMR** (400 MHz, $CDCl_3$) δ (ppm): 8.68 (4H, d, J = 4.8 Hz,), 8.20 (2H, s), 7.81 (4H, d, J = 8.0 Hz), 7.73 (4H, dt, J = 7.5 Hz, 1.8 Hz), 7.66 (4H, s), 7.23 (4H, ddd, J = 7.4, 4.8, 1.2 Hz), 4.33 (4H, t, J = 4.8 Hz), 3.91 (4H, t, J = 5.2 Hz), 3.73 (8H, m). **^{13}C-NMR** (101 MHz, $CDCl_3$) δ (ppm): 159.7, 156.9, 149.5, 141.1, 136.7, 122.3, 120.8, 118.2, 113.8, 70.9, 70.7, 69.8, 67.8. **Elem. Anal**. **Calcd** for $C_{40}H_{38}N_4O_{55} \cdot 0.5H_2O$: C, 72.38; H, 5.92; N, 8.44. **Found:** C, 72.07; H, 5.85; N, 8.26.

Pt_2(4-eg) and Pt(3-eg). The dipyridylbenzene ligand **24** (500 mg, 0.8 mmol) was dissolved in deaerated CH_3CN (27 mL), and an aqueous solution of K_2PtCl_4 (950 mg, 2.4 mmol in 9 mL water) was added under argon atmosphere. The mixture was heated at reflux under argon for 2 days. After cooling to room temperature and filtering the solution, CH_2Cl_2 was added and the organic phase was separated, dried on $MgSO_4$ and dried in vacuo. The two products were obtained by precipitation in CH_2Cl_2/Et_2O as orange powders (**Pt(3-eg)Cl**: 55 mg, **Pt_2(4-eg)Cl_2**: 100 mg). **Pt_2(4-eg), Yield:** 11%. **^{1}H-NMR** (400 MHz, CD_2Cl_2) δ (ppm): 9.18 (4H, m), 7.93 (4H, t, J = 7.8 Hz), 7.59 (4H, d, J = 7.7 Hz), 7.29 (4H, d, J = 6.3 Hz), 7.05 (4H, s), 4.17 (4H, t, J = 4.7 Hz), 3.88 (4H, t, J = 4.7 Hz), 3.76 (8H, m). **HR-MS (FTMS[+]):** **[M-Na][+] Calculated:** ($C_{40}H_{36}N_4O_5Cl_2Pt_2Na$): 1135.12507 **Found:** 1135.1236. **Elem. Anal**. **Calcd** for $C_{41}H_{39}Cl_2N_4O_5Pt_2 \cdot Et_2O$: C, 44.93; H, 4.11; N, 4.66. **Found:** C, 44.99; H, 4.08; N, 4.58.

Pt(3-eg), **Yield:** 11%. **^{1}H NMR** (400 MHz, CD_2Cl_2) δ (ppm): 9.24 (2H, dt, J = 5.6 Hz, J_{Pt-H} = 44 Hz), 7.96 (2H, t, J = 7.8 Hz), 7.68 (2H, d, J = 7.7 Hz), 7.30 (2H, d, J = 6.3 Hz), 7.18 (2H, s), 4.20 (2H, t, J = 4.7 Hz), 3.86 (2H, t, J = 4.7 Hz), 3.70 (6H, m), 3.58 (2H, m).

2.3.2. Synthesis of Pt₂(alk-4-eg)
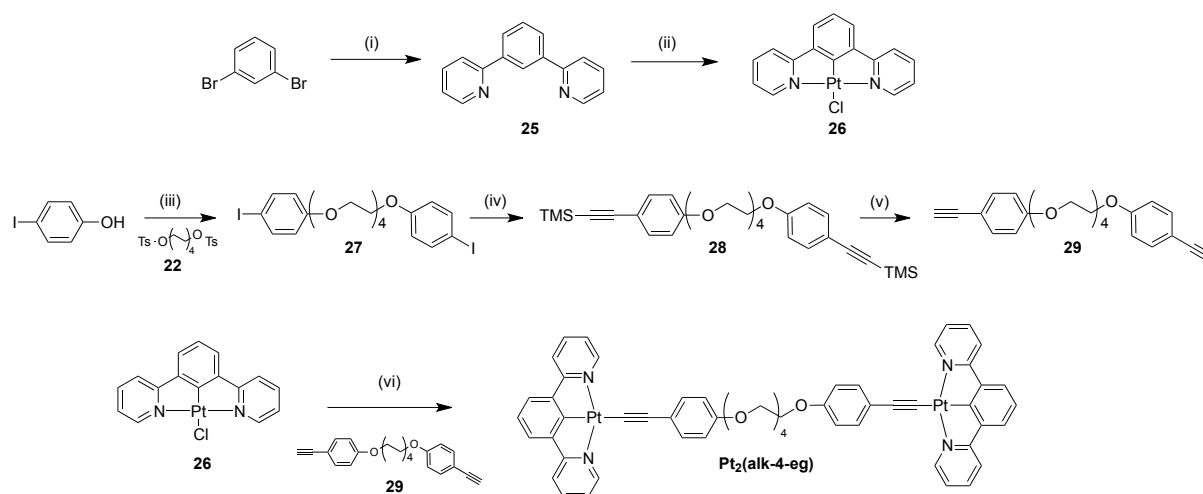
Scheme 10. Reagents and conditions: (i) 2-(tri-*n*-butylstannyl)pyridine, LiCl, PdCl₂(PPh₃)₂, toluene, 110°C, 48 h; (ii) K₂PtCl₄, AcOH, 118°C, 3 days; (iii) K₂CO₃, CH₃CN, 85°C, 12 h; (iv) PdCl₂(PPh₃)₂, CuI, Me₃N, THF, 30°C, 30 min; TMSA, 50°C, 24 h; (v) K₂CO₃, CH₂Cl₂/MeOH 1:1, 3 h; (vi) NaOH, MeOH, 30 min; CH₂Cl₂/MeOH 1:1, rt, 40 h.

25. Procedure (II): 1,3-dibromobenzene (2 g, 8.5 mmol), 2-(tri-*n*-butylstannyl)pyridine (7.8 g, 21.2 mmol), PdCl₂(PPh₃)₂ (295 mg, 0.4 mmol), LiCl (2.88 g, 98 mmol). Solvents: Toluene (70 mL). Purification: The crude product was purified by column chromatography (silica, petroleum ether:Et₂O, from 6:4 to 2:8) to obtain **7** as a white/bluish oil (1.36 mg). **Yield:** 69%. **¹H-NMR** (400 MHz, CDCl₃) δ (ppm): 8.69 (2H, ddd, *J* = 4.9, 1.8, 0.9 Hz), 8.65 (1H, t, *J* = 1.8 Hz), 8.05 (2H, dd, *J* = 7.7, 1.8 Hz), 7.79 (2H, d, *J* = 8.0 Hz), 7.69 (2H, td, *J* = 7.7, 1.8 Hz), 7.55 (1H, t, *J* = 7.8 Hz), 7.18 (2H, ddd, *J* = 7.4, 4.8, 1.1 Hz).

26. Compound **25** (440 mg, 1.89 mmol) was dissolved in acetic acid (30 ml). The solution was degassed through freeze-pump-thaw cycles. K₂PtCl₄ was added and the mixture was heated at reflux for 3 days. A yellow precipitate formed: it was filtered, washed with MeOH, H₂O, EtOH and Et₂O and dried under vacuum to obtain pure **8** (690 mg). **Yield:** 79%. **¹H-NMR** (400 MHz, CD₂Cl₂) δ (ppm): 9.32 (2H, m), 8.02 (2H, td, *J* = 7.8, 1.7 Hz), 7.78 (2H, m), 7.55 (2H, m), 7.36 (2H, m), 7.30 (1H, t, *J* = 7.7 Hz).

27. 4-iodophenol (1 g, 2.0 mmol) was dissolved in CH₃CN (80 mL) under argon. Compound **22** (875 mg, 4.0 mmol) and K₂CO₃ (414 mg, 3.0 mmol) were added to the solution. The mixture was heated at reflux for 12 hours under inert atmosphere. Then, water was added, the crude was extracted in CH₂Cl₂, the organic layer was dried over MgSO₄ and the solvent was removed under reduced pressure. The crude was purified by column chromatography to give **27** as a yellow sticky solid (178 mg). **Yield:** 92%. **¹H-NMR** (400 MHz, CDCl₃) δ (ppm): 7.45 (4H, d, *J* = 8.0 Hz), 6.87 (4H, d, *J* = 8.0 Hz), 3.84 (12H, s), 3.02 (4H, s).

28. Compound **27** (1.1 g, 1.8 mmol) was dissolved in a mixture of trimethylamine (10 mL) and THF (20 ml). The solution was degassed, Pd(PPh₃)₂Cl₂ (64 mg, 0.09 mmol) and CuI (17 mg, 0.09 mmol) were

added and the mixture was heated at 30°C for 30 minutes. Then trimethylsilylacetylene (0.65 mL, 4.5 mmol) was added dropwise and the dark solution was stirred at 50°C for 24 hours. Then the solvent was evaporated, water was added, the crude was extracted in CH_2Cl_2, the organic layer was dried over $MgSO_4$ and the solvent was removed under reduced pressure. The residue was purified by column chromatography (silica, AcOEt/petroleum ether, 3:7) to give 5 as a white solid (319 mg). **Yield:** 33%.
^{1}H-NMR (400 MHz, $CDCl_3$) δ (ppm): 7.38 (4H, d, J = 8.8 Hz), 6.81 (4H, m, J = 8.8 Hz), 4.0 (4H, t, J = 4.7 Hz), 3.83 (4H, t, J = 4.9 Hz), 3.68 (8H, m), 0.23 (18H, s). **^{13}C-NMR** (101 MHz, $CDCl_3$) δ (ppm): 159.07, 133.56, 115.56, 114.58, 105.28, 92.61, 70.99, 70.81, 69.76, 67.57, 0.21.

29. Compound **28** (200 mg, 0.37 mmol) and K_2CO_3 (512 mg, 3.7 mmol) were dissolved in a mixture of CH_2Cl_2/MeOH 1:1 (6 mL). The mixture was stirred at room temperature for 3 hours. Then, water was added, the crude was extracted in CH_2Cl_2, the organic layer was dried over $MgSO_4$ and the solvent was removed under reduced pressure to give **6** as a yellowish oil (138 mg). **Yield:** 95%. **^{1}H-NMR** (400 MHz, $CDCl_3$) δ (ppm): 7.40 (4H, d, J = 8.8 Hz), 6.84 (4H, d, J = 8.8 Hz), 4.10 (4H, t, J = 4.6 Hz), 3.84 (4H, t, J = 5.1 Hz), 3.69 (8H, m), 3.00 (2H, s). **^{13}C-NMR** (400 MHz, $CDCl_3$) δ (ppm): 159.25, 133.65, 114.69, 114.43, 83.73, 75.98, 70.95, 70.77, 69.71, 67.57.

Pt_2(alk-4-eg). Compound **29** (70 mg, 0.18 mmol) and NaOH (20 mg, 0.5 mmol) were dissolved in MeOH (2 mL) and the mixture was stirred at room temperature for 30 minutes. Then compound **26** (164 mg, 0.36 mmol) was dissolved in a mixture of MeOH/CH_2Cl_2 1:1 (16 mL) and added to the ligand solution. The mixture was stirred at room temperature for 40 hours. Then the solvent was evaporated, the crude was dissolved in CH_2Cl_2 and precipitated with Et_2O to obtain the desired product as a yellow powder (105 mg). **Yield:** 47% yield. **^{1}H-NMR** (400 MHz, CD_2Cl_2) δ (ppm): 9.49 (4H, m), 7.96 (4H, t, J = 7.9 Hz), 7.72 (4H, d, J = 8.2 Hz), 7.56 (4H, d, J = 7.6 Hz), 7.48 (4H, d, J = 8.7 Hz), 7.26 (6H, m), 6.89 (4H, d, J = 8.7 Hz), 4.16 (4H, t, J = 4.4 Hz), 3.87 (4H, t, J = 4.8 Hz), 3.72 (8H, m). **^{13}C-NMR** (101 MHz, CD_2Cl_2) δ (ppm): 178.74, 169.55, 156.62, 155.30, 143.09, 138.64, 135.02, 132.50, 123.75, 123.58, 122.93, 121.41, 119.42, 114.24, 110.72, 70.75, 70.61, 69.71, 67.52. **Elem. Anal**. **Calcd** for $C_{56}H_{46}N_4O_5Pt_2$: C, 54.02; H, 3.72; N, 4.50. **Found:** C, 53.96; H, 3.70; N, 4.48.

2.4. Synthesis of the photochromic Pt(II) complexes
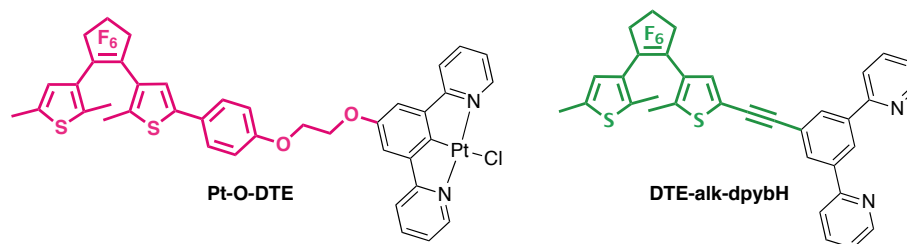
Figure 151. The Pt(II) complexes bearing a DTE moiety.

2.4.1. Synthesis of Pt-O-DTE
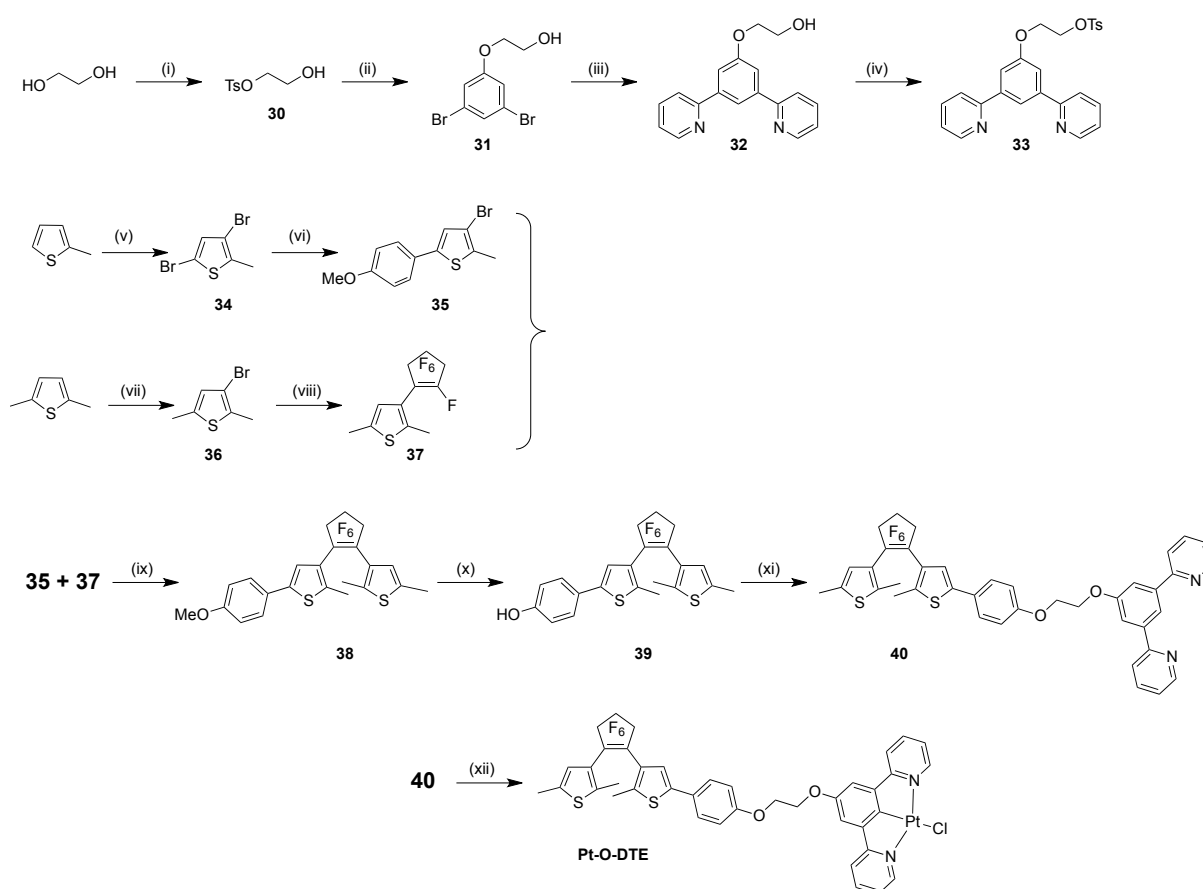
Scheme 11. Reagents and conditions: (i) TsCl, pyridine, CHCl$_3$, -20°C, 5 h; (ii) K$_2$CO$_3$, DMF, 155°C, 12 h; (iii) 2-(tri-n-butylstannyl)pyridine, LiCl, PdCl$_2$(PPh$_3$)$_2$, toluene, 110°C, 48 h; (iv) TsCl, pyridine, CHCl$_3$, -20°C, 5 h; (v) N-bromosuccinimide, AcOH, 15 h, dark; (vi) PdCl$_2$(PPh$_3$)$_2$, Na$_2$CO$_3$, THF/H$_2$O, 100°C, 15 h; (vii) N-bromosuccinimide, AcOH, 15 h, dark; (viii) n-BuLi, perfluorocyclopentene, THF, -78°C, 1 h → rt, 15 h; (ix) n-BuLi, THF, -78°C, 1 h → rt, 15 h; (x) BBr$_3$, CH$_2$Cl$_2$, -78°C, 3 h → rt, 4 days; (xi) K$_2$CO$_3$, DMF, 155°C, 12 h; (xii) K$_2$PtCl$_4$, AcOH, 118°C, 2 days.

30. Ethylene glycol (1.00 mL, 18.0 mmol) was dissolved in anhydrous CHCl$_3$ (50 ml). The solution was cooled to −20°C in a NaCl ice bath. Tosyl chloride (3.43 g, 18.0 mmol) and anhydrous pyridine (40 mL) were added sequentially while keeping the temperature of the solution below 0°C. After 5 hours stirring

at –20°C, CHCl$_3$ and pyridine were removed under reduced pressure. Cold water (60 mL) was added and the solution was extracted with CH$_2$Cl$_2$ (3 x 50 mL). The organic phase was washed twice with HCl 2N (65 mL), saturated NaHCO$_3$ (50 mL) and water (50 mL) sequentially. The organic layer was dried over MgSO$_4$ and the solvent was removed under reduced pressure. The crude was purified by column chromatography (silica, AcOEt:petroleum ether, 8:2) to give **30** as a colorless oil (1.77 g). **Yield:** 46%. **^{1}H-NMR** (400 MHz, CDCl$_3$) δ (ppm): 7.75 (2H, d, J = 8.3 Hz), 7.30 (2H, d, J = 8.1 Hz), 4.06 (2H, m), 3.73 (2H, t, J = 4.8 Hz), 2.39 (3H, s).

31. To a solution of 3,5-dibromophenol (3 g, 11.9 mmol) in 50 mL of DMF, 2-hydroxyethyltosilate (3.85 g, 17.8 mmol) and anhydrous K$_2$CO$_3$ (3.45 g, 25.0 mmol) were added. The mixture was refluxed under argon atmosphere for 12 hours. The resulting suspension was cooled to room temperature, diluted with AcOEt (50 mL) and washed with brine. The organic layer was dried over MgSO$_4$ and dried in vacuo. The crude residue was purified by column chromatography (silica, petroleum ether:AcOEt, from 8:2 to 7:3) to give the desired product as a yellowish oil (2.26 mg). **Yield:** 65%. **^{1}H-NMR** (400 MHz, CDCl$_3$) δ (ppm): 7.29 (1H, m), 7.04 (2H, d, J = 1.6 Hz), 4.07 (2H, t, J = 4.7 Hz), 3.98 (2H, m).

32. Procedure (II). Reactants: **31** (2.26 g, 7.75 mmol), 2-(tri-n-butylstannyl)pyridine (8.56 g, 23.3 mmol), PdCl$_2$(PPh$_3$)$_2$ (163 mg, 0.23 mmol), LiCl (2.96 g, 69.8 mmol). Solvents: Toluene (30 mL). Purification: The crude product was purified by column chromatography (silica, petroleum ether:AcOEt, from 2:8 to 1:9) to obtain **32** as a white solid (1.48 mg). **Yield:** 65%. **^{1}H-NMR** (400 MHz, CDCl$_3$) δ (ppm): 8.73 (2H, d, J = 4.8 Hz), 8.22 (1H, s), 7.85 (1H, d, J = 7.9 Hz), 7.79 (2H, td, J = 7.7, 1.8 Hz), 7.69 (2H, s), 7.28 (2H, m), 4.30 (2H, t, J = 4.5 Hz), 4.03 (2H, m).

33. Compound **32** (1.48 g, 5.05 mmol) was dissolved in anhydrous chl CHCl$_3$ oroform (20 ml). The solution was cooled to –20°C in a NaCl ice bath. Tosyl chloride (1.44 g, 7.58 mmol) and anhydrous pyridine (15 mL) were added sequentially while keeping the temperature of the solution below 0°C. After 5 hours stirring at –20°C, CHCl$_3$ and pyridine were removed under reduced pressure. Cold water (60 mL) was added and the solution was extracted with CH$_2$Cl$_2$ (3 x 50 mL). The organic phase was washed twice with HCl 2N (65 mL), saturated NaHCO$_3$ (50 mL) and water (50 mL) sequentially. The organic layer was dried over MgSO$_4$ and the solvent was removed under reduced pressure. The crude was purified by column chromatography (silica, AcOEt) to give **33** as a white paste (1.49 g). **Yield:** 67%. **^{1}H-NMR** (400 MHz, CDCl$_3$) δ (ppm): 8.70 (2H, d, J = 4.6 Hz), 8.20 (1H, s), 7.83 (4H, m), 7.77 (2H, td, J = 7.6, 1.7 Hz), 7.54 (2H, d, J = 1.2 Hz), 7.33 (2H, d, J = 8.1 Hz), 7.26 (2H, m), 4.44 (2H, m), 4.34 (2H, m), 2.40 (3H, s). **^{13}C-NMR** (101 MHz, CDCl$_3$) δ (ppm): 158.98, 156.72, 149.62, 144.90, 141.25, 136.78, 132.98, 129.86, 128.04, 122.50, 120.76, 118.60, 113.74, 68.24, 65.75, 21.63.

34. 2-methylthiophene (1.00 g, 10.2 mmol) was dissolved in 15 mL acetic acid. N-bromosuccinimide (3.98 g, 22.4 mmol) was added in 4 times over 1 hour while stirring. The mixture was stirred at room temperature protected from the light overnight. The following day, 30 mL H$_2$O and 50 mL Na$_2$S$_2$O$_4$

were added, the mixture was stirred for 10 minutes, then extracted wit Et_2O (3 x 60 mL). The organic phase was washed with a saturated solution of K_2CO_3 (80 mL), then dried over $MgSO_4$ and the solvent removed under reduced pressure. The crude product was purified by flash chromatography (silica, petroleum ether 100%) to obtain **34** as a yellowish oil (1.48 g). **Yield:** 57%. **^{1}H-NMR** (400 MHz, $CDCl_3$) δ (ppm): 6.77 (1H, s), 2.32 (3H, s).

35. (4-methoxyphenyl)boronic acid (1.6 g, 10.5 mmol), **34** (2.1 g, 8.1 mmol) and $PdCl_2(PPh_3)_2$ (168 mg, 0.2 mmol) were dissolved in 25 mL of THF in a Schlenk tube. A solution of Na_2CO_3 (2.5 g, 23.6 mmol) in 25 mL H_2O was added and the mixture was heated at reflux overnight. After cooling to room temperature, the mixture was extracted with CH_2Cl_2 (3 x 50 mL) and washed with brine. The organic layer was dried over $MgSO_4$ and concentrated in vacuo. The crude product was purified by flash chromatography (silica, from petroleum ether 100% to petroleum ether:CH_2Cl_2, 1:9) to obtain **35** as a white solid (1.05 g). **Yield:** 65%. **^{1}H-NMR** (400 MHz, $CDCl_3$) δ (ppm): 7.43 (2H, d, $J = 8.8$ Hz), 6.99 (1H, s), 6.90 (2H, d, $J = 8.7$ Hz), 3.83 (3H, s), 2.40 (3H, s).

36. 2,5-dimethylthiophene (1.00 g, 8.9 mmol) was dissolved in 15 mL acetic acid. *N*-bromosuccinimide (1.58 g, 8.9 mmol) was added in 4 times over 1 hour while stirring. The mixture was stirred at room temperature protected from the light overnight. The following day, 30 mL H_2O and 50 mL $Na_2S_2O_4$ were added, the mixture was stirred for 10 minutes and then extracted wit Et_2O (3 x 60 mL). The organic phase was washed with a saturated solution of K_2CO_3 (80 mL), then dried over $MgSO_4$ and the solvent was removed under reduced pressure. The crude product was purified by flash chromatography (silica, petroleum ether 100%) to obtain **36** as a yellowish oil (1.06 g). **Yield:** 63%. **^{1}H-NMR** (400 MHz, $CDCl_3$) δ (ppm): 6.62 (1H, s), 2.47 (3H, s), 2.42 (3H, s).

37. Compound **36** (3.00 g, 15.7 mmol) was dissolved in dry THF (120 mL) in a Schlenk tube under argon. The reaction mixture was cooled to -78°C and *n*-BuLi solution (1.6 M in hexane, 9.80 mL, 15.7 mmol) was added dropwise. The reaction solution became pale yellow, was stirred for 1 hour at -78°C and then cannulated into a solution of perfluorocyclopentene (9.98 g, 6.40 mL, 47.1 mmol) in 90 mL of THF at -78°C. The yellow mixture was stirred at -78°C for 1 hour, then allowed to warm up at room temperature and stirred overnight. The solution was washed twice with brine, the organic layer was dried over $MgSO_4$ and the solvent was removed under reduced pressure. The crude product was purified by column chromatography (silica, petroleum ether) to obtain the pure product as a colorless oil (2.82 g). **Yield:** 59%. **^{1}H-NMR** (400 MHz, $CDCl_3$) δ (ppm): 6.75 (1H, s), 2.46 (3H, s), 2.41 (3H d, $J = 3.3$ Hz).

38. Compound **35** (2.88 g, 10.2 mmol) was dissolved in 70 mL of dry THF in a Schlenk tube under argon. The reaction mixture was cooled to -78°C and *n*-BuLi solution (1.6 M in hexane, 6.9 mL, 11.1 mmol) was added dropwise. The reaction solution became pale yellow, was stirred for 1 hour at -78°C and then cannulated into a solution of **37** (2.81 g, 9.25 mmol) in 70 mL of THF at -78°C. The deep red mixture was stirred at -78°C for 1 hour, then allowed to warm up at room temperature and stirred

overnight. The solution was washed twice with brine, the organic layer was dried over $MgSO_4$ and the solvent was removed under reduced pressure. The crude product was purified by column chromatography (silica, petroleum ether:CH_2Cl_2, 9:1) to obtain the pure product as a white powder (3.37 g). **Yield:** 74%. **^{1}H-NMR** (400 MHz, $CDCl_3$) δ (ppm): 7.46 (2H, d, J = 8.7 Hz), 7.13 (1H, s), 6.91 (2H, d, J = 8.7 Hz), 6.73 (1H, s), 3.83 (3H, s), 2.42 (3H, s), 1.90 (3H, s), 1.87 (3H, s).

39. To a stirred solution of **38** (3.00 g, 6 mmol) in anhydrous CH_2Cl_2 (180 mL) at -78°C, a BBr_3 solution (1 M in CH_2Cl_2, 13.7 mL, 13.7 mmol) was added dropwise under an argon atmosphere. The solution was stirred for 3 hours at -78°C, and then for 4 days at room temperature. The reaction mixture was quenched with water and extracted with Et_2O. The organic layer was washed with brine, then dried over $MgSO_4$, and the solvent was removed under reduced pressure. The crude product was purified by column chromatography (silica, petroleum ether:AcOEt, 7:3) to obtain the pure product as a brown oil (2.71 g). **Yield:** 92%. **^{1}H-NMR** (400 MHz, $CDCl_3$) δ (ppm):7.41 (2H, d, J = 8.6 Hz), 7.13 (1H, s) 6.85 (2H, d, J = 8.7 Hz), 6.73 (1H, s), 5.02 (1H, bs), 2.42 (3H, s), 1.90 (3H, s), 1.86 (3H, s).

40. To a solution of **39** (497 mg, 1.0 mmol) in 6 mL of DMF, **4** (600 mg, 1.3 mmol) and anhydrous K_2CO_3 (300 mg, 2.2 mmol) were added. The mixture was refluxed under argon atmosphere for 12 hours. The resulting suspension was cooled to room temperature, diluted with AcOEt (30 mL) and washed with brine. The organic layer was dried over $MgSO_4$ and the solvent was removed under reduced pressure. The crude was purified by column chromatography (petroleum ether/AcOEt, 1:1). The desired ligand **40** was obtained as an orange powder (675 mg). **Yield:** 88%. **^{1}H-NMR** (400 MHz, CD_2Cl_2) δ (ppm): 8.69 (2H, m), 8.30 (1H, t, J = 1.4 Hz), 7.85 (2H, d, J = 8.0 Hz), 7.78 (2H, td, J = 7.7, 1.8 Hz), 7.72 (2H, d, J = 1.4 Hz), 7.49 (2H, d, J = 8.8 Hz), 7.27 (2H, ddd, J = 7.3, 4.8, 1.1 Hz), 7.16 (1H, s), 6.99 (2H, d, J = 8.8 Hz), 6.74 (1H, s), 4.51 (2H, m), 4.41 (2H, m), 2.41 (3H, s), 1.91 (3H, s), 1.87 (3H, s). **^{13}C-NMR** (400 MHz, CD_2Cl_2) δ (ppm): 159.87, 158.91, 156.87, 149.92, 141.55, 138.37, 137.05, 127.19, 126.90, 124.88, 122.81, 121.75, 120.83, 118.55, 115.38, 113.92, 105.31, 67.26, 67.20, 15.14, 14.48, 14.40. **^{19}F-NMR** (376.5 MHz, CD_2Cl_2) δ (ppm): -109 (4F, d), -132 (2F, m). **Elem. Anal**. **Calcd** for $C_{40}H_{30}N_2O_2F_6S_2$: C, 64.75; H, 4.58; N, 4.24. **Found:** C, 64.48; H, 4.40, N, 4.02, S.

Pt-O-DTE. Acetic acid (13 mL) was degassed through freeze-pump-thaw cycles, then the ligand **40** (300 mg, 0.40 mmol) and K_2PtCl_4 (183 mg, 0.44 mmol) were added. The mixture was refluxed under argon atmosphere for 48 hours. The resulting suspension was cooled to room temperature, the precipitate was separated from the solution, washed sequentially with MeOH, H_2O, EtOH, and Et_2O and dried under vacuum to obtain **Pt-O-DTE** as a yellow powder (260 mg). **Yield:** 66%. **^{1}H-NMR** (400 MHz, CD_2Cl_2) δ (ppm): 8.69 (2H, m), 8.30 (1H, t, J = 1.4 Hz), 7.85 (2H, d, J = 8.0 Hz), 7.78 (2H, td, J = 7.7, 1.8 Hz), 7.72 (2H, d, J = 1.4 Hz), 7.49 (2H, d, J = 8.8 Hz), 7.27 (2H, ddd, J = 7.3, 4.8, 1.1 Hz), 7.16 (1H, s), 6.99 (1H, d, J = 8.8 Hz), 6.74 (1H, s), 4.51 (2H, m), 4.41 (2H, m), 2.41 (3H, s), 1.91 (3H, s), 1.87 (3H, s). **^{13}C-NMR** (101 MHz, CD_2Cl_2) δ (ppm): 167.64, 164.36, 159.12, 156.64, 155.24, 152.62, 152.33, 142.41, 141.97, 139.79, 138.67, 127.50, 127.23, 125.15, 124.12, 122.05, 120.08, 115.64, 112.43, 112.27, 73.67,

73.42, 68.36, 67.50, 65.94, 15.42, 14.75, 14.68. **^{19}F-NMR** (376.5 MHz, CD_2Cl_2): δ = -110 (4F, d), -132 (2F, m). **Elem. Anal**. **Calcd** for $C_{40}H_{29}N_2O_2F_6ClS_2Pt$ + 1 CH_2Cl_2: C, 46.32; H, 2.94; N, 2.63. **Found:** C, 46.15; H, 2.90; N, 3.16.

2.4.2. Synthesis of DTE-alk-dpyb
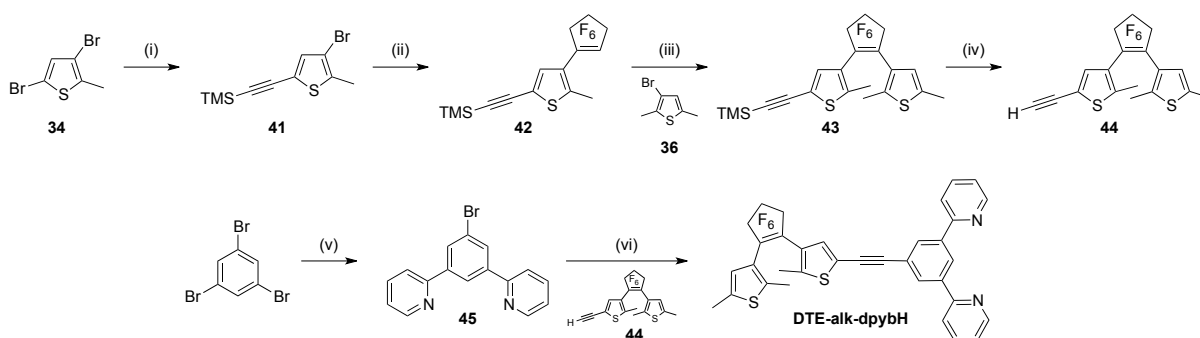
Scheme 12. Reagents and conditions: (i) PdCl$_2$(PPh$_3$)$_2$, CuI, TMSA, *i*-Pr$_2$NH, 50°C, 24 h; (ii) *n*-BuLi, perfluorocyclopentene, THF, -78°C, 1 h → rt, 15 h; (iii) *n*-BuLi, THF, -78°C, 1 h → rt, 15 h; (iv) K$_2$CO$_3$ MeOH/CH$_2$Cl$_2$, 3 h; (v) 2-(tri-*n*-butylstannyl)pyridine, LiCl, PdCl$_2$(PPh$_3$)$_2$, toluene, 110°C, 48 h; (vi) PdCl$_2$(PPh$_3$)$_2$, CuI, *i*-Pr$_2$NH, 50°C, 24 h.

41. 3,5-dibromo-2-methylthiophene (1.50 g, 5.8 mmol) was dissolved in 30 mL *i*-Pr$_2$NH and 10 mL THF in a Schlenk tube equipped with magnetic stirrer. Argon was then bubbled for 10 minutes and CuI (45 mg, 0.28 mmol) and PdCl$_2$(PPh$_3$)$_2$ were added. The mixture was stirred at 45°C for 45 minutes, then trimethylsilylacetylene (570 mg, 5.8 mmol) was added to the mixture which was stirred at 50°C for 24 hours. Then, the mixture was allowed to cool to room temperature, extracted with CH$_2$Cl$_2$/H$_2$O, the organic phase was dried over MgSO$_4$ and the solvent was removed under reduced pressure. The crude product was purified by flash chromatography (silica, petroleum ether 100%) to obtain **41** as a white solid (1.18 g). **Yield:** 74%. **^{1}H-NMR** (500 MHz, CDCl$_3$) δ (ppm): 7.05 (1H, s), 2.38 (3H, s) 0.24 (9H, s).

42. Compound **41** (1.18 g, 4.32 mmol) was dissolved in dry THF (40 mL) in a Schlenk tube under argon. The reaction mixture was cooled to -78°C and *n*-BuLi solution (2.5 M in hexane, 1.7 mL, 4.32 mmol) was added dropwise. The reaction solution became pale yellow, was stirred for 1 hour at -78°C and then cannulated into a solution of perfluorocyclopentene (2.74 g, 1.76 mL, 12.95 mmol) in 20 mL of THF at -78°C. The yellow mixture was stirred at -78°C for 1 hour, then allowed to warm up at room temperature and stirred overnight. The solution was washed twice with brine, the organic layer was dried over MgSO$_4$ and the solvent was removed under reduced pressure. The crude product was purified by column chromatography (silica, petroleum ether) to obtain the pure product as a colorless oil (904 g). **Yield:** 54%. **^{1}H-NMR** (500 MHz, CDCl$_3$) δ (ppm): 7.20 (1H, s), 2.43 (3H, d, *J* = 3.0 Hz), 0.26 (9H, s).

43. Compound **36** (490 mg, 2.58 mmol) was dissolved in dry THF (15 mL) in a Schlenk tube under argon. The reaction mixture was cooled to -78°C and *n*-BuLi solution (2.5 M in hexane, 1.3 mL, 2.82 mmol) was added dropwise. The reaction solution became pale yellow, was stirred for 1 hour at -78°C and then cannulated into a solution of **42** (907 g, 2.35 mmol) in 15 mL of THF at -78°C. The deep red mixture was stirred at -78°C for 1 hour, then allowed to warm up at room temperature and stirred overnight in the dark. The solution was washed twice with brine, the organic layer was dried over MgSO$_4$

and the solvent was removed under reduced pressure. The crude product was purified by column chromatography (silica, petroleum ether) to obtain the pure product as a yellowish oil (904 mg). **Yield:** 54%. **^{1}H-NMR** (500 MHz, CDCl$_3$) δ (ppm): 7.23 (1H, s), 6.70 (1H, s), 2.42 (3H, s), 1.87 (3H, d), 1.85 (3H, d), 0.25 (9H, s).

44. Compound **43** (550 mg, 1.14 mmol) and K$_2$CO$_3$ (2 g, 11.4 mmol) were suspended in a mixture of 8 mL MeOH and 8 mL CH$_2$Cl$_2$ in a Schelnk tube under argon. The mixture was stirred 3 hours at room temperature, then H$_2$O and CH$_2$Cl$_2$ were added, the phases were separated, the organic layer was dried over MgSO$_4$ and the solvent was removed under reduced pressure. The crude product was purified by column chromatography (silica, CH$_2$Cl$_2$:petroleum ether, 8:2) to obtain the pure product as a white sticky solid (407 mg). **Yield:** 88%. **^{1}H-NMR** (500 MHz, CDCl$_3$) δ (ppm): 7.26 (1H, s), 6.73 (1H, s), 3.35 (1H, s), 2.43 (3H, s), 1.91 (3H, s), 1.87 (3H, s).

45. 1,3,5-tribromobenzene (1.43 g, 4.55 mmol), PdCl$_2$(Ph$_3$)$_2$ (190 mg, 0.27 mmol) and LiCl (1.56 g, 36.7 mmol) were dissolved in 15 mL of dry toluene in a Schlenk tube under argon. 2-(tri-n-butylstannyl)pyridine was added and the mixture was stirred at 120°C for 1 day. Then H$_2$O and CH$_2$Cl$_2$ were added, the phases were separated, the organic layer was dried over MgSO$_4$ and the solvent was removed under reduced pressure. The crude product was purified by column chromatography (silica, CH$_2$Cl$_2$:petroleum ether, 1:1) to obtain the pure product as a white solid (400 mg). **Yield:** 30%. **^{1}H-NMR** (300 MHz, CDCl$_3$) δ (ppm): 8.71 (2H, dt, J = 4.7, 1.3 Hz), 8.55 (1H, t, J = 1.6 Hz), 8.22 (2H, d, J = 1.6 Hz), 7.79 (4H, m), 7.27 (2H, ddd, J = 6.8, 4.8, 1.8 Hz).

DTE-alk-dpybH. Compund **45** (400 mg, 1.3 mmol) was dissolved in 10 mL i-Pr$_2$NH and 50 mL THF in a Schlenk tube equipped with magnetic stirrer. Argon was then bubbled for 10 minutes and CuI (10 mg, 0.05 mmol) and PdCl$_2$(PPh$_3$)$_2$ (35 mg, 0.05 mmol) were added. The mixture was stirred at 45°C for 45 minutes. then **44** (407 mg, 1.0 mmol) was added and the mixture was stirred at 50°C for 24 hours. Then, the mixture was allowed to cool to room temperature, extracted with CH$_2$Cl$_2$/H$_2$O, the organic phase was dried over MgSO$_4$ and the solvent was removed under reduced pressure. The crude product was purified by flash chromatography (silica, CH$_2$Cl$_2$ 100%) to obtain **DTE-alk-dpybH** as a greenish solid (53 mg). **Yield:** 6%. **^{1}H-NMR** (400 MHz, CDCl$_3$) δ (ppm): 7.26 (2H, d, J = 4.0 Hz), 8.67 (1H, t, J = 1.7 Hz), 8.24 (2H, d, J = 1.7 Hz), 7.89 (2H, d, J = 8.0 Hz), 7.83 (2H, dd, J = 7.5, 1.8 Hz), 7.31 (3H, m), 6.74 (1H, s), 2.45 (3H, s), 1.94 (3H, s), 1.90 (3H, s). **^{13}C-NMR** (101 MHz, CDCl$_3$) δ (ppm): 156.21, 149.78, 143.37, 140.20, 139.92, 137.97, 136.88, 131.78, 130.16, 125.67, 125.30, 124.53, 124.27, 123.64, 122.66, 121.36, 120.70, 93.66, 82.09, 15.12, 14.39, 14.34.

3. Synthesis of the Iridium (III) complexes

3.1. General synthetic methods

Fac-**Ir(4methyl-2-ppy)₃** and its precursors were prepared according to the literature,[399] and the neutral iridium complexes were prepared following a reported procedure.[400] **4,4'-*p*-[(*N,N*-diethyl)aminostyryl]-2,2'-bipyridine**[401], **4-(*N*-diethyl)aminostyryl]-2-phenylpyridine**[402] and the iridium dimer precursor or **Ir-5**[178] were prepared as reported.
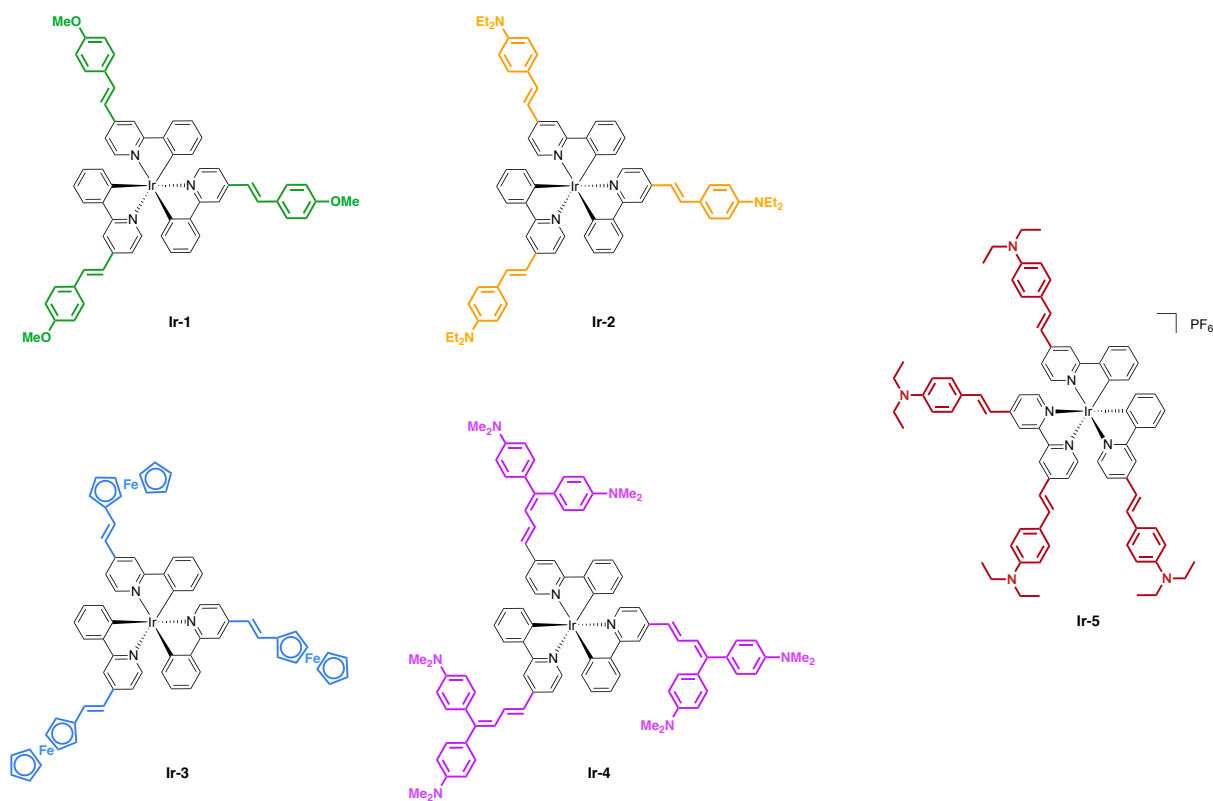
Figure 152. The Ir(III) complexes.

3.2. Synthesis of the neutral Ir(ppy)₃ complexes
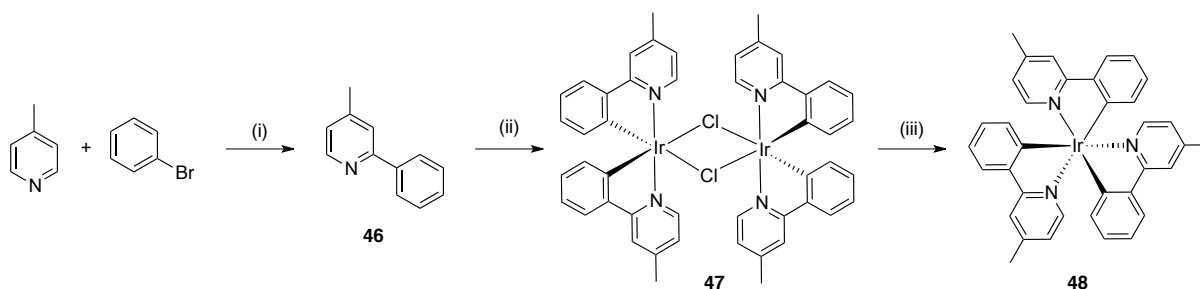
Scheme 13. Reagents and conditions: (i) Li, Et₂O, toluene, 0°C, 20 min → 30°C, 24 h; (ii) IrCl₃ · 3H₂O, 2-ethoxyethanol/H₂O, 100°C, 24 h; (iii) K₂CO₃, glycerol, 200°C, 3 days.

46. An excess of lithium (1.82 g, 272 mmol) was suspended in 40 mL of Et₂O. The suspension was cooled down to 0°C and bromobenzene (21.34 g, 136 mmol) in 50 mL of Et₂O was added dropwise during 20 minutes. The reaction mixture was stirred for overnight at room temperature. The freshly-prepared phenyllithium was added dropwise to a solution of 4-picoline (3.16 g, 34 mmol) in 90 mL toluene. The reaction was stirred at 30°C for 24 hours, distilled water was added dropwise, the residue was extracted with CH₂Cl₂, washed with water, dried over MgSO₄ and the solvent was removed under reduced pressure. The product was purified by column chromatography (silica, *n*-heptane:AcOEt, 9:1) to afford **46** as an orange\brown solid (2.44 g). **Yield:** 42%. **¹H-NMR** (400 MHz, CDCl₃) δ (ppm): 8.58 (1H, d, *J* = 5.0 Hz), 8.00 (2H, d, *J* = 7.2 Hz), 7.57 (1H, s), 7.49 (2H, t, *J* = 7.4 Hz), 7.43 (1H, t, *J* = 7.2 Hz), 7.08 (1H, d, *J* = 4.9 Hz), 2.44 (3H, s).

47. IrCl₃ · 3H₂O (500 mg, 1.675 mmol) and **46** (850 mg, 5.025 mmol) were suspended in a mixture of 2-ethoxyethanol/H₂O 3:1 (40 mL) in a Schlenk tube under inert atmosphere. The reaction mixture was heated at reflux for 24 h. The precipitate was decanted by centrifugation and the product was then washed with H₂O, EtOH and Et₂O. The solvent was removed by cannula to afford **47** as a yellow powder (682 mg). **Yield:** 72%. **¹H-NMR** (400 MHz, CDCl₃) δ (ppm): 9.06 (1H, d, *J* = 5.8 Hz), 7.69 (1H, s), 7.48 (1H, d, *J* = 7.6 Hz), 6.74 (1H, t, *J* = 7.2 Hz), 6.57 (1H, t, *J* = 6.8 Hz), 5.97 (1H, d, *J* = 7.9 Hz), 2.67 (1H, s).

48. Complex **47** (644 mg, 0.57 mmol), **46** (251 mg, 1.43 mmol) and K₂CO₃ (609 mg, 5.70 mmol) were suspended in 10 mL of glycerol in a Schlenk tube under inert atmosphere. The reaction mixture was heated at 200°C for 3 days, quenched with 15 mL of distilled water and the precipitate was decanted by centrifugation. The product was then washed with H₂O, EtOH and Et₂O. After every washing a centrifugation was made and the solvent was removed by cannula to afford **48** as a yellow powder (654 mg). **Yield:** 82%. **¹H-NMR** (400 MHz, CD₂Cl₂) δ (ppm): 7.77 (1H, s), 7.68 (1H, d, *J* = 7.7 Hz), 7.46 (1H, d, *J* = 5.6 Hz), 6.89 (1H, t, *J* = 7.2 Hz), 6.77 (3H, m), 2.46 (3H, s).
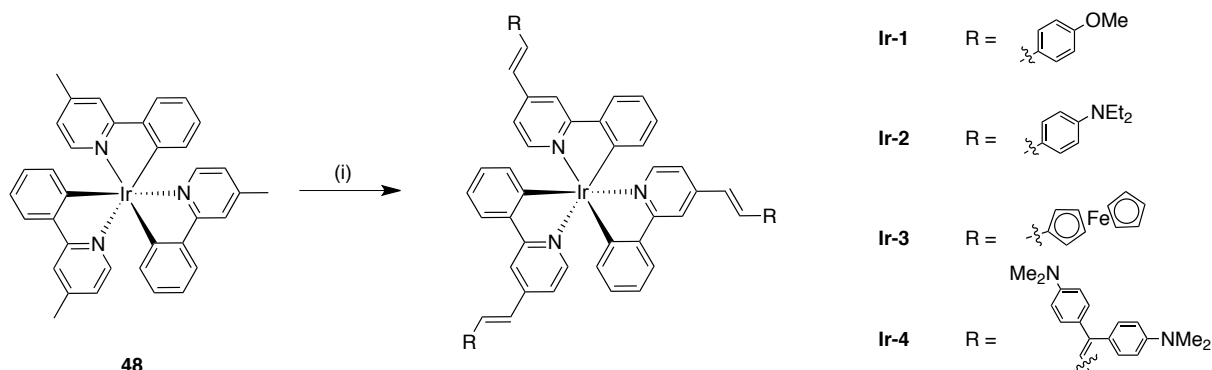
Scheme 14. Reagents and conditions: (i) *t*-BuOK , DMF, rt, 15 h.

General procedure:

Compound **48**, the appropriate aldehyde and *t*-BuOK were dissolved in DMF in a Schlenk tube under argon. The reaction mixture was stirred overnight at room temperature, quenched with H_2O and the precipitate was decanted by centrifugation. The product was then washed with methanol, diethyl ether and crystallized in a mixture of dichloromethane/diethyl ether to afford the desired complex as a red or orange powder.

Ir-1. Reactants: **48** (150 mg, 0.215 mmol), 4-methoxybenzaldehyde (117 mg, 0.861 mmol), *t*-BuOK (97 mg, 0.861 mmol). Solvents: DMF (15 mL). **Yield:** 36% (82 mg). **¹H-NMR** (400 MHz, CD_2Cl_2) δ (ppm): 8.01 (3H, bs), 7.75 (3H, d, *J* = 8.2 Hz), 7.66 (3H, d, *J* = 6.1 Hz), 7.54 (6H, d, *J* = 8.8 Hz), 7.32 (3H, d, *J* = 16.2 Hz), 7.08 (3H, dd, *J* = 6.0 Hz, 1.3 Hz), 7.01 (3H, d, *J* = 16.2 Hz), 6.99 (6H, d, *J* = 8.9 Hz), 6.94 (3H, m), 6.84 (6H, m), 3.89 (9H, s).

Ir-2. Reactants: **48** (150 mg, 0.215 mmol), 4-diethylaminobenzaldehyde (184 mg, 0.861 mmol), *t*-BuOK (97 mg, 0.861 mmol). Solvents: DMF (15 mL). **Yield:** 70% (177 mg). **¹H-NMR** (400 MHz, CD_2Cl_2) δ (ppm): 7.98 (3H, bs), 7.70 (3H, d, *J* = 7.8 Hz), 7.57 (3H, d, *J* = 5.8 Hz), 7.44 (6H, d, *J* = 8.9 Hz), 7.29 (3H, d, *J* = 16.1 Hz), 7.05 (3H, dd, *J* = 5.8 Hz, 1.1 Hz), 6.89 (12H, m), 6.71 (6H, d, *J* = 8.9 Hz), 3.41 (6H, q, *J* = 6.6 Hz), 1.19 (9H, t, *J* = 6.6 Hz).

Ir-3. Reactants: **48** (150 mg, 0.215 mmol), ferrocenecarboxaldehyde (184 mg, 0.861 mmol), *t*-BuOK (97 mg, 0.861 mmol). Solvents: DMF (15 mL). **Yield:** 71% (197 mg). **¹H-NMR** (400 MHz, CD_2Cl_2) δ (ppm): 7.92 (3H, s), 7.80 (3H, d, *J* = 7.2 Hz), 7.64 (3H, d, *J* = 6.2 Hz), 7.22 (3H, d, *J* = 16.1 Hz), 7.02 (3H, d, *J* = 6.3 Hz), 6.95 (3H, t, *J* = 7.8 Hz), 6.87 (6H, m), 6.77 (3H, d, *J* = 16.1 Hz), 4.56 (6H, m), 4.40 (6H, m), 4.18 (15H, s).

Ir-4. Reactants: **48** (150 mg, 0.215 mmol), 3,3-bis(4-(dimethylamino)phenyl)acrylaldehyde (260 mg, 0.861 mmol), *t*-BuOK (97 mg, 0.861 mmol). Solvents: DMF (15 mL). **Yield:** 68% (223 mg). **¹H-NMR** (400 MHz, CD_2Cl_2) δ (ppm): 7.75 (3H, s), 7.65 (3H, d, *J* = 7.7 Hz), 7.40 (3H, d, *J* = 6.1 Hz), 7.25 (9H, m), 7.14 (6H, d, *J* = 8.2 Hz), 6.88 (3H, m), 6.71 (24H, m), 6.62 (3H, d, *J* = 15.8 Hz), 3.04 (18H, s), 3.0 (18H, s).

3.3. Synthesis of the cationic Ir(ppy)₂(bpy) complex
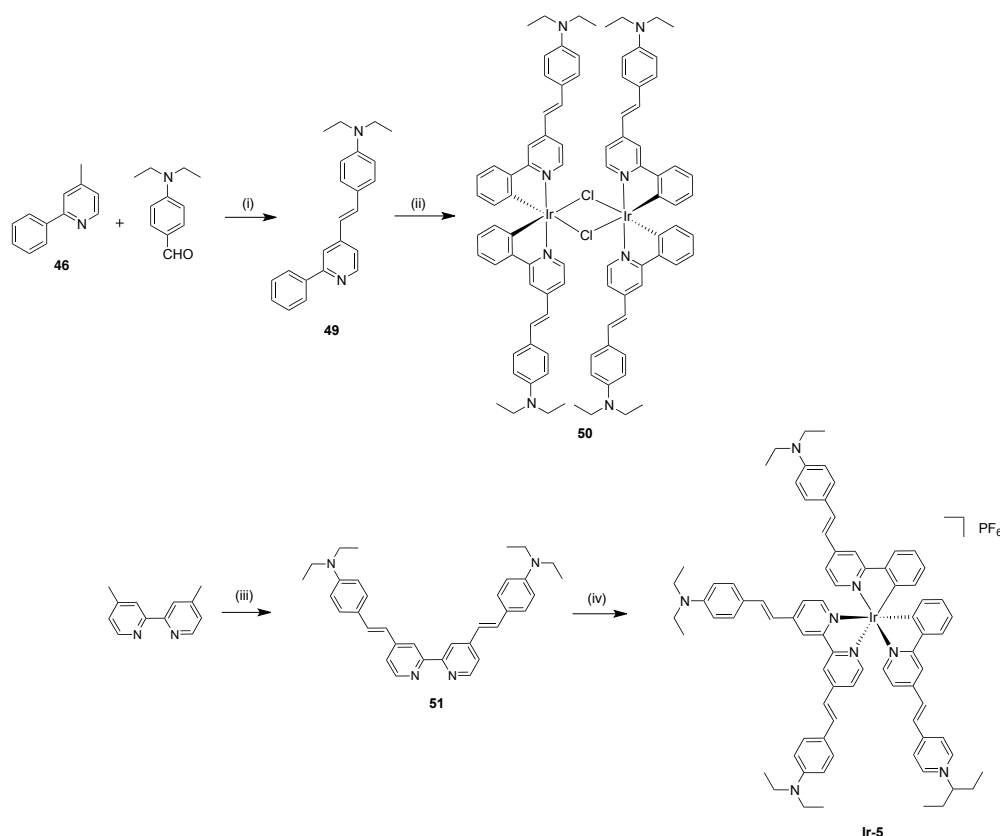
Scheme 15. (i) *t*-BuOK, DMF, 155°C, 15 h; (ii) IrCl₃·3H₂O, 2-ethoxyethanol/H₂O, 100°C, 24 h; (iii) a) *n*-BuLi, iPr₂NH, *p*-(N,N-diethyl)aminobenzaldehyde, THF, 0°C → -78°C → rt, 15 h; b) PPTS, toluene, 110°C, 4 h; (iv) AgPF₆, 1,2-dichloroethane, 84°C, 2 h → rt, 15 h.

49. 4-Methyl-2-phenylpyridine (500 mg, 2.96 mmol), 4-*N,N*-diethylaminobenzaldehyde (620 mg, 3.5 mmol) and *t*-BuOK (700 mg, 6.2 mmol) were dissolved in DMF (20 mL). The reaction mixture was heated at reflux overnight, then CH₂Cl₂ (150 mL) was added. The organic phase was washed with water and an aqueous solution of 1 M KOH, dried with MgSO₄ and the solvent was removed under reduced pressure. The crude product was purified by column chromatography (silica, CH₂Cl₂/petroleum ether 7:3) to obtain **49** as a yellow powder (546 mg). **Yield:** 56%. **¹H-NMR** (400 MHz, CDCl₃) δ (ppm): 8.61 (1H, d, *J* = 5.2 Hz), 8.06 (2H, d, J = 7.2 Hz), 7.75 (1H, s) 7.51 (2H, t, *J* = 7.4 Hz), 7.45 (3H, d, *J* = 8.5 Hz), 7.30 (1H, d, *J* = 16.3 Hz), 7.26 (1H, m), 6.86 (1H, d, *J* = 16.2 Hz), 6.68 (2H, d, *J* = 8.8 Hz), 3.40 (4H, q, *J* = 7.1 Hz), 1.20 (6H, t, *J* = 7.0 Hz).

50. IrCl₃·3H₂O (165 mg, 0.55 mmol) and **49** (550 mg, 1.66 mmol) were suspended in a mixture of 2-ethoxyethanol/H₂O 3:1 (16 mL) in a Schlenk tube under inert atmosphere. The reaction mixture was heated at reflux for 24 h. The precipitate was decanted by centrifugation and the product was then washed with H₂O, EtOH and Et₂O. The solvent was removed with cannula to afford **50** as an orange powder (290 mg). **Yield:** 30%. **¹H-NMR** (400 MHz, CD₂Cl₂) δ (ppm): 9.12 (4H, d, J = 5.9 Hz), 7.94

(4H, s), 7.63 (4H, d, J = 7.1 Hz), 7.41 (12H, m), 7.04 (4H, d, J = 16 Hz), 6.93 (4H, m), 6.83 (4H, t, J = 7.0 Hz), 6.64 (12H, m), 6.05 (4H, d, J = 8.0 Hz), 3.48 (16H, q, J = 6.8 Hz), 1.25 (24H, t, J = 6.8 Hz).

51. Diisopropylamine (607.1 mg, 6 mmol) was dissolved in THF (2.5 mL) in a Schlenk tube and the mixture was cooled to 0°C. *n*-BuLi solution (1.6 M in hexane, 3.75 mL, 6 mmol) was added slowly. After stirring one hour, the solution was cooled to -78°C and 4,4'-dimethyl-2,2'-bipyridine (501.1 mg, 2.72 mmol) in THF (13 mL) was added dropwise and the mixture stirred at low temperature for 2 hours. *p*-(N,N-diethyl)aminobenzaldehyde (957.1 mg, 5.4 mmol) was dissolved in 6 mL of THF (6 mL) and added slowly. The resulting mixture was stirred for one hour at low temperature and overnight at room temperature. After hydrolyzing with distilled water (12 mL), the phases were separated, the organic phase was dried over MgSO$_4$, filtered and the solvent was removed under reduced pressure. The dialcol was dissolved in toluene (40 mL) in a round-bottomed flask and PPTS (67.6 mg, 0.27mmol) was added. The mixture was heated at reflux for 4 hours. After cooling to room temperature, the solvent was removed under reduced pressure and dichloromethane (16 mL) was added. The mixture was washed with a saturated solution of NaHCO$_3$. The bipyridine precipitated, was filtered, abundantly washed with H$_2$O and Et$_2$O to obtain **51** as an orange powder (970 mg). **Yield:** 71%. **^{1}H-NMR** (400 MHz, CD$_3$Cl) δ (ppm): 8.63 (2H, d, J = 5.1 Hz), 8.48 (2H, s), 7.47 (4H, d, J = 8.9 Hz), 7.42 (2H, d, J = 16.2 Hz), 7.36 (2H, dd, J = 5.3, 1.8 Hz), 6.92 (4H, d, J = 16.2 Hz), 6.71 (2H, d, J = 8.9 Hz), 3.43 (8H, q, J = 7.1 Hz), 1.22 (12 H, t, J = 7.1 Hz).

Ir-5. A suspension of **50** (250 mg, 0.14 mmol), **51** (178 mg, 0.35 mmol) and AgPF$_6$ (88 mg, 0.35 mmol) in 1,2-dichloroethane (20 mL) was kept at reflux for 2 hours and stirred at room temperature for 16 hours. The solvent was removed under reduced pressure leaving a residue which was washed with Et$_2$O (3 x 20 mL). The compound was precipitated from Et$_2$O/CH$_2$Cl$_2$ giving **Ir-5** as a red solid after filtration (50 mg). **Yield:** 13%. **^{1}H-NMR** (500 MHz, CD$_2$Cl$_2$) δ (ppm): 8.32 (2H, s), 7.93 (2H, s), 7.84 (2H, d, J = 5.7 Hz), 7.80 (2H, d, J = 7.4 Hz), 7.42 (18H, m,), 7.08 (2H, t, J = 7.7 Hz), 7.02 (2H, d, J = 4.5 Hz), 6.95 (4H, m), 6.86 (2H, d, J = 16.0 Hz), 6.68 (8H, dd, J = 16, 8.9 Hz), 6.46 (2H, d, J = 7.9 Hz), 3.41 (16H, m), 1.20 (24H, m). **Elem. Anal. Calcd** for C$_{80}$H$_{84}$F$_6$IrN$_8$P: C, 64.24; H, 5.66; N, 7.50. **Found:** C, 64.28; H, 5.57; N, 7.31.

4. Synthesis of the Ruthenium(II) complex

Compounds **52** and **53** were synthesized following slightly modified procedures,[340] compound **58** and its precursors were prepared following a reported procedure.[339]
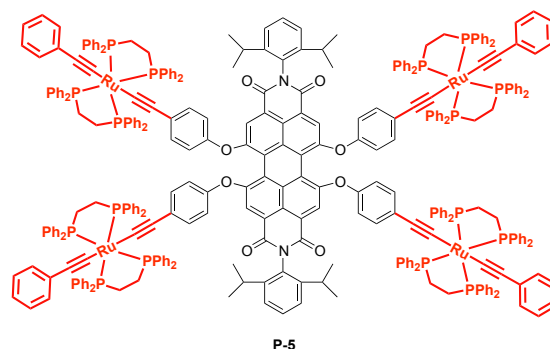
Figure 153. The Ru(II) perylene derivative.

4.1. Synthetic procedure
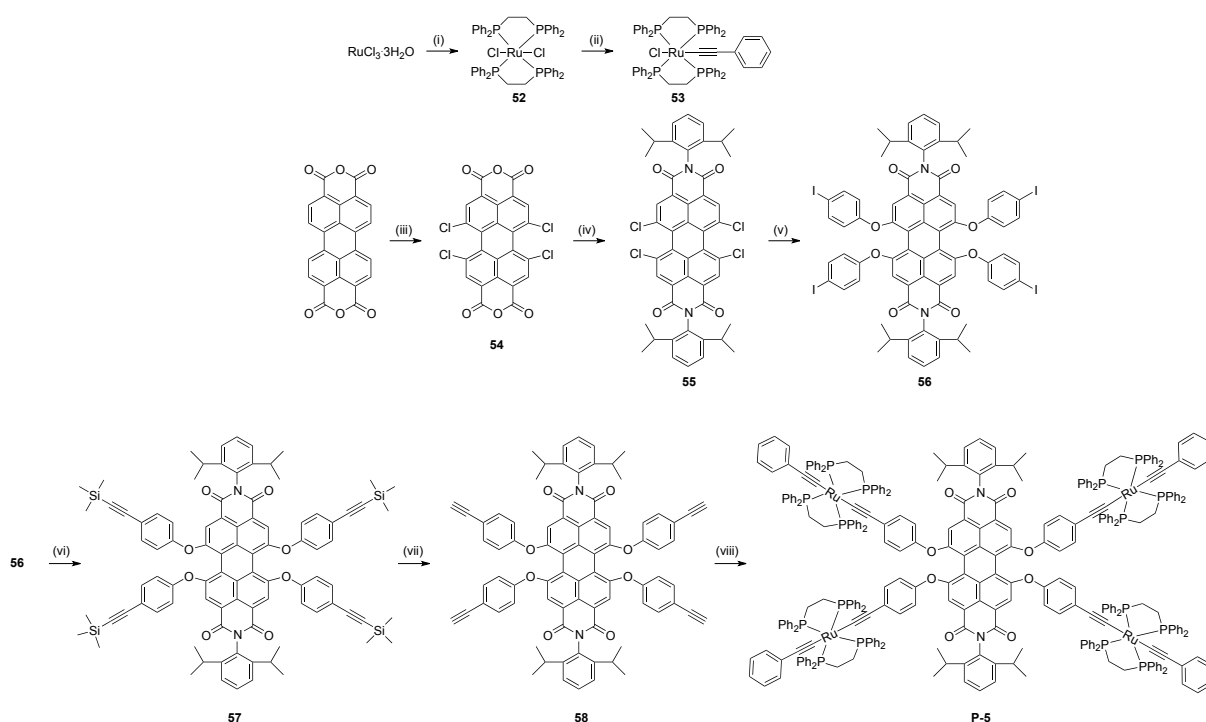
Scheme 16. Reagents and conditions: (i) 1,2-bis(diphenylphosphino)ethane, Bu$_4$NCl, CH$_2$Cl$_2$, rt, 12 h; (ii) phenylacetylene, NaPF$_6$, Et$_3$N, CH$_2$Cl$_2$, rt, 24 h; (iii) HClSO$_3$, I$_2$, 70°C, 5 h; (iv) 2,6-diisopropylaniline, propionic acid, 140°C, 24 h; (v) 4-iodophenol, K$_2$CO$_3$, N-Methyl-2-pyrrolidone, 70°C, 16 h; (vi) TMSA, PdCl$_2$(PPh$_3$)$_2$, CuI, PPh$_3$, Et$_3$N, THF, 70°C, 12 h; (vii) K$_2$CO$_3$, CH$_2$Cl$_2$, MeOH, rt, 24 h; (viii) **53**, NaPF$_6$, Et$_3$N, CH$_2$Cl$_2$, rt, 12 h.

52. RuCl$_3$·3 H$_2$O (412 mg, 1.58 mmol) and 1,2-bis(diphenylphosphino)ethane (1.33 g, 3.32 mmol) were mixed in a mortar and the mixture is mashed, then dissolved in CH$_2$Cl$_2$ (100 mL) with Bu$_4$NCl (440 mg, 1.58 mmol) and stirred for 12 hours. The mixture was then filtered, the solid was dissolved in a minimum

amount of CH_2Cl_2 and recrystallized from pentane to obtain **52** as an orange powder (1.19 g). **Yield:** 78%. **^{1}H-NMR** (400 MHz, CD_2Cl_2) δ (ppm): 7.30 (24H, m), 7.05 (16H, m), 2.77 (8H, m).

53. Complex **52** (100 mg, 0.1 mmol) and phenylacetylene (12 μL, 0.1 mmol) were dissolved in CH_2Cl_2 (10 mL). Et_3N (70 μL, 0.5 mmol) and $NAPF_6$ (9 mg, 0.05 mmol) were added and the mixture was stirred at room temperature for 24 hours. The yellow solid that formed was filtered and dried, to obtain pure **53** (82 mg). **Yield:** 79%. **^{1}H-NMR** (400 MHz, CD_2Cl_2) δ (ppm): 7.45 (18H, m), 7.02 (27H, m), 2.63 (8H, m).

54. Perylene-3,4,9,10-tetracarboxylic dianhydride (2.0 g, 5.1 mmol) and iodine (340 mg, 1.34 mmol) were dissolved in $HClSO_3$ (20 mL) in a Schlenk tube under argon. The mixture was heated at 70°C stirring for 5 hours. The reaction mixture was added dropwise into ice cold water and the resulting precipitate was filtered, washed generously with water and dried in under wacuum to obtain **54** as an orange solid (2.4 g). **Yield:** 89%. **^{1}H-NMR** (400 MHz, CD_2Cl_2) δ (ppm): 8.77 (4H, s).

55. Compound **54** (1.06 g, 2.0 mmol) and 2,6-diisopropylaniline (1.7 mL, 10.0 mmol) were dissolved in propionic acid (13 mL) under argon atmosphere. The mixture was heated at 140°C stirring for 24 hours. Afterwards, it was cooled to room temperature and added dropwise to a saturated $NaHCO_3$ solution, CH_2Cl_2 was added, the organic phase was separated and washed with water. The crude product was purified by column chromatography (silica, hexane:CH_2Cl_2, 1:1). The desired product was obtained as a red powder (1.58 g) **Yield:** 93%. **^{1}H-NMR** (400 MHz, $CDCl_3$) δ (ppm): 8.90 (4H, s), 7.66 (2H, t, J = 7.8 Hz), 7.49 (4H, d, J = 7.8 Hz), 3.04 (2H, m), 2.67 (12H, m).

56. Compound **55** (696 mg, 0.82 mmol) and p-iodophenol (1.02 g, 4.64 mmol) were dissolved in N-methyl-2-pyrrolidone (35 mL) in a Schlenk tube under argon. K_2CO_3 (480 mg, 3.11 mmol) was added and the mixture was heated at 70°C stirring overnight. The reaction mixture was cooled to room temperature and HCl 2 N (114 mL) was added. The precipitated product was dissolved in AcOEt, washed with water, the solvent was evaporated and the crude product was a purified by column chromatography (silica, hexane:AcOEt, 9:1) to give pure **56** as a red solid (1.06 g) **Yield:** 82%. **^{1}H-NMR** (400 MHz, $CDCl_3$) δ (ppm): 8.26 (4H, s), 7.61 (2H, d, J = 8.7 Hz), 7.47 (16H, m), 7.30 (4H, t, J = 7.7 Hz), 2.70 (4H, m), 1.18 (24H, m)

57. Compound **56** (304 mg, 0.19 mmol), trimethylsilylacetylene (160 μL, 1.14 mmol), $PdCl_2(PPh_3)_2$ (8 mg, 0.011), CuI (1 mg, 0.005 mmol) and PPh_3 (4.2 mg, 0.011 mmol) were dissolved in THF (12 mL) in a Schlenk tube under argon. Et_3N (8 mL) was added and the mixture was heated at 70°C for 12 hours. The mixture was then cooled to room temperature, the solvent was evaporated and the crude product was purified by column chromatography (silica, hexane:CH_2Cl_2, 1:1). The desired product was obtained as a red powder (230 mg) **Yield:** 83%. **^{1}H-NMR** (400 MHz, $CDCl_3$) δ (ppm): 8.23 (4H, s), 7.47 (2H, d, J = 7.8 Hz), 7.44 (16H, d, J = 3.4 Hz), 7.29 (4H, d, J = 7.8 Hz), 2.70 (4H, m), 1.15 (24H, d, J = 6.8 Hz), 0.27 (36H, s).

58. Compound **57** (157 mg, 0.11) was dissolved in a mixture of CH_2Cl_2 (1 mL) and MeOH (3 mL). K_2CO_3 was added and the mixture was stirred at room temperature for 24 hours. Then the solvent was evaporated, the crude product dissolved in CH_2Cl_2 and washed with water. The crude product was purified by column chromatography (silica, hexane:CH_2Cl_2, 3:7). The desired product was obtained as a red powder (124 mg) **Yield:** 96%. **^{1}H-NMR** (400 MHz, CDCl$_3$) δ (ppm): 8.28 (4H, s), 7.48 (2H, d, J = 7.8 Hz), 7.44 (16H, d, J = 3.4 Hz), 7.29 (4H, t, J, = 7.8 Hz), 3.09 (4H, s), 2.7 (4H, m), 1.15 (24 H, d, J = 6.8 Hz). **Elem. Anal. Calcd** for $C_{80}H_{58}N_2O_8$: C, 81.75; H, 4.97; N, 2.38. **Found:** C, 81.72; H, 5.04; N, 2.37.

P-5. Complex **53** (73 mg, 0.07 mmol) and compound **58** (20 mg, 0.016) were dissolved in CH_2Cl_2 in a Schlenk tube under argon. $NaPF_6$ (14.7 mg, 0.07 mmol) and Et$_3$N (25 μL) were added and the mixture was stirred at room temperature protected from the light overnight. The solvent was then evaporated and the crude product was purified by column chromatography (silica, hexane:CH_2Cl_2, 1:1). The desired product was obtained as a violet solid (48 mg) **Yield:** 58%. **^{1}H-NMR** (400 MHz, CD$_2$Cl$_2$) δ (ppm): 8.26 (4H, s), 7.65 (72H, m), 7.16 (134H, m), 2.73 (32H, m), 1.13 (24H, d, J = 7.0 Hz). **Elem. Anal. Calcd** for $C_{320}H_{266}N_2O_8P_{16}Ru_4$: C, 74.38; H, 5.19; N, 0.54. **Found:** C, 74.31; H, 5.22; N, 0.53.

5. X-ray crystal structures

5.1. Pt(3-eg)

Orange crystals were grown by slow diffusion of Et_2O into a concentrated CH_2Cl_2 solution of **Pt(3-eg)**. A crystal of dimensions 0.45 mm x 0.36 mm x 0.1 mm mounted on a cryoloop was used for data collection. Intensity data were collected at 150 K in a D8 VENTURE Bruker AXS diffractometer. Crystal data for $C_{22} H_{22} Cl N_2 O_4 Pt$) ($M$ = 608.95): Mo-Kα radiation (λ = 0.71073 Å), T = 150 K; Monoclinic $P 2_1/c$ (I.T.#14), a = 14.7007(18), b = 17.547(2), c = 8.3565(9) Å, β = 105.283(4) °, V = 2079.3(4) Å^3. Z = 4, d = 1.945 g.cm^{-3}, μ = 6.909 mm^{-1}. The structure was solved by direct methods using the *SHELXT* program,[403] and then refined with full-matrix least-square methods based on F^2 (*SHELXL-2014*).[404] All non-hydrogen atoms were refined with anisotropic atomic displacement parameters. H atoms were finally included in their calculated positions. A final refinement on F^2 with 4760 unique intensities and 271 parameters converged at $\omega R(F^2)$ = 0.1689 ($R(F)$ = 0.0538) for 3997 observed reflections with $I > 2\sigma(I)$.

CCDC: 1556598 contains the supplementary crystallographic data. These data are provided free of charge by The Cambridge Crystallographic Data Centre. Table 25 contains a summary of crystallographic data.

Empirical formula	$C_{22} H_{22} Cl N_2 O_4 Pt$
Formula weight	608.95
Temperature	150 *K*
Wavelength	0.71073 Å
Crystal system	Monoclinic
Space group	$P\ 2_1/c$
a (Å)	14.7007(18)
b (Å)	17.547(2)
c (Å)	8.3565(9)
α (°)	90
β (°)	105.283(4)
γ (°)	90
Volume (Å^3)	2079.3(4)
Z	4
ρ_{calcd} (g cm^{-3})	1.945
μ (mm^{-1})	6.909
F(000)	1180
Crystal size (mm^3)	0.450 x 0.360 x 0.100
Crystal colour	Orange
θ range	3.099-27.483
h_min, h_max	-19, 19
k_min, k_max	-21, 22

l_min, l_max	-10, 10
Reflections collected / unique	23629 / 4760 [R(int)[a] = 0.0533]
Reflections [I>2σ]	3997
Completeness to theta_max	0.998
Absorption correction type	Multi-scan
Max. and min. transmission	0.501-0.261
Refinement method	Full-matrix least-squares on F^2
Data / restraints / parameters	4760 / 0 / 271
[b]Goodness-of-fit	1.504
Final R indices [I>2σ]	$R1^c = 0.0538$, $wR2^d = 0.1689$
R indices (all data)	$R1^c = 0.0643$, $wR2^d = 0.1837$
Largest diff. peak and hole	2.509, -2.731 e⁻.Å⁻³

Table 25. Crystallographic data for complex **Pt(3-eg)**.
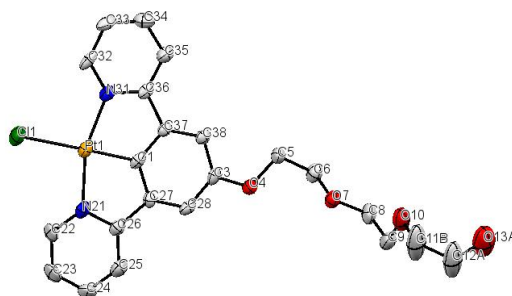
Bond lengths:

Pt1 - C1 = 1.899(8) Å, Pt1 - N31 = 2.041(7) Å, Pt1 - N21 = 2.043(7) Å, Pt1 - Cl1 = 2.417(2) Å, C3 - O4 = 1.357(10) Å.

Angles:

C1 – Pt1 - N31 = 81.0(3), C1 - Pt1 - N21 = 80.0(3), N31 - Pt1 – Cl1 = 99.9(2), N21- Pt1 - Cl1 = 99.2(2), C3 - O4 - C5 = 116.7(7).

5.2. Pt-DTE(o)

Yellow crystals were grown by slow diffusion of Et_2O into a concentrated CH_2Cl_2 solution of **Pt-DTE(o)**. A yellow crystal of dimensions 0.30 mm x 0.04 mm x 0.03 mm mounted in a glass capillary was used for data collection. Intensity data were collected at 150 K in a D8 VENTURE Bruker AXS diffractometer. Crystal data for C_{33} H_{23} Cl_3 F_6 N_2 Pt S_2 (M = 927.09): Mo-Kα radiation (λ = 0.71073 Å), T = 150 K; triclinic P -1 (I.T.#2), a = 8.6967(6), b = 9.2285(5), c = 21.3827(13) Å, α = 96.101(2), β = 100.242(2), γ = 101.099(2) °, V = 1639.55(18) Å^3. Z = 2, d = 1.878 g.cm^{-3}, μ = 4.713 mm^{-1}. The structure was solved by dual-space algorithm using the *SHELXT* program,[403] and then refined with full-matrix least-square methods based on F^2 (*SHELXL-2014*).[404] All non-hydrogen atoms were refined with anisotropic atomic displacement parameters. H atoms were finally included in their calculated positions. A final refinement on F^2 with 7495 unique intensities and 427 parameters converged at $\omega R(F^2)$ = 0.1018 ($R(F)$ = 0.0392) for 6666 observed reflections with I > 2σ(I).

CCDC: 1516131 contains the supplementary crystallographic data. These data are provided free of charge by The Cambridge Crystallographic Data Centre. Table 26 contains a summary of crystallographic data.

Empirical formula	C_{33} H_{23} Cl_3 F_6 N_2 Pt S_2
Formula weight	927.09
Temperature	150 K
Wavelength	0.71073 Å
Crystal system	Triclinic
Space group	P -1
a (Å)	8.6967(6)
b (Å)	9.2285(5)
c (Å)	21.3827(13)
α (°)	96.101(2)
β (°)	100.242(2)
γ (°)	01.099(2)
Volume (Å^3)	1639.55(18)
Z	2
ρ_{calcd} (g cm^{-3})	1.878
μ (mm^{-1})	4.713 mm-1
F(000)	900
Crystal size (mm^3)	0.300 x 0.040 x 0.030
Crystal colour	Yellow
θ range	2.935-27.483
h_min, h_max	-11, 11
k_min, k_max	-10, 11
l_min, l_max	-27, 27
Reflections collected / unique	32167 / 7495 [R(int)^a = 0.0530]

Reflections [I>2σ]	6666
Completeness to theta_max	0.998
Absorption correction type	Multi-scan
Max. and min. transmission	0.868 , 0.651
Refinement method	Full-matrix least-squares on F^2
Data / restraints / parameters	7495 / 0 / 427
[b]Goodness-of-fit	1.059
Final R indices [I>2σ]	$R1^c$ = 0.0392, $wR2^d$ = 0.1018
R indices (all data)	$R1^c$ = 0.0473, $wR2^d$ = 0.1063
Largest diff. peak and hole	4.501-1.190 e$^-$.Å^{-3}

Table 26. Crystallographic data for complex **Pt-DTE(o)**.

Bond lengths:

Pt1 - C7 = 1.903(5) Å, Pt1 - N1 = 2.028(5) Å, Pt1 - N2 = 2.037(4) Å, Pt1 - Cl1 = 2.412(1) Å, C17 - C18 = 1.360(8) Å, C18 - C19 = 1.430(7) Å, C20 - C24 = 1.360(8) Å, S1 - C17 = 1.741(6) Å, S1 - C31 = 1.731 (6) Å.

Angles:

N2 - Pt1 - N1= 161.01(18), C7 - Pt1 - N1 = 80.70(2), C7 - Pt1 - N2 = 80.36(19).

Torsions:

C15 - C16 - C17 - C18 = 37.10(9).
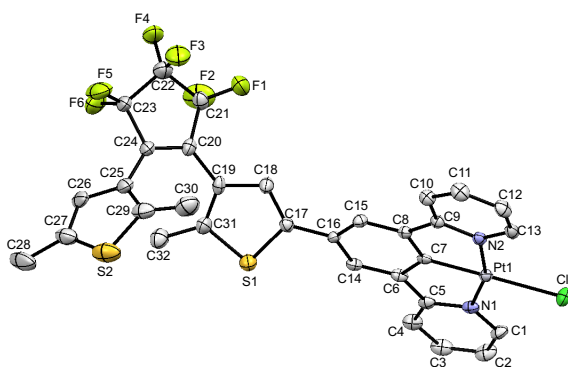
5.3. Pt-DTE(c)

Dark blue crystals were grown by slow diffusion of Et_2O into a concentrated CH_2Cl_2 solution of **Pt-DTE(c)**. A blue crystal of dimensions 0.20 mm x 0.08 mm x 0.03 mm mounted in a glass capillary was used for data collection. Intensity data were collected at 150 K in a D8 VENTURE Bruker AXS diffractometer. Crystal data for $C_{32} H_{21} Cl F_6 N_2 Pt S_2$ (M = 842.17): Mo-Kα radiation (λ = 0.71073 Å), T = 150 K; triclinic P -1 (I.T.#2), a = 7.3571(15), b = 9.5278(19), c = 21.126(4) Å, α = 92.202(7), β = 93.515(7), γ = 101.166(6) °, V = 1448.2(5) Å^3. Z = 2, d = 1.931 g.cm^{-3}, μ = 5.147 mm^{-1}. The structure was solved by dual-space algorithm using the *SHELXT* program,[403] and then refined with full-matrix least-square methods based on F^2 (*SHELXL-2014*).[404] All non-hydrogen atoms were refined with anisotropic atomic displacement parameters. H atoms were finally included in their calculated positions. A final refinement on F^2 with 6497 unique intensities and 320 parameters converged at $\omega R(F^2)$ = 0.1386 ($R(F)$ = 0.0637) for 4883 observed reflections with $I > 2\sigma(I)$.

CCDC: 1517807 contains the supplementary crystallographic data. These data are provided free of charge by The Cambridge Crystallographic Data Centre. Table 27 contains a summary of crystallographic data.

Empirical formula	$C_{32} H_{21} Cl F_6 N_2 Pt S_2$
Formula weight	842.17
Temperature	150 *K*
Wavelength	0.71073 Å
Crystal system	Triclinic
Space group	*P* -1
a (Å)	7.3571(15)
b (Å)	9.5278(19)
c (Å)	21.126(4)
α (°)	92.202(7)
β (°)	93.515(7)
γ (°)	101.166(6)
Volume (Å^3)	1448.2(5)
Z	2
ρ_{calcd} (g cm^{-3})	1.931
μ (mm^{-1})	5.147
F(000)	816
Crystal size (mm^3)	0.200 x 0.080 x 0.030
Crystal colour	Orange
θ range	2.925-27.483
h_min, h_max	-9, 9
k_min, k_max	-12, 12
l_min, l_max	-27, 27
Reflections collected / unique	24789 / 6497 [R(int)^a = 0.1058]

Reflections [I>2σ]	4883
Completeness to theta_max	0.976
Absorption correction type	Multi-scan
Max. and min. transmission	0.857 , 0.617
Refinement method	Full-matrix least-squares on F^2
Data / restraints / parameters	6497 / 0 / 320
[b]Goodness-of-fit	1.025
Final R indices [I>2σ]	$R1^c = 0.0637$, $wR2^d = 0.1386$
R indices (all data)	$R1^c = 0.0994$, $wR2^d = 0.1574$
Largest diff. peak and hole	5.567-2.358 $e^-.Å^{-3}$

Table 27. Crystallographic data for complex **Pt-DTE(c)**.

Bond lengths:

Pt1 - C7 = 1.903(10) Å, Pt1 - N1 = 2.017(9) Å, Pt1 - N2 = 2.036(8) Å, Pt1 - Cl1 = 2.401(3) Å, C17 - C18 = 1.350(15) Å, C18 - C19 = 1.399(10) Å, C20 - C24 = 1.413(17) Å, S1 - C17 = 1.741(6) Å, S1 - C31 = 1.731 (6) Å.

Angles:

N2 - Pt1 - N1= 161.00(18), C7 - Pt1 - N1 = 79.90(4), C7 - Pt1 - N2 = 81.20(4).
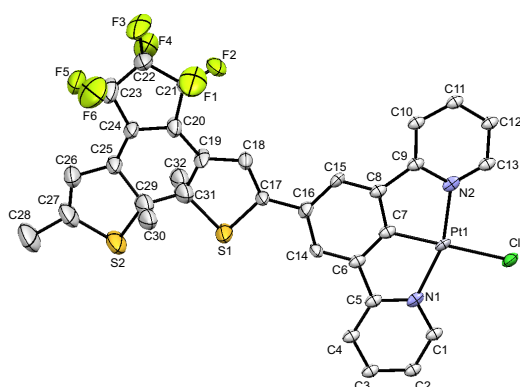
Torsions:

C15 - C16 - C17 - C18 = -7.00(2).

6. Preparation of composite films and SHG measurements

Thin films of the complex Pt-DTE in open form (5% w/w relative to the polymer) dispersed in poly(methyl methacrylate) (PMMA) or polystyrene (PS) were prepared by spin-coating a few drops of a dichloromethane solution on ordinary non-pretreated glass substrates (thickness 1 mm) previously cleaned with water/acetone. The spinning parameters were set at the following values: RPM 1 = 800; ramp 1 = 1 s, time 1 = 5 s; RPM 2 = 2000; ramp 2 = 4 s, time 2 = 83 s. Closed form of the Pt-DTE film in PS or PMMA matrix was obtained from Pt-DTE in open form after irradiation with UV light at 325 nm (continuous wave (cw) mode power, 15 mW) for 15 minutes (Figure 154)
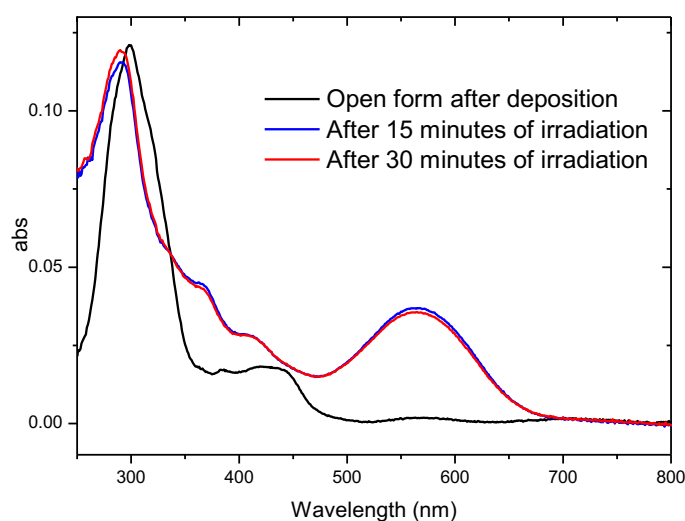
Figure 154. Switching of the **Pt-DTE**/PMMA film from open to closed form by irradiation with UV light at 325 nm.

The thickness of the films: 1.83 ± 0.11 μm for PS and 0.96 ± 0.06 μm for PMMA matrix were measured using an α-step stylus profilometer DektaK XT. Electronic absorption spectra of the composite films were recorded by a spectrophotometer Mahamatzu 3600.

Corona Poling Setup

The fundamental incident light was generated by a 1064 nm Q-switched Nd:YAG laser. The output pulse was attenuated to 0.5 mJ and was focused on the sample, placed over the hot stage. Moreover, the fundamental beam was polarized in the incidence plane (p-polarized) with an incidence angle of about 55° respect to the sample in order to optimize the SHG signal. Poling process was performed in a N_2 atmosphere and a corona-wire voltage (up to 10 kV across a 10 mm gap) was applied. After rejection of the fundamental beam by an interference filter and a glass cutoff filter, the p-polarized SHG signal at 532 nm was detected with a UV-vis photomultiplier (PT). The output signal from the PT was set to a digital store oscilloscope and then processed by a computer with dedicated software.

Maker Fringe and Second Harmonic Photoswitch

In the Maker fringe experiment, the SH intensity was detected as a function of the incidence angle of the fundamental beam and normalized with respect to that of a calibrated quartz crystal wafer (X-cut) 1 mm thick whose d_{11} is 0.46 pm/V. The incidence angle was changed by rotating the poled film, while the polarization of the fundamental and SH beam could be changed by a half-wave plate and a cube beam splitter, respectively. In order to determine the nonzero independent components of the susceptibility tensor for poled films ($C_{\infty v}$ symmetry) Maker fringe measurements were conducted with different polarizations: $p \rightarrow p$, $s \rightarrow p$, and $45 \rightarrow s$. In the SHG photoswitch experiment the poled film was rotated at incidence angle of 55° and the fundamental and SH beams were p-polarized. With the purpose of changing the photocyclization state, the poled film was alternately irradiated with UV light at 325 nm (continuous wave (cw) mode power, 15mW) and visible light with a cutoff filter at 550 nm (cw mode power, 140 mW).

IV. CONCLUSION

During my PhD, I prepared, fully characterized and studied the luminescent and nonlinear optical properties of many new organometallic compounds.

At first, the luminescent properties of two new flexibly-linked dinuclear platinum(dipyridylbenzene) complexes and a mononuclear reference were presented. The flexible tetra(oxyethylene) tether has a fundamental role in favouring the formation of excimers through face-to-face interaction. While the mononuclear **Pt(3-eg)** does not emit as excimer in solution, the dinuclear **Pt$_2$(4-eg)** gives rise to an additional emission band in the near-IR attributed to excimer emission, while **Pt$_2$(alk-4-eg)** shows higher propensity to form excimers in solution. This is due both to the presence of the flexible linker and the absence of the electron-donating substituents on the dipyridylbenzene ligand, which were previously proved to inhibit excimer formation. By controlling the solvent and reversibly binding metal cations, we could modulate the emission wavelength from the green to the red. These are the first examples of binuclear platinum complexes in which the two metal centres are linked by a flexible chain and that exhibit spectral changes purely due to excimeric formation. The results that we obtained will be useful for the future design of switchable and deep-red triplet emitters. In the near future, the second-order NLO properties of such complexes will be studied in solution and in a polymeric matrix: we expect a modulation of the NLO properties by going from the linear to the bent form.

The photochromic behaviour of two platinum(dipyridylbenzene) complexes bearing a dithienylethene fragment were then discussed. In the two complexes, the photochromic unit is linked to the platinum fragment in different ways to modulate the electronic communication between the two moieties. Both complexes show photochromic behaviour in solution with almost quantitative conversion from the open to the closed form upon irradiation, with superior performances compared to those of the respective ligands, confirming that the coordination to the platinum imparts stability to the molecule. The complexes are weakly emissive in solution because the photocyclization reaction of the DTE fragment quenches the fluorescence, but they are emissive in a rigid matrix at 77 K. Emission studies at different temperatures revealed that the presence of different linkers between the platinum and the DTE moieties has an influence on the photochromic properties of the complexes. In particular, if the photochrome is directly linked to the platinum centre, the electronic communication between the two units is better. The second-order NLO response of such complexes in solution was studied and it was observed that the value of $\mu\beta$ was greatly enhanced upon ring-closing: this is explained by a delocalization increase of the π-electron system in the closed isomer. Surprisingly, even though the tether between the two units is not π-conjugated, complex **Pt-O-DTE** shows a high NLO activity: this is the very first time that such behaviour is observed and it opens new routes for the design of photoswitchable NLO compounds.

The NLO response of **Pt-DTE** was also studied in a rigid polymeric film: it has a typical behaviour with fairly good second-order susceptibility tensor values. Polymeric films with commutable NLO response were prepared: unfortunately, due to the irreversible loss of orientation through the photoisomerization processes, they lose some SHG signal during the switches. An important objective to achieve in the future is to improve the stability of such films by using, for example, the cross-linking technique for preparation of the polymer films in order to inhibit the reorientation of the chromophores during photoisomerization.

A series of Pt(II) 1,3-di(2-pyridyl)benzene complexes with different aromatic pendants, linked to the platinum unit with different linkers, were synthesized and their second-order NLO properties were studied. As a general trend, the $\mu\beta_{EFISH}$ values increase with the electron-richness of the aromatic pendants and with the planarity of the system. By substituting the double bond with the thiophene, as a linker, we expected an increase in the NLO properties. This happens if the pendant is a pyrene, but the trend is not reproducible: when the aromatic substituent is a triphenylamine, the $\mu\beta_{EFISH}$ value decreases upon insertion of a thiophene in the molecular structure. This is probably due to some torsions within the molecule and indicates that the geometry must be taken into account when trying to predict the NLO behaviour of a complex. Besides, substitution of the alkenyl linker with an alkynyl did not lead to any particular benefit. Our study made evident that, in our case, it is not necessary to have a strong donor substituent on the styryl group in order to reach a high second-order NLO response, but it is mandatory to have a flat structure. The simple **Pt-1**, bearing a cyclometallated 5-styryl-1,3-di(2-pyridyl)benzene already shows a good quadratic hyperpolarizability and has a great potential for application in photonics.

In the last part, the TPA properties of four new 3,4,9,10-perylenetetracarboxylic diimide derivatives substituted at the 1,6,7,12-bay positions with highly conjugated groups were presented. The compounds demonstrated a good TPA response, in line with the best performing PTDCIs reported to date. The TPA activity was higher for the compound bearing 4,7-di(2-thienyl)benzo[c][1,2,5]thiadiazole, strong planar electron-withdrawing substituents. The TPA cross-section values decreased when smaller electron-donating substituents were used and dropped if the conjugation between the central PTCDI core and the lateral group was interrupted. A novel metal complex composed by a central PTDCI core and four Ru(II) σ-acetylide units at the 1,6,7,12-bay positions was successfully synthesized and characterized: this complex is expected to possess a remarkably high TPA activity, by virtue of the four Ru(II) units, which will be studied soon.

TPA cross-sections of one mononuclear and one dinuclear Ru^{II} complexes were measured. The values we found were moderately good: as expected by the presence of two metal units, the binuclear complex **Ru-2** displays better nonlinear absorption. These complexes are of particular interest because they undergo a photochemical reaction upon irradiation with the laser beam. Even though this phenomenon caused some difficulties in the measurement of the TPA response, it prompted us to use these complexes as initiators for two-photon induced polymerization.

Finally, the TPA activity of a neutral and cationic iridium(III) complexes with cyclometalated ligands was reported. The neutral complexes have good TPA cross sections on a wide range of wavelengths, which are higher than that of the unsubstituted Ir(ppy)$_3$ complex reported in literature. This remarkable activity is reached with relatively small molecules with simple substituents. The highest TPA cross-section values were found for the complex that bears the most electron-donating substituents and has the most extended π-conjugated system.

The cationic Ir(III) compound demonstrated to be a multifunctional complex. Its luminescent properties were first studied: it is not emissive at room temperature because the *cis-trans* isomerization of double bonds provides an efficient non-radiative decay pathway, but it is emissive at 77 K in a rigid matrix. It has a good second-order NLO response, moderately high if compared to cationic Ir(III) complexes reported in literature, and also a very good TPA activity, higher than that of reported compounds of the same class. This complex will be tested in biomedical research.

In summary, the great potential of several organometallic complexes in optoelectronics was demonstrated. We highlighted how, by choosing the appropriate ligands and coordination sphere it is possible to tune and enhance the photophysical properties of many coordination compounds

V. BIBLIOGRAPHY

[1] R. C. Evans, P. Douglas, C. J. Winscom, *Coord. Chem. Rev.* **2006**, *250*, 2093−2126.

[2] B. J. Coe, in *Comprehensive Coord. Chem. II*, Vol. 9, **2004**, Elsevier: Oxford, U.K.

[3] a) B. Valeur, *Molecular fluorescence: principles and applications*, **2001**, Wiley WHC; b) M. Sauer, J. Hofkens, J. Enderlein, *Handbook of fluorescence spectroscopy and imaging: from ensemble to single molecules*, **2011**, Wiley, WHC.

[4] H. Yersin, A. F. Rausch, R. Czerwieniec, T. Hofbeck, T. Fischer, *Coord. Chem. Rev*. **2011**, *255*, 2622−2652.

[5] a) Y. Chi, P.-T. Chu, *Chem. Soc. Rev.* **2010**, *39*, 638−655; b) H. Xu, R. Chen, Q. Sun, W. Lai, Q. Su, W. Huang, X. Liu, *Chem. Soc. Rev.* **2014**, *43*, 3259−3302; c) V. W.-W. Yam, K. M.-C. Wong, *Chem. Commun.* **2011**, *47*, 11579−11592.

[6] K. Li, G. S. M. Tong, Q. Wan, G. Cheng, W.-Y. Tong, W.-H. Ang, W.-L. Kwong, C.-M. Che, *Chem. Sci.* **2016**, *7*, 1653−1673.

[7] J. A. G. Williams, S. Develay, D. L. Rochester, L. Murphy, *Coord. Chem. Rev.* **2008**, *252*, 2596−2611.

[8] a) M. Mauro, A. Aliprandi, D. Septiadi, N. S. Kehr, L. De Cola, *Chem. Soc. Rev.* **2014**, *43*, 4144−4166; b) E. Baggaley, J. A. Weinstein, J. A. G. Williams, *Coord. Chem. Rev.* **2012**, *256*, 1762−1785.

[9] P.-H. Lanoë, J.-L. Fillaut, L. Toupet, J. A. G. Williams, H. Le Bozec, V. Guerchais, *Chem. Commun.* **2008**, 4333−4335.

[10] W. B. Connick, R. E. Marsh, W. P. Schaefer, H. B. Gray, *Inorg. Chem.* **1997**, *36*, 913−922.

[11] J. A. G. Williams, *Top. Curr. Chem.* **2007**, *281*, 205−268.

[12] V. M. Miskovski, V. H. Houlding, C.-M. Che, Y. Wang, *Inorg. Chem.* **1993**, *32*, 2518−2524.

[13] a) J. Brooks, Y. Babayan, S. Lamansky, P. I. Djurovich, I. Tsyba, R. Bau, M. E. Thompson, *Inorg. Chem.* **2002**, *41*, 3055−3066; b) X. Yang, X. Xu, J. Zhao, J.-S. Dang, Z. Huang, X. Yan, G. Zhou, D. Wang, *Inorg. Chem.* **2014**, *53*, 12986−13000; c) Y. Xing, C. Liu, X. Song, J. Li, *J. Mater. Chem. C* **2015**, *3*, 2166−2174; d) E. Anger, M. Rudolph, C. Shen, N. Vanthuyne, L. Toupet, C. Roussel, J. Autschbach, J. Crassous, R. Reau, *J. Am. Chem. Soc.* **2011**, *133*, 3800−3803.

[14] a) Y. Unger, D. Meyer, O. Molt, C. Schildknecht, I. Münster, G. Wagenblast, T. Strassner, *Angew. Chem. Int. Ed.* **2010**, *49*, 10214−10216; b) A. Tronnier, A. Pöthig, S. Metz, G. Wagenblast, I. Münster, T. Strassner, *Inorg. Chem.* **2014**, *53*, 6346−6356.

[15] G. R. Freeman, J. A. G. Williams, *Top. Organomet. Chem.* **2013**, *40*, 89−130.

[16] a) H.-K. Yip, L.-K. Cheng, K.-K. Cheung, C.-M. Che, *J. Chem. Soc. Dalton Trans.* **1993**, 2933−2938; b) J. F. Michalec, S. A. Bejune, D. G. Cuttell, G. C. Summerton, J. A. Gertenbach, J. S. Field, R. J. Haines, D. R. McMillin, *Inorg. Chem.* **2001**, *40,* 2193−2200.

[17] V. W.-W. Yam, R. P.-L. Tang, K. M.-C. Wong, K.-K. Cheung, *Organometallics* **2001**, *20,* 4476−4482.

[18] M. H. Wilson, L. P. Ledwaba, J. S. Field, D. R. McMillin, *Dalton. Trans.* **2005**, 2574−2579.

[19] S. Huo, J. Carroll, D. A. K. Vezzu, *Asian J. Org. Chem*. **2015**, *4*, 1210−1245.

[20] a) W. Lu, M. C. W. Chan, K.-K. Cheung, C.-M. Che *Organometallics* **2001**, *20*, 2477−2486; b) V. W.-W. Yam, R. P.-L. Tang, K. M.-C. Wong, X.-X. Lu, K.-K. Cheung, N. Zhu, *Chem. Eur. J.* **2002**, *8*, 4066−4076; c) J. R. Berenguer, E. Lalinde, J. Torroba, *Inorg.Chem.* **2007**, *46*, 9919−9930.

[21] S. C. F. Kui, F.-F. Hung, S.-L. Lai, M.-Y. Yuen, C.-C. Kwok, K.-H. Low, S. S.-Y. Chui, C.-M. Che,

Chem. Eur. J. **2012**, *18*, 96–109.

[22] G. S.-M. Tong, C.-M. Che, *Chem. Eur. J.* **2009**, *15*, 7225–7237.

[23] S.-W. Lai, M. C.-W. Chan, T.-C. Cheung, S.-M. Peng, C.-M. Che, *Inorg. Chem.* **1999**, *38,* 4046–4055.

[24] P.-K. Chow, G. Cheng, G. S. M. Tong, W.-P. To, W.-L. Kwong, K.-H. Low, C.-C. Kwok, C. Ma, C.-M. Che, *Angew. Chem. Int. Ed.* **2015**, *54*, 2084–2089.

[25] For pyrazolyl-based ligands see: a) S. Develay, O. Blackburn, A. L. Thompson, J. A. G. Williams, *Inorg. Chem.* **2008**, *47*, 11129–11142; b) A. Y.-Y. Tam, D. P.-K. Tsang, M.-Y. Chan, N. Zhu, V. W.-W. Yam, *Chem. Commun.* **2011**, *47*, 3383–3385. For 2,6-bis(benzimidazol-2'-yl)pyridine)-based ligands see: c) A. Y.-Y. Tam, W. H. Lam, K. M.-C. Wong, N. Zhu, V. W.-W. Yam, *Chem. Eur. J.* **2008**, *14*, 4562–4576; d) E. S.-H. Lan, D. P.-K. Tsang, W. H. Lam, A. Y.-Y. Tam, M.-Y. Chan, W.-T. Wong, V. W.-W. Yam, *Chem. Eur. J.* **2013**, *19*, 6385–6397; e) C. Po, A. Y.-Y. Tam, V. W.-W. Yam, *Chem. Sci.* **2014**, *5*, 2688–2695; f) Z. Wang, Z. Sun, X.-Q. Hao, J.-L Niu, D. Wei, T. Tu, J.-F. Gong, M.-P. Song, *Organometallics* **2014***, 33*, 1563–1573. For pyrimidine-based ligands see: g) X. Li, J. Hu, Y. Wu, R. Li, D. Xiao, W. Zeng, D. Zhang, Y. Xiang, W. Jin, *Dyes and Pigments* **2017**, *141*, 188–194. For 6-membered chelated rings see: h) K. L. Garner, L. F. Parkes, J. D. Piper, J. A. G. Williams, *Inorg. Chem.* **2010**, *49*, 476–487; i) D. A. K. Vezzu, D. Ravindranathan, A. W. Garner, L. Bartolotti, M. E. Smith, P. D. Boyle, S. Huo, *Inorg. Chem.* **2011***, 50,* 8261–8273.

[26] M. Beley, J.-P. Collin, R. Louis, B. Metz, J.-P. Sauvage, *J. Am. Chem. Soc*. **1991**, *113*, 8521–8522.

[27] J. A. G. Williams, *Chem. Soc. Rev.* **2009**, *38*, 1783–1801.

[28] D. J. Cárdenas, A. M. Echavarren, M. C. R. de Arellano, *Organometallics* **1999**, *18*, 3337–3341.

[29] J. A. G. Williams, A. Beeby, E. S. Davies, J. A. Weinstein, C. Wilson, *Inorg. Chem.* **2003**, *42*, 8609–8611.

[30] A. F. Rausch, L. Murphy, J. A. G. Williams, H. Yersin, *Inorg. Chem.* **2009**, *48*, 11407–11414.

[31] W. Sotoyama, T. Satoh, H. Sato, A. Matsuura, N. Sawatari, *J. Phys. Chem. A* **2005**, *109,* 9760–9766.

[32] S. J. Farley, D. L. Rochester, A. L. Thompson, J. A. K. Howard, J. A. G. Williams, *Inorg. Chem.* **2005**, *44*, 9690–9703.

[33] R. A. Marcus, *J. Phys. Chem*. **1965**, *43*, 1261–1274.

[34] E. Rossi, L. Murphy, P. L. Brothwood, A. Colombo, C. Dragonetti, D. Roberto, R. Ugo, M. Cocchi, J. A. G. Williams, *J. Mater. Chem*. **2011**, *21*, 15501–1551.

[35] D. L. Rochester, S. Develay, S. Záliš, J. A. G. Williams, *Dalton. Trans.* **2009**, 1728–1741.

[36] J. F. Michaelec, S. A. Bejune, D. R. McMillin, *Inorg. Chem.* **2000**, *39*, 2708–2709.

[37] Q.-Z. Yang, Q.-X. Tong, L.-Z. Wu, Z.-X. Wu, L.-P. Zhang, C.-H. Tung, *Eur. J. Inorg. Chem.* **2004**, 1948–1954.

[38] M. Cocchi, D. Virgili, V. Fattori, D. L. Rochester, J. A. G. Williams, *Adv. Funct. Mater.* **2007**, *17*, 285–289.

[39] a) M. A. Baldo, D. F. O'Brien, Y. You, A. Shoustikov, S. Sibley, M. E. Thompson, S. R. Forrest, *Nature* **1998**, *395*, 151–154; b) M. A. Baldo, S. Lamansky, P. E. Burrows, M. E. Thompson, S. R. Forrest, *Appl. Phys. Lett.* **1999**, *75,* 4–6; c) C. Adachi, M. A. Baldo, S. R. Forrest, M. E. Thompson, *Appl. Phys. Lett.* **2000**, *77,* 904–906.

[40] C. Sekine, Y. Tsubata, T. Yamada, M. Kitano, S. Doi, *Sci. Technol. Adv. Mater.* **2014**, *15*, 034203.

[41] M. Cocchi, D. Virgili, V. Fattori, J. A. G. Williams, J. Kalinovski, *Appl. Phys. Lett.* **2007**, *90*, 023506.

[42] B. D'Andrade, S. R. Forrest, *Chem. Phys.* **2003**, *286*, 321–335.

238

[43] J. Kalinovski, M. Cocchi, D. Virgili, V. Fattori, J. A. G. Williams, *Adv. Mater.* **2007**, *19*, 4000−4005.

[44] A. F. Rausch, L. Murphy J. A. G. Williams, H. Yersin, *Inorg. Chem.* **2012**, *51*, 312−319.

[45] X. Yang, Z. Wang, S. Madakuni, J. Li, G. E. Jabbour, *Adv. Mater.* **2008**, *20*, 2405−2409.

[46] L. Murphy, P. Brulatti, V. Fattori, M. Cocchi, J. A. G. Williams, *Chem. Commun.* **2012**, *48*, 5817−5819.

[47] M. Cocchi, J. Kalinowski, L. Murphy, J. A. G. Williams, V. Fattori, *Org. Electron.* **2010**, *11*, 388−396.

[48] J. Kalinowski, M. Cocchi, L. Murphy, J. A. G. Williams, V. Fattori, *Chem. Phys.* **2010**, *378*, 47−57.

[49] E. Rossi, L. Murphy, P. L. Brothwood, A. Colombo, C. Dragonetti, D. Roberto, R. Ugo, M. Cocchi, J. A. G. Williams, *J. Mater. Chem.* **2011**, *21*, 15501−15510.

[50] W. Mroz, C. Botta, U. Giovanella, E. Rossi, A. Colombo, C. Dragonetti, D. Roberto, R. Ugo, A. Valore, J. A. G. Williams, *J. Mater. Chem.* **2011**, *21*, 8653−8661.

[51] F. Nisic, A. Colombo, C. Dragonetti, D. Roberto, A. Valore, J. M. Malicka, M. Cocchi, G. R. Freeman, J. A. G. Williams, *J. Mater. Chem. C* **2014**, *2*, 1791−1800.

[52] B. Yin, F. Niemeyer, J. A. G. Williams, J. Jiang, A. Bouccekine, L. Toupet, H. Le Bozec, V. Guerchais, *Inorg. Chem.* **2006**, *45*, 8584−8596.

[53] T. Kayano, S. Takayasu, K. Shinozaki, *Chem. Eur. J.* **2014**, *20*, 16583−16589.

[54] a) S. Develay, J. A. G. Williams, *Dalton Trans.* **2008**, 4562−4564; b) R. Munoz-Rodriguez, E. Bunuel, J. A. G. Williams, D. J. Cárdenas, *Chem. Commun.* **2012**, *48*, 5980−5982.

[55] A. M. Smith, M. C. Mancini, S. Nie, *Nat. Nanotechnol.* **2009**, *4*, 710−711.

[56] S. W. Botchway, M. Charnley, J. W. Haycock, A. W. Parker, D. L. Rochester, J. A. Weinstein, J. A. G. Williams, *PNAS* **2008**, *105*, 16071−16076.

[57] E. Baggaley, S. W. Botchway, J. W. Haycock, H. Morris, I. V. Sazanovich, J. A. G. Williams, J. A. Weinstein, *Chem. Sci.* **2014**, *5*, 879−886.

[58] A. Colombo, F. Fiorini, D. Septiadi, C. Dragonetti, F. Nisic, A. Valore, D. Roberto, M. Mauro, L. De Cola, *Dalton Trans.* **2015**, *44*, 8478−8487.

[59] V. N. Kozhevnikov, B. Donnio, D. W. Bruce, *Angew. Chem. Int. Ed.* **2008**, *47*, 6286−6289.

[60] a) V. N. Kozhevnikov, B. Donnio, B. Heinrich, J. A. G. Williams, D. W. Bruce, *J. Mater. Chem. C* **2015**, *3*, 10177−10187; b) V. N. Kozhevnikov, B. Donnio, B. Heinrich, D. W. Bruce, *Chem. Commun.* **2014**, *50*, 14191−14193.

[61] C.-J. Lin, Y.-H. Liu, S.-M. Peng, T. Shinmyozu, J.-S. Yang, *Inorg. Chem.* **2017**, *56*, 4978−4989.

[62] S. J. Choi, J. Kubawara, Y. Nishimura, T. Arai, T. Kanbara, *Chem. Lett.* **2012**, *41*, 65−67.

[63] C. Baik, W.-S. Han, Y. Kang, S. O. Kang, J. Ko, *J. Organomet. Chem.* **2006**, *691*, 5900−5910.

[64] Z. Wang, E. Turner, V. Mahoney, S. Madakuni, T. Groy, J. Li, *Inorg. Chem.* **2010**, *49*, 11276−11286.

[65] W. A. Tarran, G. R. Freeman, L. Murphy, A. M. Benhan, R. Kataky, J. A. G. Williams, *Inorg. Chem.* **2014**, *53*, 5738−5749.

[66] Y. Chen, K. Li, W. Lu, S. S.-Y. Chui, C.-W. Ma, C.-M. Che, *Angew. Chem. Int. Ed.* **2009**, *48*, 9909−9913.

[67] E. Rossi, A. Colombo, C. Dragonetti, D. Roberto, R. Ugo, A. Valore, L. Falciola, P. Brulatti, M. Cocchi, J. A. G. Williams, *J. Mater. Chem.* **2012**, *22*, 10650−10655.

[68] Y. Chen, W. Lu, C.-M. Che, *Organometallics* **2013**, *32*, 350−353.

[69] V. V. Sivchik, E. V. Grachova, A. S. Melnikov, S. N. Smirnov, A. Y. Ivanov, P. Hirva, S. P. Tunik, I. O. Koshevoy, *Inorg. Chem.* **2016**, *55*, 3351−3363.

[70] a) Y. J. Tian, E. W. Meijer, F. Wang, *Chem. Commun.* **2013**, *49*, 9197–9199; b) M. Mauro, A. Aliprandi, C. Cebrián, D. Wang, C. Kübel, L. De Cola, *Chem. Commun.* **2014**, 7269–7272.

[71] T.-F. Fu, L. Ao, Z.-C. Gao, X.-L. Zhang, F. Wang, *Chinese Chem. Lett.* **2016**, *27*, 1147–1154.

[72] a) J. A. Bailey, M. G. Hill, R. E. Marsh, V. M. Miskowski, W. P. Schaefer, H. B. Gray, *Inorg. Chem.* **1995**, *34*, 4591–4599; b) D. R. McMillin, J. J. Moore, *Coord. Chem. Rev.* **2002**, *229*, 113–121.

[73] a) V. W.–W. Yam, R. P.-L. Tang, K. M.-C. Wong, K.-K. Cheung, *Organometallics* **2001**, *20*, 4476–4482; b) Q.-Z. Yang, L.-Z. Wu, Z.-X. Wu, L. P. Zhang, C. H. Tung, *Inorg. Chem.* **2002**, *41*, 5653–5655.

[74] K. M.-C. Wong, V. W.-W. Yam, *Coord. Chem. Rev.* **2007**, *251*, 2477–2488.

[75] T. J. Wadas, Q.-M. Wang, Y.-J. Kim, C. Flaschenreim, T. N. Blanton, R. Eisenberg, *J. Am. Chem. Soc.* **2004**, *126*, 16841–16849.

[76] M. C.-L. Yeung, V. W.-W. Yam, *Chem. Soc. Rev.* **2015**, *44*, 4192–4202.

[77] S.-W. Lai, H.-W. Lam, W. Lu, K.-K. Cheung, C.-M. Che, *Organometallics* **2002**, *21,* 226–234.

[78] a) V. W.-W. Yam, K. M.-C. Wong, N. Zhu, *J. Am. Chem. Soc.* **2002**, *124*, 6506–6507; b) V. W.-W. Yam, K. H.-Y. Chan, K. M.-C. Wong, N. Zhu, *Chem. Eur. J.* **2005**, *11*, 4535–4543; c) A. Amar, H. Meghezzi, J. Boixel, H. Le Bozec, V. Guerchais, D. Jacquemin, A. Bouccekine, *J. Phys. Chem. A* **2014**, *118*, 6278–6286.

[79] C. Po, A. Y.-Y. Tam, K. M.-C. Wong, V. W.-W. Yam, *J. Am. Chem. Soc.* **2011**, *133*, 12136–12143.

[80] H. L.-K. Fu, C. Po, S. Y.-L. Leung, V. W.-W. Yam, *ACS Appl. Mater. Interfaces* **2017**, *9*, 2786–2795.

[81] C. Y.-S. Chung, S. P.-Y. Li, K. K.-W. Lo, V. W.-W. Yam, *Inorg. Chem.* **2016**, *55*, 4650–4663.

[82] K. M.-C. Wong, W.-S. Tang, X.-X. Lu, N. Zhu, V. W.-W. Yam, *Inorg. Chem.* **2005**, *44*, 1492–1498.

[83] J. L.-L. Tsai, T. Zou, J. Liu, T. Chen, A. O.-Y. Chan, C. Yang, C.-N. Lok, C.-M. Che, *Chem. Sci.* **2015**, *6*, 3823–3830.

[84] C. Yu, K. M.-C. Wong, K. H.-Y. Chan, V. W.-W. Yam, *Angew. Chem. Int. Ed.* **2005**, *44*, 791−794.

[85] C. Yu, K. H.-I. Chan, K. M.-C. Wong, V. W.-W. Yam, *Chem. Eur. J.* **2008**, *14*, 4577–4584.

[86] C. Yu, K. H.-Y. Chan, K. M.-C. Wong, V. W.-W. Yam, *PNAS* **2006**, *52*, 19652–19657.

[87] K. H.-Y. Chan, J. W.-Y. Lam, K. M.-C. Wong, B.-Z. Tang, V. W.-W. Yam, *Chem. Eur. J.* **2009**, *15*, 2328–2334.

[88] K. M.-C. Wong, N. Zhu, V. W.-W. Yam, *Chem. Commun.* **2006**, 3441–3443.

[89] a) W. Lu, M. C.-W. Chan, K.-K. Cheung, C.-M. Che, *Organometallics* **2001**, *20*, 2477–2486; b) W. Lu, M. C.-W. Chan, C.-M. Che, C. Li, Z. Hui, *J. Am. Chem. Soc.* **2004**, *126*, 7639–7651.

[90] S. Y.-L. Leung, W. H. Lam, V. W.-W. Yam, *PNAS* **2013**, *110*, 7986–7991.

[91] M. S. Gin, T. Yokozawa, R.B. Prince, J. S. Moore, *J. Am. Chem. Soc.* **1999**, *121*, 2643–2644.

[92] Y. Cao, M. O. Wolf, B. O. Patrick, *Inorg. Chem.* **2013**, *52*, 5636–5638.

[93] I. Kajitani, K. Tsuge, Y. Sasaki, M. Kato, *Chem. Eur. J.* **2012**, *18*, 11196−11200.

[94] a) T. V. Jones, M. M. Slutsky, R. Laos, T. F. A. de Greef, G. N. Tew, *J. Am. Chem. Soc.* **2005**, *127*, 17235−17240; b) T. V. Jones, M. M. Slutsky, G. N. Tew, *New J. Chem.* **2008**, *32*, 676–679; c) R. B. Prince, L. Brunsveld, E. W. Meijer, J. S. Moore, *Angew. Chem. Int. Ed.* **2000**, *39*, 228–230.

[95] M.-X- Zhu, W. Lu, N. Zhu, C.-M. Che, *Chem. Eur. J.* **2008**, *14*, 9736–9746.

[96] S. Y.-L. Leung, A. Y.-Y. Tam, C.-H. Tao, H. S. Chow, V. W.-W. Yam, *J. Am. Chem. Soc.* **2012**, *134*, 1047−1056.

[97] S. Y.-L. Leung, K. M.-C. Wong, V. W.-W. Yam, *PNAS* **2016**, *113*, 2845−2850.

[98] a) K. H.-Y. Chan, H.-S. Chow, K. M.-C. Wong, M. C.-L. Yeung, V. W.-W. Yam, *Chem. Sci.* **2010**, *1*, 477–482; b) V. W.-W. Yam, K. H.-Y. Chan, K. M.-C. Wong, B. W.-K. Chu, *Angew. Chem. Int. Ed.* **2006**, *45*, 6169–6173.

[99] a) Y. Hu, K. H.-I. Chan, C. Y.-S. Chung, V. W.-W. Yam, *Dalton Trans.* **2011**, *40*, 12228–12234; b) C. Y.-S. Chung, V. W.-W. Yam, *Chem. Eur. J.* **2013**, *19*, 13182–13192.

[100] X.-S. Xiao, W. Lu, C.-M. Che, *Chem. Sci.* **2014**, *5*, 2482–2488.

[101] I. Stengel, C. A. Strassert, L. De Cola, P. Bäuerle, *Organometallics* **2014**, *33*, 1345–1355.

[102] a) M. H. Keefe, K. D. Benkstein, J. T. Hupp, *Coord. Chem. Rev.* **2000**, *205*, 201–228; b) S.-S. Sun, A. J. Lees, *Coord. Chem. Rev.* **2002**, *230*, 171–192; c) Q. Zhao, F. Li, C. Huang, *Chem. Soc. Rev.* **2010**, *39*, 3007–3030; d) C. W. Rogers, M. O. Wolf, *Coord. Chem. Rev.* **2002**, *233–234*, 341–350.

[103] a) V. Guerchais, J. L. Fillaut, *Coord. Chem. Rev.* **2011**, *255*, 2448–2457; b) M. C.-L. Yeung, V. W.-W. Yam, *Chem. Soc. Rev.* **2015**, *44*, 4192–4202.

[104] T. Förster, *Ann. Phys.* **1948**, *2*, 55–75.

[105] C. J. Pedersen, *J. Am. Chem. Soc.* **1967**, *89*, 2495–2496.

[106] a) Y. Nakahara, Y. Matsumi, W. Zhang, T. Kida, Y. Nakatsuji, I. Ikeda, *Org. Lett.* **2002**, *4*, 2641–2644; b) Y. Nakahara, T. Kida, Y. Nakatsuji, M. Akashi, *J. Org. Chem.* **2004**, *69*, 4403–4411.

[107] V. W.-W. Yam, R. P.-L. Tang, K. M.-C. Wong, C.-C. Ko, K.-K. Cheung, *Inorg. Chem.* **2001**, *40*, 571–574.

[108] V. W.-W. Yam, R. P.-L. Tang, K. M.-C. Wong, K.-K. Cheung, *Organometallics* **2001**, *20*, 4476–4482.

[109] W.-S. Tang, X.-X. Lu, K. M.-C. Wong, V. W.-W. Yam, *J. Mater. Chem.* **2005**, *15*, 2714–2720.

[110] Q.-Z. Yang, L.-Z. Wu, H. Zhang, B. Chen, Z.-X. Wu, L.-P. Zhang, C.-H. Tung, *Inorg. Chem.* **2004**, *43*, 5195–5197.

[111] S. Sinn, F. Biedermann, M. Vishe, A. Aliprandi, C. Besnard, J. Lacour, L. De Cola, *Chem. Phys. Chem.* **2016**, *17*, 1829–1834.

[112] E. Garoni, J. Boixel, V. Dorcet, T. Roisnel, D. Roberto, D. Jaquemin, V. Guerchais, *Dalton Trans.* **2018**, *47*, 224–232.

[113] a) J. K. Stille, *Angew. Chem. Int. Ed. Engl.* **1986**, *25*, 508–524; b) N. Miyaura, A. Suzuki, *Chem. Rev.* **1995**, *95*, 2457–2483; c) W. Goodall, K. Wild, K. J. Arm, J. A. G. Williams, *J. Chem. Soc., Perkin Trans. 2* **2002**, 1669–1681.

[114] Solar Active, https://www.solaractive.com/ (accessed January 2018)

[115] Nanomatrix, https://www.nanomatrixsecure.com/en/security-products/security-features/security-ink-coating/photochromic-ink (accessed January 2018)

[116] a) Serengeti sunglasses, http://www.serengeti-eyewear.com/Technology/Photochromic.aspx (accessed January 2018); b) Framesdirect, https://www.framesdirect.com/landing/a/photochromic-sunglasses-lenses.html (accessed January 2018).

[117] a) N. Soh, K. Yoshida, H. Nakajima, K. Nakano, T. Imato, T. Fukaminato, M. Irie, *Chem. Commun.* **2007**, 5206–5208; b) X. Piao, Y. Zou, J. Wu, C. Li, T. Yi, *Org. Lett.* **2009**, *11*, 3818–3821.

[118] a) D. Lam, R. N. Branda, A. Spantulescu, J. G. Finden, A. Hayek, K. A. Hope-Ross, S. Siridov, U.S. Patent 0250392, **2013**; b) M. Uchida, M. Irie, JP Patent 04257560, **1992**.

[119] a) S. Ovshinsky, U.S. Patent 3530441, **1970**; b) M. Irie, T. Fukaminato, K. Matsuda, S. Kobatake, *Chem. Rev.* **2014**, *114*, 12174–12277.

[120] A. Fihey, A. Perrier, W. R. Browne, D. Jacquemin, *Chem. Soc. Rev.* **2015**, *44*, 3719–3759.

[121] D. H. Waldeck, *Chem. Rev.* **1991**, 415–436.

[122] M. Irie, M. Mohri, *J. Org. Chem.* **1988**, *53*, 803–808.

[123] R. M. Kellogg, M. B. Groen, H. J. Wynberg, *J. Org. Chem.* **1967**, *32*, 3093–3100.

[124] S. Nakamura, M. Irie, *J. Org. Chem.* **1988**, *53*, 6136–6138.

[125] a) Y. Nakayama, K. Hayashi, M. Irie, *J. Org. Chem.* **1990**, *55*, 2592–2596; b) K. Uchida, T. Matsuoka, K. Sayo, M. Iwamoto, H. Hayashi, M. Irie, *Chem. Lett.* **1999**, 835–836.

[126] a) S. Gilat, S. H. Kawai, J.-M. Lehn, *J. Chem. Soc. Chem. Commun.* **1993**, 1439–1442; b) K. Uchida, E. Tsuchida, Y. Aoi, S. Nakamura, M. Irie, *Chem. Lett.* **1999**, 63–64.

[127] a) Y. P. Strokach, T. M. Valova, Z. O. Golotyuk, V. A. Barachevsky, O. Y. Kuznetsova, V. N. Yarovenko, S. L. Semenov, I. V. Zavarzin, V. Z. Shirinian, M. M. Krayushkin, *Opt. Spectrosc.* **2005**, *99*, 573–578; b) T. Yamaguchi, K. Uchida, M. Irie, *J. Am. Chem. Soc.* **1997**, *119*, 6066–6071; c) A. Staykov, K. Yoshizawa, *J. Phys. Chem. C.* **2009**, *113*, 3826–3834.

[128] L. N. Lucas, J. V. Esch, R. M. Kellogg, B. L. Feringa, *Chem. Commun.* **1998**, 2313–2314.

[129] a) K. A. Muszkat, S. Sharafy, *J. Am. Chem. Soc.* **1971**, *93*, 4119–4125; b) G. Hohlneicher, M. Müller, M. Demmer, J. Lex, J. H. Penn, L.-X. Gan, P. D. Loesel, *J. Am. Chem. Soc.* **1988**, *110*, 4483–4494; c) J. H. Frederick, Y. Fujiwara, J. H. Penn, K. Yoshihara, H. Petek, *J. Phys. Chem.* **1991**, *95*, 2845–2858.

[130] M. Irie, T. Lifka, K. Uchida, S. Kobatake, Y. Shindo, *Chem. Commun.* **1999**, 747–750.

[131] a) R. Hoffmann, R. B. Woodward, *Acc. Chem. Res*, **1968**, *1*, 17–22; b) R. B. Woodward, R. Hoffmann, *Angew. Chem. Int. Ed.* **1969**, *8*, 781–932.

[132] a) F. Stellacci, C. Bertarelli, F. Toscano, M. C. Gallazzi, G. Zolti, G. Zerbi, *Adv. Mater.* **1999**, *11*, 292–295; b) G. Pariani, R. Castagna, G. Dassa, S. Hermes, C. Vailati, A. Bianco, C. Bertarelli, *J. Mater. Chem.* **2011**, *21*, 13223–13231.

[133] Y. Nakayama, K. Hayashi, M. Irie, *Bull. Chem. Soc. Jpn.* **1991**, *64*, 789–795.

[134] a) M. Irie, *Chem. Rev.* **2000**, *100,* 1685–1716; b) M. Irie, T. Fukaminato, K. Matsuda, S. Kobatake, *Chem. Rev.* **2014**, *114*, 12174–12277; c) H. Tian, S. Yang, *Chem. Soc. Rev.* **2004**, *33*, 85–97; d) S. Kawata, Y. Kawata, *Coord. Chem. Rev.* **2000**, *100,* 1777–1788.

[135] M. Irie, *Photochem. Photobiol. Sci.* **2010**, *9*, 1535–1542.

[136] C.-C. Ko, V. W.-W. Yam, *J. Mater. Chem.* **2010**, *20*, 2063–2070.

[137] G. M. O. Máille, S. M. Draper, *Spectrosc. Prop. Inorg. Organomet. Compd.* **2012**, *43*, 166–215.

[138] a) E. C. Harvey, B. L. Feringa, J. C. Vos, W. R. Browne, M. T. Pryce, *Coord. Chem. Rev.* **2015**, *282–283*, 77–86; b) V. Guerchais, L. Ordronneau, H. Le Bozec, *Coord. Chem. Rev.* **2010**, *254*, 2533–2545; c) H. Le Bozec, V. Guerchais, *C. R. Chimie.* **2013**, 1172–1182.

[139] a) R. T. F. Jukes, V. Adamo, F. Hartl, P. Belser, L. De Cola, *Inorg. Chem.* **2004**, *34*, 2779–2792; b) C.-C. Ko, W.-M. Kvok, V. W.-W. Yam, D. L. Phillips, *Chem. Eur. J.* **2006**, *12*, 5840–5848.

[140] a) A. Fernandez-Acebes, J.-M. Lehn, *Chem. Eur. J.* **1999**, *5*, 3285–3292; b) X. He, L. Norel, Y.-M. Hervault, R. Métivier, A. D'Aléo, O. Maury, S. Rigaut, *Inorg. Chem.* **2016**, *55*, 2635–12643; c) I. Lee, Y. You, S.-J. Lim, S. Y. Park, *Chem. Lett.* 2**007**, *36*, 888–889; d) W. Tan, Q. Zhan, J. Zhang, H. Tian, *Org. Lett.* **2009**, *11*, 161–164.

[141] J. K.-W. Lee, C.-C. Ko, K. M.-C. Wong, N. Zhu, V. W.-W. Yam, *Organometallics* **2007**, *26*, 12–15.

[142] a) J. C.-H. Chan, W. H. Lam, H.-L. Wong, N. Zhu, W.-T. Wong, V. W.-W. Yam, *J. Am. Chem. Soc.* **2011**, *133*, 12690–12705; b) H.-L. Wong, N. Zhu, V. W.-W. Yam, *J. Organomet. Chem.* **2014**, *751*, 430–437.

[143] A. Presa, R. F. Brissos, A. B. Caballero, I. Borilovic, L. Korrodi-Gregório, R. Pérez-Tomás, O. Roubeau, P. Gamez, *Angew. Chem. Int. Ed*. **2015**, *54*, 4561−4565.

[144] I. Jung, H. Choi, E. Kim, C.-H. Lee, S. O. Kang, J. Ko, *Tetrahedron* **2005**, *61*, 12256−12263.

[145] S. K. Brayshaw, S. Schiffers, A. J. Stevenson, S. J. Teat, M. R. Warren, R. D. Bennett, I. V. Sazanovich, A. R. Buckley, J. A. Weinstein, P. R. Raithby, *Chem. Eur. J.* **2011**, *17*, 4385−4395.

[146] J. Boixel, Y. Zhu, H. Le Bozec, M. A. Benmensour, A. Boucekkine, K. M.-C. Wong, A. Colombo, D. Roberto, V. Guerchais, D. Jacquemin, *Chem. Commun.* **2015**, *52*, 9833−9836.

[147] M. N. Roberts, C.-J. Carling, J. K. Nagle, . R. Branda, M. O. Wolf, *J. Am. Chem. Soc.* **2009**, *131*, 6644−16645.

[148] H.-L. Wong, C.-H. Tao, N. Zhu, V. W.-W. Yam, *Inorg. Chem*. **2011**, *50*, 471−481.

[149] a) B. Li, H.-M. Wen, J.-Y. Wang, L.-X. Shi, Z.-N. Chen, *Inorg. Chem.* **2013**, *52*, 12511−12520; b) B. Li, H.-M. Wen, J.-Y. Wang, L.-X. Shi, Z.-N. Chen, *Inorg. Chem.* **2015**, *54*, 11511−11519.

[150] a) M. N. Roberts, J. K. Nagle, J. G. Finden, N. R. Branda, M. O. Wolf, *Inorg. Chem.* **2009**, *48*, 19−21; b) M. N. Roberts, J. K. Nagle, M. B. Majewski, J. G. Finden, N. R. Branda, M. O. Wolf, *Inorg. Chem.* **2011**, *50*, 4956−4966.

[151] M. H.-Y. Chan, H.-L. Wong, V. W.-W. Yam, *Inorg. Chem.* **2016**, *55*, 5570−5577.

[152] a) D. Dulic, T. Kudernac, A. Puzys, B. L. Feringa, B. J. van Wees, *Adv. Mater.* **2007**, *19*, 2898−2902; b) T. Kudernac, T. Kobayashi, A. Uyama, K. Uchida, S. Nakamura, B. L. Feringa, *J. Phys. Chem. A* **2013**, *117*, 8222−8229; c) J M. Cox, I. M. Walton, D. G. Patel, M. Xu, Y.-S. Chen, J. B. Benedict, *J. Phys. Chem. A* **2015**, *119*, 884−888.

[153] a) Y. Chi, P. T. Chou, *Chem. Soc. Rev.* **2010**, *39*, 638−655; b) G. Zhou, W. Y. Wong, X. Yang, *Chem. Asian J.* **2011**, *6*, 1706−1727; c) I. Omae, *Coord. Chem. Rev.* **2016**, *310*, 154−169; d) C.-L. Ho, H. Li, W.-Y. Wong, *J. Organomet. Chem.* **2014**, *751*, 261−285; e) K. P. Silva Zanoni, R. Lopes Coppo, R. Costa Amaral, N. Y. Murakami Iha, *Dalton Trans*. **2015**, *44*, 1455−14573.

[154] a) E. Baranoff, J.-H. Yum, M. Graetzel, M. K. Nazeeruddin, *J. Organomet. Chem.* **2009**, *694*, 2661−2670; b) E. I. Mayo, K. Kilsa, T. Tirrell, P. I. Djurovich, A. Tamayo, M. E. Thompson, N. S. Lewis, H. B. Gray, *Photochem. Photobiol. Sci.* **2006**, *5*, 871−873.

[155] a) K. K.-W. Lo, D. C.-M. Ng, C.-K. Chung, *Organometallics* **2001,** *20,* 4999−5001; b) K. K. Lo, *Acc. Chem. Res*. **2015**, *48*, 2985−2995; c) D.-L. Ma, H.-J. Zhong, W.-C. Fu, D. S.-H. Chan, H.-Y. Kwan, W.-F. Fong, L.-H. Chung, C.-Y. Wong, C.-H. Leung, *PLoS ONE* **2013**, *8*, e55751; d) K. K.-W. Lo, C.-K. Chung, T. K.-M. Lee, L.-H Lui, K. H.-K. Tsang, N. Zhu, *Inorg. Chem.* **2003**, *42*, 6886−6897.

[156] H. N. Kagalwala, D. N. Chirdon, I. N. Mills, N. Budwal, S. Bernhard, *Inorg. Chem.* **2017**, *56*, 10162−10171.

[157] D. Ma, T. Tsuboi, Y. Qiu, L. Duan, *Adv. Mater.* **2017**, *29*, 1603253, and references therein.

[158] G. E. Schneider, H. J. Bolink, E. C. Constable, C. D. Ertl, C. E. Housecroft, A. Pertegas, J. A. Zampese, A. Kanitz, F. Kessler, S. B. Meier, *Dalton Trans.* **2014**, *43*, 1961−1964.

[159] M. G. Colombo, A. Hausel, H. U. Güdel, *Inorg. Chem* **1993**, *32*, 3088−3092.

[160] F. Neve, A. Crispini, S. Campagna, S. Serroni, *Inorg. Chem.* **1999,** *38,* 2250−2258.

[161] J. D. Slinker, A. A. Gorodetsky, M. S. Lowry, J. Wang, S. Parker, R. Rohl, S. Bernhard, G. G. Malliaras, *J. Am Chem. Soc.* **2004**, *126*, 2763−2767.

[162] a) R. D. Costa, E. Ortí, H. J. Bolink, S. Graber, S. Schaffner, M. Neuburger, C. E. Housecroft, E. C. Constable, *Adv. Funct. Mater.* **2009**, *19*, 3456–3463; b) R. Terki, L.-P. Simoneau, A. Rochefort, *J. Phys. Chem. A* **2009**, *113*, 534–541.

[163] H. F. Henwood, E. Zysman-Colman, *Chem. Commun.* **2017**, *53*, 807–827.

[164] a) K. Hasan, L. Donato, Y. Shen, J. D. Slinker, E. Zysman-Colman, *Dalton Trans.* **2014**, *43*, 13672–13682; b) S. Ladouceur, D. Fortin, E. Zysman-Colman, *Inorg. Chem.* **2010**, *49*, 5625–5641.

[165] a) A. F. Henwood, S. Evariste, A. M. Z. Slawin and E. Zysman-Colman, *Faraday Discuss.* **2014**, *174*, 165–182; b) S. B. Meier, W. Sarfert, J. M. Junquera-Hernández, M. Delgado, D. Tordera, E. Ortì, H. J. Bolink, F. Kessler, R. Scopelliti, M. Grätzel, M. K. Nazeeruddind, E. Baranoff, *J. Mater. Chem. C* **2013**, *1*, 58–68; c) F. Monti, A. Baschieri, I. Gualandi, J. J. Serrano-Pérez, J. M. Junquera-Hernández, D. Tonelli, A. Mazzanti, S. Muzzioli, S. Stagni, C. Roldan-Carmona, A. Pertegás, H. J. Bolink, E. Ortí, L. Sambri, N. Armaroli, *Inorg. Chem.* **2014**, *53*, 7709–7721.

[166] a) S. Ladouceur, E. Zysman-Colman, *Eur. J. Inorg. Chem.* **2013**, 2985–3007; b) C. Dragonetti, A. Valore, A. Colombo, S. Righetto, V. Trifiletti, *Inorg. Chim. Acta* **2012**, *388*, 163–167; c) C. Dragonetti, L. Falciola, P. Mussini, S. Righetto, D. Roberto, R. Ugo, A. Valore, *Inorg. Chem.* **2007**, *46*, 8533–8547.

[167] K. Hasan, A. K. Bansal, I. D. W. Samuel, C. Roldán-Carmona, H. J. Bolink, E. Zysman-Colman, *Sci. Reports* **2015**, *5*, 12325.

[168] Q. Zhao, S. Liu, M. Shi, C. Wang, M. Yu, L. Li, F. Li, T. Yi, C. Huang, *Inorg. Chem.* **2006**, *45*, 6152–6160.

[169] O. Lohio, L. Viau, O. Maury, H. Le Bozec, *Tetrahedron Lett.* **2007**, *48*, 1229–1232.

[170] a) M. K. Nazeeruddin, R. T. Wegh, S. Klink, M. Grätzel, C. N. Klein, Patent WO2007004113, **2007**; b) M. K. Nazeeruddin, E. D. Baranoff, M. Grätzel, Patent WO2008148830, **2008**.

[171] A. L. Medina-Castillo, J. F. Fernandez-Saanchez, C. Klein, M. K. Nazeeruddin, A. Segura-Carretero, A. Fernandez-Gutierrez, M. Gräzel, U. E. Spichiger-Keller, *Analyst* **2007**, *132*, 929–936.

[172] J. C. Araya, J. Gajardo, S. A. Moya, P. Aguirre, L. Toupet, J. A. G. Williams, M. Escadeillas, H. Le Bozec, V.Guerchais, *New J. Chem.* **2010**, *34*, 21–24.

[173] V. Aubert, L. Ordronneau, M. Escadeillas, J. A. G. Williams, A. Boucekkine, E. Coulaud, C. Dragonetti, S. Righetto, D. Roberto, R. Ugo, A. Valore, A. Singh, J. Zyss, I. Ledoux-Rak, H. Le Bozec, V. Guerchais, *Inorg. Chem.* **2011**, *50*, 5027–5038.

[174] S. Sinha, S. Mandal, P. Gupta, *RSC Adv.* **2015**, *5*, 99529–99539.

[175] M. Zaarour, A. Singh, C. Latouche, J. A. G. Williams, I. Ledoux-Rak, J. Zyss, A. Bouccekine, H. Le Bozec, V. Guerchais, C. Dragonetti, A. Colombo, D. Roberto, A. Valore, *Inorg. Chem.* **2013**, *52*, 7987–7994.

[176] A. Colombo, E. Garoni, C. Dragonetti, S. Righetto, D. Roberto, N. Baggi, M. Escadeillas, V. Guerchais, K. Kamada, *Polyhedron* **2018**, *140*, 116–121.

[177] T. Le Bouder, L. Viau, J.-P. Guégan, O. Maury, H. Le Bozec, *Eur. J. Org. Chem.* **2002**, 3024–3033.

[178] M. Lepeltier, T. K.-M. Lee, K. K.-W. Lo, L. Toupet, H. Le Bozec, V. Guerchais, *Eur. J. Inorg. Chem.* **2007**, 2734–2747.

[179] P. A. Franke, A. E. Hill, C. W. Peters, G. Weinreich, *Phys. Rev. Lett.* **1961**, *7*, 118–119.

[180] N. Bloembergen, *Nonlinear Optics*, **1965**, Benjamin, New York.

[181] S. Di Bella, C. Dragonetti, M. Pizzotti, D. Roberto, F. Tessore, R. Ugo, *Top. Organomet. Chem.* **2010**, *28*, 1–55.

[182] a) J. L. Oudar, D. S. Chemla, *J. Chem. Phys.* **1977**, *66*, 2664−2668; b) J. L. Oudar, *J. Chem. Phys.* **1977**, *67*, 446−457.

[183] a) O. Riant, G. Bluet, S. Brasselet, N. Druze, I. Ledoux, F. Lefloch, A. Skibniewski, J. Zyss, *Mol. Cryst. Liq. Cryst.* **1998**, *322*, 35−42; b) J. Zyss, I. Ledoux, *Chem. Rev.* **1994**, *94*, 77−105; c) H. Le Bozec, T. Le Bouder, O. Maury, I. Ledoux, J. Zyss, *J. Opt. A: Pure Appl. Opt.* **2002**, *4*, S189−S196.

[184] A. Ashkin, G. D. Boyd, J. M. Dziedzic, *IEEE J. Quantum Electron.* **1966**, *2*, 109−124.

[185] M. Bass, P. A. Franken, J. F. Ward, G. Weinreich, *Phys. Rev. Lett.* **1962**, *9*, 446−448.

[186] R. W. Boyd, *Nonlinear Optics 3rd edition*, **2008**, Academic Press.

[187] a) I. Ledoux, J. Zyss, *J. Chem. Phys.* **1982**, *73*, 203−213; b) G. R. Meredith, *Rev. Sci. Instrum.* **1982**, *53*, 48−53; c) K. D. Singer, A. F. Garito, *J. Chem. Phys*. **1981**, *75*, 3572−3580; d) C. G. Bethea, *Appl. Opt.* **1975**, *14*, 1447−1451.

[188] D. J. Williams, *Angew. Chem. Int. Ed. Engl.* **1984**, *23*, 690−703.

[189] K. Clays, A. Persoons, *Phys. Rev. Lett.* **1991**, *66*, 2980−2983.

[190] W. M. Laidlaw, R. G. Denning, T. Verbiest, E. Chauchard, A. Persoons, *Proc. SPIE Int. Soc. Opt. Eng.* **1994**, *2143*, 14−19.

[191] S. Bruni, E. Cariati, F. Cariati, F. A. Porta, S. Quici, D. Roberto, *Spectrochimica Acta Part A* **2001**, *57*, 1417−1426.

[192] C. H. Wang, J. N. Woodford, A. K.-Y. Jen, *Chem. Phys.* **2000**, *262*, 475−487.

[193] D. R. Kanis, M. A. Ratners, T. J. Marks, *Chem. Rev.* **1994***, 94*, 195−242.

[194] L.-T. Cheng, W. Tam, S. H. Stevenson, G. R. Meredith, G. Rikken, S. R. Marder, *J. Phys. Chem.* **1991**, *95*, 10631−10643.

[195] L.-T. Cheng, W. Tam, S. R. Marder, A. E. Stiegman, G. Rikken, C. W. Spangler, *J. Phys. Chem.* **1991**, *95*, 10643−10652.

[196] a) S. R. Marder, D. N. Beratan, L.-T. Cheng, *Science* **1991**, *252*, 103−106; b) F. Meyers, S. R. Marder, B. M. Pierce, J. L. Bredas, *J. Am. Chem. Soc.* **1994**, *116*, 10703−10714; c) C. B. Gorman, S. R. Marder, *Proc. Natl. Acad. Sci. USA* **1993**, *90*, 11297−11301.

[197] S. R. Marder, B. Kippelen, A. K.-Y. Jen, N. Peyghambarian, *Science*, **1997**, *388*, 845−851.

[198] a) I. D. L. Albert, T. J. Marks, M. A. Ratner, *J. Am. Chem. Soc.* **1997**, *119*, 6575−6582; b) C.-F. Shu, Y.-K. Wong, *J. Mater. Chem.* **1998**, *8*, 833−835.

[199] P. R. Varanasi, A. K.-Y. Jen, J. Chandrasekhar, I. N. N. Namboothiri, A. Rathna, *J. Am. Chem. Soc.* **1996,** *118,* 12443−12448.

[200] a) V. P. Rao, K. Y. Wong, A. K.-Y. Jen, K. J. Drost, *Chem. Mater.* **1994**, *6*, 2210−2212; b) E. M. Breitung, C.-F. Shu, R. J. McMahon, *J. Am. Chem. Soc.* **2000**, 1*22*, 1154−1160.

[201] a) A. K.-Y. Jen, V. P. Rao, K. Y. Wong, K. J. Drost, *J. Chem. Soc. Chem. Commun.* **1993**, 90−92; b) V. P. Rao, A. K.-Y. Jen, K. Y. Wong, K. J. Drost, *Tetrahedron Lett.* **1993**, *34*, 1747−1750.

[202] Y. K. Wang, C.-F. Shu, E. M. Breitung, R. J. McMahon, *J. Mater. Chem.* **1999**, *9*, 449−1452.

[203] A. K.-Y. Jen, Y. Cai, P. W. Bedworth, S. R. Marder, *Adv. Mater.* **1997**, *9*, 132−135.

[204] K. D. Singer, J. E. Sohn, L. A. King, H. M. Gordon, *J. Opt. Soc. Am. B* **1989**, *6*, 1339−1350.

[205] S. J. Benight, D. H. Bale, B. C. Olbricht, L. R. Dalton, *J. Mater. Chem.* **2009**, *19*, 7466−7475.

[206] S. K. Kurtz, T. T. Perry, *J. Appl. Phys.* **1968**, *39*, 3798−3813.

[207] D. Espa, L. Pilia, L. Marchiò, F. Artizzu, G. Di Carlo, D. Marinotto, A. Serpe, F. Tessore, P. Deplano, *Dalton Trans.* **2016**, *45*, 17431−17438.

[208] P. D. Maker, R. W. Terhune, M. Nisenoff, C. M. Savage, *Phys. Rev. Lett.* **1962**, *8*, 21−22.

[209] a) J. Jerphagnon, S. K. Kurtz, *Phys. Rev. B: Solid State* **1970**, *1*, 1739−1744; b) W. N. Herman, L. M. Hayden, *J. Opt. Soc. Am. B* **1995**, *12*, 416−427.

[210] D. Marinotto, R. Castagna, S. Righetto, C. Dragonetti, A. Colombo, C. Bertarelli, M. Garbugli, G. Lanzani, *J. Phys. Chem. C* **2011**, *115*, 20425−20432.

[211] a) E. Cariati, M. Pizzotti, D. Roberto, F. Tessore, R. Ugo, *Coord. Chem. Rev.* **2006**, *250*, 1210−1233; b) O. Maury, H. Le Bozec, *Metal-Based Quadratic Nonlinear Optical Materials*, **2010**, John Wiley & Sons, Ltd, Chichester, UK; c) N. J. Long, *Angew. Chem. Int. Ed. Engl.* **1995**, *34*, 21−38.

[212] M. L. H. Green, S. R. Marder, M. E. Thompson, J. A. Bandy, D. Bloor, P. V. Kolinsky, R. J. Jones, *Nature* **1987**, *330*, 360−362.

[213] S. Barlow, S. R. Marder, *Chem. Commun.* **2000**, 1555−1562.

[214] J. C. Calabrese, L.-T. Cheng, J. C. Green, S. R. Marder, W. Tam, *J. Am. Chem. Soc.* **1991**, *113*, 7227−7232.

[215] J. A. Mata, E. Peris, I. Asselberghs, R. Van Boxel, A. Persoons, *New J. Chem.* **2001**, 299−304.

[216] T. Farrell, A. R. Manning, T. C. Murphy, T. Meyer-Friedrichsen, J. Heck, I. Asselberghs, A. Persoons, *Eur. J. Inorg. Chem.* **2001**, 2365−2375.

[217] V. Alain, M. Blanchard-Desce, C.-T. Chen, S. R. Marder, A. Fort, M. Barzoukas, *Synth. Met.* **1996**, 133−136.

[218] S.-J. Wang, Y.-F. Wang, C. Cai, *J. Phys. Chem. C* **2015**, *119*, 16256−16262.

[219] a) C. E. Powell, M. G. Humphrey, *Coord. Chem. Rev.* **2004**, *248*, 725−756; b) M. P. Cifuentes, M. G. Humphrey, *J. Organomet. Chem.* **2004**, *689*, 3968−3981.

[220] F. Nisic, A. Colombo, C. Dragonetti, E. Garoni, D. Marinotto, S. Righetto, F. De Angelis, M. G. Lobello, P. Salvatori, P. Biagini, F. Melchiorre, *Organometallics* **2015**, *34*, 94−104.

[221] L.-T. Cheng, W. Tam, G. R. Meredith, S. R. Marder, *Mol. Cryst. Liq. Cryst.* **1990**, *189*, 137−153.

[222] D. Roberto, R. Ugo, S. Bruni, E. Cariati, F. Cariati, P. C. Fantucci, I. Invernizzi, *Organometallics* **2000**, *19*, 1775−788.

[223] L.-T. Cheng, W. Tam, D. F. Eaton, *Organometallics* **1990**, *9*, 2856−2857.

[224] a) D. R. Kanis, P. G. Lacroix, M. A. Ratner, T. J. Marks, *J. Am. Chem. Soc.* **1994**, *116*, 10089−10102; b) D. W. Bruce, A. Thornton, *Mol. Cryst. Liq. Cryst.* **1993**, *231*, 253−256.

[225] a) F. Tessore, D. Roberto, R. Ugo, P. Mussini, S. Quici, I. Ledoux-Rak, J. Zyss, *Angew. Chem. Int. Ed.* **2003**, *42*, 456−459; b) F. Tessore, D. Locatelli, S. Righetto, D. Roberto, R. Ugo, *Inorg. Chem.* **2005**, *44*, 2437−2442.

[226] B. J. Coe, M. C. Chamberlain, J. P. Essex-Lopresti, S. Gaines, J. C. Jeffery, S. Houbrechts, A. Persoons, *Inorg. Chem.* **1997**, *36*, 3284−3292.

[227] B. J. Coe, J. P. Essex-Lopresti, J. A. Harris, S. Houbrechts, A. Persoons, *Chem. Commun.* **1997**, 1645−1646.

[228] B. J. Coe, L. A. Jones, J. A. Harris, E. E. Sanderson, B. S. Brunschwig, I. Asselberghs, K. Clays, A. Persoons, *Dalton Trans.* **2003**, 2335−2341.

[229] B. J. Coe, J. A. Harris, L. J. Harrington, J. C. Jeffery, L. H. Rees, S. Houbrechts, A. Persoons, *Inorg. Chem.* **1998**, *37*, 3391−3399.

[230] B. J. Coe, L. A. Jones, J. A. Harris, B. S. Brunschwig, I. Asselberghs, K. Clays, A. Persoons, J. Garin, J. Orduna, *J. Am. Chem. Soc.* **2004**, *126*, 3880−3891.

246

[231] a) B. J. Coe, J. A. Harris, B. S. Brunschwig, *Dalton Trans.* **2003**, 2384–2386; b) B. J. Coe, S. P. Foxon, E. C. Harper, M. Helliwell, J. Raftery, C. A. Swanson, B. S. Brunschwig, K. Clays, E. Franz, J. Garin, J. Orduna, P. N. Horton, M. B. Hursthouse, *J. Am. Chem. Soc.* **2010**, *132*, 1706–1723; c) B. J. Coe, *Acc. Chem. Res.* **2006**, *39*, 383–393.

[232] a) M. Bourgault, C. Mountassir, H. Le Bozec, I. Ledoux, G. Pucetti, J. Zyss, *J. Am. Chem. Soc. Chem. Commun.* **1993**, 1623–1624; b) A. Hilton, T. Renouard, O. Maury, H. Le Bozec, I. Ledoux, J. Zyss, *Chem. Commun.* **1999**, 2521–2522.

[233] M. Bourgault, K. Baum, H. Le Bozec, G. Pucetti, I. Ledoux, J. Zyss, *New J. Chem.* **1998**, 517–522.

[234] D. Roberto, R. Ugo, F. Tessore, E. Lucenti, S. Quici, S. Vezza, S. Bruni, I. Ledoux-Rak, J. Zyss, *Organometallics* **2002**, *21*, 161–170.

[235] T. Renouard, H. Le Bozec, I. Ledoux, J. Zyss, *Chem. Commun.* **1999**, 871–872.

[236] K. Sénéchal, O. Maury, H. Le Bozec, I. Ledoux, J. Zyss, *J. Am. Chem. Soc.* **2002**, *124*, 4561–4562.

[237] a) O. Maury, L. Viau, K. Sénéchal, B. Corre, J.-P. Guégan, T. Renouard, I. Ledoux, J. Zyss, H. Le Bozec, *Chem. Eur. J.* **2004**, *10*, 4454–4466; b) C. Feuvrie, O. Maury, H. Le Bozec, I. Ledoux, J. P. Morral, G. T. Dalton, M. Samoc, M. G. Humphrey, *J. Phys. Chem. A* **2007**, *111*, 8980–8985.

[238] a) D. Roberto, F. Tessore, R. Ugo, S. Bruni, A. Manfredi, S. Quici, *Chem. Commun.* **2002**, 846–847; b) S. De Angelis, S. Fantacci, A. Sgamelotti, F. Cariati, D. Roberto, F. Tessore, R. Ugo, *Dalton Trans.* **2006**, 6707–6714.

[239] A. Colombo, D. Locatelli, D. Roberto, F. Tessore, R. Ugo, M. Cavazzini, S. Quici, F. De Angelis, S. Fantacci, I. Ledoux-Rak, N. Tancrez, J. Zyss, *Dalton Trans.* **2012**, *41*, 6707–6714.

[240] M. O. Senge, M. Fazekas, E. G. A. Notaras, W. J. Blau, M. Zawadzka, O. B. Locos, E. M. Ni Mhuircheartaigh, *Adv. Mater.* **2007**, *19*, 2737–2774.

[241] a) S. M. Le Cours, H.-W. Guan, S. G. Di Magno, C. H. Wang, M. J. Therien, *J. Am. Chem. Soc.* **1996**, *118*, 1497–1503; b) L. Karki, F. W. Vance, J. T. Hupp, S. M. Le Cours, M. J. Therien, *J. Am. Chem. Soc.* **1998**, *120*, 2606–2611.

[242] M. Pizzotti, E. Annoni, R. Ugo, S. Bruni, S. Quici, P. C. Fantucci, M. Bruschi, G. Zerbi, M. Del Zoppo, *J. Porph. Phthal.* **2004**, *8*, 1311–1324.

[243] M. Pizzotti, F. Tessore, A. Orbelli Biroli, R. Ugo, F. De Angelis, S. Fantacci, A. Sgamellotti, D. Zuccaccia, A. Macchioni, *J. Phys. Chem. C* **2009**, *113*, 11131–11141.

[244] A. Nayak, J. Park, K. De Mey, X. Hu, T. V. Duncan, D. N. Beratan, K. Clays, M. J. Therien, *ACS Cent. Sci.* **2016**, *2*, 954–966.

[245] a) P. G. Lacroix *Eur. J. Inorg. Chem.* **2001**, 339–348; b) S. Di Bella, I. Fragalà, I. Ledoux. M. A. Diaz-Garcia, T. J. Marks, *J. Am. Chem. Soc.* **1997**, *119*, 9550–9557.

[246] a) G.-J. Zhou, W.-Y. Wong, *Chem. Soc. Rev.* **2011**, *40*, 2541–2566; b) G.-J. Zhou, W.-Y. Wong, Z. Lin, C. Ye, *Angew. Chem. Int. Ed.* **2006**, *45*, 6189–6193.

[247] a) W.-Y. Wong, C.-L. Ho, *Acc. Chem. Res.* **2010**, *43*, 1246–1256; b) F.-R. Dai, H.-M. Zhan, Q. Liu, Y.-Y. Fu, J.-H. Li, Q.-W. Wang, Z. Xie, L. Wang, F. Yan, W.-Y. Wong, *Chem. Eur. J.* **2012**, *18*, 1502–1511; c) Q. Wang, W.-Y. Wong, *Polym. Chem.* **2011**, *2*, 432–440; d) F.-R. Dai, Y.-C. Chen, L.-F. Lai, W.-J. Wu, C.-H. Cui, G.-P. Tan, X.-Z. Wang, J.-T. Lin, H. Tian, W.-Y. Wong, *Chem. Asian J.* **2012**, *7*, 1426–1434.

[248] G. G. Dubinina, R. S. Price, K. A. Abboud, G. Wicks, P. Wnuk, Y. Stepanenko, M. Drobizhev, A. Rebane, K. S. Schanze, *J. Am. Chem. Soc.* **2012**, *134*, 19346–19349.

[249] R. Liu, N. Dandu, C. McCleese, Y. Li, T. Lu, H. Li, D. Yost, C. Wang, S. Kilina, C. Burda, W. Sun, *Eur. J. Inorg. Chem.* **2015**, 5241–5253.

[250] P. Nguyen, G. Lesley, T. B. Marder, *Chem. Mater.* **1997**, *9*, 406–408.

[251] A. Colombo, F. Nisic, C. Dragonetti, D. Marinotto, I. P. Oliveri, S. Righetto, M. G. Lobello, F. De Angelis, *Chem. Commun.* **2014**, *50*, 7986–7989.

[252] R. Durand, S. Gauthier, S. Achelle, S. Kahlal, J.-Y. Saillard, A. Barsella, L. Wojcik, N. Le Poul, F. Robin-Le Guen, *Dalton Trans.* **2017**, *46*, 3059–3069.

[253] a) A. Valore, A. Colombo, C. Dragonetti, S. Righetto, D. Roberto, R. Ugo, F. De Angelis, S. Fantacci, *Chem. Commun.* **2010**, *46*, 2414–2416; b) A. Colombo, C. Dragonetti, D. Marinotto, S. Righetto, D. Roberto, S. Tavazzi, M. Escadeillas, V. Guerchais, H. Le Bozec, A. Boucekkine, C. Latouche, *Organometallics* **2013**, *32*, 3890–3894.

[254] G. D. Batema, M. Lutz, A. L. Spek, C. A. Van Walree, S. de Mello Donegá, A. Meijerink, R. W. A. Havenith, J. Pérez-Moreno, K. Clays, M. Büchel, A.Van Dijken, D. L. Bryce, G. P. M. Van Klink, G. Van Koten, *Organometallics* **2008**, *27*, 1690–1701.

[255] A. Scarpaci, C. Monnereau, N. Hergué, E. Blart, S. Legoupy, F. Odobel, A. Gorfo, J. Pérez-Moreno, K. Clays, I. Asselberghs, *Dalton Trans*. **2009**, 4538–4546.

[256] E. Rossi, A. Colombo, C. Dragonetti, S. Righetto, D. Roberto, R. Ugo, A. Valore, J. A. G. Williams, M. G. Lobello, F. De Angelis, S. Fantacci, I. Ledoux-Rak, A. Singh, J. Zyss, *Chem. Eur. J.* **2013**, *19*, 9875–9883.

[257] T. T. Dang, J.-F. Soulé, H. Doucet, M. A. Benmensour, A. Boucekkine, A. Colombo, C. Dragonetti, S. Righetto, D. Jacquemin, J. Boixel, V. Guerchais, *Eur. J. Inorg. Chem.* **2016**, 4774–4782.

[258] a) J. A. Delaire, K. Nakatani, *Chem. Rev.* **2000**, *100*, 1817–1845; b) F. Mançois, J.-L. Pozzo, J. Pan, F. Adamietz, V. Rodriguez, L. Ducasse, F. Castet, A. Plaquet, B. Champagne, *Chem. Eur. J.* **2009**, *15*, 2560–2571; c) V. Guerchais, J. Boixel, H. Le Bozec, *Photon-working Switches*, **2017**, 363–384, Springer Japan, Tokyo; d) K. A. Green, M. P. Cifuentes, M. Samoc, M. G. Humphrey, *Coord. Chem. Rev.* **2001**, *255*, 2530–2541; e) S. Di Bella, I. P. Oliveri, A. Colombo, C. Dragonetti, S. Righetto, D. Roberto, *Dalton Trans.* **2012**, *41*, 7013–7016.

[259] B. J. Coe, S. Houbrechts, I. Asselberghs, A. Persoons, *Angew. Chem. Int. Ed.* **1999**, *38*, 366–369.

[260] S. K. Hurst, M. P. Cifuentes, J. P. L. Morrall, N. T. Lucas, I. R. Whittall, M. G. Humphrey, I. Asselberghs, A. Persoons, M. Samoc, B. Luther-Davies, A. C. Willis, *Organometallics* **2001**, *20*, 4664–4675.

[261] a) V. Aubert, V. Guerchais, E. Ishow, K. Hoang-Thi, I. Ledoux, K. Nakatani, H. Le Bozec, *Angew. Chem. Int. Ed.* **2008**, *47*, 577–580; b) L. Ordronneau, H. Nitadori, L. Ledoux, A. Singh, J. A. G. Williams, M. Akita, V. Guerchais, H. Le Bozec, *Inorg. Chem.* **2012**, *51*, 5627–5636; c) H. Le Bozec, V. Guerchais, *C. R. Chimie* **2013**, *16*, 1172–1182.

[262] a) H. Nitadori, L. Ordronneau, J. Boixel, D. Jacquemin, A. Boucekkine, A. Singh, M. Akita, I. Ledoux, V. Guerchais, H. Le Bozec, *Chem. Commun*. **2012**, *48*, 10395–10397; b) L. Ordronneau, V. Aubert, V. Guerchais, A. Boucekkine, H. Le Bozec, A. Singh, I. Ledoux, D. Jacquemin, *Chem. Eur. J.* **2013**, *19*, 5845–5848.

[263] M.-Y. Zhang, C.-H. Wang, W.-Y. Wang, N.-N. Ma, S.-L. Sun, Y.-Q. Qiu, *J. Phys. Chem. A* **2013**, *117*, 12497–12510.

[264] J. Lin, R. Sa, M. Zhang, K. Wu, *J. Phys. Chem. A*. **2015**, *119*, 8174–8181.

[265] a) J. Boixel, V. Guerchais, H. Le Bozec, A. Chantzis, D. Jacquemin, A. Amar, A. Boucekkine, A. Colombo, C. Dragonetti, D. Marinotto, D. Roberto, S. Righetto, R. De Angelis, *J. Am. Chem. Soc.* **2014**, *136*, 5367–5375; b) J. Boixel, V. Guerchais, H. Le Bozec, A. Chantzis, D. Jacquemin, A. Colombo, C. Dragonetti,

D. Marinotto, D. Roberto, *Chem. Commun.* **2015**, *51*, 7805−7080.

[266] N. Baggi, E. Garoni, A. Colombo, C. Dragonetti, S. Righetto, D. Roberto, J. Boixel, V. Guerchais, S. Fantacci, *Polyhedron* **2018**, *140*, 74−77.

[267] F. Nisic, E. Cariati, A. Colombo, C. Dragonetti, S. Fantacci, E. Garoni, E. Lucenti, S. Righetto, D. Roberto, J. A. G. Williams, *Dalton Trans.* **2017**, *46*, 1179−1185.

[268] a) R. H. Page, M. C. Jurich, B. Beck, A. Sen, R. J. Twieg, J. D. Swalen, G. C. Bjorklund, C. G. Wilson, *J. Opt. Soc. Am. B* **1990**, *7*, 1239−1250; b) M. A. Mortazavi, A. Knoesen, S. T. Kowel, B. G. Higgins, A. Dienes, *J. Opt. Soc. Am. B* **1989**, *6*, 733−741.

[269] a) P. N. Prasad, D. J. Williams, *Introduction to Nonlinear Optical Effects in Molecules and Polymers*, **1991**, Wiley, New York; b) D. M. Burland, R. D. Miller, C. Walsh, *Chem. Rev.* **1994**, *94*, 31−75; c) F. Ghebremichael, M. G. Kuzyk, H. S. Lackritz, *Prog. Polym. Sci.* **1997**, *22*, 1147−1201.

[270] a) G. Rojo, F. Agullò-Lòpez, B. Del Rey, T. J. Torres, *Appl. Phys.* **1998**, *84*, 6507−6512; b) S. Di Bella, I. Fragalà, *New J. Chem.* **2002**, *26*, 285−290.

[271] a) D. Roberto, F. Tessore, R. Ugo, S. Bruni, A. Manfredi, S. Quici, *Chem. Commun.* **2002**, 846−847; b) F. Tessore, D. Roberto, R. Ugo, M. Pizzotti, S. Quici, M. Cavazzini, S. Bruni, F. De Angelis, *Inorg. Chem.* **2005**, *44*, 8967−8978.

[272] V. Calabrese, S. Quici, E. Rossi, E. Cariati, C. Dragonetti, D. Roberto, E. Tordin, F. De Angelis, S. Fantacci, *Chem. Commun.* **2010**, 8374−8376.

[273] a) A. Valore, E. Cariati, C. Dragonetti, S. Righetto, D. Roberto, R. Ugo, F. De Angelis, S. Fantacci, A. Sgamellotti, A. Macchioni, D. Zuccaccia, *Chem. Eur. J.* **2010**, *16*, 4814−4825; b) I. González, D. Cortés-Arriagada, P. Dreyse, L. Sanhueza-Vega, I. Ledoux-Rak, D. Andrade, I. Brito, A. Toro-Labbé, M. Soto-Arriaza, S. Caramori, B. Loeb, *Eur. J. Inorg. Chem.* **2015**, 4946−4955.

[274] C. Dragonetti, S. Righetto, D. Roberto, R. Ugo, A. Valore, S. Fantacci, A. Sgamellotti, F. De Angelis, *Chem. Commun.* **2007**, 4116−4118.

[275] a) C. Dragonetti, S. Righetto, D. Roberto, A. Valore, *Phys. Status Solidi C* **2009**, *S1*, S50−S53; b) C. Dragonetti, S. Righetto, D. Roberto, A. Valore, T. Benincori, F. Sannicolò, F. De Angelis, S. Fantacci, *J. Mater. Sci.: Mater. Electron.* **2009**, *20*, S460−S464; c) C. Dragonetti, S. Righetto, D. Roberto, R. Ugo, A. Valore, F. Demartin, F. De Angelis, A. Sgamellotti, S. Fantacci, *Inorganica Chim. Acta* **2008**, *361*, 4070−4076.

[276] C. Dragonetti, A. Colombo, D. Marinotto, S. Righetto, D. Roberto, A. Valore, M. Escadeillas, V. Guerchais, H. Le Bozec, A. Boucekkine, C. Latouche, *J. Organomet. Chem.* **2014**, *751*, 568−572.

[277] C. Dragonetti, A. Valore, A. Colombo, D. Roberto, S. Righetto, G. Rampinini, F. Colombo, L. Rocchigiani, A. Macchioni, *Inorganica Chim. Acta* **2012**, *382*, 72−78.

[278] M. Zaarour, V. Guerchais, H. Le Bozec, C. Dragonetti, S. Righetto, D. Roberto, F. De Angelis, S. Fantacci, M. G. Lobello, *Dalton Trans.* **2013**, *42*, 155−159.

[279] B. J. Coe, *Comprehensive Coordination Chemistry II*, Vol. 9, **2004**, Elsevier Pergamon: Oxford, U.K.

[280] M. G. Humphrey, M. P. Cifuentes, M. Samoc, *Top. Organomet. Chem.* **2010**, *28*, 57−73.

[281] M. Goeppert-Mayer, *Ann. Phys.* **1931**, *9*, 273−294.

[282] W. Kaiser, C. G. B. Garrett, *Phys. Rev. Lett.* **1961**, *7*, 229−231.

[283] G. Lemercier, J.-C. Mulatier, C. Martineau, R. Anémian, C. Andraud, I. Wang, O. Stéphan, N. Amari, P. Baldeck, *C. R. Chimie* **2005**, *8*, 1308−1316.

[284] K. Ogawa, *Appl. Sci.* **2014**, *4*, 1−18.

[285] K. Y. Zhang, K. K.-W. Lo, *Metal complexes for cell and organism imaging, in inorganic chemical biology: principles, techniques and applications*, **2014**, John Wiley & Sons, Ltd, Chichester, UK.

[286] R. L. Sutherland, *Handbook of nonlinear optics, 2nd edn.* **2003**, Marcel Dekker, New York.

[287] Notes from lessons of Dr. K. Kamada, AIST Osaka, Japan.

[288] a) C. Xu, W. W. Webb, *J. Opt. Soc. Am. B* **1996**, *13*, 481−491; b) M. Drobizev, Y. Stepanenko, Y. Dzenis, A. Karotki, A. Rebane, P. N. Taylor, H. L. Anderson, *J. Phys. Chem. B* **2005**, *109*, 7223−7236.

[289] a) M. Sheik-Bahae, A. A. Said, T.-H. Wei, D. J. Hagan, E. W. Van Striland, *IEEE J. Quantum. Electron.* **1990**, *26*, 760−769; b) K. Kamada, *Proc. SPIE* **2004**, *5516*, 97−105.

[290] K. Kamada, K. Matsunaga, A. Yoshino, K. Ohta, *J. Opt. Soc. Am. B* **2003**, *20*, 529−537.

[291] K. Kamada, K, Ohta, Y. Iwase, K. Kondo, *Chem. Phys. Lett.* **2003**, *372*, 386−393.

[292] N. S. Makarov, M. Drobizhev, A. Rebane, *Opt. Express* **2008**, *16*, 4029-4047.

[293] G. S. He, L.-S. Tang, Q. Zheng, P. N. Prasad, *Chem. Rev.* **2008**, *108*, 1245−1330.

[294] W. L. Peticolas, J. P. Goldsborough, K. E. Rieckhoff, *Phys. Rev. Lett.* **1963**, *10*, 43−45.

[295] N. Hu, Y. Gong, X. Wang, Y. Lu, G. Peng, L. Yang, S. Zhang, Z. Luo, H. Li, F. Gao, *J. Fluoresc.* **2015**, *25*, 1559−1566.

[296] a) J. E. Ehrlich, X. L. Wu, I.-Y. S. Lee, Z.-Y. Hu, H. Röckel, S. R. Marder, J. W. Perry, *Opt. Lett.* **1997**, *22*, 1843−1845; b) M. Albota, D. Beljonne, J.-L. Brédas, J. E. Ehrlich, J.-Y. Fu, A. A. Heikal, S. E. Hess, T. Kogej, M. D. Levin, S. R. Marder, D. McCord-Maughon, J. W. Perry, H. Röckel, M. Rumi, G. Subramaniam, W. W. Webb, X.-L. Wu, C. Xu, *Science* **1998**, *281*, 1653−1656.

[297] B. Strehmel, S. Amthor, J. Schelter, C. Lambert, *Chem. Phys. Chem.* **2005**, *6*, 893−896.

[298] O. Mongin, L. Porrès, M. Charlot, C. Katan, M. Blanchard-Desce, *Chem. Eur. J.* **2007**, *13*, 1481−1498.

[299] S. K. Lee, W. J. Yang, J. J. Choi, C. H. Kim, S.-J. Jeon, B. R. Cho, *Org. Lett.* **2005**, *7*, 323−326.

[300] L. Beverina, M. Crippa, P. Salice, R. Ruffo, C. Ferrante, I. Fortunati, R. Signorini, C. M. Mari, R. Bozio, A. Facchetti, G. A. Pagani, *Chem. Mater.* **2008**, *20*, 3242−3244.

[301] S.-J. Chung, K.-S. Kim, T.-C. Lin, G. S. He, J. Swiatkiewicz, P. N. Prasad, *J. Phys. Chem. B* **1999**, *103*, 10741−10745.

[302] O. Mongin, J. Brunel, L. Porrès, M. Blanchard-Desce, *Tetrahedron Lett.* **2003**, *44*, 2813−2816.

[303] L. Porrès, C. Katan, O. Mongin, T. Pons, J. Mertz, M. Blanchard-Desce, *J. Mol. Struct.* **2004**, *704*, 17−24.

[304] B. R. Cho, K. H. Son, S. H. Lee, Y.-S. Song, Y.-K. Lee, S.-J. Jeon, J. H. Choi, H. Lee, M. Cho, *J. Am. Chem. Soc.* **2001**, *123*, 10039−10045.

[305] B. R. Cho, M. J. Piao, K. H. Son, S. H. Lee, S. J. Yoon, S.-J. Jeon, M. Cho, *Chem. Eur. J.* **2002**, *8*, 3907−3916.

[306] W. J. Yang, C. H. Kim, M.-Y. Jeong, S. K. Lee, M. J. Piao, S.-J. Jeon, B. R. Cho, *Chem. Mater.* **2004**, *16*, 2783−2789.

[307] Z. Zeng, Z. Guan, Q.-H. Xu, J. Wu, *Chem. Eur. J.* **2011**, *17*, 3837−3841.

[308] J. Yoo, S. K. Yang, M.-Y. Jeong, H. C. Ahn, A.-J. Jeon, B. R. Cho, *Org. Lett.* **2003**, *5*, 645−648.

[309] P. Macak, Y. Luo, H. Norman, H. J. Ågren, *Chem. Phys.* **2000**, *113*, 7055−7061.

[310] W. J. Yang, D. Y. Kim, C. H. Kim, M.-Y. Jeong, S. K. Lee, S.-J. Jeon, B. R. Cho, *Org. Lett.* **2004**, *6*, 1389−1392.

[311] G. J. Lee, S. H. Lee, B. R. Cho, *Curr. Appl. Phys.* **2004**, *4*, 573−576.

[312] L. Porrès, O. Mongin, C. Katan, M. Charlot, T. Pons, J. Mertz, M. Blanchard-Desce, *Org. Lett.* **2004**, *6*, 47–50.

[313] B. J. Zhang, S.-J. Jeon, *Chem. Phys. Lett.* **2003**, *377*, 210–216.

[314] a) M. Drobizhev, A. Karotki, Y. Dzenis, A. Rebane, Z. Suo C. W. Spangler, *J. Phys. Chem. B* **2003**, *107*, 7540–7543; b) O. Varnavski, X. Yan, O. Mongin, M. Blanchard-Desce, T. Goodson III, *J. Phys. Chem. C* **2007**, *111*, 149–162; c) B. Xu, H. Fang, F. Chen, H. Lu, J. He, Y. Li, O. Chen, H. Sun, W. Tian, *New J. Chem.* **2009**, *33*, 2457–2464; d) B. Xu, J. Zhang, H. Fang, S. Ma, O. Chen, H. Sun, C. Im, W. Tian, *Polym. Chem.* **2014**, *5*, 479–488.

[315] G. S. He, J. Swiatkiewicz, Y. Jiang, P. N. Prasad, B. A. Reinhardt, L.-S. Tan, R. Kannan, *J. Phys. Chem. A* **2000**, *104*, 4805–4810.

[316] O. Mongin, L Porrès, C. Katan, T. Pons, J. Mertz, M. Blanchard-Desce, *Tetrahedron Lett.* **2003**, 44, 8121–8125; b) T.-C. Lin, C.-Y. Liu, B.-R. Huang, J.-H. Lin, Y.-K. Shen, C.-Y. Wu, *Eur. J. Org. Chem.* **2013**, 498–508.

[317] A. A. Tracton, *Coating Technology Handbook* **2005**, CRC Press.

[318] C. Huang, S. Barlow, S. R. Marder, *J. Org. Chem.* **2011**, *76*, 2386–2407.

[319] a) L. De Boni, C. J. L. Constantino, L. Misoguti, R. F. Aroca, S. C. Zilio, C. R. Mendonça, *Chem. Phys. Lett.* **2003**, 371, 744–749; b) S. L. Oliveira, D. S. Corrêa, L. Misoguti, C. J. L. Constantino, R. F. Aroca, S. C. Zilio, C. R. Mendonça, *Adv. Mater.* **2005**, *17*, 1890–1893; c) D. S. Correa, S. L. Oliveira, L. Misoguti, S. C. Zilio, R. F. Aroca, C. J. L. Constantino, C. R. Mendonça, *J. Phys. Chem. A* **2006**, *110*, 6433–6438.

[320] G. Horowitz, F. Kouki, P. Spearman, D. Fichou, C. Nogues, X. Pan, F. Garnier, *Adv. Mater.* **1996**, *8*, 242–245.

[321] a) E. Piovesan, D. L. Silva, L. De Boni, F. E. G. Guimaraes, L. Misoguti, R. Zalesny, W. Bartowiak, C. R. Mendonça, *Chem. Phys. Lett.* **2009**, 479, 52–55; b) L. De Boni, A. A. Andrade, L. Misoguti, C. R. Mendonça, S. C. Zilio, *Opt. Express* **2004**, *12*, 3921–3927.

[322] K. D. Belfield, M. V. Bondar, F. E. Hernandez, O. V. Przhonska, *J. Phys. Chem. C* **2008**, *112*, 5618–5622.

[323] Z. An, S. A. Odom, R. F. Kelley, C. Huang, X. Zhang, S. Barlow, L. A. Padilha, J. Fu, S. Webster, D. J. Hagan, E. W. Van Stryland, M. R. Wasielewski, S. R. Marder, *J. Phys. Chem. A* **2009**, *113*, 5585–5593.

[324] L. Cao, L. Xu, D. Zhang, Y. Zhou, Y. Zheng, Q. Fu, X.-F. Jiang, F. Lu, *Chem. Phys. Lett.*, **2017**, *682*, 133–139.

[325] B. Pagoaga, O. Mongin, M. Caselli, D. Vanossi, F. Momicchioli, M. Blanchard-Desce, G. Lemercier, N. Hoffmann, G. Ponterini, *Phys. Chem. Chem. Phys.* **2016**, *18*, 4924–4941.

[326] A. Marginenanu, J. Hofkens, M. Cotlet, S. Habuchi, A. Stefan, J. Qu, C. Kohl, K. Müllen, J. Vercammen, Y. Engelborghs, T. Gensch, F. C. De Schryver, *J. Phys. Chem. B* **2004**, *108*, 12242–12251.

[327] J. Zhang, M. K. R. Fischer, P. Bäuerle, T. Goodson III, *J. Phys. Chem. B* **2013**, *117*, 4204–4215.

[328] a) C. Huang, M. M. Sartin, N. Siegel, M. Cozzuol, Y. Zhang, J. M. Hales, S. Barlow, J. W. Perry, S. R. Marder, *J. Mater. Chem.* **2011**, *21*, 16119–16128; b) C. Huang, M. M. Sartin, M. Cozzuol, N. Siegel, S. Barlow, J. W. Perry, S. R. Marder, *J. Phys. Chem. A* **2012**, *116*, 4305–4317.

[329] B. Gao, C. Lu, J. Xu, F. Meng, Y. Cui, H. Tian, *Chem. Lett.* **2006**, *35*, 1416–1417.

[330] Z. Cai, R. J. Vaźquez, D. Zhao, L. Li, W.-Y. Lo, N. Zhang, Q. Wu, B. Keller, A. Eshun, N. Abeyasinghe, H. Banaszak-Holl, T. Goodson III, L. Yu, *Chem. Mater.* **2017**, *29*, 6726–6732.

[331] a) X. Huang, Q. Shi, W.-Q. Chen, C. Zhu, W. Zhou, Z. Zhao, X.-M. Duan, X. Zhan, *Macromolecules* **2010**, *43*, 9620-9626; b) J. Luo, S. Lee, M. Son, B. Zheng, K.-W. Huang, Q. Qi, W. Zeng, G. Li, D. Kim, J. Wu, *Chem. Eur. J.* **2015**, *21*, 3708–3715.

[332] M. Adachi, Y. Murata, S. Nakamura, *J. Phys. Chem.* **1995**, *99*, 14240–1424.

[333] C. Huang, M. M. Sartin, N. Siegel, M. Cozzuol, Y. Zhang, J. M. Hales, S. Barlow, J. W. Perry, S. M. Marder, *J. Mater. Chem*. **2011**, *21*, 16119–16128.

[334] M. Lan, K. Ikegami, *Colloids and Surfaces A: Physicochem. And Eng. Aspects*, **2005**, *257*, 225–229.

[335] X. T. Liu, Y. Zhao, A.-M. Ren, J.-K. Feng, *J. Mol. Model.* **2011**, *17*, 1413–1425.

[336] a) S. Lentijo, G. Aullón, J. A. Miguel, P. Espinet, *Dalton Trans*. **2013**, *42*, 6353–6365; b) J. E. Expósito, M. Álvarez-Paíno, G. Aullón, J. A. Miguel, P. Espinet, *Dalton Trans*. **2015**, *44*, 16164–16176; c) M. K. Brennaman, M. R. Norris, M. K. Gish, E. M. Grumstrup, L. Alibabaei, D. L. Ashford, A. M. Lapides, J. M. Papanikolas, J. L. Templeton, T. J. Meyer, *J. Phys. Chem. Lett*. **2015**, *6*, 4736–4742.

[337] a) V. L. Gunderson, E. Krieg, M. T. Vagnini, M. A. Iron, B. Rybtchinski, M. R. Wasielewski, *J. Phys. Chem. B* **2011**, *115*, 7533–7540; b) M. L. Hassan, C. M. Moorefield, H. S. Elbatal, G. R. Newkome, D. A. Modarelli, N. C. Romano, *Mater. Sci. Eng. B* **2012**, *177*, 350–358; c) M. Schulze, A. Steffen, F. Würthner, *Angew. Chem. Int. Ed.* **2015**, *54*, 1570–1573; d) F. Nastasi, G. La Ganga, S. Campagna, Z. Syrgiannis, F. Rigodanza, S. Vitale, A. Licciardello, M. Prato, *Phys. Chem. Chem. Phys*. **2017**, *19*, 14055–14065.

[338] B. Liu, W. Zhu, W. Wu, K. M. Ri, H. Tian, *J. Photochem. Photobiol. A, Chem.* **2008**, *194*, 268–274.

[339] a) B. E. Partridge, P. Leowanawat, E. Aqad, M. R. Imam, H.-J. Sun, M. Peterca, P. A. Heiney, R. Graf, H. W. Spiess, X. Zeng, G. Ungar, V. Percec, *J. Am. Chem. Soc*. **2015**, *137*, 5210–5224; b) J. Qu, N. D. Pschirer, D. Liu, A. Stefan, F. C. De Schryver, K. Müllen, *Chem. Eur. J.* **2004**, *10*, 528–537.

[340] a) D. Touchard, P. Haquette, S. Guesmi, L. Le Pichon, A. Daridor, L. Toupet, P. H. Dixneuf, *Organometallics* **1997**, *16*, 3640–3648; b) M. A. Fox, J. E. Harris, S. Heider, V. Pérez-Gregorio, M. E. Zakrzewska, J. D. Farmer, D. S. Yufit, J. A. K. Howard, P. J. Low, *J. Organomet. Chem.* **2009**, *694*, 2350–2358.

[341] J. Sun, Q. Ren, X.-Q. Wang, G.-H. Zhang, D. Xu, *Opt. Laser Technol.* **2009**, *41*, 209–212.

[342] E. Akhüseyin, O. Türkmen, B. Küçüköz, H. Yilmaz, A. Karatay, G. Sevinç, K. Xu, M. Hayvali, H. G. Yaglioglu, *Phys. Chem. Chem. Phys,* **2016**, *18*, 4451–4459.

[343] Y. Sekiguchi, T. Yamashita, M. Vacha, *J. Lumin.* **2008**, *128*, 848–850.

[344] B. J. Coe, J. Fielden, S. P. Foxon, B. S. Brunschwig, I. Asselberghs, K. Clays, A. Samoc, M. Samoc, *J. Am. Chem. Soc.* **2010**, *132*, 3496–3513.

[345] P. Shi, B. J. Coe, S. Sanchez, D. Wang, Y. Tian, M. Nyk, M. Samoc, *Inorg. Chem.* **2015**, *54*, 11450–11456.

[346] a) S. Mazzucato, I. Fortunati, S. Scolaro, M. Zerbetto, C. Ferrante, R. Signorini, D. Pedron, R. Bozio, D. Locatelli, S. Righetto, D. Roberto, R. Ugo, A. Abbotto, G. Archetti, L. Beverina, S. Ghezzi, *Phys. Chem. Chem. Phys*. **2007**, *9*, 2999–3005, b) C. Dragonetti, M. Balordi, A. Colombo, D. Roberto, R. Ugo, I. Fortunati, E. Garbin, C. Ferrante, R. Bozio, A. Abbotto, H. Le Bozec, *Chem. Phys. Lett.* **2009**, *475*, 245–249.

[347] a) B. J. Rudresha, K. B. Manjunatha, G. Umesh, B. Ramachandra Bhat, *Chem. Phys. Lett.* **2012**, *542*, 159–163; b) C. Nie, Q. Zhang, H. Ding, B. Huang, X. Wang, X. Zhao, S. Li, H. Zhou, J. Wu, Y. Tian, *Dalton Trans*. **2014**, *43*, 599–608.

[348] F. Jin, C. Pan, W. Zhang, L. Sun, X. Hu, R. Liao, D. Tao, *J. Lumin.* **2016**, *172*, 264–269.

[349] a) G. G. Dubinina, R. S. Price, K. A. Abboud, G. Wicks, P. Wnuk, Y. Stepanenko, M. Drobizhev, A. Rebane, K. S. Schanze, *J. Am. Chem. Soc.* **2012**, *134*, 19346−19349; b) M. G. Vivas, L. De Boni, T. M. Cooper, C. R. Mendonca, *ACS Photonics* **2014**, *1*, 106−113.

[350] H.-P. Zhou, D.-M. Li, P. Wang, L.-H. Cheng, Y.-H. Gao, Y.-M. Zhu, J.-Y. Wu, Y.-P. Tian, X.-T. Tao, M.-H. Jiang, H.-K. Fun, *J. Mol. Struct.* **2007**, *826*, 205−210.

[351] B. J. Coe, M. Samoc, A. Samoc, L. Zhu, Y. Yi, Z. Shuai, *J. Phys. Chem. A* **2007**, *111*, 472−478.

[352] C. Feuvrie, O. Maury, H. Le Bozec, I. Ledoux, J. P. Morrall, G. T. Dalton, M. Samoc, M. G. Humphrey, *J. Phys. Chem. A* **2007**, *111*, 8980−8985.

[353] a) C. Girardot, B. Cao, J.-C. Mulatier, P. L. Baldeck, J. Chauvin, D. Riehl, J. A. Delaire, C. Andraud, G. Lemercier, *ChemPhysChem* **2008**, *9*, 1531−1535; b) M. Four, D. Riehl, O. Mongin, M. Blanchard-Desce, L. M. Lawson-Daku, J. Moreau, J. Chauvin, J. A. Delaire, G. Lemercier, *Phys. Chem. Chem. Phys.* **2011**, *13*, 17304−17312; c) O. Mongin, M. Four, S. Chevreux, M. Blanchard-Desce, G. Lemercier, *Chimia* **2015**, *69*, 666−669.

[354] P. Hanczyc, B. Nordena, M. Samoc, *Dalton Trans.* **2012**, *41*, 3123−3125.

[355] J. Liu, Y. Chen, G. Li, P. Zhang, C. Jin, L. Zeng, L. Ji, H. Chao, *Biomaterials* **2015**, *56*, 140−153.

[356] L. Q. Xu, *Eur. Polym. J.* **2015**, *71*, 279−288.

[357] K. A. Green, M. P. Cifuentes, M. Samoc, M. G. Humphrey, *Coord. Chem. Rev.* **2011**, *255*, 2025−2038.

[358] A. M. McDonagh, M. G. Humphrey, M. Samoc, B. Luther-Davies, *Organometallics* **1999**, *18*, 5195−5197.

[359] a) A. M. McDonagh, M. G. Humphrey, M. Samoc, B. Luther-Davies, S. Houbrechts, T. Wada, H. Sasabe, A. Persoons, *J. Am. Chem. Soc.* **1999**, *121*, 1405−1406; b) S. K. Hurst, M. G. Humphrey, T. Isoshima, K. Wostyn, I. Asselberghs, K. Clays, A. Persoons, M. Samoc, B. Luther-Davies, *Organometallics* **2002**, *21*, 2024−2026; c) S. K. Hurst, N. T. Lucas, M. G. Humphrey, T. Isoshima, K. Wostyn, I. Asselberghs, K. Clays, A. Persoons, M. Samoc, B. Luther-Davies, *Inorg. Chim. Acta* **2003**, *350*, 62−76.

[360] H. S. Nalwa, T. Watanabe, S. Miyata, *Nonlinear Optics of Organic Molecules and Polymers*, **1997**, CRC Press, Boca Raton, FL.

[361] M. Samoc, J. P. Morrall, G. T. Dalton, M. P. Cifuentes, M. G. Humphrey, *Angew. Chem. Int. Ed*. **2007**, *46*, 731−733.

[362] R. L. Roberts, T. Schwich, T. C. Corkery, M. P. Cifuentes, K. A. Green, J. D. Farmer, P. J. Low, T. B. Marder, M. Samoc, M. G. Humphrey, *Adv. Mater.* **2009**, *21*, 2318−2322.

[363] T. Schwich, M. P. Cifuentes, P. A. Gugger, M. Samoc, M. G. Humphrey, *Adv. Mater.* **2011**, *23*, 1433−1435.

[364] K. A. Green, P. V. Simpson, T. C. Corkery, M. P. Cifuentes, M. Samoc, M. G. Humphrey, *Macromol. Rapid Commun.* **2012**, *33*, 573−578.

[365] P. V. Simpson, L. A. Watson, A. Barlow, G. Wang, M. P. Cifuentes, M. G. Humphrey, *Angew. Chem. Int. Ed.* **2016**, *55*, 2387−2391.

[366] G. T. Dalton, M. P. Cifuentes, L. A. Watson, S. Petrie, R. Stranger, M. Samoc, M. G. Humphrey, *Inorg. Chem*. **2009**, *48*, 6534−6547.

[367] Z. Chen, C J. Jeffery, M. Morshedi, G. J. Moxey, A. Barlow, X. Yang, B. A. Babgi, G. T. Dalton, M. D. Randles, M. K. Smith, C. Zhang, M. Samoc, M. P. Cifuentes, M. G. Humphrey, *ChemPlusChem* **2015**, *80*, 1329−1340.

[368] F. Malvolti, C. Rouxel, G. Grelaud, L. Toupet, T. Roisnel, A. Barlow, X. Yang, G. Wang, F. I. Abdul Razak, R. Stranger, M. P. Cifuentes, M. G. Humphrey, O. Mongin, M. Blanchard-Desce, C. O. Paul-Roth, F. Paul, *Eur. J. Inorg. Chem.* **2016**, 3868−3882.

[369] K. Onitsuka, N. Ohara, F. Takei, S. Takahashi, *Dalton Trans.* **2006**, 3693−3698.

[370] A. M. McDonagh, C. E. Powell, J. P. Morrall, M. P. Cifuentes, M. G. Humphrey, *Organometallics* **2003**, *22*, 1402−1413.

[371] C. E. Powell, M. P. Cifuentes, A. M. McDonagh, M. G. Humphrey, M. Samoc, B. Luther-Davies, G. A. Heath, *J. Am. Chem. Soc.* **2003**, *125*, 602−610.

[372] A. Colombo, C. Dragonetti, D. Roberto, R. Ugo, L. Falciola, S. Luzzati, D. Kotowski, *Organometallics* **2011**, 30, 1279−1281.

[373] R. M. Edkins, S. L. Bettington, A. E. Goeta, A. Beeby, *Dalton Trans.* **2011**, *40*, 12765−12770.

[374] C.-L. Ho, K.-L. Wong, H.-K. Kong, Y.-M. Ho, C. T.-L. Chan, W.-M. Kwok, K. S.-Y. Leung, H.-L. Tam, M. H.-W. Lam, X.-F. Ren, A.-M. Ren, J.-K. Fengf, W.-Y. Wong, *Chem. Commun.* **2012**, *48*, 2525−2527.

[375] Y. Fan, D. Ding, D. Zhao, *Chem. Commun.* **2015**, *51*, 3446−3449.

[376] A. Colombo, C. Dragonetti, D. Roberto, A. Valore, C. Ferrante, I. Fortunati, A. L. Picone, F. Todescato, J. A. G. Williams, *Dalton Trans.* **2015**, *44*, 15712−15720.

[377] H. Moritomo, A. Fujii, Y. Suzuki, T. Yoshihara, S. Tobita, J. Kawamata, *Jpn. J. Appl. Phys.* **2016**, *55*, 092041.

[378] M. Lepeltier, F. Appaix, Y. Y. Liao, F. Dumur, J. Marrot, T. Le Bahers, C. Andraud, C. Monnereau, *Inorg. Chem.* **2016**, *55*, 9586−9595.

[379] L. S. Natrajan, A. Toulmin, A. Chewa, S. W. Magennis, *Dalton Trans.* **2010**, *39*, 10837−10846.

[380] W.-J. Xu, S.-J. Liu, X. Zhao, N. Zhao, Z.-Q. Liu, H. Xu, H. Liang, Q. Zhao, X.-Q. Yu, W. Yuang, *Chem. Eur. J.* **2013**, *19*, 621−629.

[381] M. Sarma, T. Chatterjee, R. Bodapati, K. N. Krishnakanth, S. Hamad, S. V. Rao, S. K. Das, *Inorg. Chem.* **2016**, *55*, 3530−3540.

[382] a) G. Li, Q. Lin, L. Sun, C. Feng, P. Zhang, B. Yu, Y. Chen, Y. Wen, H. Wang, L. Ji, H. Chao, *Biomaterials* **2015**, *53*, 285−295; b) C. Jin, J. Liu, Y. Chen, L. Zeng, R. Guan, C. Ouyang, L. Ji, H. Chao, *Chem. Eur. J.* **2015**, *21*, 12000−12010; c) L. Sun, Y. Chen, S. Kuang, G. Li, R. Guan, J. Liu, L. Ji, H. Chao, *Chem. Eur. J.* **2016**, *22*, 8955−8965.

[383] M. Lepeltier, H. Le Bozec, V. Guerchais, T. K.-M. Lee, K. K.-W. Lo, *Organometallics* **2005**, *24*, 6069−6072.

[384] J. N. Demas, G. A. Crosby, *J. Phys. Chem.* **1971**, *75*, 991−1024.

[385] a) C. G. Bethea B. F. Levine, *Appl. Phys. Lett.* **1974**, *24*, 445–447; b) C. G. Bethea B. F. Levine. *J. Chem. Phys.* **1975**, *62*, 2666–2682; c) J. Zyss I. Ledoux, *J. Chem. Phys.* **1982**, *73*, 203–213.

[386] E. Diez-Barra, J. C. Garcia-Martinez, S. Merino, R. Del Rey, J. Rodriguez-Lopez, P. Sanchez-Verdu, J. Tejeda, *J. Org. Chem.* **2001**, *66*, 5664−5670.

[387] X.-S. Xiao, W. Lu, C.-M. Che, *Chem. Sci.* **2014**, *5*, 2482−2488.

[388] T. N. Y Hoang, M. Humbert-Droz, T. Dutronc, L. Guénée, C. Besnard, C. Piguet, *Inorg. Chem.* **2013**, 52, 5570−5580.

[389] S. M. Johnson, S. Connelly, I. A. Wilson, J. W. Kelly *J. Med. Chem.*, **2008**, *51*, 6348−6358.

[390] W. Treibe, *Tetrahedron Lett.* **1967**, 4707−4709.

[391] W. Wu, C. Cheng, C., W. Wu, H. Guo, S. Ji, P. Song, K. Han, J. Zhao, X. Zhang, Y. Wu, G. Du, *Eur. J. Inorg. Chem.* **2010**, 4683−4696.

[392] Y. Liu, A. Kuzuya, R. Sha, J. Guillaume, R. Wang, J. W. Canary, N. C. Seeman, *J. Am. Chem. Soc.* **2008**, *130*, 10882−10883.

[393] F. Nisic, A. Colombo, C. Dragonetti, D. Roberto, A. Valore, J. M. Malicka, M. Cocchi, G. R. Freeman, J. A. G. Williams, *J. Mater. Chem. C*, **2014**, *2*, 1791−1800.

[394] J. A. G. Williams, A. Beeby, E. S. Davies, J. A. Weinstein, C Wilson, *Inorg. Chem.* **2003**, *42*, 8609−8611.

[395] X. Zhu, M. C. Traub, D. A. Vanden Bout, K. N. Plunkett, *Macromolecules* **2012**, *45*, 5051−5057.

[396] a) J. S. Bradshaw, K. E. Krakoviak, G. C. LindH, R. M. Izath *Tetrahedron* **1987**, *43*, 4271−4276.

[397] a) A. J. Myles, T. J. Wigglesworth, N. R. Branda, *Adv. Mater.* **2003**, *15*, 9, 745−748; b) S.-J. Lim, B.-K. An, S. Y. Park, *Macromol.* **2005**, *38*, 6236−6239; c) S, Pu, W. Liu, W. Miao, *J. Phys. Org. Chem.* **2009**, *22*, 954−963; d) S. Pu, D. Jiang, W. Liu, G. Liu, S. Cui, *J. Mater. Chem.* **2012**, *22*, 3517−3526.

[398] J. Boixel, V. Guerchais, H. Le Bozec, A. Chantzis, D. Jacquemin, A. Colombo, C. Dragonetti, D. Marinotto, D. Roberto, *Chem. Commun.* **2015**, *51*, 7085−7088.

[399] M. Lepeltier, H. Le Bozec, V. Guerchais, T. K.-M. Lee, K. K.-W. Lo *Organometallics* **2005**, *24*, 6069−6072.

[400] M. Zaarour, A. Singh, C. Latouche, J. A. G. Williams, I. Ledoux-Rak, J. Zyss, A. Boucekkine, H. Le Bozec, V. Guerchais, C. Dragonetti, A. Colombo, D. Roberto, A. Valore, *Inorg. Chem.* **2013**, *52*, 7987−7994.

[401] T. Le Bouder, L. Viau, J.-P. Guégan, O. Maury, H. Le Bozec, *Eur. J. Org. Chem.* **2002**, 3024−3033.

[402] M. Lepeltier, T. K.-M. Lee, K. K.-W. Lo, L. Toupet, H. Le Bozec, V. Guerchais, *Eur. J. Inorg. Chem.* **2007**, 2734−2747.

[403] G. M. Sheldrick, *Acta Cryst. A71*, **2015**, 3−8.

[404] G.M. Sheldrick, *Acta Cryst. C71*, **2015**, 3−8.